Light-activated Caged Iron Chelators (CICs) for Skin Photoprotection

Hampshire, Annabel

Award date:
2019

Awarding institution:
University of Bath

Light-activated Caged Iron Chelators (CICs) for Skin Photoprotection

Annabel Hampshire

A thesis submitted for the degree of Doctor of Philosophy

University of Bath

Department of Pharmacy and Pharmacology

May 2019

DECLARATION OF ANY PREVIOUS SUBMISSION OF THE WORK

The material presented here for examination for the award of a higher degree by research has not been incorporated into a submission for another degree.

Candidate's signature:

DECLARATION OF AUTHORSHIP

I am the author of this thesis, and the work described therein was carried out by myself personally.

Candidate's signature:

Whether your target is big or small, grand or simple, ambitious or personal, I've always believed that success comes from not letting your eyes stray from that target. Anyone who wants to achieve a dream must stay strong, focused and steady. She must expect and demand perfection and never settle for mediocrity.
-Estée Lauder, 1985

In memory of Aunty Sue

Table of Contents

Abstract

UV radiation from the sun to which the skin is exposed is largely UVA. UVA is oxidative in nature and may generate redox-active labile iron within skin cells, inducing severe damage through the production of reactive oxygen species (ROS), and leading to skin photoaging and cancer. Light-activated caged iron chelators (CICs) are compounds that become active when exposed to environmentally relevant doses of UVA, releasing a potent iron-trapping agent or chelator, and providing UVA dose-dependent protection from harmful labile iron.

This work describes first the optimisation of the synthesis of CICs where the iron-binding capability of the well-known iron chelators SIH, PIH and deferasirox (EXJADE®) was masked with a cinnamic acid photo-cleavable caging group. UVA irradiation uncaged the CICs to give the free iron chelator and a photoproduct, generated from cyclization of the caging group. The CICs were assessed for photoprotective ability in human skin fibroblasts (FEK4) by use of the MTT assay after a dose of 500 kJ/m^2 UVA irradiation. One such CIC **51** (20 μM) provided significant photoprotection upon UVA irradiation, increasing the number of viable cells compared to cells irradiated without addition of the CIC. A second series of CICs was then synthesised by rational design; caging groups were selected based on the antioxidant potential of their carbostyril photoproducts. Two lead carbostyrils were identified which could significantly quench UVA-induced ROS especially in combination with an iron chelator, as determined by flow cytometry using the oxidative stress indicator, CM-H_2DCFDA. This analysis led to the synthesis of the corresponding multi-functional CIC **115**, which also showed significant photoprotection in the MTT assay. The capacity of sub-optimal thicknesses of commercially available sunscreen formulations to provide photoprotection against UVA-induced cell death and labile iron release was also investigated using the calcein assay. At a thickness of 0.5 mg/cm^2, UVA-induced labile iron was generated in all cases at fold-increases of 1.63-2.08 compared to the unirradiated control. The cell death consequences of this effect were confirmed by flow cytometry with annexin V/PI staining. The addition of CICs significantly reversed UVA-induced cell death and generation of labile iron, showing the potential real-world impact of combining a CIC with UVA/B filters in a sunscreen formulation. Finally a synthetic pathway to the natural iron chelator pulcherrimic acid was developed, followed by an investigation into its photoprotective potential.

Acknowledgements

I am hugely grateful to my supervisors Dr Ian Eggleston and Dr Charareh Pourzand, firstly for giving me the opportunity to undertake this PhD research and secondly for their constant support and guidance. Much of my perseverance in the laboratory stemmed from your 'can-do', positive attitudes.

I am especially grateful to Ian for the long hours of discussing chemistry and reading drafts of this thesis! Charareh, thank you for being a great female role model for me in the world of academia, and for always offering your help and a cup of tea.

To my parents and brothers, for your love and belief and for always finding a way to re-energise me.

To Joe, for your patience… and humour when I needed it the most, for putting up with me talking about my thesis in my sleep, and for helping me to believe in myself.

To my laboratory and office colleagues; Joanna Watt, Beccie Martin, Nour Alhusein, Dana Beiki, Bayan Alkhawaja, Scott Alan and Kunal Tewari. I am very lucky to have shared this time with you. I am particularly thankful to Jo, you have made undertaking my PhD very enjoyable and you have always gone out of your way to help or counsel me and make me laugh when experiments didn't work. Beccie, I hope you can find a replacement partner for the Christmas tree angel competition!

To Yarac, for making me smile as the sun rose before a day in the lab.

I would also like to thank the Faculty of Science at the University of Bath and the British Skin Foundation for providing the funding for this research.

Abbreviations

AcOH	acetic acid
Bn	benzyl
BCC	basal cell carcinoma
CA-AM	calcein acetoxymethyl ester
CDP	cyclic dipeptide
CIC	caged iron chelators
CMP	collagen mimetic peptides
CPD	cyclobutane pyrimidine dimer
m-CPBA	*meta*-chloroperbenzoic acid
DCFDA	2',7'-dichlorofluorescin diacetate
DCM	dichloromethane
DIPEA	*N,N*-diisopropylethylamine
DMAP	4-dimethylaminopyridine
DMF	*N,N*-dimethylformamide
DPPH	2, 2-diphenyl-1-picrylhydrazyl
ECETP	(carbethoxyethylidene)triphenylphosphorane
EDC.HCl	*N-(*3-dimethylaminopropyl)-*N'*-ethylcarbodiimide
ESR	electron spin resonance spectroscopy
FA	formic acid
FAS	ferrous ammonium sulphate
FDA	Food and Drug Administration
INH	isonicotinylhydrazide
KC	keratinocyte cancer
LIP	labile iron pool
MED	minimal erythema dose
MTT	3-(4,5-dimethylthiazol-2-yl)-2,5-diphenyltetrazolium bromide
NMSC	non-melanoma skin cancer
O/N	overnight

PI	propidium iodide
PIH	pyridoxal isonicotinoyl hydrazine
PPG	photocleavable protecting group
ROS	reactive oxygen species
RSF	radical skin protection factor
RT	room temperature
SCC	squamous cell carcinoma
SIH	salicylaldehyde isonicotinoyl hydrazone
SPF	sun protection factor
SSR	solar-simulated radiation
TFA	trifluoroacetic acid
THF	tetrahydrofuran
UVR	ultraviolet radiation
2,5-DKP	2,5-diketopiperazine

CHAPTER 1: INTRODUCTION

1. Sunlight and skin cancer

1.1 The spectrum of sunlight and penetration through skin

The sun provides us with a vital source of energy for human life in the form of light. Sunlight is crucial to photosynthesis, the process performed by plants to convert light energy into chemical energy that fuels cellular activity. Sunlight is composed of infrared, visible and ultraviolet (UV) electromagnetic radiation in the range of 100 nm - 1 mm. UV radiation (UVR) from the sun compromises the 100-400 nm portion, which is further divided into UVC (100-280 nm), UVB (280-320 nm), UVA2 (320-340 nm) and UVA1 (340-400 nm).[1] UVC is absorbed by the ozone layer and therefore human exposure is unlikely, whereas UVB is also substantially absorbed, though not completely, by the ozone layer. However, ozone is transparent to UVA and therefore the UVR that reaches the Earth's surface is up to 95% UVA.[2,3] A wide range of applications of UVR in healthcare and medicine have been identified since the discovery of UVR by Johann Wilhelm Ritter in 1801. In the late 18th century, the cytotoxic effect of UVC irradiation on bacteria was discovered, and hence the possibility of using short wavelength UVR in the sterilization of food was realised.[1] In 1903, UVR was used along with X-ray radiation to treat the facial swellings of patients with *Lupus* (a chronic inflammatory disease),[4] and following this in 1927 the First International Conference on Light and Heat in London included abstracts on the application of UVR for curing a range of 'human ills' with the suggestion being made that 'man was on the threshold of something that would be of great advantage'.[5]

Human skin is the interface between a person and their environment, and as such it is exposed to UVR very regularly. Factors that increase the amount of UVR an individual's uncovered skin is exposed to include: spending time outdoors during the summer months, being at a high altitude, living close to the equator and the amount of ozone in the atmosphere.[6] Human skin is separated into two main sections: the epidermis and the dermis. The epidermis is the outer cellular layer and has an depth of 50-150 μm. 95% of the cells in the epidermis are

keratinocytes, with the remainder being melanocytes and Langerhans cells.[7] Keratinocytes are derived from the basal layer (*stratum basale*) of the epidermis which sits on the basement membrane, next to the dermis (shown in Figure 1). Keratinocytes from the *stratum basale* will differentiate and then migrate, whilst maturing, to the surface of the skin (*stratum corneum*) through a series of defined layers (described in Figure 1), this process takes approximately one month in humans. The *stratum corneum* has between 10-20 layers of dead keratinocytes (corneocytes) with a thickness of approximately 10 μm. Over the course of their differentiation from the *stratum basale* to the *stratum corneum*, keratinocytes build up proteins such that they become surrounded by a cornified envelope. At this stage the keratinocytes are termed corneocytes, and their cornified envelope consists of involucrin cross-linked with insoluble keratin which acts as a very important physical barrier for the body against pathogenic invasion, heat and water loss and to defend against UVR.[8] Turnover of the epidermis is tightly controlled so that corneocyte loss (desquamation) and keratinocyte division are at equilibrium.[9]

Underneath the epidermis sits the mainly non-cellular dermis, which is 3-5 mm thick and contains fibroblasts and mast cells surrounded by an extracellular matrix of collagen and elastin fibres. In the uppermost layer of the dermis (the papillary layer), capillary loops are connected to small veins which then travel down through the lower dermis (reticular layer) to connect with cutaneous veins.[7]

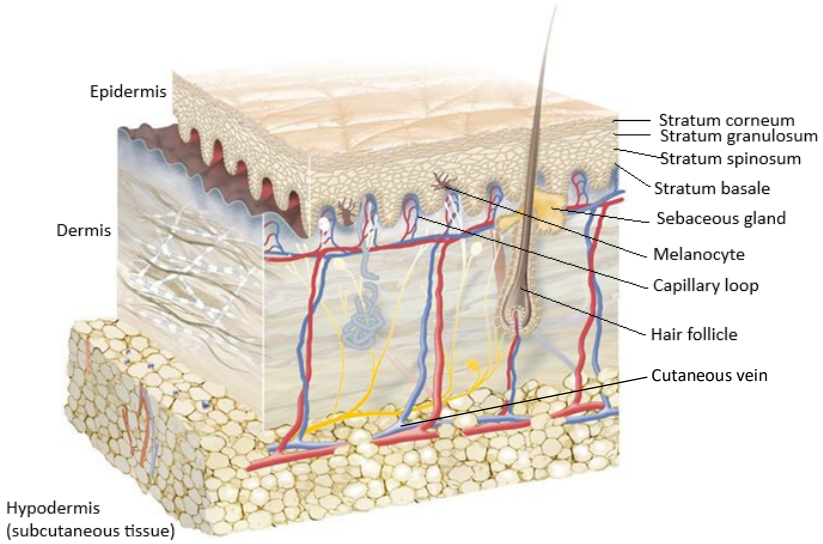

Figure 1. Structure of the human skin (adapted from www.eucerin.co.uk/about-skin/basic-skin-knowledge/skin-structure-and-function).[10] The epidermal layer consists of keratinocytes differentiating and maturing upwards from the lowest level the *stratum basale*, through the *stratum spinosum* and the *stratum granulosum* before reaching the outermost skin surface, the *stratum corneum*.[3] The dermal layer sits underneath the epidermis and consists mainly of fibrous materials (collagen and elastin) and vasculature along with fibroblast cells.[9]

The constituent molecules in the skin contain a range of chromophores, which are the parts of a molecule responsible for its colour *via* the absorption of radiation, often through a conjugated system. Each chromophore has a characteristic absorption spectrum and as such the extent of absorption of a specific wavelength of radiation by the skin is dependent on the endogenous chromophores present, for example urocanic acid, DNA and proteins containing tyrosine or tryptophan.[9] These chromophores all have maximal absorbance primarily in the UVC-UVB range (260-320 nm) with minimal UVA absorbance, see Table 1.

Table 1. Examples of endogenous epidermal chromophores and their maximal absorbance wavelengths.[9]

Chromophore	Structure	Maximal absorbance wavelength (nm)
Urocanic acid	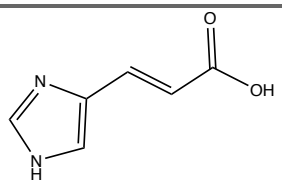	268-280
Tyrosine	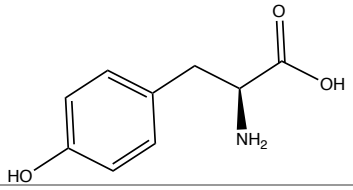	275
Tryptophan	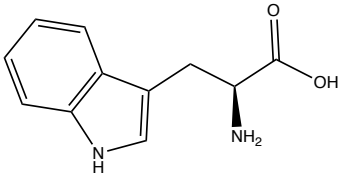	280
DNA bases	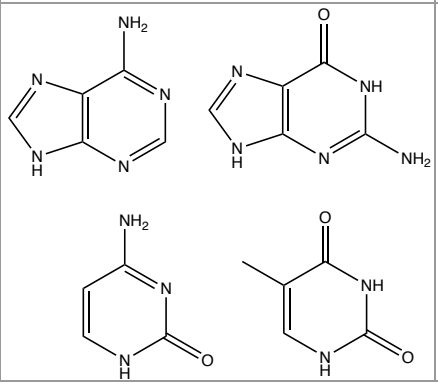	260

As long wavelength UVA is not absorbed by the majority of epidermal chromophores, it is able to penetrate further into the skin and reach the dermal layer.[3] It is estimated that up to 50% of UVA can reach melanocytes on the basal membrane compared to only around 14% of UVB.[11] Longer wavelength UVA can also penetrate through unprotected car and office windows.[11] A computational study was carried out by Ash *et al.* to analyse the tissue penetration of different wavelengths of light, confirming that UVA penetrates further into the skin than UVB (approximately 500 µm to 1000 µm for UVB and UVA respectively, Figure 2).[12]

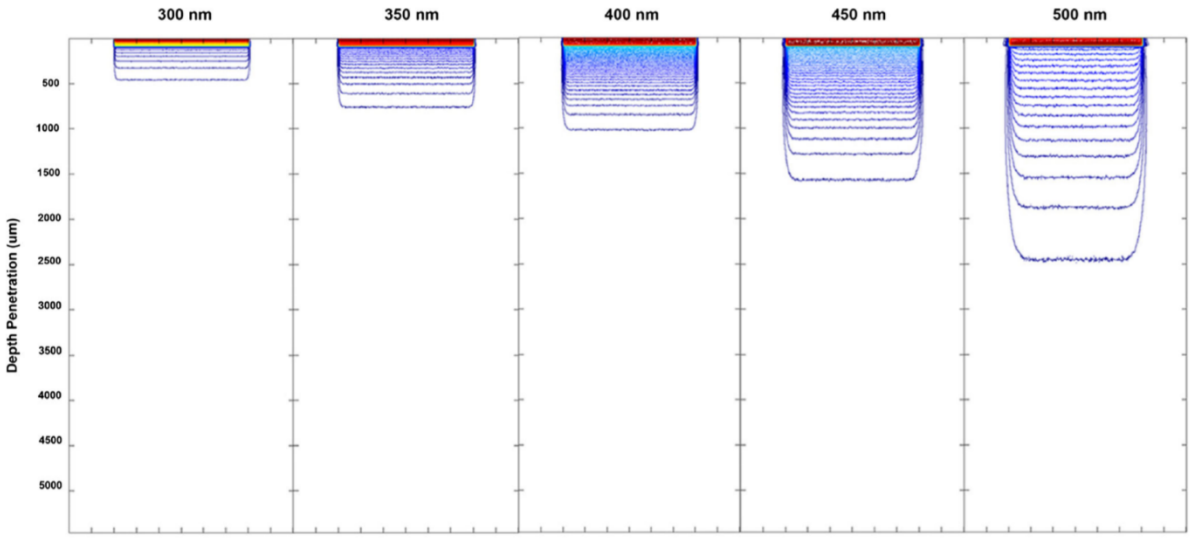

Figure 2. Depth penetration of 300-500 nm wavelengths of light into computational tissue matrix from Ash *et al.*[12] The tissue matrix was modelled as an 80 μm thick epidermis with a 5% melanin concentration and a melanin-free dermis. The model was calibrated against thermography measurements of Caucasian, Indian and Afro Caribbean skin tones exposed to a range (2-20 J/cm^2) of intense pulsed light (IPL). The simulated photon distribution was subsequently calculated using the Monte Carlo process.[12]

1.2 Types of skin cancer

Overexposure to UVR is known as the major risk factor associated with skin cancer[13] as well as promoting skin ageing, wrinkling and pigmentation and immune system suppression. Skin cancers can be classified into two groups known as non-melanoma skin cancer (NMSC) and malignant melanoma, with the classification being based on the cell type where the tumour originates. NMSCs are derived from keratinocytes and as such may also be termed keratinocyte cancers (KCs). NMSCs are sub-divided into basal cell carcinoma (BCC) and squamous cell carcinoma (SCC). NMSC is the most common skin cancer, with the worldwide incidence being 18-20 times higher than for malignant melanoma.[14] A systematic review by Lomas *et al.* in 2012 revealed that the incidence of NMSC has been increasing worldwide over the past 50 years.[15] Of the NMSC category of skin cancers approximately 20-30% are SCC and 70-80% are BCC.[14] More than 80% of NMSC are found on areas of the body susceptible to life-long cumulative sun-exposure such as ears, nose, cheeks and the top of hands.[14] Typically NMSC has a good prognosis as the metastatic capacity of these cancers is low compared to

melanoma skin cancer. Thus although the incidence of NMSC is far higher, the mortality rate is lower.[16]

Malignant melanoma are tumours that originate from the melanocytes, which are found at the basement membrane of the epidermis and produce the skin pigment melanin. Although this form of cancer is the least common, it is responsible for approximately 80% of skin cancer-related deaths due to its high propensity to metastasise.[16] The prognosis for metastatic melanoma is between 12-28% survival after 5 years.[17]

Figure 3 shows the number of deaths from malignant melanoma in England over a 25 year period from 1985 to 2010, divided into age groups. It indicates that the number of deaths for under 44-year-olds is reasonably stable, while deaths in the 45-64 year old group increased until the year 2000 but have since stabilised. However, the number of deaths in people above the age of 65 has increased rapidly since 1985 and shows no sign of diminishing. This may simply be due to increased life expectancy [18] and therefore the accumulation of many more years of sun exposure. Travel abroad to hot countries has also become increasingly easy and cheap, and sun-filled holidays are now much more common, exposing unconditioned skin to high UVR intensities.[19] The introduction of UVR tanning beds and the desire to have a tanned skin complexion may be another factor that could contribute to the increasing number of deaths.[3]

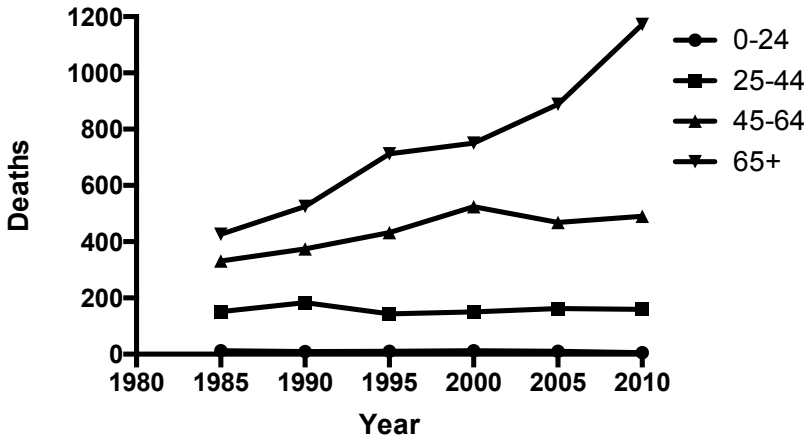

Figure 3. Graph showing the number of deaths from malignant melanoma in England over a 25 year period, divided into four age groups. Data from the Office for National Statistics, UK.[20]

The role of the melanocyte pigment melanin with respect to UVR-protection is currently not very well understood,[21] and more knowledge is required to help interpret this interaction in terms of the transformation to malignant cells. Melanin exists in two different forms, pheomelanin and eumelanin. The relative proportions of these melanins, along with the way that they are packaged and distributed in melanosomes determines the colour of the skin.[21] Melanosomes are organelles specific to melanocytes where melanin is biosynthesized (melanogenesis). Melanin is then distributed to adjacent keratinocytes through dendritic projections, where it subsequently accumulates.[21] Melanin is thought to shield DNA from UVR by scattering it, however the specific chromophore and thus absorption spectrum of natural melanin has not been identified due to its insolubility.[9] Tyrosine is the fundamental structural unit of melanins, and the first step of melanogenesis is the conversion of tyrosine to dopaquinone *via* oxidation by the enzyme tyrosinase.[22] In the absence of cysteine, dopaquinone forms 5,6-dihydroxyindole (DHI), 5,6-dihydroxyindole-2-carboxylic acid (DHICA) and their oxidised forms which are polymerized to give eumelanin. In the presence of cysteine, dopaquinone is oxidised to benzothiazine intermediates which are polymerized to pheomelanin.[22] The macromolecules are highly conjugated and cross linked through heteroaromatic units *via* C-C bonds, making them non-hydrolysable.[22,23] The type and amount of melanin produced by melanocytes is mainly influenced by the individual's genetics as well as a range of factors such as hormonal changes, inflammation, age and exposure to UVR.[24] It has been suggested that UVR-induced photodamage and the subsequent repair process induces melanogenesis and therefore increases tanning.[24] Due to this, melanin has been termed an endogenous 'sunscreen' with a sun protection factor (SPF, see Section 2.1) of approximately 3-5.[25] There is an inverse relationship between the amount of skin pigmentation and the incidence of melanoma cancer.[25]

1.3 Mechanisms of UVB damage

The damaging effects of UVB radiation are initiated through the direct absorption of UVB by consituents of the skin.[26] UVB radiation is associated with the painful experience of sunburn through an inflammatory response induced by over-exposure to the sun. Inflammatory mediators such as interleukin-1, IL-6, IL-8 and IL-10, as well as tumour necrosis factor-α, are produced in keratinocytes upon UVB radiation.[27] The absorption spectrum of DNA overlaps

mainly with the UVC radiation wavelength range, however a significant portion lies in the UVB range.[9] Therefore in the context of sunlight reaching the human skin, most UVB radiation will be absorbed by epidermal DNA. The predominant feature of UVB-induced skin damage is the formation of two types of DNA-damage photoproducts between adjacent pyrimidine bases: cyclobutane pyrimidine dimer (CPD) and pyrimidine 6-4 pyrimidone (6-4PP), shown in Scheme 1.

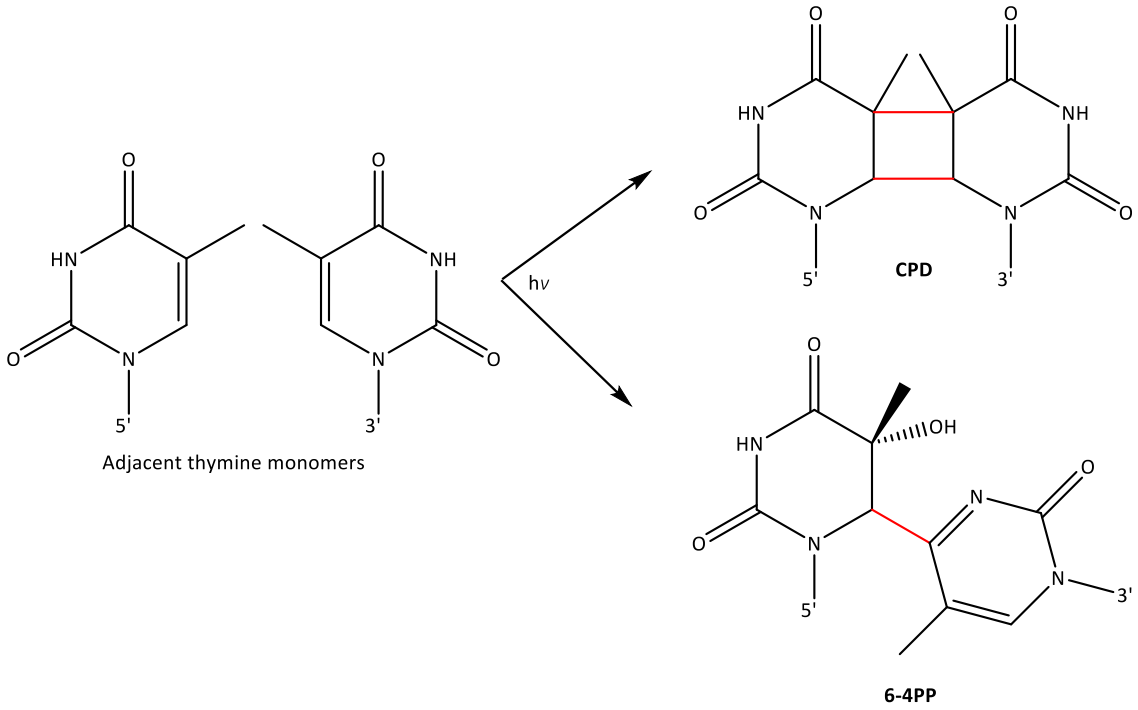

Scheme 1. The formation of the two DNA photoproducts; cyclobutane pyrimidine dimer (CPD) and pyrimidine 6-4 pyrimidone (6-4PP) upon UVB absorption by two adjacent thymine bases.

CPDs are observed at a 5-10-fold higher frequency than 6-4PP.[28] These lesions in DNA can lead to the transition of C to T and CC to TT. Such mutations have been found to be the most frequent (50-90%) in *p53* (tumour suppressor gene).[28] Post-UVR exposure, there is normally a transcriptional activation of *p53* leading to the induction of high levels of the p53 protein in cells.[29] The p53 protein triggers cell cycle arrest (G1 and G2) which allows the repair of DNA lesions prior to DNA synthesis and mitosis. It also initiates apoptosis, therefore DNA-damaged cells are either usually repaired or eliminated by the increased expression of this protein.[29] Ananthaswamy *et al.* demonstrated that mutations in *p*53 were first detectable 6 weeks after cumulative irradiation of mouse skin with UVB.[30] In their *in vivo* progression model for UVB-induced skin carcinogenesis, Tyagi *et al.* demonstrated that after repetitive exposure of HaCaT

(immortalized human epidermal keratinocytes) cells to UVB radiation, they exhibited an enhanced proliferation rate, apoptotic resistance and colony and sphere-forming abilities. Furthermore, inoculation of these cells into mice led to the formation of aggressive SCC.[31] Thus UVB induced formation of CPD and 6-4PP photolesions leads to mutations in the *p53* gene and a reduction in the expression of the p53 protein which subsequently initiates skin carcinogenesis.

Lesions cause torsional strain of the DNA double helix and under normal circumstances mutagenic photodimers such as CDPs and 6-4PPs are often removed by nucleotide excision repair (NER), a repair pathway for regions of DNA damage up to 30 bases in length.[32] However when exposed to high-dose UVB, the NER process can become saturated and lead to an accumulation of mutations.[32] Differences in the expression of repair genes may also account for varying levels of unrepaired damage between individuals.[32] Inherited genetic diseases such as xeroderma pigmentosum (XP), Cockayne syndrome (CS) and trichothiodystrophy (TTD) are all caused by mutations to genes which encode for critical NER proteins. XP patients have a >10,000-fold increased risk of skin cancer in exposed parts of the body in comparison to a healthy individual.[33]

UVR from the sun is only 5-10% UVB with the remaining 90-95% being UVA.[3] With this in mind, the ability of UVB radiation to behave as a strong carcinogen is quite surprising, one would expect UVA radiation to be approximately 9 times more dangerous. However the action spectrum (a plot of wavelength against the dose required for a given biological outcome) of UVB shows that it is approximately 1000 times more effective at developing erythema than UVA per unit dose (kJ/cm^2).[34] The relative erythemogenic weighting of UVB radiation is due to its action as a 'direct' carcinogen. Skin constituents directly absorb the lower wavelength but higher frequency energy, as described above, which makes UVB radiation a significant carcinogen. This is worsened in areas with low ozone as a higher percentage of UVB radiation will reach the surface of the Earth.[35] Conversely UVA radiation is termed an 'indirect' carcinogen despite being responsible for a larger portion of the total UVR from the sun. The mechanisms of action of UVA radiation damage are described in the following section.

1.4 Mechanisms of UVA damage

Whereas the mechanisms of UVB-induced skin damage have been long studied, UVA-induced damage has received less attention as it was not considered a direct DNA damaging agent.[11,36] There is now substantial evidence to support the claim that UVA plays a significant role in the pathogenesis of skin cancers. UVA-damage results from the reactivity of endogenous (porphyrins, riboflavin, melanin) and exogenous (thiopurine drugs, fluoroquinolone antibiotics) photosensitizers which generate ROS, for example singlet oxygen, hydrogen peroxide, superoxide anion. These ROS lead to serious oxidative stress causing DNA single strand breakage, nuclear base damage, protein, membrane and organelle damage.[11] Peak *et al.* showed that there was a >20-fold higher number of DNA single strand breaks in human teratocarcinoma cells that were irradiated with monochromatic UVA at 365 nm in comparison to UVB at 313 nm, with 9000 lesions/cell and 430 lesions/cell respectively.[37] Following this, it was found that DNA single-stranded breaks found in melanocytes after UVA exposure were most likely initiated by a photosensitizing reaction with pheomelanin.[38] 40 times more DNA single-stranded breaks were observed in melanocytes in dark skin compared to melanocytes in light skin.[39] This evidence suggests that the oxidative nature of UVA may play a crucial role in the positive progression of melanoma skin cancer.

The monomeric lesion 7,8-dihydro-8-oxoguanine (8-oxoG) is a frequently observed oxidatively damaged DNA guanine base and is classed as a pre-mutagenic photoproduct[40] (see Scheme 2). Analysis of the effect of monochromatic radiation ranging from UVB (312 nm) to visible light (434 nm) on human skin fibroblasts demonstrated that UVA radiation above 334 nm was responsible for almost all of the yield of 8-oxoG.[40] It was estimated that the total amount of 8-oxoG formed by sunlight exposure would be equal to or exceed the amount of direct DNA damage and CPD formation.[40] In relation to this it has also been determined that the level of 8-oxoG formation induced by UVA irradiation in melanocytes is 2-fold higher than in keratinocytes.[41]

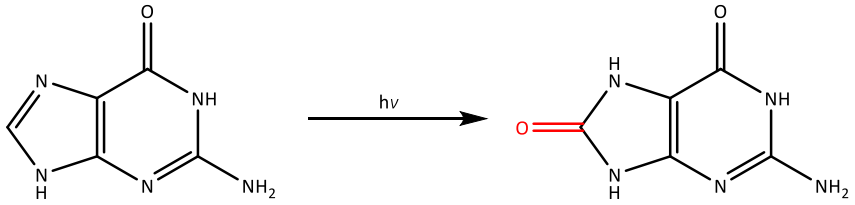

8-oxoG

Scheme 2. The monomeric photolesion 7,8-dihydro-8-oxoguanine (8-oxoG) formed through UVA-induced oxidation of a guanine DNA base.

Mouret *et al.* demonstrated in 2006 that CPDs, typically a hallmark of UVB-induced damage, were significantly produced in whole human skin exposed to UVA. Furthermore, a recent *in vivo* study by Tewari *et al.* showed a significant increase in CPD with increasing skin depth after irradiation with UVA.[42] The mechanism for this occurrence is unknown, and it was also shown by Mouret *et al.* that the rate of removal of UVA-induced CPDs was slower than that of UVB-induced CPDs.[43] This suggests that the repair of CPDs is compromised by the longer wavelength UVA. Consistent with this is the knowledge that UVA radiation can cause extensive protein unfolding and aggregation, leading to changes in cellular signalling and homeostasis.[44] Tryptophan, tyrosine, phenylalanine, methionine and histidine side chains have all been shown to be susceptible to photo-oxidation.[44] There is also evidence that direct absorption of UVR by disulphide bonds between two cysteine residues causes homolytic cleavage of the bond to form two thiyl radicals ($RS^{\cdot}$).[44] The CPD repair NER proteins are a possible oxidation target and therefore UVA radiation could compromise the DNA repair in cells *via* inhibition of the activity of NERs, subsequently prolonging the repair process. Other DNA repair proteins known to be targets for UVA-induced oxidation include PARP-1, APE-1 and XPE.[45]

Oxidative stress of cells is usually managed by endogenous antioxidant defences working in unison, for example the enzymes superoxide dismutase (SOD), catalase and glutathione peroxidases (GPx).[46] SOD catalyses the conversion of the superoxide anion (O_2^{-}) into oxygen and hydrogen peroxide (H_2O_2). H_2O_2 can then be converted to water and oxygen by catalase[46]:

$$2HO_2 \rightarrow O_2 + H_2O_2$$

$$2H_2O_2 \rightarrow O_2 + 2H_2O$$

GPx catalyses the conversion of H_2O_2 to water through the transformation of glutathione (GSH) to glutathione disulphide (GS-SG)[47]:

$$2GSH + H_2O_2 \rightarrow GS\text{-}SG + 2H_2O$$

GSH can also neutralise lipid peroxides, and the GS-SG formed can be reduced back to GSH through the action of glutathione reductase.[47] The excessive ROS that are generated intracellularly through UVA-radiation affect the oxidative homeostasis of cells, overcoming the neutralising of ROS by enzymes.[48] The negative balance of ROS is also aided by UVA irradiation significantly decreasing the activity of catalase and SOD in human keratinocytes.[49] This was demonstrated by Hoerter *et al.*, who assessed the impact of UVA radiation in the presence of an incompletely functioning antioxidant enzyme system using a mutant strain of *E.coli* lacking SOD. A 9-fold increase in mutagenesis occurred when the mutant bacterial strain was UVA-irradiated in comparison to the wild-type.[50]

Iron is a redox-active transition metal and therefore can cycle between its two principal oxidation states, Fe^{3+} and Fe^{2+}. Ferrous iron (Fe^{2+}) is well known as being capable of catalysing redox reactions *in vitro*,[51] and in the presence of hydrogen peroxide, ferrous iron can catalyse the formation of the hydroxyl radical through Fenton chemistry:

$$Fe^{2+} + H_2O_2 \rightarrow OH^{\cdot} + OH^{-} + Fe^{3+}$$

Excessive intracellular ROS generated by UVA-irradiation via this pathway can be exacerbated through iron-catalysed lipid peroxidation of membranes in human primary fibroblasts and keratinocytes, with the formation of harmful alkoxyl and peroxyl radicals.[52] There is an accessible intracellular pool of metabolically and catalytically active 'free' iron, termed the labile iron pool (LIP) which is thought to be bound to low molecular weight ligands (glutathione, citrate[53], phosphate).[54] Iron that is not metabolically required is stored in the

iron storage protein ferritin (Ft) with up to 4,500 atoms of ferric (Fe^{3+}) iron being stored and protected from reduction in a single protein molecule.[55] The LIP is monitored by the cytosolic iron regulatory proteins 1 and 2 (IRPs) which regulate the uptake and distribution of iron throughout cells. Increased iron supply will inactivate IRP-1 and degrade IRP-2 leading to synthesis of Ft. Pourzand *et al.* showed that upon UVA irradiation of human skin fibroblasts (FEK4 cells) there was an immediate loss of activity in IRP-1 binding which returned after 6 h.[56] At higher doses of UVA radiation the reduction was present 24 h post irradiation. This result correlated with a dose-dependent decrease in Ft levels, which suggests that there is a release of free iron due to degradation of Ft upon UVA radiation.[56] This phenomenon was reversed by the addition of the protease inhibitor chymostatin, which is known to specifically block the activity of lysosomal chymotrypsin. This indicated that the release of free iron from Ft was *via* proteolysis by lysosomal proteases.[56] The stability of lysosomal membranes after UVA-irradiation was assessed using a fluorescent probe. The result demonstrated the loss of integrity of the lysosomal membrane and subsequently the leakage of lysosomal contents into the cytosol.[56] Figure 4 outlines the molecular mechanisms described above.

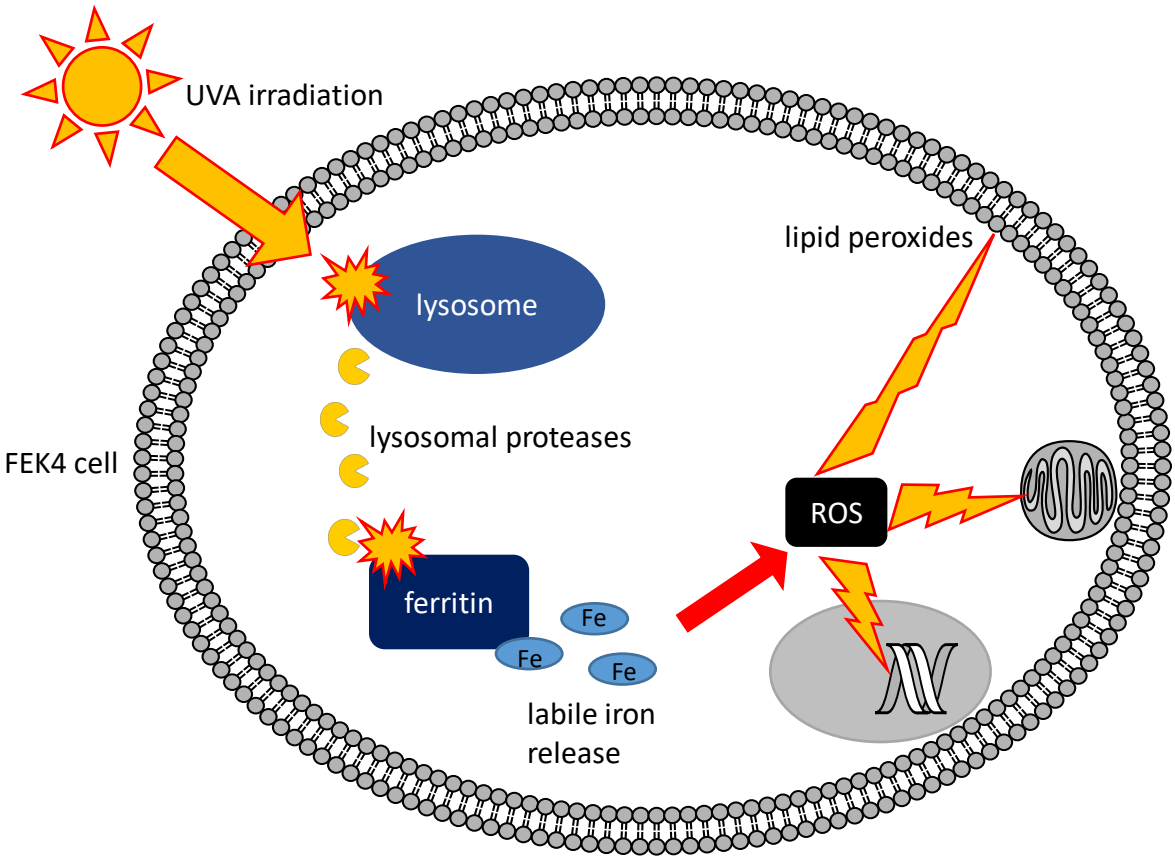

Figure 4. Representation of UVA-induced oxidative stress and labile iron release in a human skin FEK4 cell. UVA irradiation destabilises the membrane integrity of lysosomes, releasing lysosomal proteases such as chymotrypsin. These proteases degrade ferritin which releases labile iron into the cytosol. Redox active iron can contribute to the generation of ROS, damaging membranes, mitochondria and DNA.[57]

2. Photoprotection

2.1 The use of sunscreens

The detrimental effects of over-exposure to UVA and UVB have been already been described in Section 1.3 and 1.4. Protection from these damaging wavelengths is crucial in order to prevent skin cancer and photoaging. Protection methods such as wearing long-sleeved clothing and hats and staying in the shade between the hours of 12-3pm, when the intensity of UVB is highest, are the best ways to stay safe in the sun.[36] The major breakthrough of sunscreen technology has enabled people to feel protected whilst spending time outdoors,

however there are gaps in consumer understanding about the proper use of sunscreens which may result in incomplete sun protection for the user.[36]

Up until the 1930s a pale complexion was fashionable in America and Europe as it was considered to indicate wealth and status, and as a result there were many cases of lead poisoning through the white lead used to whiten faces and necks.[58] The fashion for a tanned, 'healthy' complexion has risen through the 19th century, opening up the sun care market for cosmetic companies. Through the lack of research into the harmful effects of UVR during these times, people were subject to high levels of exposure. Certain products on the market provided a damage-inducing effect rather than being protective, such as the photosensitizing product Sun-bi-Sun.[59] One of the most common reasons for using sunscreens is to prevent the painful sunburn experience, and for this reason the first sunscreens invented were biased towards UVB protection and did not contain any UVA protection, therefore the user was lulled into a false sense of security in terms of skin cancer prevention. This may have increased the incidence of skin cancers including melanoma as people felt they could spend more time outdoors and not be sunburned, but were subject to high doses of UVA radiation.[11,36]

As early as 1985, Diffey *et al.* highlighted the need to include protection against UVA when this was still not a general consideration.[60] Once the role of UVA in photocarcinogenesis and ageing was better understood, a change to sunscreen formulation was brought about which introduced 'broad spectrum' UVA/UVB protection.[36] In a study by Young *et al* the use of a daily-care broad spectrum sunscreen was shown to inhibit most of the damage caused by daily sub-erythemal (sunburn) exposure.[61] The SPF of a sunscreen relates to the relative protection that a product provides against UVB radiation. It is calculated using the ratio of UVR doses required to trigger erythema on human skin with and without the sunscreen formulation, the dose required is termed the minimal erythema dose (MED). The testing is performed using solar-simulated radiation (SSR); a lamp which emits the specified percentages of UVA and UVB radiation to act as a 'solar mimic'.[34] There is a true relationship between the factorial difference in SPF values and the protection afforded by the sunscreens. For example, an SPF 15 sunscreen applied correctly absorbs 93.3% of erythemogenic UVB rays, whereas an SPF 30 sunscreen absorbs 96.7%. Therefore the amount of UVB rays

transmitted through the skin using an SPF 15 sunscreen (6.7%) is double that of the SPF 30 sunscreen (3.3%), relating to half the protection (shown in Figure 5).[62]

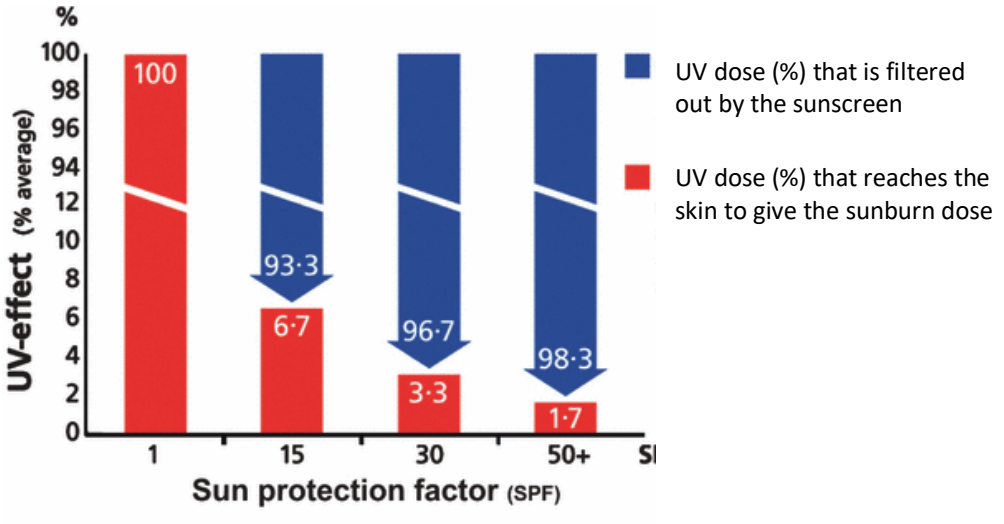

Figure 5. Graph from Osterwalder *et al.* showing the absorbance and transmittance of UVB irradiation through sunscreens of varying SPF.[62]

The UVA protection (PF-UVA) is analysed by either an *in vivo* method based on UVA-induced persistent pigment darkening (PPD) or an *in vitro* method based on UVA transmittance through a film of the formulation. Sunscreens are now tightly regulated in the EU and the UK so that the SPF/PF-UVA ratio must be less than or equal to 3, *i.e* a SPF 30 sunscreen must have a PF-UVA of at least 10 to pass, and the sunscreen must be clearly labelled with the outcome.[36] However as the biological outcomes of UVA and UVB damage are very different, the question should be asked as to whether there is a better way of testing UVA protection that involves the direct biological endpoint of UVA, namely ROS. One such test is the radical sun protection factor (RSF) which is a ratio of the detected amount of radicals generated in unprotected skin compared to protected skin using electron spin resonance (ESR). A significant correlation has been found between PF-UVA and RSF values for a range of sunscreen formulations, therefore this may be a more appropriate test for the UVA protection afforded by sunscreens.[63,64]

Consumer compliance is a huge factor in the misuse of sunscreens, along with a lack of understanding of proper use of sunscreens. There are many reasons why people use sunscreens sparingly or not at all, such as: it takes too much time to apply, it is greasy, it is expensive, it prevents a tan, they have skin that 'does not burn easily,' or they have a

'protective tan'.[65] These reasons include many that are relevant to the formulation of the sunscreen and therefore it is in the hands of cosmetic companies to make more user- friendly sunscreens. Public health education is also paramount to increasing compliance in sunscreen use to prevent skin cancers,[66,67] indeed in a study by Ghiasvand *et al.* the general use of a SPF >15 sunscreen was estimated to reduce the incidence of melanoma by 18%.[68] Poor compliance leads to the incorrect use of sunscreens, for example applying the formulation unevenly or not rubbing it in, not reapplying after water immersion or towelling, and not applying the recommended amount of sunscreen (2 mg/cm^2).[65] When the SPF of a product is determined, 2 mg/cm^2 of formulation is used in the testing procedure, therefore using less than 2 mg/cm^2 will significantly lower the SPF (and subsequently PF-UVA) protection provided by the sunscreen. There are many human sunscreen studies which indicate that typically people apply much less than the recommended amount of sunscreen, with amounts varying between 0.5 and 1.5 mg/cm^2.[69-71] This is worsened especially when using 'physical' sunscreens containing TiO_2 or ZnO, as these tend to leave a white film on the skin. It is postulated that most sunscreen users achieve a protection between 20-50% of the labelled SPF value, as there is a logarithmic relationship between application thickness and SPF value.[71] This again raises the question of a need to change the SPF testing method.

Solar UVB radiation is a critical environmental trigger for the biosynthesis of vitamin D, with all other vitamin D sources being through the diet. Along with calcium, vitamin D is essential for healthy bones especially in growing children. There are concerns over the inhibition of vitamin D biosynthesis whilst using sunscreen formulations.[62] A human study using 32 healthy children indicated that a low daily dose of UVR gave a modest but significant improvement in 25-hydroxyvitamin D_3 (a widely used serum marker for vitamin D status) of 24%, however there was a 1162% increase in the level of skin CPDs generated.[72] If there are changes made to the SPF testing method along with increased public health campaigns to apply more sunscreen, it is feasible that vitamin D biosynthesis from UVB could be compromised.[73] However a recent study by Young *et al.* into the impact of sunscreen on vitamin D status showed that the application of two sunscreens during a week long holiday in Tenerife prevented sunburn whilst there was also a significant increase in the level of 25-hydroxyvitamin D_3 across the cohort, thus providing evidence that sunscreen application does not prevent vitamin D biosynthesis.[74] A daily 15 min exposure to sunlight is adequate to

provide an individual's vitamin D requirements from spring until autumn, however in winter there is insufficient UVB to synthesise vitamin D.[2] For these reasons it is essential that the vitamin D requirements of the human body are sufficiently supplemented through the diet, as would be the case throughout the winter months.

2.2 Types of UVR filters, their efficiency and new developments

The UVR filters used in sunscreen can be categorized as either organic or inorganic. The two approved inorganic UVR filters are titanium dioxide (TiO_2) and zinc oxide (ZnO) which are classed as broad spectrum filters that form a physical barrier to scatter, absorb and reflect UVR.[75] The main drawback of these filters is the white film that the particulates leave behind on the skin[65], and because of this the use of ZnO and TiO_2 in sunscreens is mostly in the nanoparticle form. The ZnO and TiO_2 nanoparticles are typically spheroidal and have average diameters of 18.2 nm and 21.5 nm respectively.[76] There is some concern over the safety of the long term use of nanoparticles due to the possibility of penetration through the skin and systemic absorption.[77] In a study by Osmond-McLeod *et al.* sunscreen formulations containing ZnO or TiO_2 nanoparticles were applied topically once a week to hairless mice.[76] The ZnO formulation did not cause any significant increase in the level of Zn in serum and internal organ tissue, however the TiO_2 formulation caused a very small increase in liver Ti although this was not deemed an adverse biological outcome.[76]

There are approximately 55 organic filters that are approved in different countries worldwide and of that number only 9 are approved for use by regulatory bodies globally due to clinical efficacy and side effect concerns. The properties of these approved filters are outlined in Table 2.[34,36,75]

Table 2. Comparison of UVR filters globally approved for use in sunscreen formulations.

Name (common name)	Structure	Class	UVR absorbing region, absorbance maximum (nm)
Benzophenone-3 (oxybenzone)	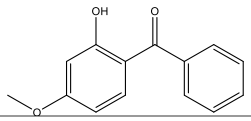	Benzophenones	UVB/UVA2, 286 and 324
Butyl methoxydibenzoyl methane (avobenzone)	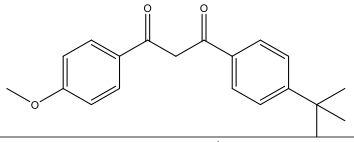	Dibenzoyl methanes	UVA1/2, 357
Ethylhexyl dimethyl PABA (padimate O)	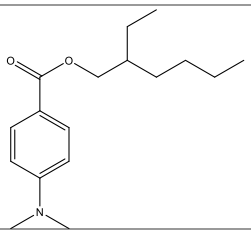	*para*-amino benzoates	UVB, 311
Ethylhexylmethoxy cinnamate (octinoxate)	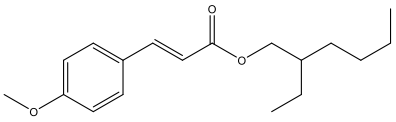	Cinnamates	UVB, 311
2-Ethylhexyl salicylate (octisalate)	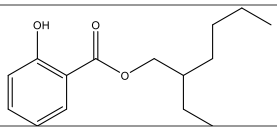	Salicylates	UVB, 305
Homomenthyl salicylate (homosalate)	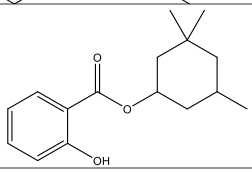	Salicylates	UVB, 306
Octocrylene	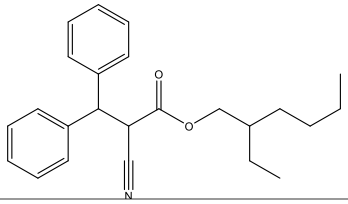	-	UVB, 303
4-aminobenzoic acid (PABA)	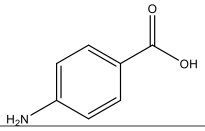	*para*-Amino benzoates	UVB, 283
Phenyl benzimidazole sulfonic acid (ensulizole)	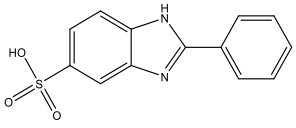	-	UVB, 302

The ability of UVR filter structures to delocalise electrons determines their maximum wavelength of absorption, and therefore the UVR region in which they absorb.[75] The PABA moiety was one of the first UVR filters to be developed. It contains an electron-donating group (NR_2) *para* to an electron-withdrawing group (CO_2R) which provides an efficient route for electron delocalization, (see Table 2).[75] However, PABA filters in sunscreens are a common cause of allergy and have also been shown to have relatively high percutaneous absorption (1.6-9.6% recovered in the urine 48 h after topical application), therefore they are rarely used in modern sunscreen formulations.[77] The structure of the salicylate group of UVR filters (seen in octisalate and homosalate, Table 2) allows electron delocalization as well as the possibility of internal hydrogen bonding through the *ortho* hydroxyl substituent.[75] This additional internal interaction lowers the HOMO-LUMO energy gap of the salicylates in comparison to PABA, and therefore increases the absorption maximum of the molecules (there is an inverse relationship between the energy of an electronic transition of a compound and the wavelength of UVR absorbance it exhibits).[75] Cinnamates (see octinoxate, Table 2) have a similar basic structure to PABA, in which the aromatic ring is 1,4-disubstituted with an electron-donating and electron-withdrawing group, however there is an extra double bond leading to additional conjugation and electron delocalization in the molecule, further increasing the UVR wavelength of absorption.[75] These filters are subject to *E*/*Z* photo-isomerisation (shown in Scheme 3) which reduces the efficiency of their UVR absorption due to the *Z* isomer being poorer at absorbing UVR. For example the molar absorption coefficients of the E and Z isomers of octinoxate are 19,500 $dm^3\ mol^{-1}\ cm^{-1}$ and 10,000 $dm^3\ mol^{-1}\ cm^{-1}$ respectively.[75]

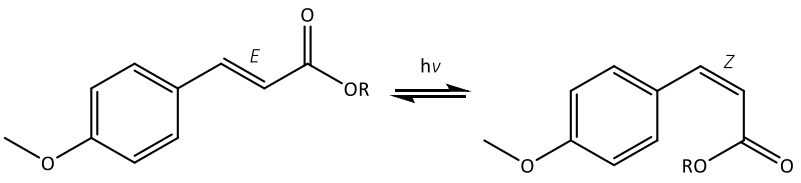

Scheme 3. Photo-isomerisation of a cinnamate UVR filter from the *E* to the *Z* isomer, which is a poorer UVR absorber.

Benzophenone derivatives have an electron-donating group in either or both of the *ortho* and *para* positions (see oxybenzone, Table 2) to increase electron delocalization, along with the possibility of an intramolecular hydrogen bond.[75] This results in the filters exhibiting two absorption maxima: 286 nm (UVB) and 324 nm (UVA2). Oxybenzone is one of the most bioavailable photoactive compounds after cutaneous application and as such its use has declined.[77] Dibenzoyl methane filters, for example avobenzone, have the lowest energy requirements of the original classes of UVR filters and therefore mainly absorb in the UVA region. This is due to their ability to undergo keto-enol tautomerism, which provides a conjugated structure that is stabilised by intramolecular hydrogen bonding, shown in Scheme 4.[75]

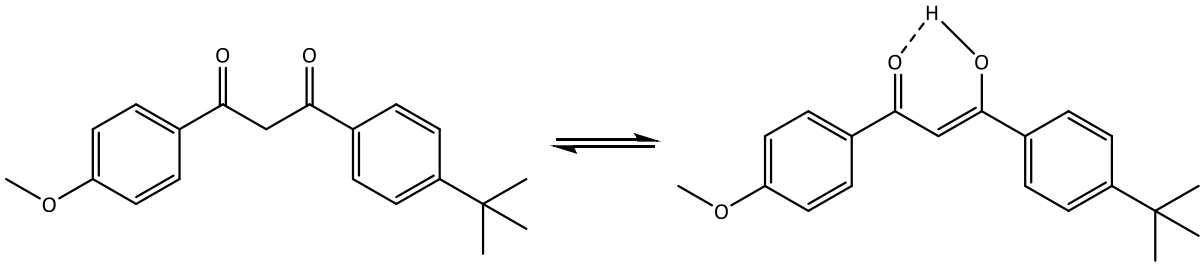

Scheme 4. The keto-enol tautomerism of avobenzone gives the UVR filter a wavelength of absorption in the UVA1/2 region.

Avobenzone is the most widely used UVA filter in sunscreens and as shown in Table 2, it is the only UVA1/2 filter to be approved for use by regulatory bodies worldwide. It has been suggested that avobenzone has poor photostability. The keto and enol forms of avobenzone are in equilibrium in solution and the equilibrium always lies in the direction of the enol tautomer, however upon UVA irradiation at 357 nm the enol form is converted to the keto form[78] (see Scheme 4). The keto form absorbs in the UVC range from 260-280 nm which therefore renders the photoprotective properties of the sunscreen inadequate.[78] Photodegradation of avobenzone also occurs through α-cleavage of the keto form to give benzoyl or phenacyl radicals.[78] Avobenzone can be stabilized by octocrylene and therefore they are often formulated together in sunscreens.[79,80] The requirement for more stable and non-toxic UVA filters is high, and one possible option is a camphor derivative, terephthalylidene dicamphor sulfonic acid (shown in Figure 6). This filter is patented by L'Oréal under the name Mexoryl SX (ecamsule)[81] and it has been approved for use globally

as a UVA filter, except in the USA. The camphor family of filters generally have high molar absorption coefficients in the UVA range and are photostable.[75] It is claimed that Mexoryl SX formulations gave higher protection than equivalent sunscreen formulations, reducing the formation of CPDs and significantly decreasing ferritin and lysosome expression induced by repeated UVA exposure.[81] In one human study it was found that a 5% formulation of Mexoryl SX gave an equal protection against photolesions and sunburn compared to a 5% formulation of a commonly used UVB filter, even though the former absorbs in the UVA region.[82]

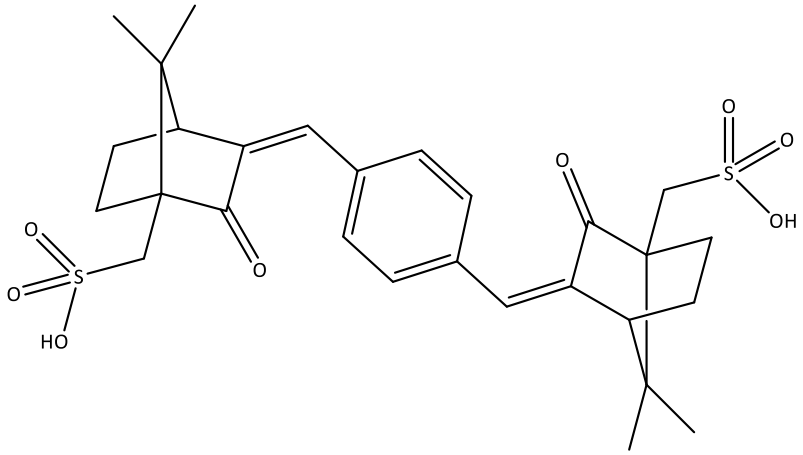

Figure 6. The structure of the UVA filter terephthalylidene dicamphor sulfonic acid, patented by L'Oréal as Mexoryl SX.

The use of sunscreens does not come without concerns about the effect on the environment. Sunscreen components can enter the environment as a result of recreational water activities, showering, rubbing off and excretion. Approximately 25% of sunscreen ingredients applied to the skin is thought to leach into the sea following a 20 minute submersion.[83] 782 ng/g of octocrylene has been found in the livers of Franciscana dolphins due to the ability of octocrylene to bioaccumulate.[84] In the same study it was reported that octinoxate caused a mortality of 33.3% and a bleaching of 83.3% in the coral species *S.caliendrum* at a dose of 1000 μg/L.[84] A recent study also showed that the UVR filters octocrylene, avobenzone, octisalate and homosalate amongst others can mimic the effect of progesterone on Ca^{2+} signalling in human sperm cells, and therefore have the potential to impair male fertility.[85] Due to the deleterious effects of synthetic sunscreen ingredients, significant research has been carried out into the potential use of natural products as photoprotectants. One example

is the protection of human HaCaT keratinocytes by palaythine (shown in Figure 7), a mycosporine-like amino acid (MAA) extracted from the red algae *Chrondus yendoi*.[86] MAAs are secondary metabolites produced by organisms that live in high sunlight environments such as shallow waters. They are natural UVR absorbers, often called 'microbial sunscreens'.[87] Palythine absorbs in the UVB and UVA2 regions with a maximum absorbance at 320 nm. In the study by Lawrence *et al.* HaCaT cells were significantly protected from solar-simulated radiation (SSR) at a 0.3% w/v palythine concentration.[86] The addition of palythine inhibited cell death, the formation of photolesions and upregulation of inflammatory cytokine genes (IL-8, 6 and 20) in irradiated cells. Palythine also exhibited antioxidant activity in irradiated HaCaT cells using the DCFDA assay.[86]

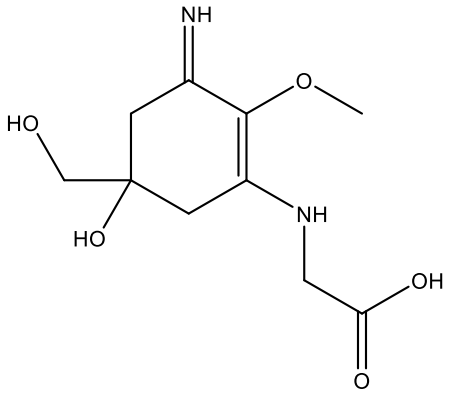

Figure 7. Structure of the natural UVB/UVA2 filter palythine, a mycosporine-like amino acid extracted from the red algae *Chrondus yendoi.*[86]

Recently Ellison *et al.* demonstrated as proof of concept that natural collagen loops or other helix interruptions in the skin could be bound by collagen mimetic peptides (CMPs) tethered to salicylic acid. Derivatives of salicylic acid form a popular class of UVB filters, including the widely used octisalate and homosalate. In this study it was shown that attachment of salicylic acid to a CMP invoked no change in the wavelength of absorption in comparison to free salicylic acid.[88] The pendant UVB filter also remained attached to the collagen surface through multiple washes.[88] This research may be useful in improving the water resistant properties of sunscreens which could lead to better photoprotection as well as a reduction in the level of UVR filters affecting aquatic life. This concept could also decrease any systemic cytotoxicity through percutaneous absorption of the filter.[88]

The inclusion of antioxidants in sunscreens and daily moisturisers is becoming ever more popular, with many sunscreens on the market containing antioxidants such as vitamin E and C, or botanical extracts that suggest an antioxidant action.[89-91] This development is rational based on the increasing body of knowledge concerning UVA-induced generation of ROS in skin.[57] In a study by Wu *et al.* HaCaT cells were incubated with a range of concentrations of α-tocopherol prior to UVA irradiation. The results demonstrated that the lowest concentration, 2.9 IU/ml, gave a significant increase in cell viability while the highest concentration, 14.7 IU/ml, returned cell viability to that of the unirradiated control, significantly reducing lipid peroxidation and preventing UVA-induced GSH depletion.[92]

3. The role of iron

3.1 Systemic iron homeostasis and dysregulation

Iron is an essential bioelement, required for human growth and development. The transition metal plays a vital role as a co-factor in many proteins and enzymes involved in oxygen transport (haemoglobin and myoglobin), energy metabolism, DNA synthesis and electron transport, for example cytochromes and ribonucleotide reductase.[93,94] In healthy adults, free iron in the body is sequestered in haemoglobin (60-70%), muscle myoglobin (10%) or in iron-sulphur clusters of proteins or heme enzymes (1%), the remainder is stored in ferritin where it is ready for use when required by the body.[93,94] The capacity of iron to lose and gain electrons is pivotal to its role in cellular function, however this property also makes it dangerous for ROS generation, and thus the presence of iron is a double-edged sword in biology.[93] This makes iron homeostasis in the body a crucial part of life. Bioavailable iron is transported in the blood by transferrin (Tf), a glycoprotein capable of binding two units of ferric iron (Fe^{3+}).[95] Two molecules of diferric-Tf can form a complex at the cell surface with the transferrin receptor (TfR), and this complex is then internalized within an endosome. A decrease in pH inside the endosome *via* a proton pump releases Fe^{3+} from Tf and reduces it to Fe^{2+}. This mediates the release of iron through the endosomal membrane and into the cell by the divalent metal transporter 1 (DMT-1).[96] Once in the cytosol, free ferrous iron (the labile

iron pool, LIP) is available for use or for uptake into the iron storage protein, ferritin. The intracellular regulation of labile iron is controlled by the iron regulatory proteins (IRPs).[97] Ferritin has the capacity to oxidise Fe^{2+} to Fe^{3+} and incorporate it anaerobically at neutral pH without natural iron-binding molecules.[53] The principal pool of ferritin and therefore iron is in the liver, which holds approximately 25% of body iron.[93] Iron can only be excreted from the body through the desquamation of the *stratum corneum*, sweat, urine, gastrointestinal secretions and menstruation in women.[93] Figure 8 outlines the processes relating to the transport and homeostasis of intracellular iron.

Over the last two decades, several genes that control iron homeostasis have been discovered. For example, in the hereditary iron overload disorder hemochromatosis, the *HFE* gene which regulates the interaction of the TfR with Tf is commonly mutated, thus increasing uptake of dietary iron into cells.[95] Regular blood transfusions are required for the treatment of β-thalassaemia, an inherited blood disorder which is characterized by abnormal haemoglobin production resulting in anaemia. These blood transfusions often lead to the excessive loading of iron into a patient, which cannot be excreted.[98] In cases of iron overload, Tf becomes saturated with iron and the excess iron is unable to bind; this is called non-transferrin bound iron (NTBI). This iron is loosely bound by citrate and albumin and can be taken up into cells independently of the TfR, and thus highly vascular organs such as the heart become iron-overloaded.[99]

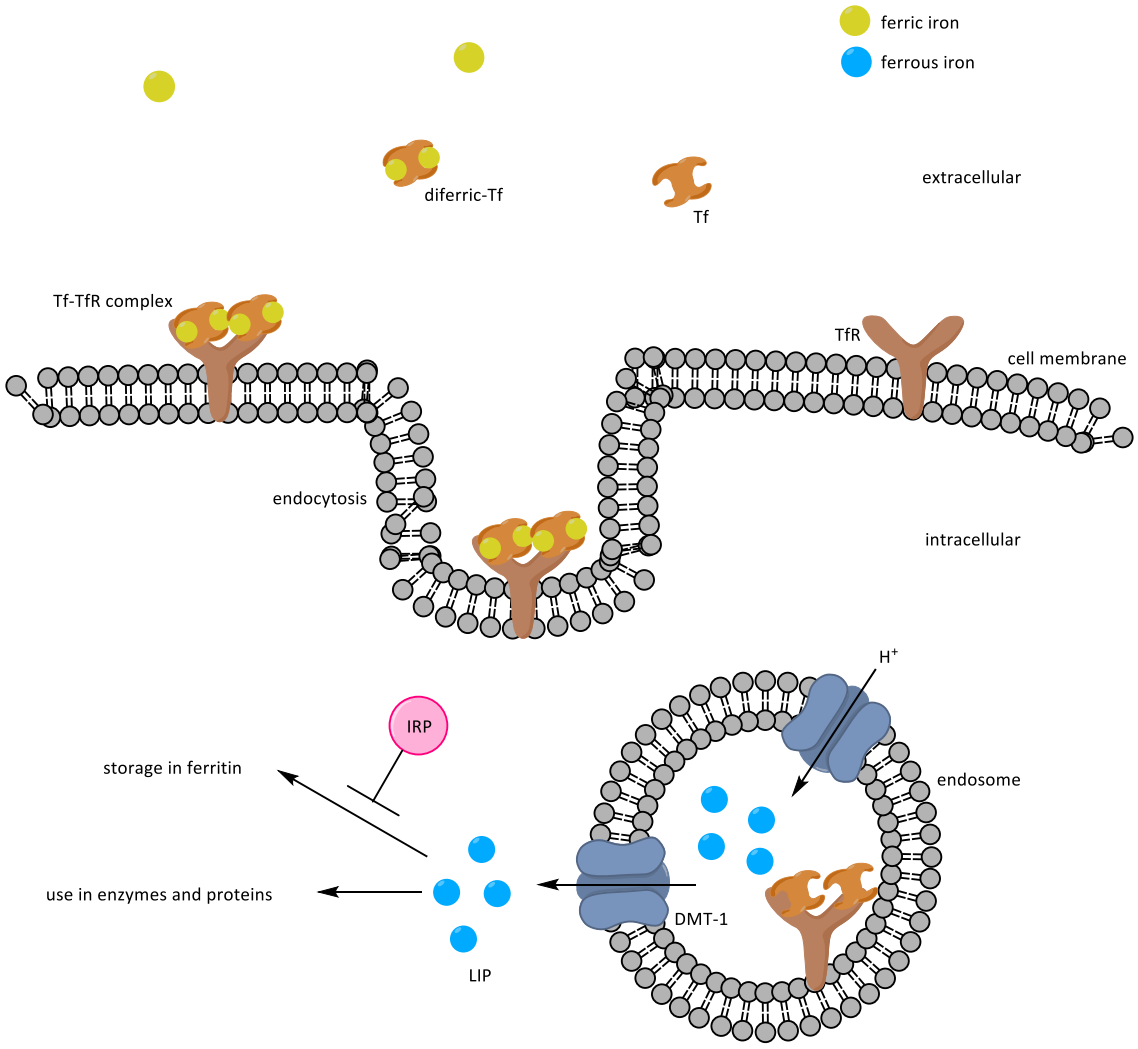

Figure 8. Diagram illustrating the uptake and cellular homeostasis of iron. Transferrin (Tf) can bind two ferric iron molecules (Fe^{3+}) in the bloodstream, and two molecules of diferric-Tf form a complex with the transferrin receptor (TfR) which is internalized in an endosome. A proton pump lowers the pH of the endosome which releases Fe^{3+} from Tf and reduces it to ferrous (Fe^{2+}) iron. Fe^{2+} is pumped out of the endosome by the divalent metal transporter (DMT-1), whereupon iron regulatory proteins (IRPs) control its destination.

For over 40 years, patients with an iron overload disorder have been treated clinically with iron chelation therapy to reduce the tissue damage caused by excess iron stored in the heart, liver and endocrine organs.[100] Systemic iron-overload has similarities with the challenge posed by UVA-induced release of labile iron and the subsequent oxidative damage that may result. There are no clinical iron chelators included in over-the-counter sunscreen formulations and with the building awareness of the UVA-induced release of labile iron in human skin cells, this is an interesting research area. Improving the photoprotective

capabilities of current sunscreen formulations with iron chelators could truly provide 'broad-spectrum' protection and could be very advantageous.

3.2 Design and critical features of iron chelators for clinical application

When designing an iron chelator for therapeutic use there are a number of features to consider. The coordination of Fe^{3+} is best fulfilled in an octahedral geometry with six donor atoms, and ligand affinity is in the general order: hexadentate>tridentate>bidentate.[99] Under biological conditions the most commonly used comparison standard for the affinity of a ligand for ferric iron is pFe^{3+}, defined as the negative logarithm of the concentration of free Fe^{3+} in solution at pH 7.4.[99] Most hexadentate ligands have high pFe^{3+} values and can scavenge Fe^{3+} efficiently at concentrations as low as 30 mg/kg/day.[101] A pFe^{3+} value of $\geq$ 20 seems to be sufficiently high to prevent the distribution of iron in the body.[99]

Fe^{3+} is a hard Lewis acid due to its high charge density and ability to readily accept 6 lone pairs into empty 4s, p and d orbitals. Therefore Fe^{3+} makes the most stable coordination complexes with hard Lewis bases, ligands which have small electronegative donor atoms (O and F). N-containing ligands are often borderline between hard and soft Lewis bases and therefore have the potential to coordinate softer Lewis acids. The most probable off-target metals that could be ligated by therapeutic N-containing iron chelators and cause toxicity are Cu^{2+} and Zn^{2+}, as these metals are borderline soft Lewis acids.[99] Zn^{2+} is required for the catalytic activity of more than 200 enzymes in the human body which have roles in the immune system, wound healing, protein synthesis and cell division.[102] Zn^{2+} also plays a key role in synaptic plasticity and thus learning. Cu^{2+} is essential for maintaining the strength of the skin, blood vessels and connective tissue.[102] Cu^{2+} is very tightly bound to proteins (such as ceruplasmin)[102] in most biological systems and is chaperoned between proteins by specialised molecules, making coordination by iron chelators improbable.[103] This knowledge helps the design of high affinity iron chelators (high pFe^{3+}) which have minimal toxicity due to off-target metal chelation. Under aerobic conditions, high affinity Fe^{3+} iron chelators have been shown to chelate Fe^{2+} and autooxidise it to Fe^{3+} to form a stable complex, therefore under most physiological conditions chelators with a high pFe^{3+} will also chelate Fe^{2+}.[104]

The key property for an orally active iron chelator is the ability to be absorbed through the gastrointestinal tract and reach the desired target areas in the body. Thus oral iron chelators need to be sufficiently lipophilic to pass across biological membranes, but not be too lipophilic to remain within the phospholipid bilayer of the plasma membrane.[99] A chelator with a logP value (water-octanol partition coefficient) above 0.2 should fulfil this requirement.[99] A molecular weight of less than 500 Da is also a crucial feature that a chelator should possess in order to ensure an efficient rate of drug absorption through non-facilitated diffusion.[99]

3.3 Types of iron chelators and their limitations

There are three clinical iron chelators used worldwide for iron overload disorders, and a comparison of their properties is presented in Table 3.

Table 3. A comparison of the properties of the three clinically used iron chelators[99,101,105]

	Desferrioxamine (DFO, desferal)	**Deferasirox (Exjade©)**	**Deferiprone (Ferriprox©)**
Molecular weight (Da)	560	373	139
Chelating property	Hexadentate	Tridentate	Bidentate
Iron binding affinity (pFe^{3+})	26.6	22.5	20.4
Delivery	Diffusion pump	Oral	Oral
Half life	20-30 min	12-16 h	3-4 h
LogP (lipid solubility)	-0.61 (low)	3.8 (high)	0.61 (medium)
Adverse effects	Ocular, auditory growth inhibition, allergy	Gastrointestinal, hepatitis	Gastrointestinal, arthralgia

Desferrioxamine (DFO, **1**) is a hexadentate iron chelator that forms a 1:1 complex with iron, shown in Figure 9. It is a naturally occurring *Streptomyces pilosus* siderophore which has been used since the 1970s and is classed as the 'gold standard' of iron chelators for its high affinity for Fe^{3+}.[99] DFO is a relatively large (MW= 560 Da) hydrophilic molecule and as such it is not orally bioavailable and has quite a short plasma half-life. Clinically, it is typically administered iv *via* a diffusion pump, which is painful and cumbersome and therefore patient compliance

is poor.[96] Hence the development of orally active iron chelators that are comparable to DFO in their affinity for iron was necessary.

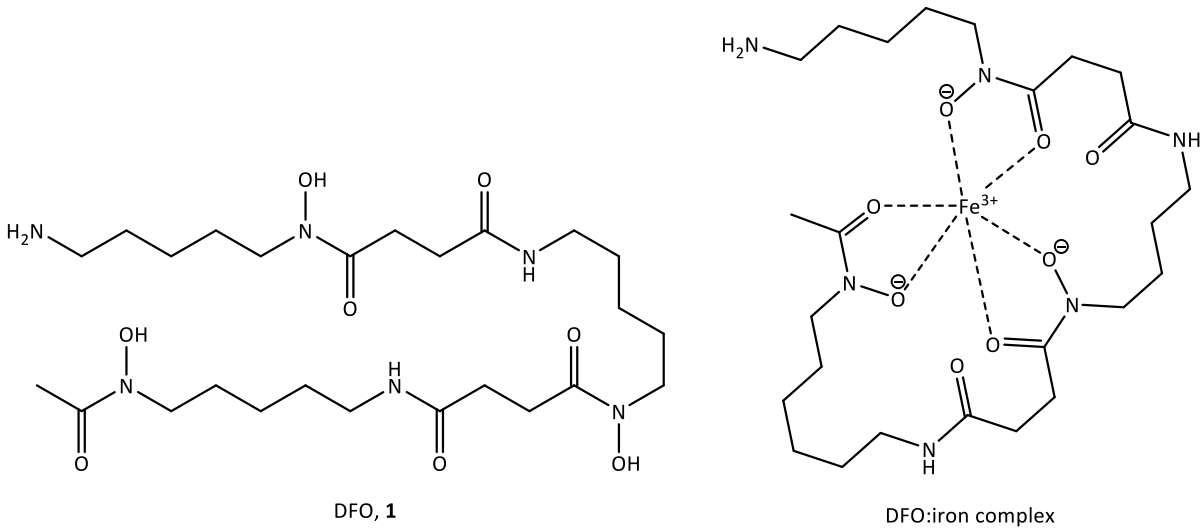

Figure 9. Structure of the hexadentate siderophore iron chelator DFO and its 1:1 complex with ferric iron.

Deferiprone **2** (Figure 10) was licensed for use in Europe in 1999 as an orally active bidentate iron chelator and has comparable effectiveness to DFO.[99] Deferiprone is a chelator of the hydroxypyridone class which coordinates iron through its two adjacent oxygen atoms to form a neutral 3:1 complex (FeL_3). This complex can also permeate biological membranes and thus is readily removed,[99] including from cardiac tissue where it has been demonstrated to reduce the myocardial iron burden in thalassemia major patients more effectively than either DFO or deferasirox **6**.[106] Despite these positive features, the results of a variety of clinical trials have led to concerns over the therapeutic value of deferiprone.[107] These concerns led to the discovery that the incompletely coordinated biscomplex $[FeL_2]^+$ (present due to the concentration of deferiprone not being high enough to fully chelate iron) can potentiate H_2O_2-mediated oxidative DNA damage in iron-loaded liver cells.[108] The incomplete coordination of deferiprone could enable reductants or oxidants to reach the metal centre, and thus in a clinical setting low Fe:L ratios may lead to long-term toxicities.[96] The deferiprone dosage required to keep an iron-overloaded patient balanced is very high (75-100 mg/kg/day) due to extensive metabolism (glucuronidation) of the 3-hydroxyl function of the chelator. As this functional group is essential for iron coordination, the efficacy of deferiprone is greatly reduced by metabolism in this way: urinary studies have shown that >85% of the administered

dose is recovered as the 3-O-glucuronide conjugate.[109] The 1,2-diethyl analogue of deferiprone (CP94, **3**), shown in Figure 10, appeared to be a more efficient derivative at mobilizing liver iron in a study using iron-overloaded rats, however the increased efficiency was not thought to translate into humans due to differences in metabolism.[110] Further analogues of deferiprone with higher iron affinities have been devised to counteract the high dosages needed to compensate for metabolism. The Novartis lead compound **4** with an aromatic substituent in the 2-position was found to be orally active in the iron- loaded rat and marmoset (Figure 10).[111] Hider and co-workers demonstrated that introducing an electron-withdrawing substituent in the 2-position of the ring (*i.e* 1-hydroxyalkyl or amido group) increased the iron affinity due to stabilisation of the negatively charged hydroxyl oxygen at physiological pH.[99] As a result of these studies, a further analogue (CP502, **5**) was identified with a pFe^{3+} of 21.7, which thus binds iron ten times more strongly than deferiprone at pH 7.4.[99]

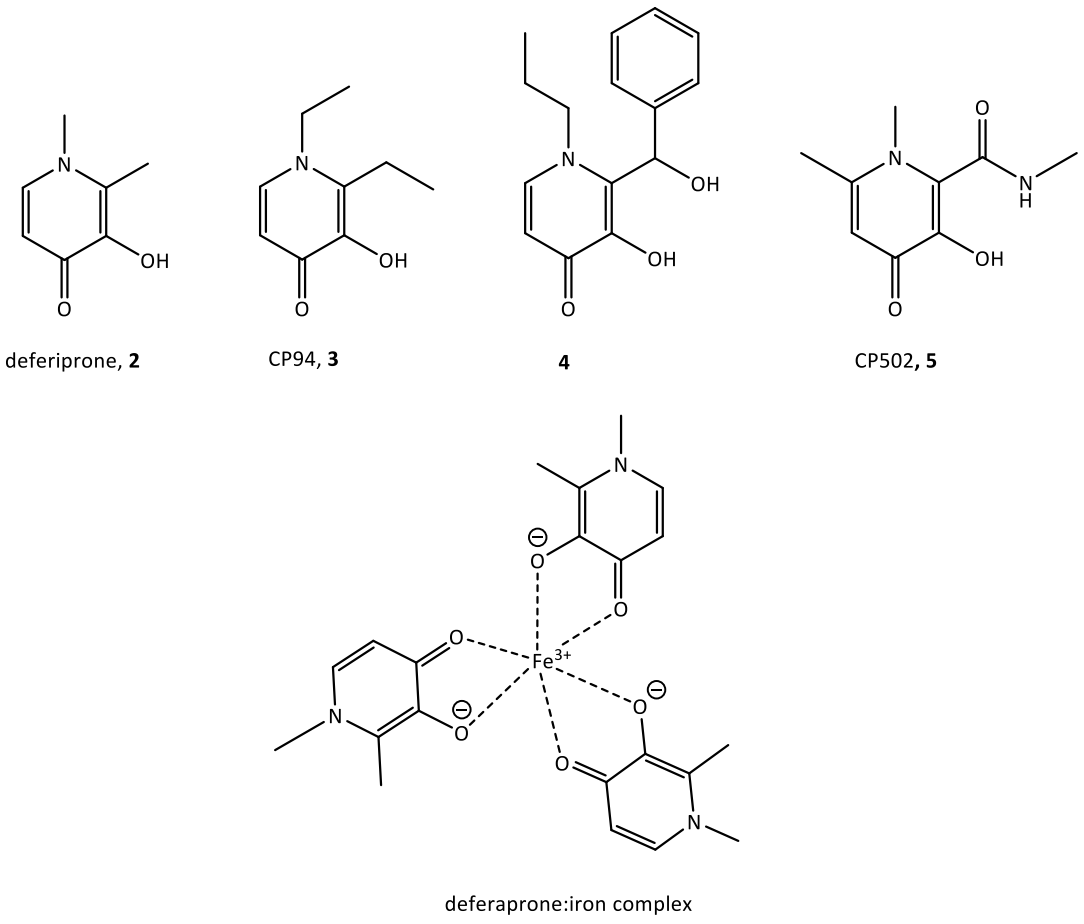

Figure 10. The structure of deferiprone **2** and subsequent analogues **3**-**5** with higher pFe^{3+} values, along with the structure of the 3:1 complex that deferiprone forms with ferric iron.

Deferasirox **6** is a triazole-based tridentate chelator which binds Fe^{3+} as a FeL_2 complex through its two phenolic oxygens and one triazolyl nitrogen, as shown in Figure 11.[98] It is relatively hydrophobic compared to the other two clinically used iron chelators with a logP value of 3.8 and can therefore easily penetrate membranes, but has good oral bioavailability.[99] The pFe^{3+} of deferasirox is 22.5,[99] indicating that it binds iron 100 times more effectively than the bidentate chelator, deferiprone (pFe^{3+}= 20.4, see Table 2). Upon chelation the deferasirox-iron complex formed has a net charge of -3 and a combined molecular weight of more than 800 Da, and for these reasons it is likely that iron complexes formed intracellularly become trapped within the cell.[99] Significantly, it has been shown that the $[ML_2]^{3-}$ deferasirox complex is redox-inactive under biological conditions.[98]

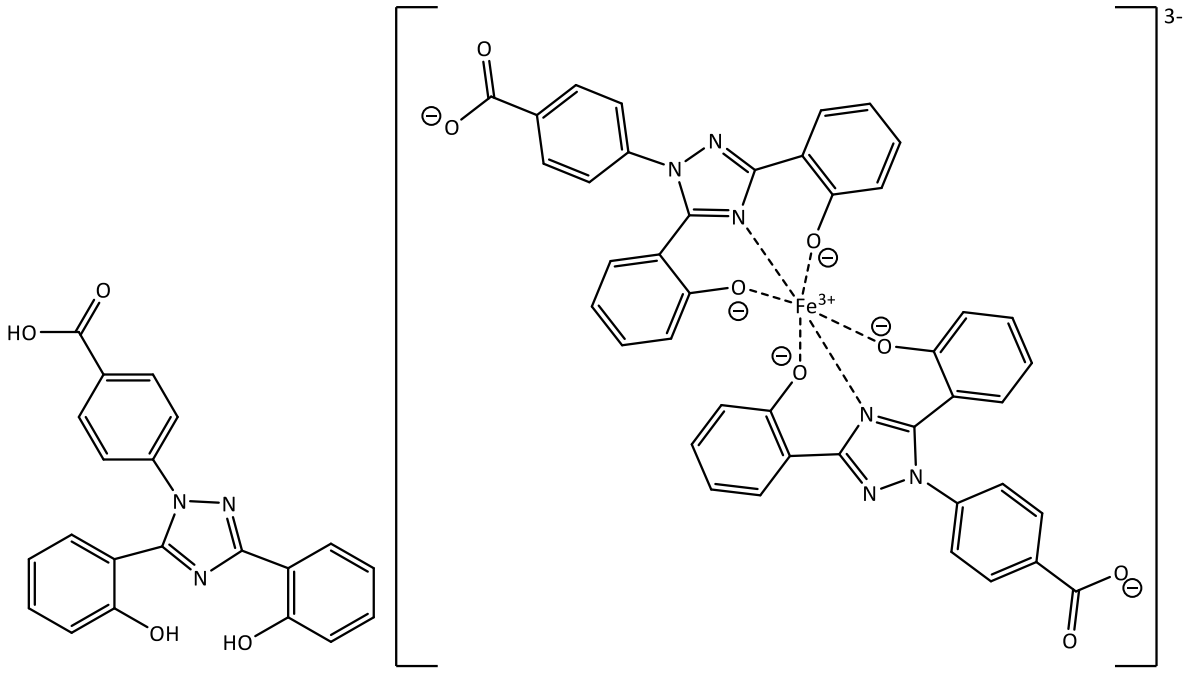

Figure 11. The structure of the tridentate iron chelator deferasirox and its 2:1 complex with ferric iron.

In a study using hypertransfused rats, deferasirox promoted the hepatocellular chelation and excretion of iron 4-5 times more effectively than DFO,[112] and has been proven to be efficient at removing liver iron from patients receiving regular transfusions.[113] There have been some concerns over the potential of the triazolyl nitrogen in deferasirox to coordinate to the divalent metal cations Zn^{2+} and Cu^{2+} since this sp^2-hybridised nitrogen atom is a somewhat softer donor (Lewis base).[98] However, steric factors are also important to consider in complex

formation, and it has been shown by Hancock that ligands forming six-membered chelate rings prefer small metal centres compared to 5-membered chelate rings which are suited to larger metals.[114] It has been shown that the bond lengths of Fe-O and Fe-N in deferasirox complexes are very short (1.60 Å and 1.90 Å respectively)[98] compared to a $[Fe(H_2O)_6]^{3+}$ complex which has an average Fe-O bond length of 2.01 Å.[115] The deferasirox:iron complex is therefore somewhat strained. The degree of strain for similar complexes will increase with increasing ionic radius of the central metal, thus binding of the larger Zn^{2+} by deferasirox is disfavoured sterically in comparison to the smaller Fe^{3+}.[98]

The aroylhydrazone family of tridentate chelators contains two analogues which have received much attention due to their noteworthy iron binding ability, namely pyridoxal isonicotinoyl hydrazone (PIH, **7**) and salicylaldehyde isonicotinoyl hydrazone (SIH, **8**),[116,117] which are shown in Figure 12. Both of these ligands bind Fe^{3+} through phenolic and carbonyl oxygens and an imine nitrogen to form $[ML_2]^-$ complexes. PIH, SIH and other analogues can easily be synthesized through Schiff base condensation of the relevant aldehyde with isonicotinylhydrazide.[116] These iron chelators are lipophilic in nature and are uncharged at physiological pH, which along with their relatively low molecular weights should in principle make them favourable for clinical use as orally active iron chelators. PIH is a member of the original '100 series' of aroylhydrazone chelators, and recently the pFe^{3+} value of PIH has been revised and is now considered to be 26.2, which is comparable to the iron-binding ability of DFO.[105] An initial study of PIH demonstrated its efficacy at removing Fe^{3+} from the mitochondria of reticulocytes, showing its ability to pass the plasma and mitochondrial membranes.[116] In a study by Baker *et al.*, PIH was found to be as efficient as DFO in preventing the uptake of ^{59}Fe by Tf in hepatocyte cells, reducing the uptake to approximately half the control value.[118] The '200 series' of aroylhydrazones was created by replacing the pyridoxal moiety with the more lipophilic salicylaldehyde group, and SIH is a member of this series. The 200 series of analogues display decreased intracellular iron mobilization capability in comparison to the 100 series,[119] for example SIH has a pFe^{3+} value of 24.6.[105] However, SIH has been used extensively by cell biologists researching the cytosolic labile iron pool, in particular in the development of fluorescent calcein-based assays.[120,121]

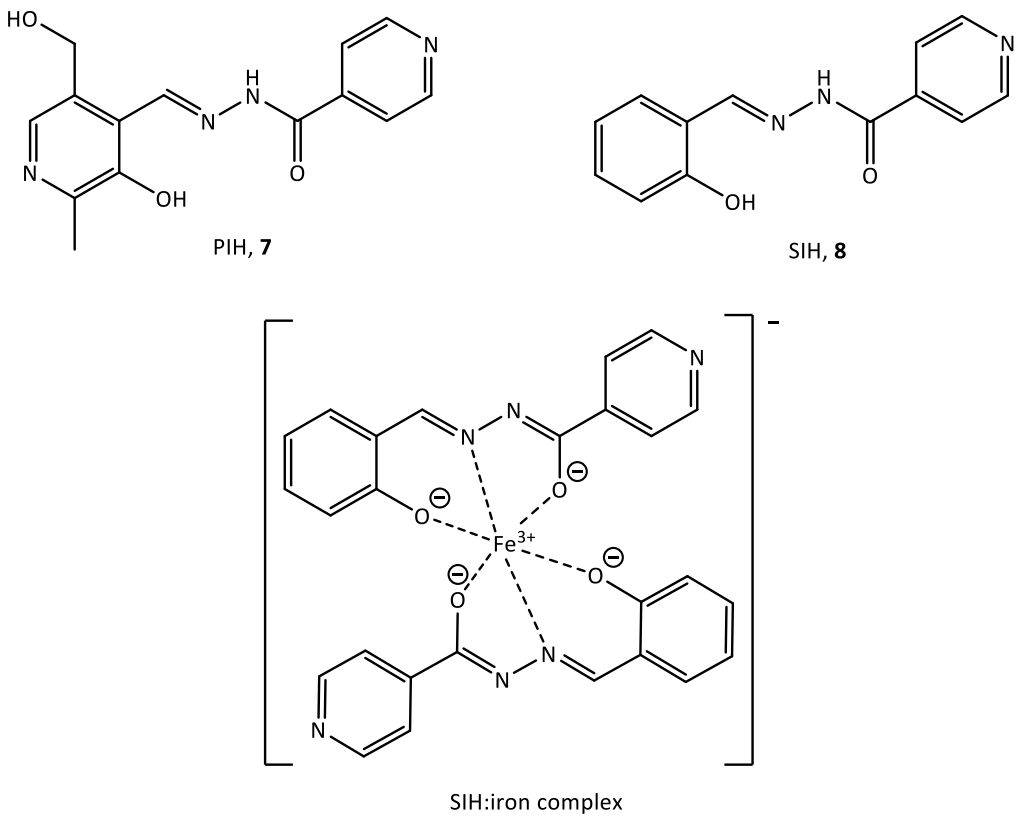

Figure 12. The structures of two tridentate aroylhydrazone iron chelators, SIH **7** and PIH **8**, along with the complex formed through ferric iron coordination by SIH.

The use of natural products in drug discovery and in cosmetics is rising due to consumer concerns about safety, toxicology and sustainability of synthetic compounds.[122,123] Indeed, a recent review by Newman *et al.* highlighted that drug discovery seemed to be moving away from large compound libraries for drug discovery and moving towards smaller, more focused libraries based around many structural aspects of natural products.[124] Siderophores excreted by bacteria and fungi, such as DFO, are naturally occurring high affinity Fe^{3+} chelators that pathogens use when in low iron environments or during host invasion.[125] Siderophore:iron complexes are internalized into the cells of pathogenic organisms and then iron is released from the complex for use.[126] The most common groups of siderophores are hydroxamates and catecholates.[125] DFO is an example of a hydroxamate chelator, with coordination of Fe^{3+} being through the hydroxyl functions on the nitrogen along with the carbonyl oxygen. Catecholates are phenolic compounds in which the 1,2-dihydroxy structural moiety coordinates Fe^{3+} in a bidentate manner, for example as in enterobactin **9** which is found in Gram-negative bacteria such as *E.coli*,[127] shown in Figure 13.

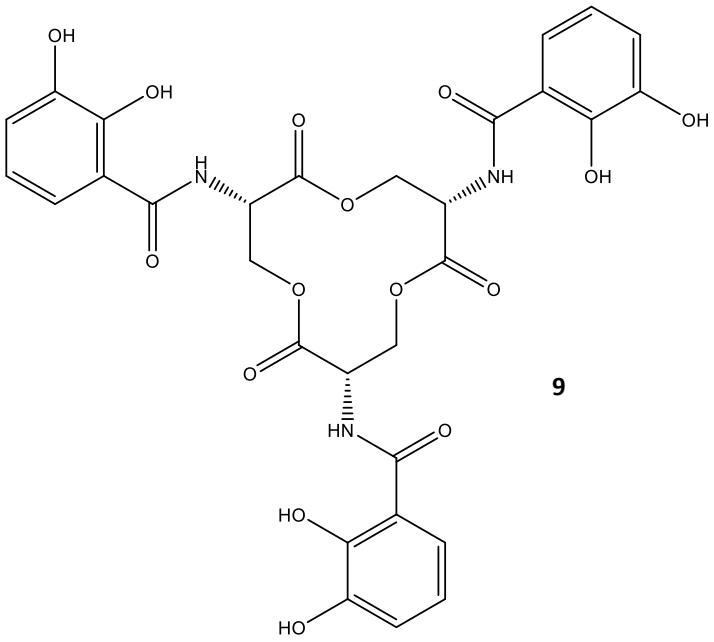

9

Figure 13. The structure of the natural hexadentate iron chelator enterobactin **9** found in *E.coli* which coordinates iron through its three catecholate moieties.

Catecholate iron chelators are of interest due to the number of plant-derived flavanols such as catechin **10** which contain the catechol moiety.[128] Many such natural products have been researched in terms of their antioxidant effects, and these studies have now progressed into investigations of their iron-binding ability.[128] For example, baicalein **11** found in the Chinese herb *Scutellaria baicalensis,* has been found to inhibit iron-induced Fenton chemistry through both its radical scavenging properties and its ability to chelate iron.[129] In one study by Zhang *et al.* both **11** and quercetin **12**, which is found in cranberries, were shown to significantly inhibit iron-induced lipid and protein peroxidation of the liver and decrease hepatic iron content in iron-overloaded mice.[130] Another naturally occurring catechin derivative which is abundant in green tea is epigallocatechin gallate (EGCG, **13**). In a study by Reznichenko *et al.*, **13** was found to have an iron-binding activity comparable to DFO.[131] Figure 14 shows the structures of the natural iron chelators described above.

Other natural products have been identified with various novel iron-binding motifs, for example the cyclodipeptide N-oxide derivative pulcherriminic acid (PA, **14),** produced by the yeasts *C. pulcherrima* and *M. pulcherrima* (found on grapes[132]) as well as the *Bacillus* family of aerobic sporeforming bacteria.[126] Cook and Slater showed that **14** depletes iron by forming

an insoluble Fe^{3+} complex called pulcherrimin.[133] Molecules such as **14** may thus provide interesting new leads for the development of therapeutic natural iron chelators.

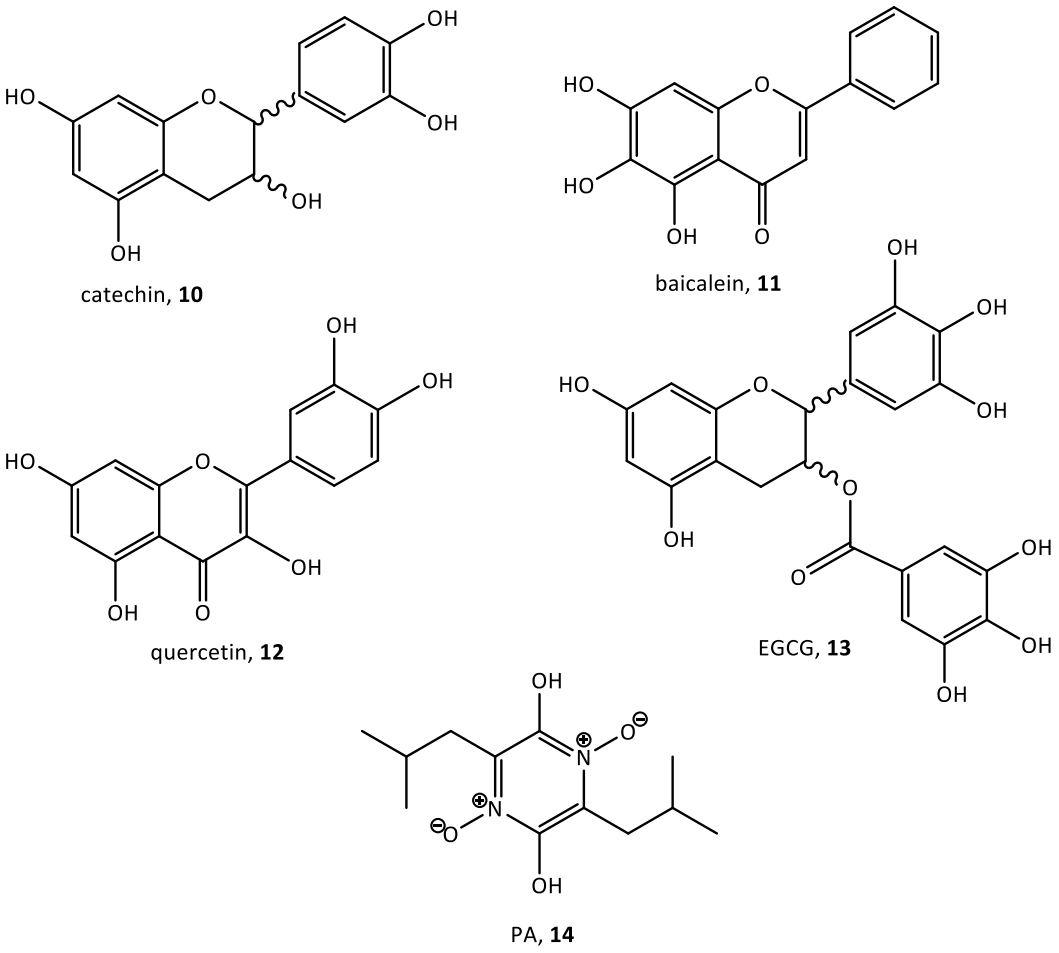

Figure 14. The structures of plant flavanol derived natural iron chelators **10**-**13** along with PA **14**, a natural N-oxide iron chelator.

3.4 Alternative uses for iron chelators

The successful clinical development of iron chelators to reduce tissue damage associated with iron overload diseases has generated interest into expanding the use of chelators for treating other iron-dependent diseases. For example, iron-promoted oxidative damage is a major contributor to neurodegenerative disorders and cardiovascular disease.[100] It could be fruitful to repurpose already clinically approved chelators for new uses, specifically for localized iron accumulation in comparison to systemic imbalance.[123] One of the many biological roles of

iron is in the enzyme ribonucleotide reductase which catalyses the rate- limiting step in the formation of deoxyribonucleotides from ribonucleotide precursors.[96] The rate of DNA synthesis and proliferation in tumour cells is higher than in normal cells, and therefore the demand for iron as a cofactor of ribonucleotide reductase is also higher. In order to meet the higher demand for iron in cancerous cells, TfR expression is upregulated and subsequently iron uptake is increased.[96] This highlights the possibility to use iron chelators as potent anti-tumour agents, for example in a study by Richardson *et al.* a series of PIH analogues were all found to inhibit tumour cell growth in culture more effectively than DFO.[134] Similarly, iron chelation may also be a suitable strategy for the development of anti-microbial agents to prevent biofilm formation (where microorganisms adhere to each other and also to a surface within an extracellular matrix of polymeric substances), especially as the resistance to current antibiotics is growing rapidly.[135]

The transition metals iron, copper and zinc have all been implicated in the neurodegenerative disorders Alzheimer's disease (AD), Parkinson's disease (PD) and Friedreich's ataxia.[131,136] Analysis of animal and human brains has shown that iron distribution in the brain is not uniform compared to other metals. The *substantia nigra*, *globus pallidus* and *dentate gyrus* are all associated with iron accumulation and also with these neurodegenerative disorders.[131] Additionally, mutations in genes that regulate iron homeostasis have also been implicated in a number of neurodegenerative diseases. Most key iron homeostasis proteins (such as Ft and TfR) contain iron-responsive elements (IREs) in the 5'-untranslated region (UTR) of their mRNA, therefore either their synthesis or degradation is promoted by the presence or absence of iron.[137] Amyloid precursor protein (APP) and α-synuclein are the major proteins implicated in accelerating the disease progression of AD and PD respectively; they also contain 5' UTR IREs.[131,137] In the case of AD, iron can promote the deposition of monomeric amyloid β (Aβ) peptides which can aggregate and form oligomers; oligomers that are misfolded then form Aβ plaques, a hallmark of AD.[138] As iron is a potent redox catalyst, its promotion of oxidative stress may also lead to neurodegeneration in parts of the brain associated with iron accumulation.[131,136] This indicates that iron chelation therapy could be at the heart of strategies of neuroprotection by preventing oxidative stress and so aggregation of Aβ and α-synuclein. In one clinical trial, DFO was found to significantly slow the progression

of AD[137] and in a study by Reznichenko *et al.* the natural iron chelator **13** (see Figure 11) reduced Aβ generation in Chinese hamster ovary cells overexpressing the APP mutation.[131] Other studies have shown the efficacy of PIH for removing iron from mitochondria and its potential usefulness for the treatment of Friedrich's ataxia, a neurodegenerative disease where mitochondria are iron-overloaded.[96]

4. Iron chelation for skin photoprotection

4.1 Phototherapy

At a basic level, light from the sun has been attributed to positive therapeutic outcomes in terms of improving mood, especially seasonal affective disorder, through the increased biosynthesis of vitamin D *via* the absorption of UVB radiation.[14] Light has also been proven to be beneficial as a targeted therapy for certain pathologies. One of the most recognised light therapies is photodynamic therapy (PDT), where a photosensitizing drug is administered to the patient prior to targeted exposure with light of the required wavelength to activate the drug.[139,140] This offers the potential of destroying the targeted tissue without damaging the surrounding tissue. The therapeutic effect depends principally on the generation of ROS at the site of action, which promote oxidative stress-induced damage to proteins, nucleic acids and lipids and subsequently cellular necrosis. The use of PDT has gained clinical recognition for the treatment of actinic keratosis (AK), BCC and SCC in many European countries including Germany, Sweden, Austria, Italy and Switzerland, as well as in the USA and Canada.[139,141,142] Very recently, a clinical trial on the use of PDT for prostate cancer treatment in 30 men has provided promising results that may lead to the widespread acceptance of this technique for the treatment of solid tumours.[143] A further development of PDT is the use of antibodies to target photosensitizers to tumour-associated antigens. Coupling photosensitizers with monoclonal antibodies can improve the specificity and efficacy of the therapy.[144] Due to the worldwide increase in antibiotic resistance, the use of PDT for the treatment of microbial infections has also been studied extensively;[145] this method could be very beneficial as it is unlikely that bacteria would develop resistance to ROS.

Atopic dermatitis and psoriasis are common chronic inflammatory skin diseases characterized by abnormally dry red skin lesions which are worsened by itching.[146] There are three main types of phototherapy that are currently used to treat inflammatory skin conditions: broadband UVB, narrowband UVB and PUVA. The type of phototherapy used depends on the specific skin condition and clinical factors such as previous patient responses to treatment.[147] In narrowband UVB a small range of UVB wavelengths is used to treat skin conditions. It is very effective for severe psoriasis and atopic dermatitis.[147] However for chronic plaque psoriasis where narrowband UVB treatment has not been effective, phototherapy *via* PUVA is recommended as well as for other skin dermatoses such as vitilago.[147,148] PUVA is the combination of UVA irradiation with the potent photosensitizing agent, 8-methoxypsoralen, which can be administered orally or topically in a bath or cream.[148] This is an example of a drug that can provide a topical or systemic therapeutic effect upon stimulation by UVA irradiation, illustrating again that the use of light to activate a pre-administered drug is an efficient and useful mechanism with proven clinical efficiency.[148,149]

4.2 Iron chelators and the UVA-induced labile iron pool

As previously described in Section 1.4, one of the hallmarks of UVA-induced damage is the release of redox-active intracellular labile iron into the LIP.[48,57] With the substantial knowledge surrounding iron chelators and their therapeutic use not solely for systemic iron overload disorders, it would appear reasonable to target UVA-induced LIP with an iron chelator in order to provide a potential photoprotective effect. In this context, Glickstein *et al.* assessed the effect of the three clinically approved iron chelators deferiprone, DFO and deferasirox along with SIH on cytosolic LIP. It was revealed that in three cultured cell lines, the lipophilic iron chelators (deferiprone, deferasirox and SIH) readily chelated labile iron in 1 h as they were able to quickly permeate the plasma membrane.[150] In contrast, prolonged treatment (12-18 h) with the hydrophilic chelator DFO was required for the chelator to enter cells by endocytosis and subsequently reduce cytosolic LIP.[150]

Zhong *et al.* sought to ascertain the importance of the level of labile iron in determining the susceptibility of both human skin keratinocytes and fibroblasts towards UVA-induced necrotic

cell death.[151] In this study, skin cells were treated with or without the iron chelator DFO 18 h prior to UVA-irradiation. Using the calcein assay, DFO treatment was shown to abolish the UVA-induced labile iron release in both keratinocytes and fibroblasts.[151] The immediate depletion of intracellular adenosine triphosphate (ATP) has been identified as a hallmark of pre-necrotic cells,[152] and pre-treatment of fibroblasts with DFO in this study was also found to significantly decrease UVA-induced ATP depletion.[151] Furthermore, it was confirmed using flow cytometry that pre-treatment with DFO did indeed significantly protect fibroblasts against UVA-induced necrotic cell death, although an important observation was the ability of DFO to completely abolish the basal level of iron without UVA-irradiation.[151] In a parallel investigation, Seité *et al.* used a reconstructed organotypic culture to analyse UVA-induced lipid peroxidation and iron chelation.[153] The organotypic culture consisted of human keratinocytes which formed a stratified epidermis, seeded on a dermal substitute containing a collagen matrix. The study pre-treated the epidermis model with the iron chelator *N,N*′-bis-(3,4,5-trimethoxybenzyl) ethylenediamine *N,N*,-diacetic acid (OR10141, **15**), shown in Figure 15, for 1 h prior to UVA exposure. The percentage of UVA-induced lipid peroxidases (LPO) was greatly reduced by use of **15**, as was the induction of ferritin synthesis.[153]

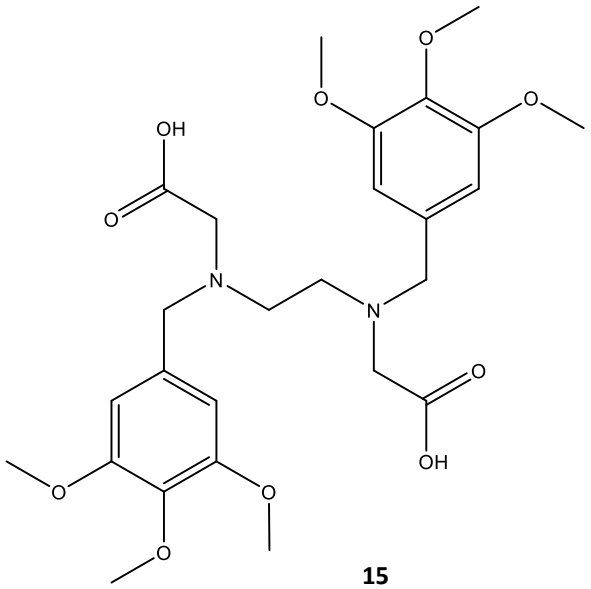

15

Figure 15. The structure of OR10141, **15**, which has been shown to greatly reduce lipid peroxidation and ferritin synthesis in an organotypic skin model.[153]

In a study by Bendova *et al.* the cytoprotective effects of the iron chelators DFO, deferiprone, deferasirox, SIH and PIH in H9c2 cells were assessed using the oxidative stress inducer *tert*-butyl hydroperoxide (*t*-BHP).[154] All chelators afforded cellular protection when co-treated for 24 h with *t*-BHP, with the relative protection from highest to lowest with respect to concentration used being in the order deferasirox > SIH > PIH >deferiprone >DFO.[154] The study also examined the cytotoxicity of the iron chelators after 72 h of treatment, and while DFO and deferiprone did not cause any significant loss of cell viability up to concentrations of 100 µM, deferasirox, SIH and PIH caused a 50% reduction in cell viability at concentrations of 3, 30 and 44 µM respectively.[154] In another study by Hasinoff *et al.*, the ability of deferasirox to protect cardiac myocytes from doxorubicin-induced oxidative damage was analysed. The results showed that exposure of myocytes to deferasirox for longer than 24 h induced cytotoxicity [155] These studies thus show that over-exposure to iron chelators, in particular high affinity lipophilic chelators can lead to detrimental effects due to the removal of essential iron from critical metalloproteins.[100,154-156]

4.3 Prochelators and their applications

Due to the potential cytotoxicity that may result from over-exposure to iron chelators, the positive therapeutic use of chelators for specific iron-related disorders also involves safety concerns. In an attempt to combat the side effects of long-term use of iron chelators but still harness their protective qualities, several studies have investigated the administration of prochelators, which are molecules that are unable to bind iron until they are activated in an oxidative atmosphere. These 'oxidative stress-activatable iron chelators' provide a means of targeting tissues that are at risk of excessive iron-induced oxidative damage.[153,157,158]

For example Kielar *et al.* masked the iron-binding ability of deferasirox through a group containing a boronic ester that is cleaved upon exposure to H_2O_2.[100] One of the phenolic oxygens required for the tridentate coordination of Fe^{3+} by deferasirox was esterified with 4-bromomethylphenylboronic acid pinacol ester before basic hydrolysis of the boronate ester to give the prochelator TIP **16,** (Scheme 5).[100] UV/Vis analysis of deferasirox and **16** ± Fe^{3+} showed no spectral change when Fe^{3+} was added to **16** compared to an observed spectral

change when Fe^{3+} was added to deferasirox, indicating that the prochelator does not bind iron.[100] Unmasking of **16** occurs *via* oxidation of the boronic acid with H_2O_2 to give a phenol intermediate which undergoes spontaneous elimination to release deferasirox and *p*-quinone methide; this by-product is converted to 4-hydroxybenzyl alcohol in water (see Scheme 5). Clean conversion of the **16** to deferasirox and 4-hydroxybenzyl alcohol upon addition of excess H_2O_2 was shown using LC/MS.[100] **16** showed a similar protective ability to deferasirox when pre-treated cells were exposed to H_2O_2, however upon exposure for 24 h, **16** exhibited greater cellular cytotoxicity compared to the parent chelator at concentrations above 25 μM.[100] The apparent cytotoxicity could be due to the ability of boronic acids to inhibit certain proteases such as subtilisin and chymotrypsin.[159]

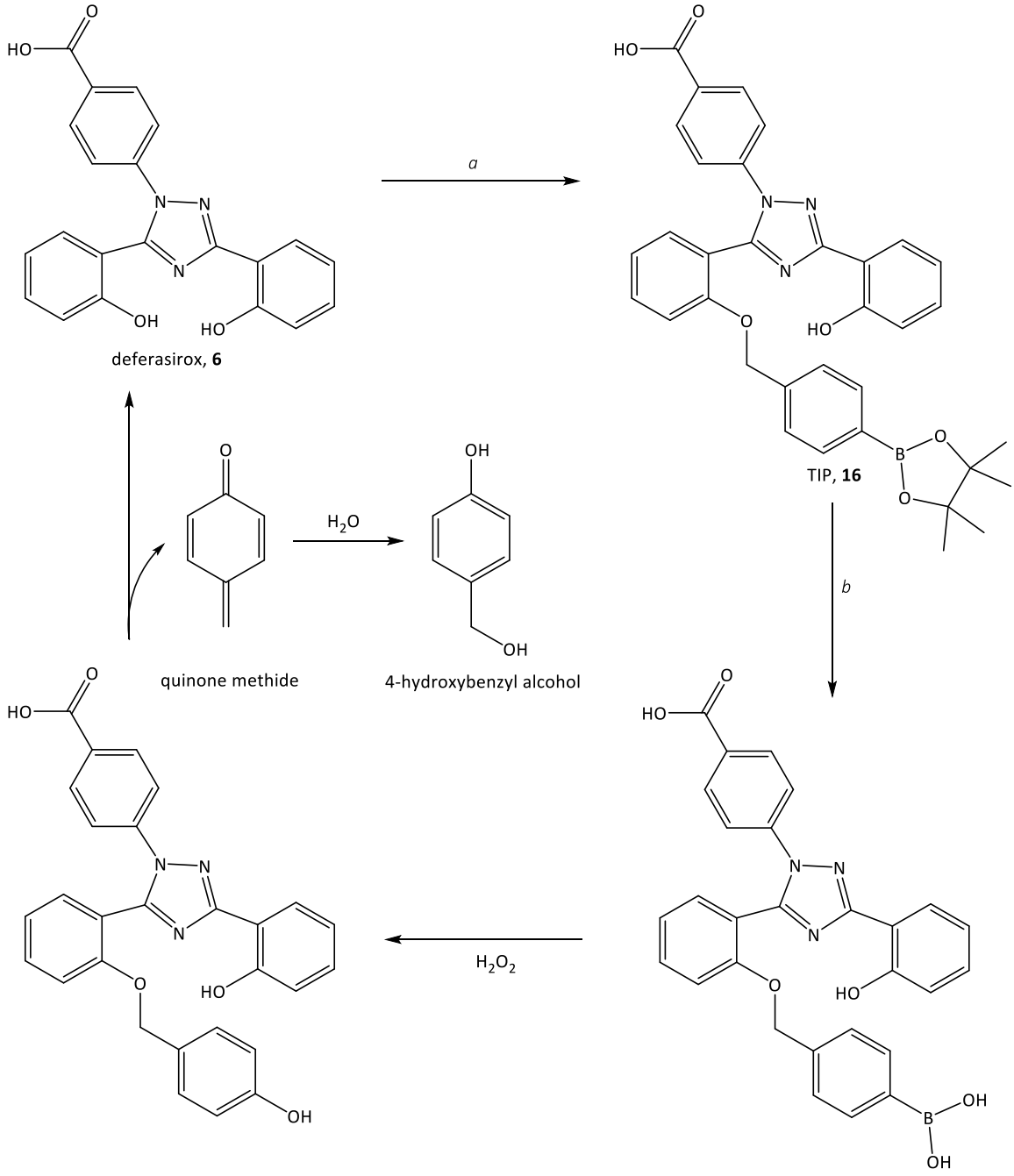

Scheme 5. The masking of deferasirox **6** to form the prochelator **16**, which is activated upon reaction with H_2O_2 to give the free iron chelator and 4-hydroxybenzyl alcohol as a by-product. *Synthesis reagents and conditions:* **a.** 4-bromomethylphenylboronic acid pinacol ester, K_2CO_3, acetonitrile; **b.** KOH, H_2O, MeOH.

In a similar study looking at protective agents for cardiomyocyte oxidative injury, the iron-coordinating phenolic oxygen of SIH was masked with a boronic ester to give the prochelator BSIH **17**,[160] shown in Figure 16. When H9c2 cardiomyoblast cells were pre-treated with **17** and

the parent chelator prior to 24 h treatment of 200 µM H_2O_2, the EC_{50} (concentration required to reduce H_2O_2 induced toxicity to 50% of the viability of the untreated control) values for SIH and **17** were 8 and 84 µM respectively, indicating that a higher concentration of **17** was required before protection was afforded.[160] However, it was discovered that **17** was less cytotoxic than SIH at the time points of 24 and 72 h exposure, and furthermore when cells were incubated with **17** for seven days no cytotoxicity was observed.[160]

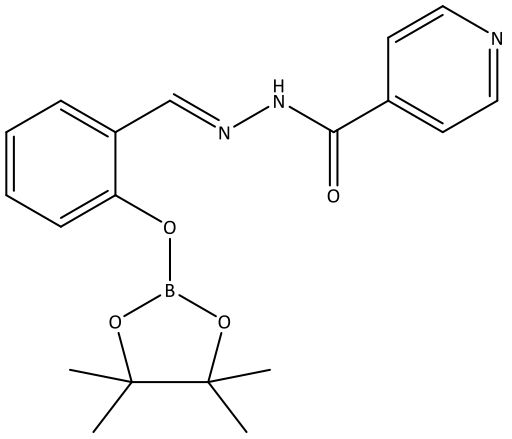

BSIH, **17**

Figure 16. The structure of the boronate prochelator BSIH **17** which is activated upon reaction with H_2O_2 to give the free iron chelator SIH **8**.

In the context of photoprotection, a study by Pygmalion *et al.* investigated UVA-induced labile iron release and oxidative stress reduction using a diisopropyl ester prochelator (Sideroxyl, **18**) of a low affinity iron chelator (DBED, **19**).[161] The aminocarboxylate **19** was hypothesised to undergo intramolecular hydroxylation in the presence of H_2O_2 to form a high affinity iron chelator (HBBED, **20**) due to the additional phenolic Fe^{3+} coordination site, shown in Scheme 6. Prior to activation, **19** would be unlikely to compete with iron contained in Tf and would only bind free Fe^{3+}.[161] **18** was found to decrease intracellular UVA-induced ROS in human fibroblasts and keratinocytes in a dose-dependent manner, however it was not shown whether the presence of **18** modulated the UVA-induced LIP level. The conversion of **18** to **19** in cell culture was also not proven, but was hypothesised to occur *via* non-specific esterase hydrolysis as such enzymes are abundant in human skin.[161] **19** is ionised at physiological pH and so cannot easily be administered in cell culture due to its poor bioavailability.[161] This novel

idea of UVA photoprotection against labile iron release is promising, however it is limited by the two-step intracellular reaction required for generation of an active chelator.

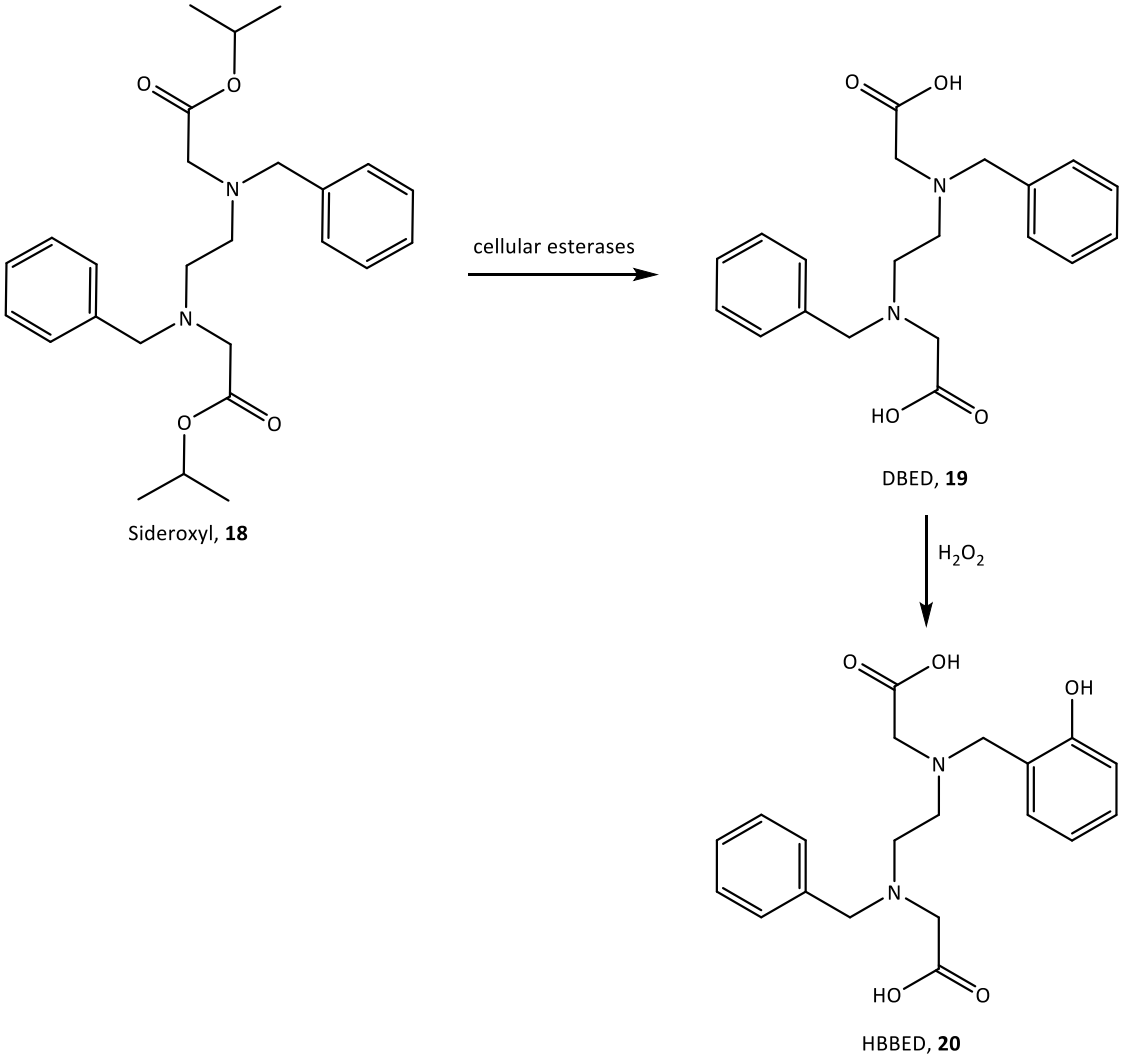

Scheme 6. Sideroxyl **18**, a diisopropyl ester, is converted to the low affinity iron chelator DBED **19** by cellular esterases. **19** is subsequently activated by H_2O_2 to give the high affinity iron chelator HBBED **20**.

4.4 Photocleavable protecting groups in caged iron chelators

Photocleavable or photolabile protecting groups (PPGs) provide an opportunity to reversibly deactivate a target biological entity, which can be released upon irradiation with a specific wavelength of light.[162] The use of PPGs to 'cage' active compounds has been valuable in chemical synthesis, biochemistry and fluorescence-based studies *in vivo* and *in vitro*.[162-166] An ideal PPG should: render the caged group inactive, have a strong absorption at the relevant

wavelength for their release, be released through a clean photoreaction with a high quantum yield (efficiency of photorelease), and be stable in the absence of light.[162] 2-Nitrobenzyl and 2-nitrophenethyl moieties, for example 1-(2-nitrophenyl) ethyl (NPE, **21**), and their alkoxy derivatives, have been some of the most commonly used PPGs (see Figure 17). The caging of ATP with **21** (giving **22**) was reported in 1988 by Walker *et al.*, with the release of free ATP from the caged product being achieved upon irradiation at 342 nm.[167] Nucleobases caged with NPE-type PGGs have also been incorporated into DNA rendering them inactive, but they could be reactivated upon irradiation at 365 nm.[168,169] However, photolysis of this class of caging group generates potentially toxic by-products, for example *o*- nitrosobenzaldehyde which has also been shown to convert to azobenzene-2,2'-dicarboxylic acid and thus compete for the incident light, reducing the efficiency of cleavage of the PPG.[162,169] Therefore the use of alternative photolabile groups that do not possess these drawbacks would be desirable.

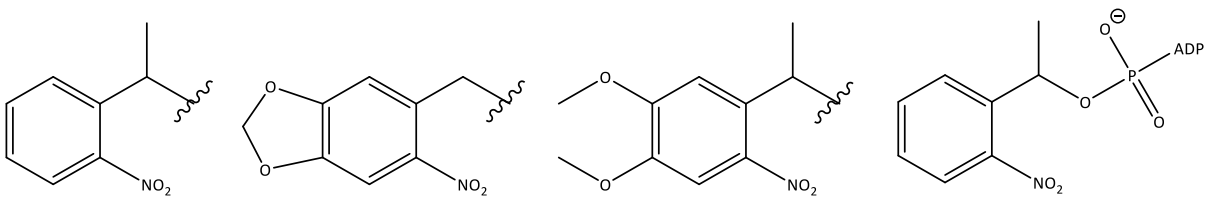

NPE, **21** NPE-ATP, **22**

Figure 17. NPE photolabile group (**21**) along with some photocleavable analogues and the first caged group, NPE-ATP (**22**).

In 1988, Turner *et al.* were the first to demonstrate the use of 2-hydroxycinnamoyl as a PPG for amines.[170] In this study, thrombin, a serine blood coagulation protease, was caged with 2-hydroxycinnamic acid to give the caged protease **23**. Photolysis of the inactivated enzyme resulted in the release of active thrombin along with a coumarin photoproduct **24** within 15 min (Scheme 7).[170] Subsequently, a series of photolabile compounds based on the 2-hydroxycinnamoyl scaffold were synthesised and tested for their ability to selectively inhibit proteases, enabling isolation and purification of these enzymes.[165]

The 2-hydroxycinnamoyl scaffold has also found use as a fluorescent reporter, termed the 'optical microsyringe'.[166,171] A simple alcohol, *e.g* ethanol, can be caged with this photolabile group, which can then be administered to probe a biological site of interest with unknown

characteristics, for example the volume of an organelle. Quantification of the fluorescent coumarin-type photoproduct released upon irradiation can then provide detailed biological insights.[166] In this context, 3,5-dibromo-2,4-dihydroxycinnamic acid has been described as a proof of concept photolabile group for the purpose of fluorescence reporting *in vivo*. The 3,5-dibromo-2,4-dihydroxycinnamoyl caged ethanol **25** is non-fluorescent, but upon irradiation at wavelengths >350 nm the fluorescent coumarin **26** is released, acting as a biomarker (Scheme 7).[171]

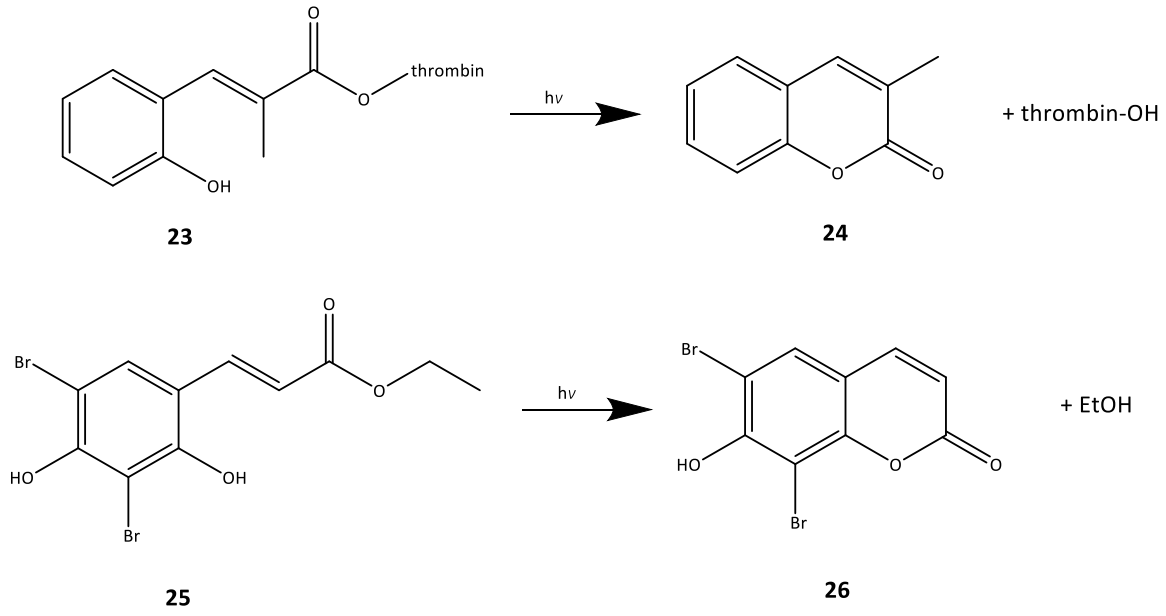

Scheme 7. Examples of 2-hydroxycinnamoyl photolabile caging groups and their coumarin photoproducts.

A development of this useful type of caging group is the 2-aminocinnamoyl caging group, which undergoes photolysis and subsequent expulsion of an alcohol or amine *via* the same mechanism as a 2-hydroxycinnamoyl derivative.[172] Aminocinnamoyl compounds may indeed provide more versatile functionality than the corresponding hydroxycinnamoyl groups. This is because the amino group provides a further site for substitution, unlike the hydroxyl group, while photocleavage results in the release of a carbostyril photoproduct as opposed to a coumarin.[172] A patent in 2000 described the use of the 2-aminocinnamic acid-derived PGGs to cage a range of amino acids in order to quantitatively measure the rise and fall of levels of certain amino acids in a biological system, for example glutamic acid[173] (Scheme 8).

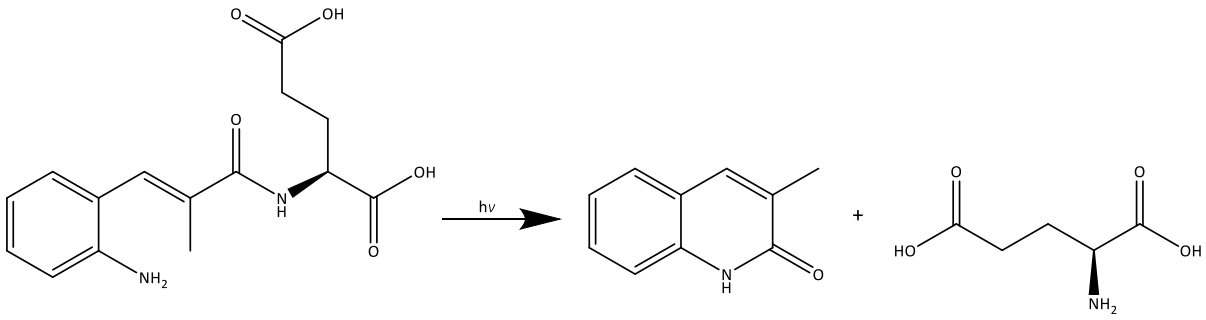

Scheme 8. An example of a 2-aminocinnamoyl-caged amino acid, glutamic acid. Upon irradiation the free amino acid and a carbostyril photoproduct are released.

The substantial information available around the use of photolabile groups and their applications in chemistry and biology led to the concept of forming a light-activated caged iron chelator (CIC) as a prodrug. Most iron chelators contain an iron-coordinating phenolic group which is a suitable moiety for caging with a PPG in order to render the iron chelator inactive. As UVA irradiation has been shown to give a substantial increase in labile iron,[57,151] the concept of a caged chelator that is activated upon UVA irradiation in order to chelate the excess iron produced is highly attractive. Yiakouvaki *et al.* investigated a proof of concept study into CICs where the phenolic groups of both SIH and PIH were masked with the photocleavable group **21** to give **27** and **28** (Scheme 9).[156] Upon UVA irradiation the free iron chelator was released along with the nitroso photoproduct. High performance liquid chromatography (HPLC) confirmed the conversion of the caged compound to the desired iron chelator upon exposure to UVA.[156] The calcein assay was used to investigate the level of UVA-induced labile iron in cells pre-treated with the caged compounds. Human fibroblasts pre-treated with CICs significantly reduced the UVA-induced labile iron in comparison to untreated UVA-irradiated cells.[156] Furthermore, the CICs did not deplete the basal levels of labile iron without UVA irradiation. However, high concentrations (100 µM) of the CICs were required to prevent UVA-induced necrotic cell death, and in particular **28** performed worse than the parent SIH for cell photoprotection.[156] It was suggested that the expected toxic properties of the nitroso photoproducts may be the cause of decreased efficiency of the CICs.[156]

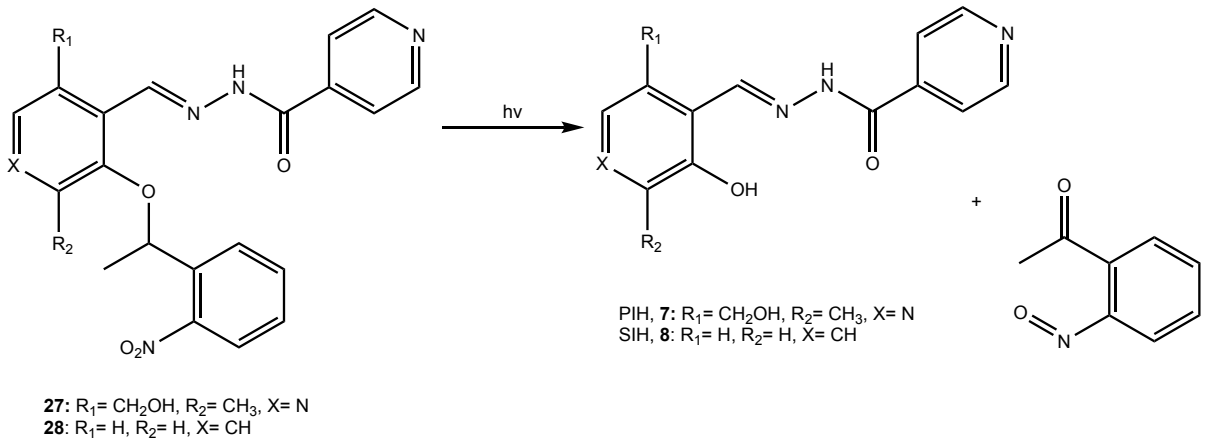

Scheme 9. Examples of CICs: NPE caged PIH **27** or SIH **28**. Upon UVA irradiation the free iron chelator PIH **7** or SIH **8** and a nitroso photoproduct are released.

In post-menopausal women, the major pathway of iron excretion is skin desquamation, and increased levels of iron in the skin have been implicated with an increase in oxidative damage here.[174] When combined with UVA exposure, this poses a serious health risk to this group of women. In a pilot study by Pelle *et al.,* the photoprotective ability of CIC **27** was also analysed in a post-menopausal cellular model.[174] At a concentration of 100 µM, **27** was able to significantly protect cells against lipid peroxidation in comparison to the untreated and irradiated control.[174]

Recently, Franks *et al.* described the caging of an aroylhydrazone chelator analogue, HAPI **29**, with an *o*-hydroxycinnamic acid PPG to give CIC **30**.[175] Upon UVA irradiation, **30** gives the free iron chelator along with a coumarin photoproduct, umbelliferone **31** (Scheme 10). **30** was analysed in terms of its ability to reduce UVA-induced ROS, and was shown to decrease ROS production in a concentration-dependant manner upon UVA irradiation.[175] **30** also showed efficient UVA photoprotection of ARPE-15 cells against necrotic cell death at concentrations up to 25 µM, which was comparable to the parent iron chelator on its own.[175] However, **30** showed a decrease in photoprotective ability at high concentrations of 50- 100 µM, which may indicate cytotoxicity.

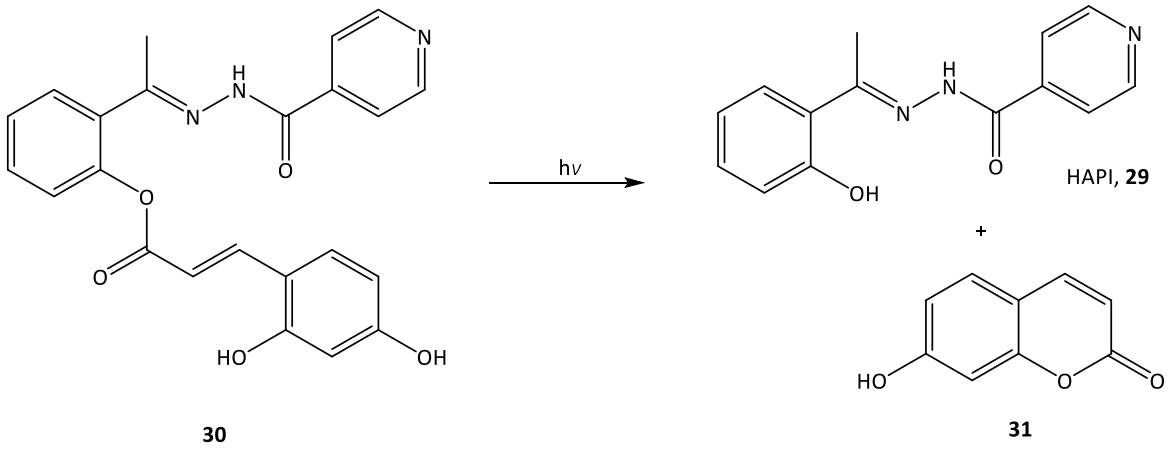

Scheme 10. The CIC **30** is cleaved upon UVA irradiation to give the free iron chelator HAPI **29** along with umbelliferone **31.**

These studies highlight the promise of light-activated CICs for combatting UVA-induced iron release, which leads to oxidative stress and subsequently photoaging and skin cancer. Further investigation into potent light-activated CICs should enable their full potential to be harnessed as prospective additions into current sunscreen formulations, to provide truly broad spectrum photoprotection and help reduce the current worldwide incidence of skin cancer.

5. Project aims

The incidence of skin cancer in the UK is increasing, and there is a direct link to over-exposure of the skin to harmful UVA and UVB radiation from the sun. The increasing incidence of skin cancer may be due to an increase in outdoor pursuits without correct photoprotection, the improper use of current sunscreen formulations, and also a lack of sunscreen ingredients that meet the necessary requirements for broad spectrum photoprotection. The mechanism of initiation of UVA-induced skin cancer is due to the oxidative nature of UVA and its ability to release intracellular labile iron (Section 1.4). Thus far there have been some attempts to develop 'activatable' iron chelators or 'prochelators' which are triggered by exogenous stimuli to release a high affinity iron chelator that can trap harmful iron. The activation of these prochelators proceeds either *via* oxidation or UVA irradiation, and these promising studies

have opened an interesting area of research into novel prochelating compounds that may add a new approach to photoprotection.

The overall aim of this project was to build upon the current strategies of activatable prochelators, and develop novel 'light-activated caged iron chelators' (CICs), capable of exhibiting a photoprotective effect in human fibroblasts when exposed to a physiological relevant dose of UVA. A key element of this work was to demonstrate the extent to which such optimised CICs may be able to complement the protection that is currently afforded by existing sunscreen products against iron-related UVA damage.

Within the overall project aim, the following detailed objectives were identified:

1. To develop an efficient synthetic pathway to a series of CICs, where well-studied iron chelators (including the clinically used deferasirox) were masked with hydroxycinnamic acid and aminocinnamic acid-derived photo-cleavable groups, and to assess the photoprotective capacity of these CICs.
2. To rationally design a novel series of CICs where the caging group is converted to an antioxidant moiety upon activation, based upon analysis of the capacity of the isolated antioxidants to scavenge UVA-induced ROS.
3. To investigate the capacity of improperly applied sunscreen formulations to prevent UVA-induced cell death and labile iron release, and the potential of CICs to augment the photoprotection afforded by sunscreen formulations.
4. To explore the synthetic pathway to a natural iron chelator, pulcherriminic acid, and assess its potential as a photoprotectant.

CHAPTER 2: RESULTS AND DISCUSSION

1. Introduction

The concept of light-activated caged iron chelators (CICs) as a tool to protect against UVA-induced labile iron release and subsequently skin cancer has been described in Section 1.4.4. In order to incorporate CICs into a suitable broad spectrum sunscreen formulation they need to have the following features: be activated readily under environmentally relevant doses of UVA irradiation e.g practical dose levels of solar UVA which would be commonly achieved whilst outdoors in the summer or on holiday; be lipophilic enough to enter skin cells easily; be non-toxic both with and without activation. Regarding toxicity, CICs should not bind iron and should not release cytotoxic photoproducts, but should provide a photoprotective effect against UVA-induced skin damage.[156] One of the most important design features of CICs is to render the parent iron chelator inactive when not exposed to UVA irradiation, as prolonged exposure to iron chelators has been shown to be harmful in a variety of cell lines.[100,154-156] For this reason, as well as the synthesis of iron chelators relevant to this work, an assessment of their cytotoxicity profiles under normal cellular conditions was initially required.

The structures and features of the three clinically used iron chelators, DFO **1**, deferiprone **2** and deferasirox **6** have been discussed in Section 1.3.3. The advantage of working with these iron chelators is that their clinical profiles have been elucidated, *i.e.* their metabolic stability, lipophilicity and dosage. DFO **1** has been long considered the 'gold standard' of iron chelators due to its high affinity for iron (pFe^{3+} = 26.6)[96] but its relatively high molecular weight and hydrophilicity, already make it unsuitable for topical application, and severely limit the scope for development of CICs . Deferiprone **2** has proven its worth as a bioavailable bidentate iron chelator, but its metabolic profile and the high dosage required to reach clinical efficiency is of concern. The tridentate iron chelator deferasirox **3** has a higher pFe^{3+} than **2** (22.5 and 20.4 respectively)[99,105] and is also more lipophilic, and these features make it the most desirable clinical iron chelator to use in a light-activated CIC. Although not used clinically, the aroylhydrazone family of iron chelators has been widely studied for therapeutic use, in particular PIH **7** and SIH **8**, as they both possess high pFe^{3+} values (26.2 and 24.6

respectively).[105] These iron chelators are lipophilic and uncharged at physiological pH, which along with their relatively low molecular weights makes them ideal for developing CICs.[96] Importantly, all of the suitable iron chelators mentioned above have structures in which one of their iron-binding functions can be readily masked or deactivated.

2. Synthesis of iron chelators and their cellular activity

The synthesis of the two aroylhydrazone iron chelators **7** and **8** *via* a simple condensation reaction is shown in Scheme 11. The required aldehyde was treated with isonicotinylhydrazide (INH) in EtOH at reflux[176] giving the desired iron chelators **7** and **8** in 85% and 95% yields respectively.

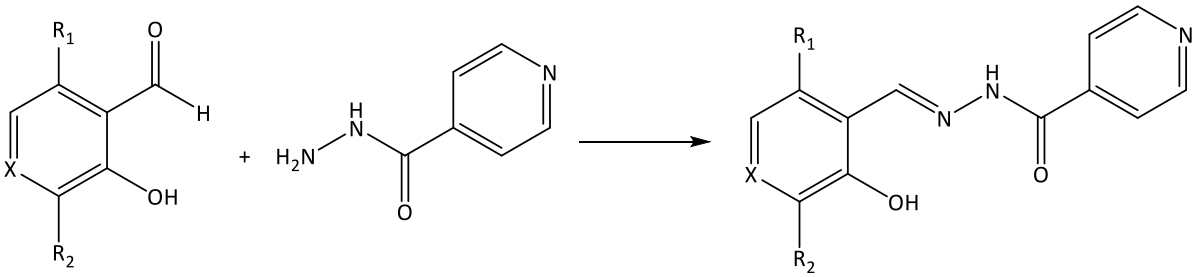

Pyridoxal HCl: R_1= CH_2OH, R_2= CH_3, X= N
Salicylaldehyde: R_1= H, R_2= H, X= CH

PIH, **7**: R_1= CH_2OH, R_2= CH_3, X= N
SIH, **8:** R_1= H, R_2= H, X= CH

Scheme 11. Synthetic route to aroylhydrazone iron chelators PIH **7** and SIH **8**. *Reagents and conditions:* **7.** EtOH, aq. NaOAc, reflux, 1.5 h, 85%; **8.** EtOH, reflux, 3 h. 95%.

The synthesis of the clinical iron chelator **6** was achieved by a straightforward two-step procedure starting from salicylic acid and salicylamide, as shown in Scheme 12.[8] In the first step, reaction of salicylic acid with thionyl chloride generates an acid chloride *in situ*, which then combines with salicylamide under reflux in xylene. This gave the water-sensitive benzoxazinone intermediate **32** in a 65% yield.[98] Condensation of **32** with 4-hydrazinobenzoic acid was then achieved by refluxing in EtOH in the presence of NEt_3 to give deferasirox **6** in 85% yield.[98] In order to simplify the subsequent preparation of CIC derivatives, the carboxylic acid function of **6** was converted to the methyl ester, which would also have the added benefit of producing CICs that would be uncharged at physiological pH and therefore would pass into

cells more easily. Esterification of **6** was simply achieved by refluxing overnight in anhydrous MeOH with a catalytic amount of H_2SO_4 to give **33** in high yield.

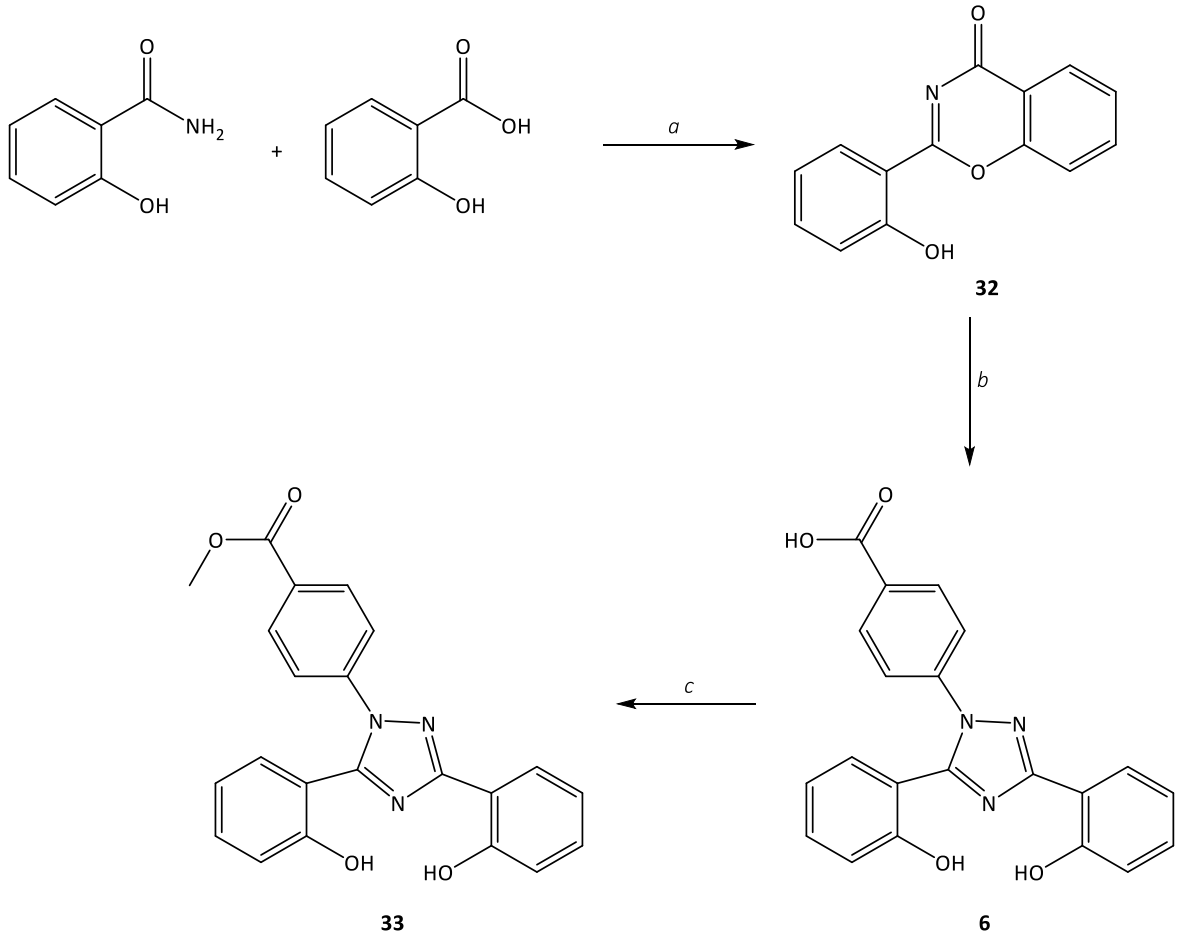

Scheme 12. Synthetic route to clinical iron chelator deferasirox **6** and deferasirox ester **33**. *Reagents and conditions:* **a.** pyridine, thionyl chloride, xylene, reflux, 3.5 h, 65%; **b.** 4-hydrazinobenzoic acid, NEt_3, EtOH, reflux, 2.5 h, 85%; **c.** MeOH, H_2SO_4, reflux, O/N, 95%.

The synthesised iron chelators **7**, **8** and **33** were analysed for their cytotoxicity under conditions of prolonged exposure in a human skin cell line. FEK4 cells, primary human dermal fibroblasts, were chosen for this work as they have been previously shown to be a good cell model in which to study the exposure of human skin to solar UVA irradiation, which penetrates as far as the dermal layer of skin.[56,156,177] Cell viability upon exposure to iron chelators was assessed using the MTT (3-(4,5-dimethylthiazol-2-yl)-2,5-diphenyl tetrazolium bromide) assay. In this simple quantitative colorimetric assay, MTT, which is colourless in solution, is converted by cellular and mitochondrial dehydrogenase enzymes into formazan,

a dark-blue material that is water-insoluble. The amount of formazan produced is directly proportional to the number of viable cells.[178] Concentrations of 10, 20 and 50 μM of iron chelators were chosen; this range was based on concentrations previously reported in studies of skin cell photoprotection with iron chelators.[48,156,174] Incubation periods of 24 and 48 h were used, as shown in Figures 18 and 19.

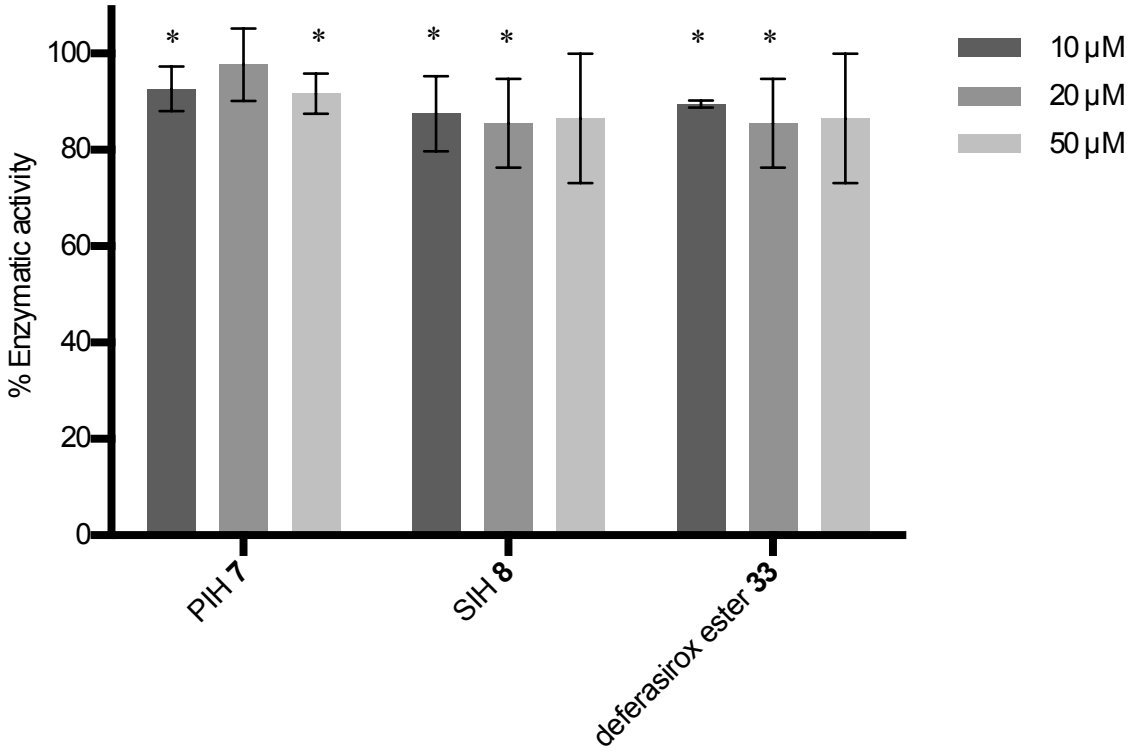

Figure 18. MTT assay evaluation of the effect of prolonged exposure of FEK4 fibroblasts to iron chelators PIH **7**, SIH **8** and deferasirox ester **33**. Cells were treated with 10, 20 and 50 μM iron chelator for 24 h followed by MTT analysis 24 h later. Data is expressed as mean ± SD compared to the untreated control, which was fixed at 100% enzymatic activity (n=3).

*= $p < 0.05$, significantly different from the untreated control.

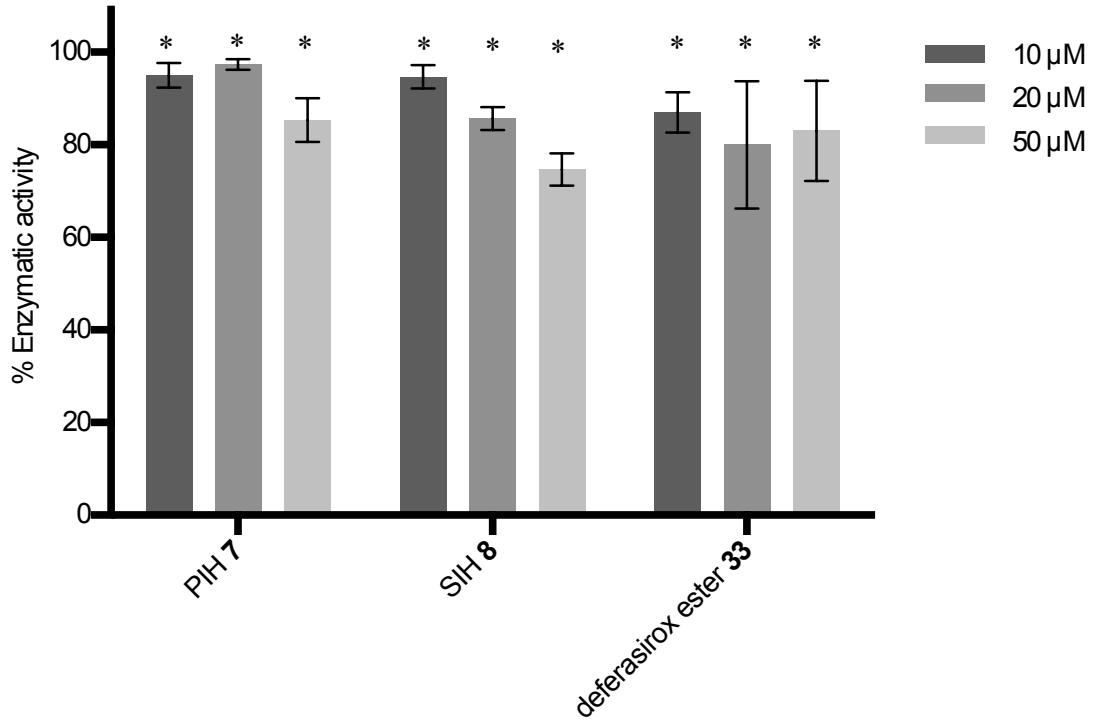

Figure 19. MTT assay evaluation of the effect of prolonged exposure of FEK4 fibroblasts to iron chelators PIH **7**, SIH **8** and deferasirox ester **33**. Cells were treated with 10, 20 and 50 µM iron chelator for 48 h followed by MTT analysis 24 h later. Data is expressed as mean ± SD compared to the untreated control, which was fixed at 100% enzymatic activity (n=3).

*= $p < 0.05$, significantly different from the untreated control.

The results of the MTT cytotoxicity assays indicated that after 24 h of exposure **8** and **33** decreased cell viability to 85-90% of the untreated control at all concentrations, however not all results were statistically significant. On the other hand, cells exposed to **7** for 24 h remained above 90% cell viability in comparison to the control. Upon exposure of FEK4 cells to **8** and **33** for 48 h, there was a marked reduction in cell viability at concentrations of 20 and 50 µM. **7** also exhibited a reduction in cell viability to 82% of the untreated control at a concentration of 50 µM. These results indicate that there is some evidence of both dose level and exposure time affecting cell viability as the iron chelators remove iron from essential enzymes. For the purpose of skin photoprotection, these findings exemplify the need to deactivate these iron chelators with a group that can be removed upon exposure to an environmentally relevant dose of UVA irradiation to release an active iron chelator.

3. Hydroxycinnamoyl-caged iron chelators

The group of Porter first introduced the hydroxycinnamoyl group as a useful PPG in work involving caged serine proteinases[165,170] as described in Section 1.4.4. The mechanism of photo-cleavage of the hydroxycinnamoyl protecting group proceeds *via* the alkene bond absorbing a photon and subsequently undergoing *E/Z* photoisomerization. This conversion of stereochemistry brings the ester carbonyl group into closer proximity with the *o*-phenolic hydroxyl group, which enables nucleophilic attack on the carbonyl and subsequent cyclization with release of an alcohol or phenol,[170] as shown in Scheme 13.

The photoproduct formed from a hydroxycinnamoyl PPG is a coumarin, which is of particular interest because of the reported antioxidant activity of coumarin-type molecules found in plants.[179,180] Various plant-derived coumarins have been investigated for their potential as therapeutic agents, for example against intestinal inflammatory disease, due to their antioxidant properties and ability to inhibit lipid peroxidation.[180] Different substituents on the benzopyrone scaffold of coumarins have been shown to alter the antioxidant potential of natural coumarins, for example umbelliferone, esculetin and scopoletin **34b**-**d** shown in Scheme 13. In particular, the presence of electron-donating groups such as hydroxy and methoxy groups seems to enhance the radical scavenging properties of these compounds.[179,180] In two recent studies on the antioxidant activity of plant-derived coumarins, it was found that **34c** (with the 6,7-dihydroxy motif) was one of the strongest ROS quenchers amongst a range of coumarin derivatives.[179,180]

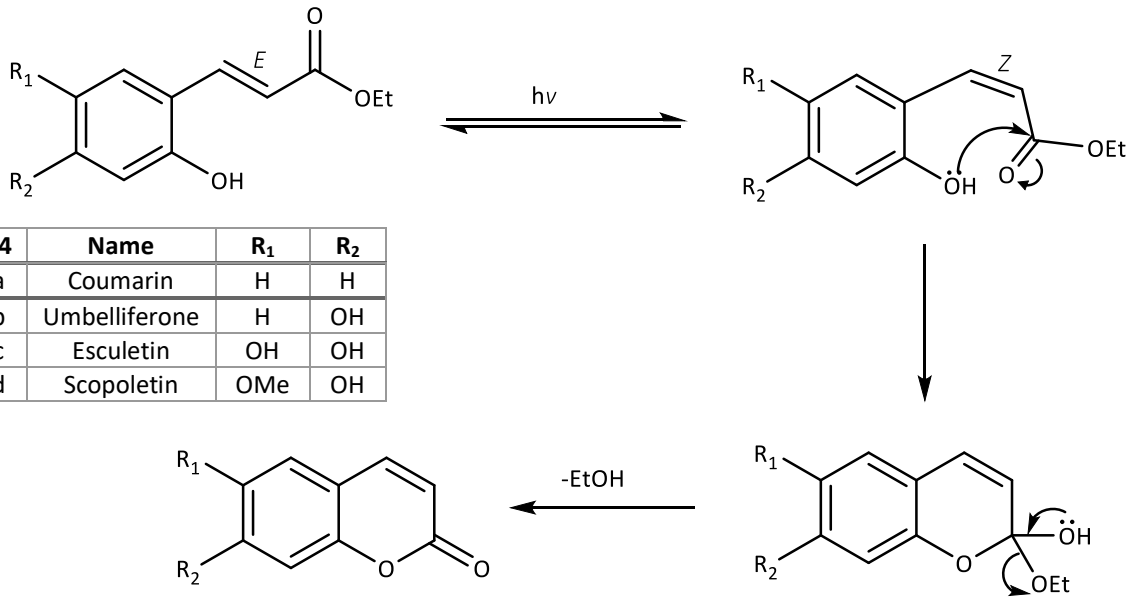

34	Name	R_1	R_2
a	Coumarin	H	H
b	Umbelliferone	H	OH
c	Esculetin	OH	OH
d	Scopoletin	OMe	OH

Scheme 13. Mechanism of photo-release of a hydroxycinnamoyl-caged alcohol upon UVA irradiation to give a coumarin photoproduct.

The hydroxycinnamoyl group is therefore an attractive PPG for an iron chelator. The phenolic group of iron chelators **7**, **8** and **33** would normally be involved in coordinating iron, consequently this phenolic group provides the perfect opportunity to mask the iron-binding capability of an iron chelator through protection as an ester. Upon cleavage of the photolabile group by UVA irradiation, an active iron chelator would be released to quench the generation of intracellular labile iron along with a coumarin fragment which could provide a complementary antioxidant effect.

To begin the synthesis of cinnamoyl-based CICs, *trans*-2-hydroxycinnamic acid **35** was chosen as the starting material as it was commercially available and upon photo-cleavage of the CIC, the simplest photoproduct **34a** would be released. The use of carbodiimide reagents is one of the most common approaches for carboxylic acid activation in order to form an ester or amide bond,[181] with the most well-known carbodiimide being *N, N*'- dicyclohexylcarbodiimide (DCC). During a coupling reaction using DCC, the by-product dicyclohexylurea (DCU) is formed, which can often be simply filtered off due to its insolubility in non-polar solvents. In many cases, *N*-ethyl-*N'-(*3-dimethylaminopropyl)carbodiimide (EDC) can be a more advantageous carbodiimide as its urea by-product is water-soluble and can therefore be removed easily in

an aqueous work-up.[181] As shown in Scheme 14, the initial reaction between a carboxylic acid and a carbodiimide activating reagent forms an *O*-acylisourea. This intermediate can either react with another carboxylate species to form a symmetric anhydride, or it may react directly with an alcohol (or amine) nucleophile to form the desired coupled product.[181] Intramolecular rearrangement of the *O*-acylisourea intermediate to an unreactive *N*-acylurea occurs readily between pH 3-6 and slowly at pH values above 7, which prevents formation of the coupled product whilst consuming the carboxylate. In the synthesis of esters this may be overcome by addition of *N,N'*-dimethylaminopyridine (DMAP) which rapidly converts the *O*-acylisourea intermediate to an acyl pyridinium species which can then react with an alcohol to give the desired ester.[181,182]

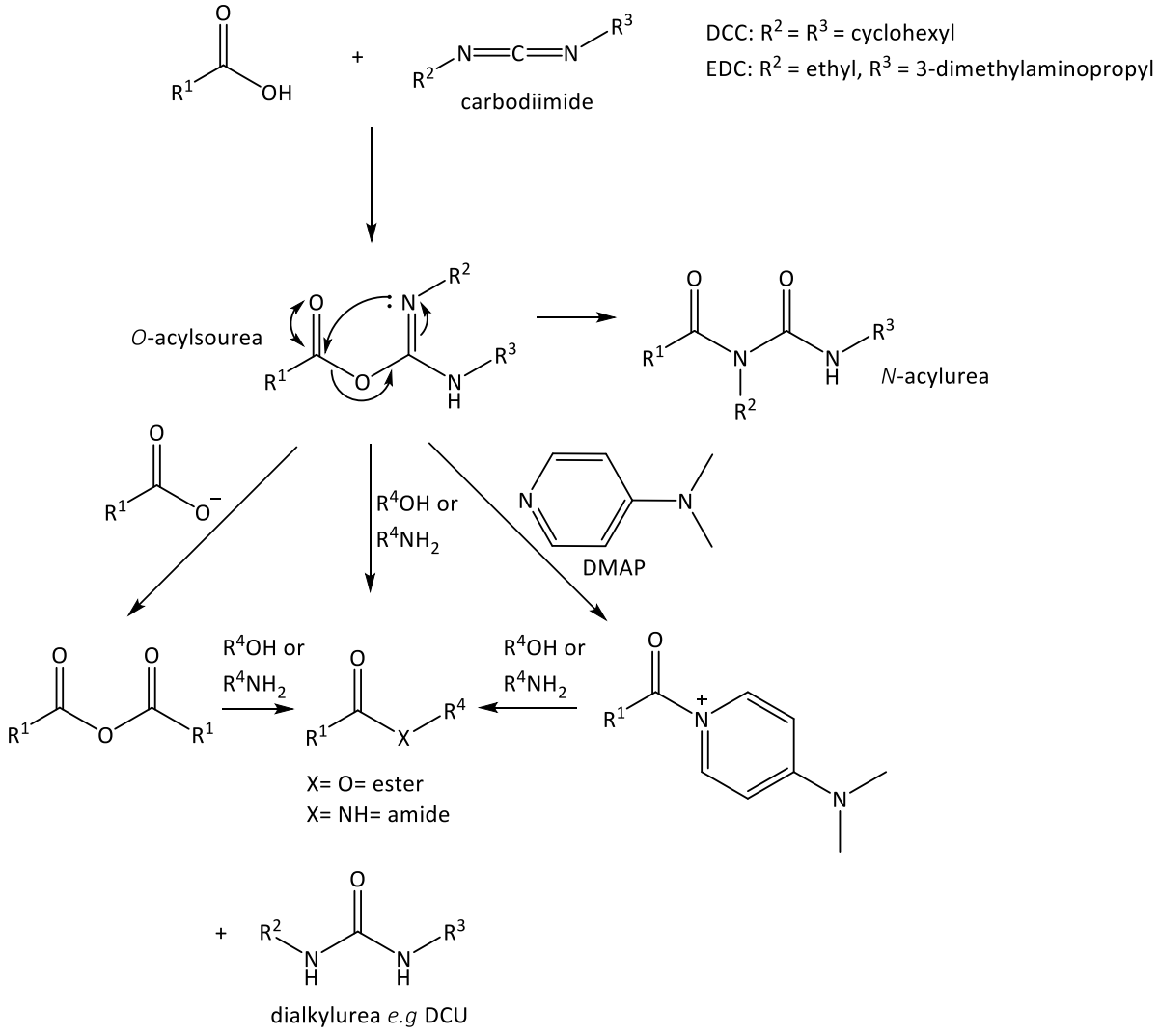

Scheme 14. Carbodiimide-mediated ester or amide formation starting from a carboxylic acid. The mechanism for rearrangement of the initial *O*-acylisourea formed to an unreactive *N*-acylurea is shown.

The acid **35** was activated with one equivalent of both EDC.HCl and DMAP at 0°C for 10 min in anhydrous DMF, before addition of the iron chelator **8** in the presence of one equivalent of diisopropylethylamine (DIPEA) in anhydrous DMF (Scheme 15). Mass spectrometry and NMR analysis of the crude reaction material indicated the presence of the desired CIC **36** along with coumarin **34a**, presumably formed by cyclisation of the activated acid **35**. The two products were impossible to separate *via* column chromatography.

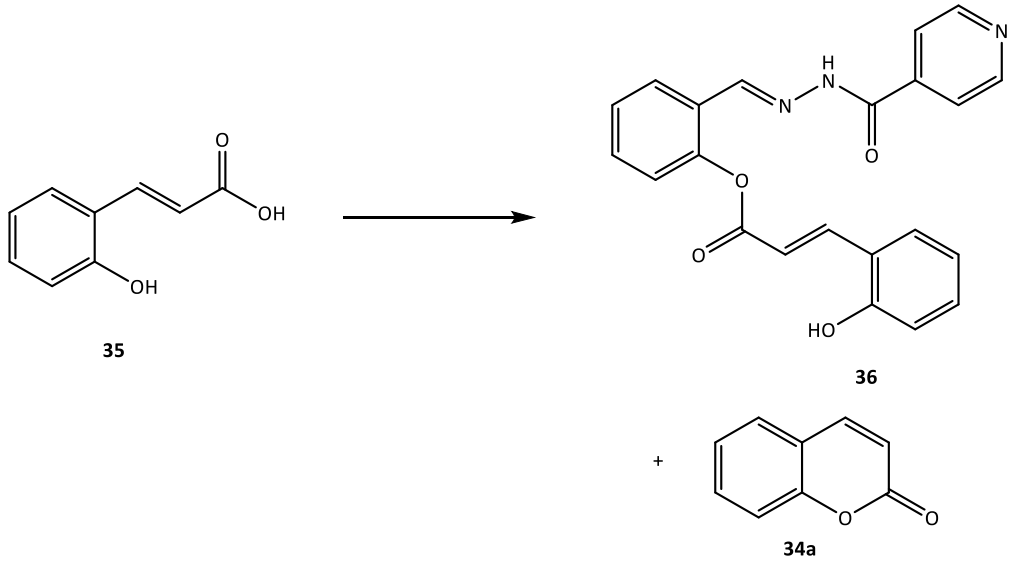

Scheme 15. Attempted synthetic route to 2-hydroxycinnamoyl SIH CIC **36** along with **34a** by-product. *Reagents and conditions:* DMAP, EDC.HCl, **8**, DIPEA, dry DMF, 0 °C → RT, O/N.

Although these results showed that the desired CIC **36** could be synthesised *via* this coupling method, the difficult purification and formation of a significant amount of **34a** was unsatisfactory. In order to prevent the formation of **34a** during the reaction, protection of the 2-hydroxyl group in **35** was required. Masking of a phenolic hydroxyl can be typically accomplished through conversion to a benzyl ether. However for our purposes protection *via* a benzyl ether was unsuitable due to the deprotection methods required. Cleavage of benzyl ethers is usually achieved by using hydrogenation or strong acid,[183] which are both incompatible with the structures of **35** or the desired CIC. For this reason, a silyl ether was a very attractive form of protection as they are easy to form and inert under a range of acidic and basic conditions,[184] but can be effectively removed in the presence of fluoride ions, for example with tetra-*N*-butylammonum fluoride (TBAF), due to the strength of the Si-F bond.[184-

[186] There is a variety of silyl ether protecting groups available with various substituents, the most commonly used being trimethylsilyl (TMS), triethylsilyl (TES), *t*-butyldimethylsilyl (TBS), triisopropylsilyl (TIPS) and *t*-butyldiphenylsilyl (TBDPS).[183] Generally the bulkier silyl groups decrease the rate of ether cleavage under acidic or basic conditions.[184] TBS was chosen as the most suitable protecting group for this work as it is reasonably stable under both acidic and basic conditions, but the alkyl substituents are not too large, and so limited interference with the acylation reaction should be expected.[186]

Silyl ether protection of the hydroxyl function of **35** was achieved by first globally protecting both the acid and hydroxyl function with TBS in the presence of imidazole as base and catalyst[185] to give **37** (Scheme 16). Selective deprotection to give the acid **38a** was first attempted under basic conditions using a method by Okamoto *et al.* which described selective cleavage of the more labile TBS ester protecting group using the mild base, K_2CO_3.[187] This method was however only partially successful as the phenolic TBS ether of **37** was also found to be cleaved under Okamoto's conditions. Switching to acidic conditions, it was found that stirring **37** in 0.3% TFA in MeCN at room temperature was an effective alternative method for selective cleavage of the TBS ester, giving excellent yields of the protected cinnamic acid **38a**. Coupling of **38a** to the iron chelator **8** was attempted using the same conditions as previously described in Scheme 15. However, no reaction was observed, possibly due in fact to the additional steric bulk of the TBS protecting group. It was therefore decided to convert **38a** into a more powerful acylating agent, an acyl halide. Acyl halides are strongly electrophilic and therefore useful for forming hindered esters.[181] Conversion of **38a** to the acid chloride **38b** using thionyl chloride proceeded well, with the TBS protecting group stable enough to withstand the HCl generated,[187] (Scheme 16). Due to the expected moisture sensitivity of **38b**, it was reacted immediately with **8** in the presence of one equivalent of pyridine and a catalytic quantity of DMAP (0.1 equivalent) in anhydrous DMF to give the desired protected CIC **39** in 27% yield. 24% of the starting acid **38a** was recovered giving an overall conversion of 36%.

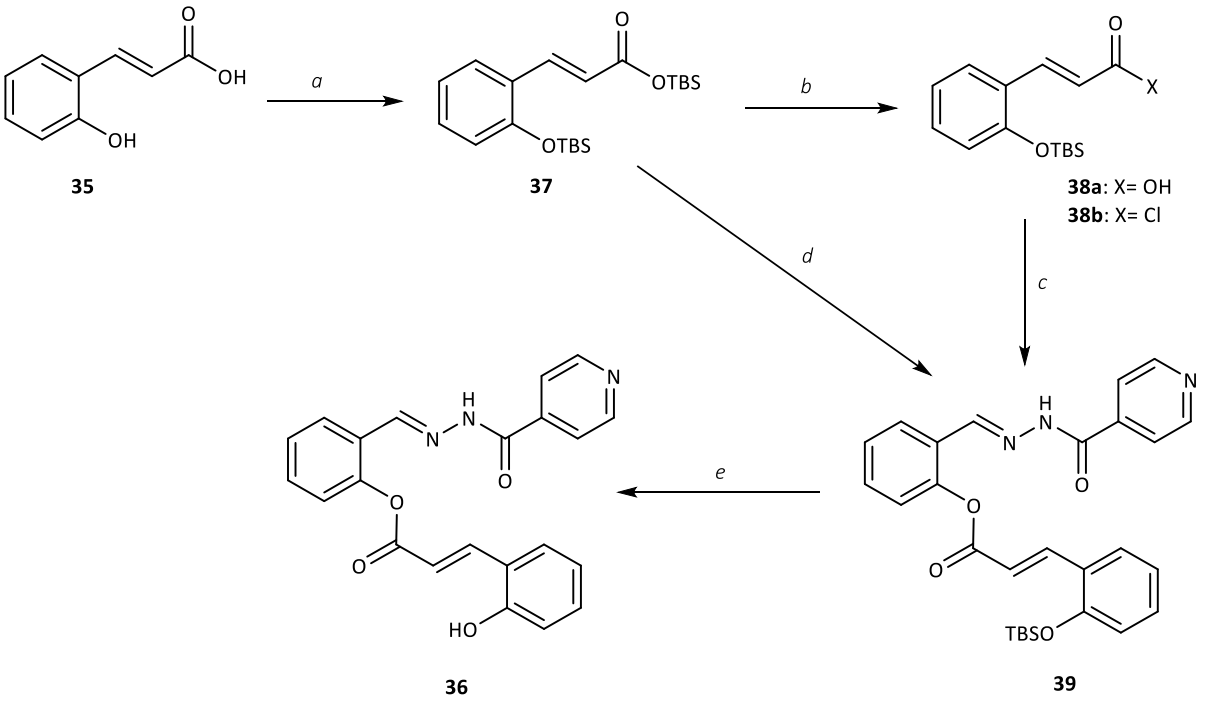

Scheme 16. Synthetic route to 2-hydroxycinnamoyl SIH CIC, **36**. *Reagents and conditions*: **a**. TBS-Cl, imidazole, anhydrous DMF, RT → 60 °C, O/N, 83%; **b.** (i) 0.3% TFA, MeCN, RT, O/N, 98%; (ii) $SOCl_2$, anhydrous DCM, reflux 4 h; **c. 8**, pyridine, DMAP, anhydrous DMF/dry DCM, 30 °C, 2 days, 27%; **d.** (i) $(COCl)_2$ in DCM, DMF, 0 °C, 3 h (ii) **8**, pyridine, DMAP, anhydrous DMF/anhydrous DCM, 30 °C, 2 days, 22-25%; **e.** TBAF, AcOH, anhydrous DMF, 0 °C, 30 min, 86%.

In order to improve the efficiency of the preparation of **39**, some variations of the acid chloride coupling were also explored. Using the same conditions but with anhydrous DCM as an alternative coupling solvent gave no increase in yield. Wissner *et al.* reported the conversion of TBS-protected carboxylic acids directly to the acid chloride using oxalyl chloride and catalytic DMF to form a Vilsmeier reagent.[188] This method was employed and **37** was directly converted to the acid chloride and coupled with SIH as previously to give **39** in a 22-25% yield depending on the chosen solvent (route d, Scheme 16). The overall conversion taking into account the recovery of **38a** was 31-35%. Cleavage of the protecting group was achieved using TBAF[186] in the presence of acetic acid, which provided a neutral reaction pH to prevent basic hydrolysis of the ester bond. This gave the final 2-hydroxycinnamoyl caged-SIH CIC **36**.

An analogous approach was taken to synthesise the 2,4-hydroxycinnamoyl-SIH CIC **44** shown in Scheme 17. Upon UVA irradiation this PPG would give the photoproduct umbelliferone **34b.** The synthesis was carried out *via* the same methodology as with the 2-hydroxy derivative and the globally silyated ester **41** was obtained in good yield (73%) and converted to the silyated cinnamic acid **42a** with 0.3% TFA in excellent yield (95%). The thionyl chloride method to convert **42a** to **42b** and subsequent esterification with SIH gave an overall conversion to the coupled product of 10-18% (4-10% yield) depending on the solvent used. Complete conversion of acid **42a** to the acid chloride **42b** was observed and no generation of umbelliferone **34b** was seen during the esterification step. HPLC analysis of the crude reaction material after two days of reaction indicated the presence of both the acid **42a** and SIH **8**.

The coupling reaction using oxalyl chloride was also attempted (route d, Scheme 17), and it was found necessary to increase the equivalents of pyridine to equal the equivalents of oxalyl chloride (3 equivalents). With fewer equivalents of pyridine, complex mixtures were observed presumably due to cleavage of the TBS groups by the HCl generated. The overall conversion to **43** using this method was 31% from a yield of 9%, as 71% of the starting acid **42a** was recovered. Similarly to the thionyl chloride method, HPLC analysis of the crude material showed that other than the coupled product **43**, only **42a** and **8** were present. Presumably the steric bulk of both the 2 and 4-TBS protecting groups again limited the reaction of the acid chloride **42b** with **8**, such that the reaction was proceeding so slowly that the acid chloride **42b** was competitively hydrolysed back to the unreactive acid **42a**. Cleavage of the protecting group was again accomplished using TBAF[186] in the presence of acetic acid to give full conversion to the final 2,4-dihydroxycinnamoyl CIC **44,** however it was very water soluble and remained in the aqueous phase upon extraction leading to only a 15% recovery.

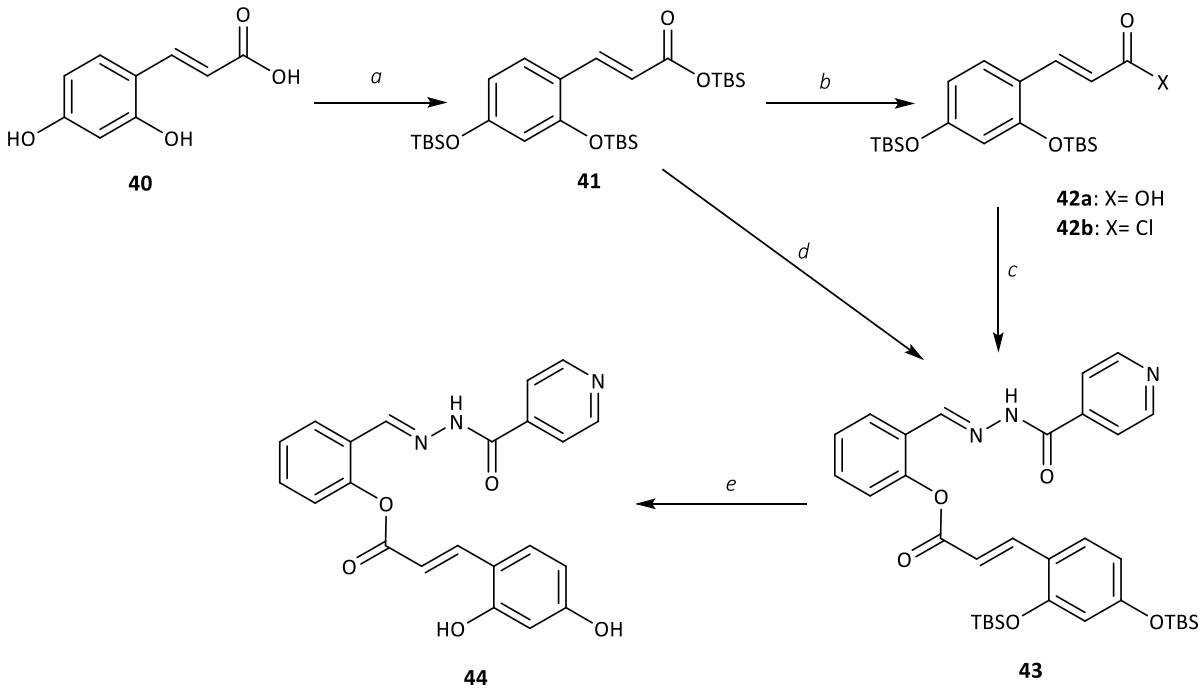

Scheme 17. Synthetic route to 2,4-hydroxycinnamoyl SIH ClC, **44**. *Reagents and conditions*: **a**. TBS-Cl, imidazole, anhydrous DMF, 60 °C, O/N, 73%; **b.** (i) 0.3% TFA, MeCN, RT, O/N, 95%; (**ii**) $SOCl_2$, anhydrous DCM, reflux 4 h; **c. 8**, pyridine, DMAP, anhydrous DMF/dry DCM, 30 °C, 2 days, 4-10%; **d.** (i) $(COCl)_2$ in DCM, DMF, 0 °C, 3 h (ii) **8**, pyridine, DMAP, anhydrous DMF, 30 °C, 2 days, 9%; **e.** TBAF, AcOH, anhydrous DMF, 0 °C, 1.5 h, 15%.

As it was envisaged that the steric bulk of both the 2 and 4-TBS protecting groups was limiting the coupling of the acid chloride **42b** with **8,** an alternative approach was explored. In order to overcome the difficulty of coupling the sterically hindered **42b** to the *ortho*-substituted phenolic component **8**, coupling of **42b** to the scaffold aldehyde of **8**, salicylaldehyde, was performed. Salicylaldehyde is a phenol with a much smaller *ortho* substituent than **8** therefore it was expected that the steric impact on the coupling reaction would be reduced. Scheme 18 shows the coupling of salicylaldehyde and **42b** which proceeded in a 33% yield to give the intermediate **45**, although full conversion of salicylaldehyde was not observed. **45** was used in the next step without purification. After refluxing **45** with INH in EtOH for 24 h, TLC analysis showed that **45** was still present in the reaction mixture, but conversion to **43** was observed. The reaction gave a 21% yield of **43**, corresponding to a 7% yield over the two steps from salicylaldehyde.

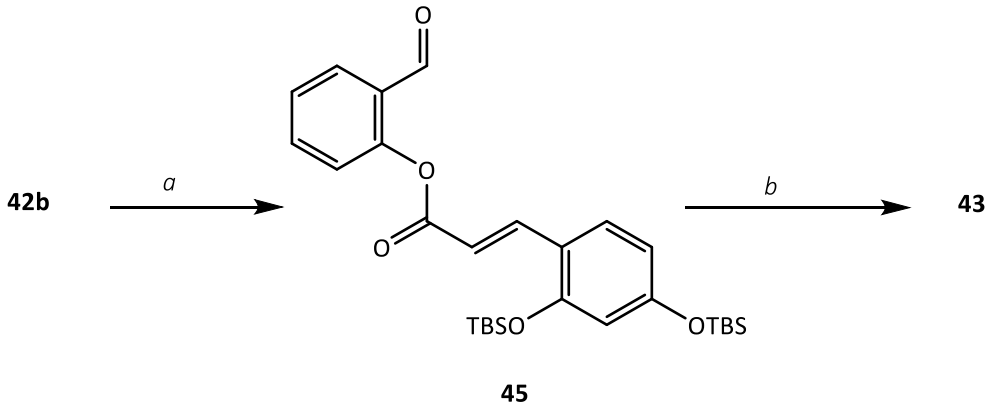

Scheme 18. Alternative synthetic route to 2,4-TBS cinnamoyl-SIH, **43**. *Reagents and conditions:* **a.** salicylaldehyde, pyridine, DMAP, anhydrous DCM, 30 ^{o}C, 2 days, 33%; **b.** INH, EtOH, 40 ^{o}C → reflux, 24 h, 21%.

The coupling reactions to form hydroxycinnamoyl-SIH CICs **36** and **44** were successful, although the yields were very modest, and so the synthesis of a hydroxycinnamoyl-caged deferasirox derivative was also attempted. Deferasirox **6** has two phenolic hydroxyl groups involved in iron coordination, which could both be masked with a photo-cleavable hydroxycinnamoyl protecting group. Both phenolic groups are chemically very similar, therefore little selectivity for the esterification of either phenolic function was anticipated, implying a mixture of products would be formed. For this reason coupling of the 2-TBS cinnamic acid chloride **38b** to the deferasirox intermediate **32** was first attempted as it only presented one phenolic hydroxyl (Scheme 19). This intermediate **32** was anticipated to be less sterically hindered than deferasirox methyl ester **33**. Unfortunately the attempted coupling with **32** to give the proposed CIC intermediate **46** failed, with neither starting material being consumed after two days of reaction, consequently this synthetic route was not pursued any further.

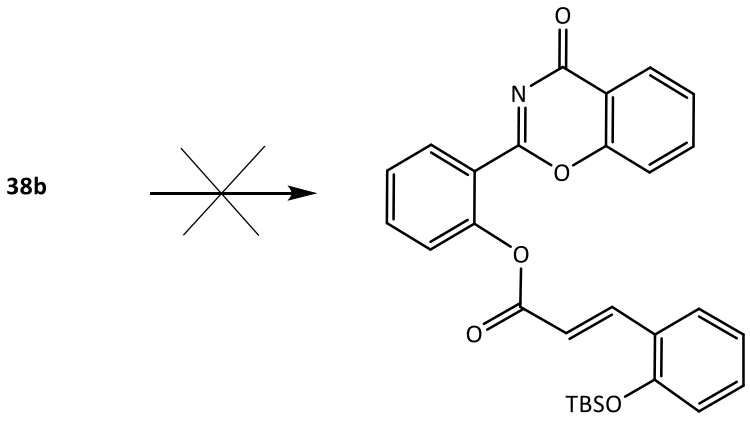

46

Scheme 19. Attempted coupling of 2-TBS cinnamic acid chloride **38b** with benzoxazinone **32**. *Reagents and conditions:* **32**, pyridine, DMAP, anhydrous DMF/anhydrous DCM, 30 °C → 100 °C, 2 days.

The UV/Vis absorbance spectra of both synthesised CICs **36** and **44** were recorded to confirm that the CICs absorbed in the relevant UVA wavelength range (320- 400 nm). Figure 20 shows that **36** absorbs maximally at 290 nm (in the UVB wavelength range) with a molar absorptivity of ε_{290}= 15,200 L mol^{-1} cm^{-1}, and continues to absorb significantly up to 380 nm, which covers a considerable portion of the UVA range.

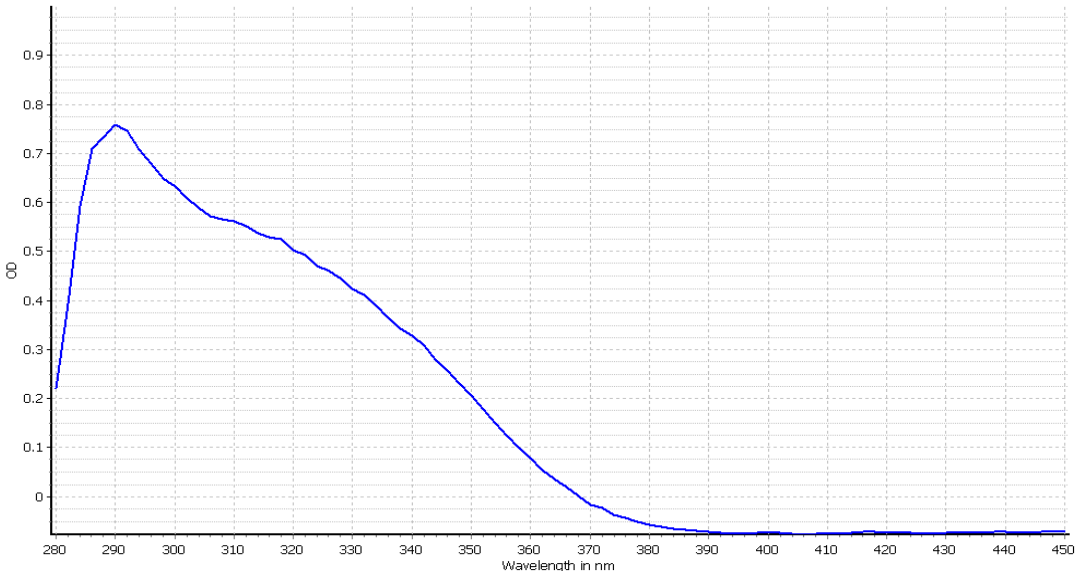

Figure 20. UV/Vis absorbance spectrum of CIC **36** in DMSO (50 μM).

The additional 4-hydroxy group in CIC **44** gives a red shift in absorbance, as shown in Figure 21. The maximal absorbance is 304 nm with a lower molar absorptivity of ε_{304}= 7,500 L mol^{-1} cm^{-1}, while **44** also continues to absorb through the UVA region to 395 nm. This corresponds to the observation of Gagey *et al.* that in a series of hydroxycinnamoyl-caged ethanol compounds, increasing the electron-donating power of substituents on the aromatic ring red-shifts the wavelength of maximum absorption.

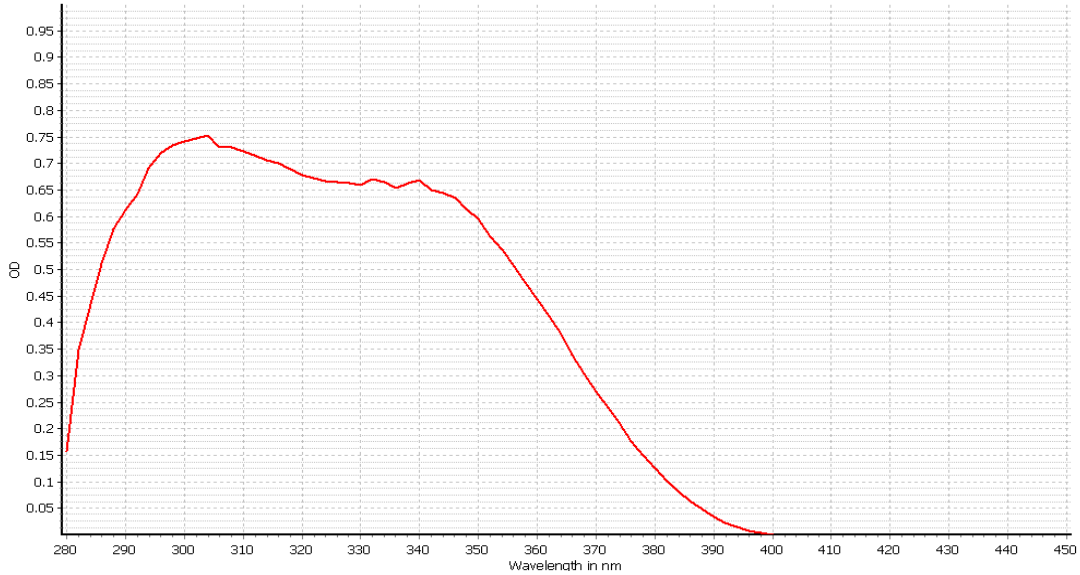

Figure 21. UV/Vis absorbance spectrum of CIC **44** in DMSO (100 μM).

As the CICs **36** and **44** were shown to absorb within the relevant UVA window, it was next important to ensure that they would be 'uncaged' by environmentally relevant doses of UVA irradiation to which a person's skin may be exposed to on a summer's day. It has previously been reported that a few hours of sun exposure at noon in Southern Europe would provide a dose of 500 kJ/m^2 of UVA radiation.[189] To confirm this, an IL1700 radiometer was used outdoors at the University of Bath on the 26th June 2017 to obtain readings for solar UVA on a British summer day. Readings were taken between 12.00 and 15.00 BST and the temperature in direct sunlight during this time was 35^{o}C. The readings indicated that a 500 kJ/m^2 UVA dose was equivalent to only 80 min in the sun on this day, which highlights the importance of adequate sunscreen protection.

The erythema response to UVR exposure is significant in SPF testing and is also a useful biological endpoint for the comparison of UVA radiation doses. Conversly to UVB-induced

erythema where damage is caused by direct absorption, UVA-induced erythema is mediated *via* ROS generation.[190] An erythemal response to UVR exposure can either be expressed as a physical dose (kJ/m^2) or as a biological dose (MED), the MED differs between individuals as skin type controls sensitivity to UVR. Therefore it is important to make reference to MED along with dose of UVA radiation used throughout this discussion. In a study by Harrison *et al.* an MED response was visualised in volunteers with skin types I and II after UVA doses ranging between 300-700 kJ/m^2, thus on average a 500 kJ/m^2 UVA dose is approximately equivalent to one MED.[190] When SSR is used rather than solely UVA radiation, one MED in skin types I and II is equivalent to a dose of approximately 40 kJ/m^2 due to the impact of the additional damaging UVB radiation.

The percentage of the incident dose of UVA radiation that would reach the accumulation of CIC in the cytosol depends largely on the individual's skin type (pigmentation), but it is estimated to be on average 10-20% of the incident dose due to absorption by chromophores.[191] For example, performing chemical (extracellular) irradiation of a CIC using a dose of 50 kJ/m^2 would be equivalent to a dose of 250-500 kJ/m^2 (0.5- 1 MED) if the CIC was in the skin. Therefore the uncaging of CICs by a dose of 50 kJ/m^2 to give a free iron chelator is critical. The intact CIC **36** was irradiated at increasing doses of UVA and the extent of uncaging was followed on analytical HPLC (the detailed method is outlined in the Experimental 7.2.4.2. The HPLC chromatograms are shown in Figure 22.

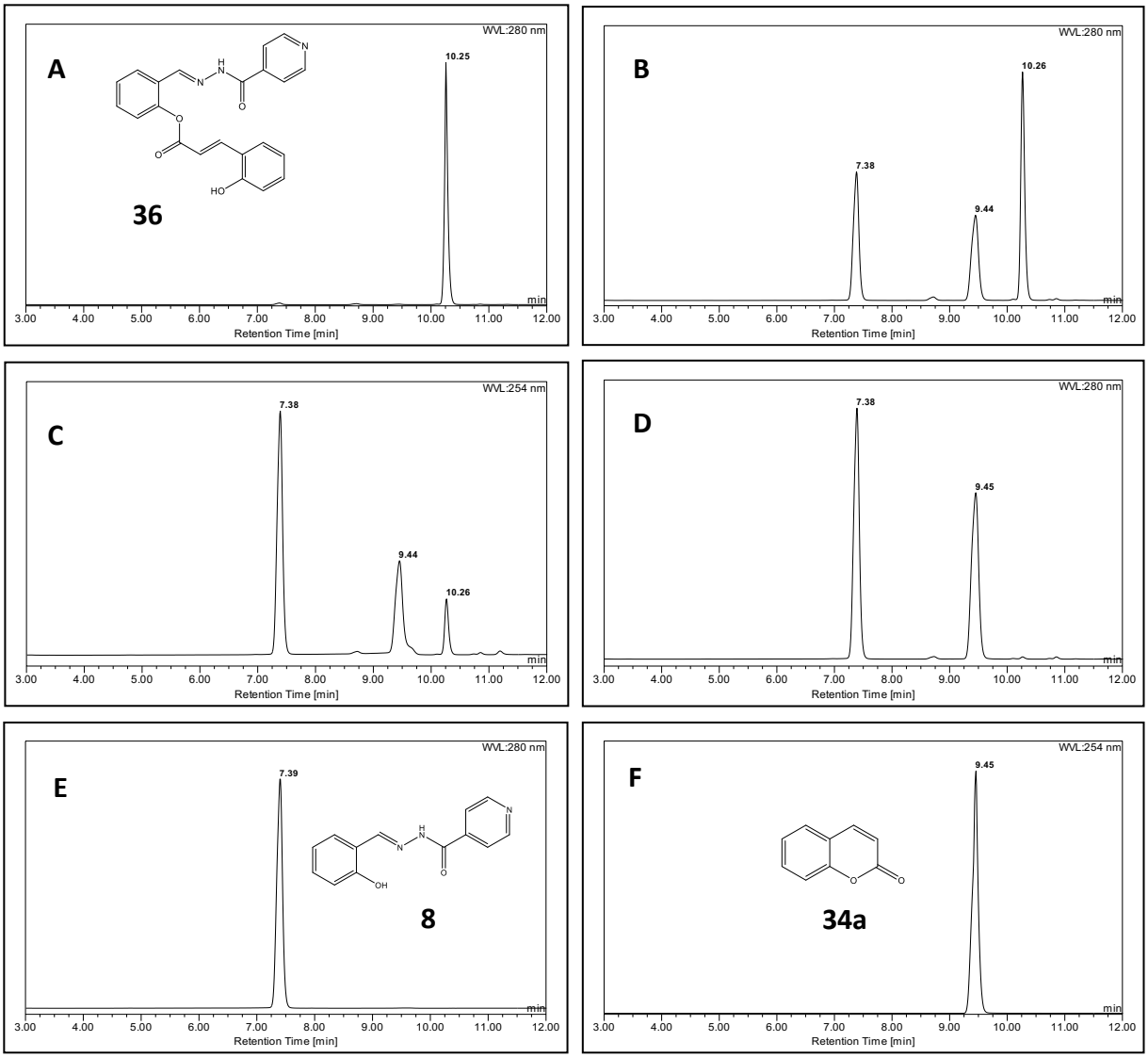

Figure 22. HPLC uncaging chromatograms of CIC **36**: **A.** Non-irradiated control of 'intact' **36**; **B.** 10 kJ/m^2 irradiation; **C.** 25 kJ/m^2 irradiation; **D.** 50 kJ/m^2 irradiation showing complete uncaging; **E.** Reference SIH **8** injection; **F.** Reference coumarin **34a** injection. Samples in DMSO solution (1 mg/mL) were irradiated with a 4 kW broad spectrum UVA lamp (Sellas, Germany).

Chromatogram **A** in Figure 22 shows that the peak at 10.25 min for pure **36** disappears to form two new peaks at 7.38 min and 9.44 min which correspond to SIH **8** and coumarin **34a**. These were both injected separately on the same gradient system of the analytical HPLC as references (chromatograms **E** and **F** respectively). **36** was completely uncaged upon 50 kJ/m^2 UVA irradiation (chromatogram **D**), equivalent to 250-500 kJ/m^2 solar UVA irradiation or 0.5-1 MED. This indicates that the CIC would be fully uncaged near to the dose required for the

appearance of minimal erythema, therefore it would exert powerful iron chelating activity at exactly the right time.

In the same manner the intact CIC **44** was also irradiated at increasing doses of UVA and the extent of uncaging was followed on analytical HPLC, with the chromatograms shown in Figure 23. The peak at 6.56 min for pure **44** (chromatogram **A**) disappears completely after 10 kJ/m^2 irradiation to form two new peaks at 5.71 min and 6.18 min, which correspond to SIH **8** and umbelliferone **34b** respectively (reference chromatograms **C** and **D**). The complete uncaging of **44** with a dose of 10 kJ/m^2 is equivalent to 100 kJ/m^2 of human skin sun exposure (1/5th MED). This efficient uncaging may limit the utility of **44** as a practical photoprotectant because the iron chelating activity would be expended after a significantly sub-erythemal dose rather than providing prolonged activity during UVA exposure. A representative comparison of the dose-dependent UVA uncaging of CICs **36** and **44** is shown in Figure 24, highlighting that the addition of the 4-hydroxyl group has a significant effect on the photostability of **44**, increasing the absorption in the UVA window.

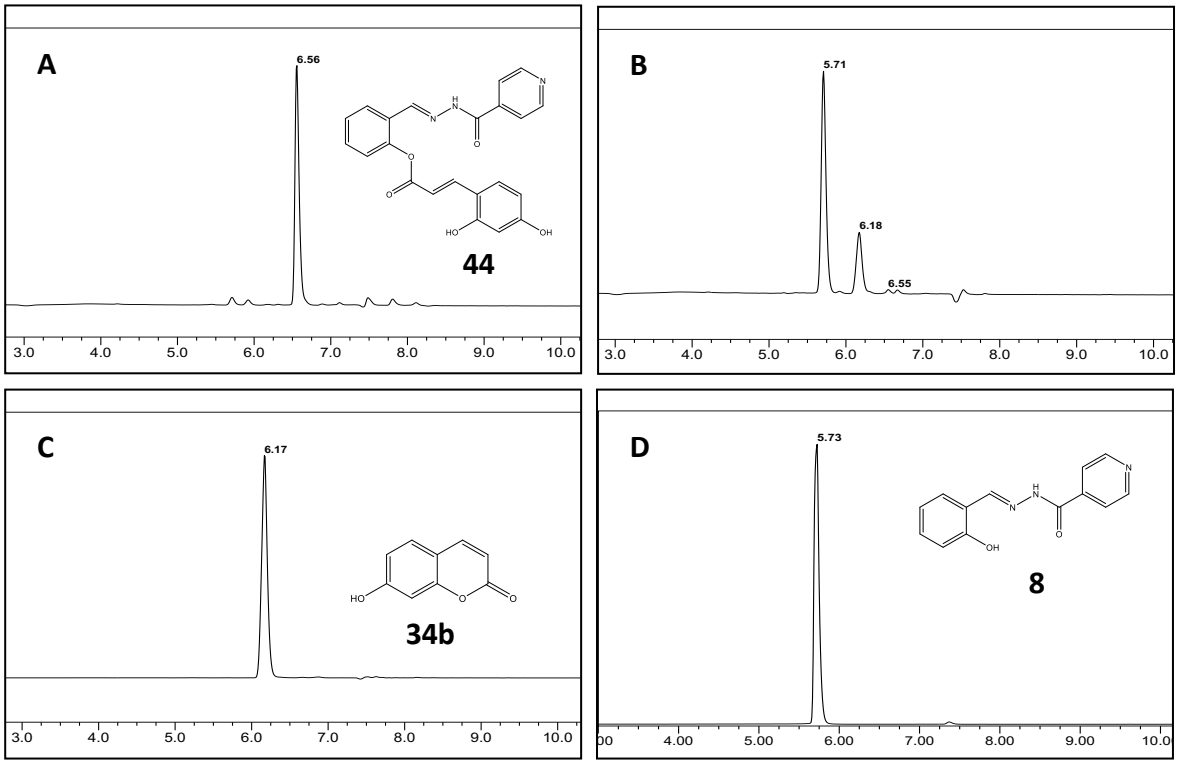

Figure 23. HPLC uncaging chromatograms of CIC **44**: **A.** Non-irradiated control of 'intact' **44**; **B.** 10 kJ/m^2 irradiation showing complete uncaging; **C.** Reference umbelliferone **34b** injection; **D.** Reference SIH **8** injection. Samples in DMSO solution (1 mg/mL) were irradiated with a 4 kW broad spectrum UVA lamp (Sellas, Germany).

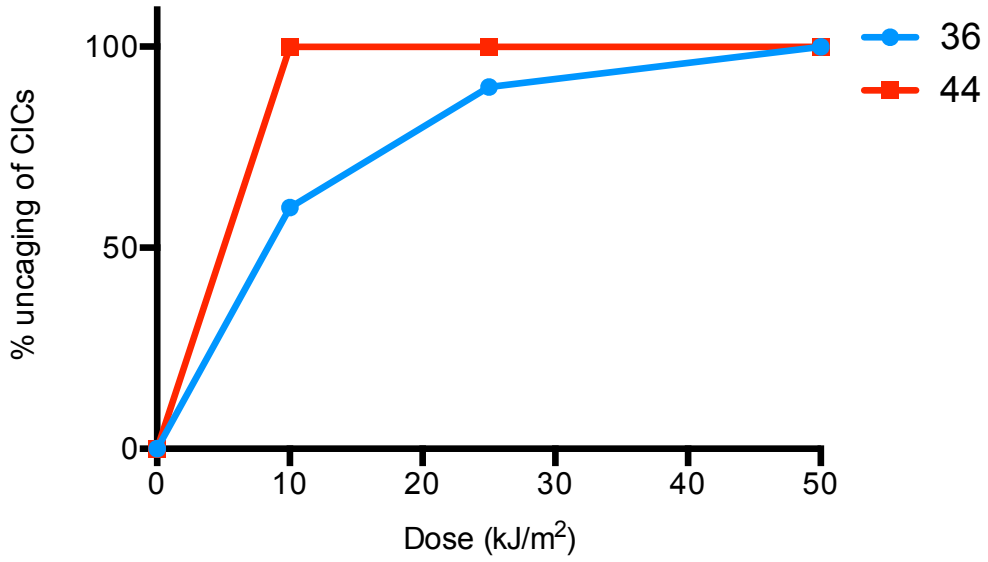

Figure 24. Representative comparison of the dose-dependent UVA uncaging of hydroxycinnamoyl-SIH CICs **36** and **44**. Percentage uncaging calculated using the peak area of the remaining CIC compared to the peak area of the unirradiated sample. Samples in DMSO solution (1 mg/mL) were irradiated with a 4 kW broad spectrum UVA lamp (Sellas, Germany).

The MTT assay was used to assess the photoprotective ability of CICs **36** and **44**. A concentration of 20 µM of CICs was used, which was incubated with the cells for 18 h before irradiation of the monolayers of cells at 500 kJ/m^2. The assay was carried out 24 h after irradiation as after this time cellular iron homeostasis would have returned to normal and therefore any reduced cell viability would reflect severe oxidative damage.[56] The results are shown in Figure 25, which show that the photoprotective effect of both **36** and **44** is less than that of the parent iron chelator **8** alone. This result is similar to the outcome seen by Franks *et al.* for their compound **30** (Scheme 10, Introduction 1.4.4), an aroylhydrazone iron chelator HAPI **29** caged with 2,4-dihydroxycinnamic acid (as seen in our CIC **44**). In concentrations above 25 µM they report that **30** is cytotoxic, which may suggest that coumarin-type photoproducts actually exhibit a pro-oxidant effect. Both CICs significantly improve the cell viability in comparison to the untreated irradiated control but are cytotoxic in unirradiated cells, similar to the cytotoxicity of **8** alone.

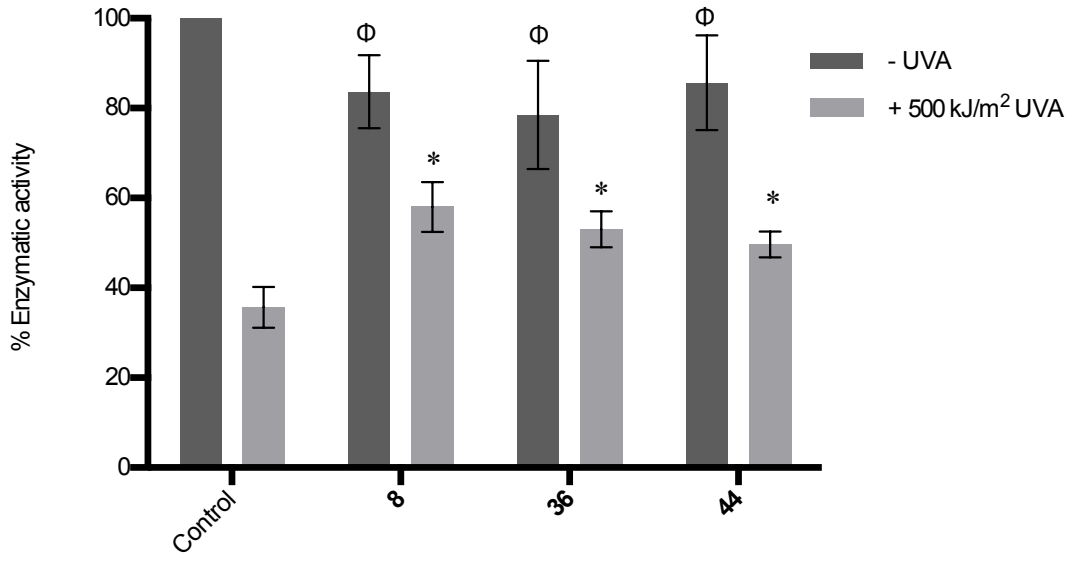

Figure 25. MTT assay evaluation of the photoprotection afforded by the hydroxycinnamoyl CICs **36** and **44** along with their parent iron chelator SIH **8** in FEK4 fibroblasts. Cells were treated with the compounds (20 μM) overnight before ± 500 kJ/m^2 UVA irradiation followed by MTT analysis 24 h later. Data is expressed as the mean ± SD compared to the untreated unirradiated control, which was fixed at 100% enzymatic activity (n=3).

*= p< 0.05, significantly different from the untreated irradiated control.

Φ= *p* <0.05, significantly different from the untreated unirradiated control.

4. Aminocinnamoyl-caged iron chelators

The aminocinnamoyl group was also introduced by Porter's laboratory as a useful photo-labile moiety and has certain advantages over the hydroxycinnamoyl group.[172] The photo-cleavage reaction follows the same mechanism as shown in Scheme 13 and the aminocinnamoyl compounds tend to absorb at slightly longer wavelengths than the corresponding hydroxycinnamoyl compounds. There is also the possibility to substitute the amino function with one or two alkyl groups which also shifts the absorption to longer wavelengths.[172] The initial work carried out in the Porter laboratory on a series of aminocinnamoyl derivatives included the 4,5-dimethoxy aminocinnamic acid **50**, which contained a methyl substituent on the double bond. This photo-cleavable group was chosen to begin studies into aminocinnamoyl CICs due to its established photo-cleavage within the UVA window and its ease of synthesis in a good yield.

4,5-Dimethoxy aminocinnamic acid **50** is not commercially available so a synthetic procedure reported by Li *et al.* was adapted.[172] Beginning with 6-nitroveratraldehyde **47,** the olefinic ethyl ester **48** was obtained *via* a Wittig reaction using (carbethoxyethylidene)triphenylphosphorane (ECETP) which proceeded in a good yield (88%), as shown in Scheme 18. The stabilised ylid should give only the *E* alkene isomer, and the stereochemistry of **48** has been previously confirmed in this laboratory by X-ray crystallography.[192] Hydrolysis of the ester with aqueous 1M NaOH in a mixture of EtOH and THF followed by an acidic work-up gave complete conversion to the carboxylic acid **49**. Reduction of the nitro group to the amine was first attempted by refluxing with iron powder and acetic acid in EtOH,[193] which gave a good conversion to the desired intermediate **50**, however it was difficult to remove impurities even after column chromatography. Applying an alternative reduction method using ferrous sulphate solution and concentrated aqueous ammonia[194] gave an excellent yield and a much purer product, which did not require column chromatography.

The coupling of **50** with both aroylhydrazone iron chelators **7** and **8** was attempted using EDC.HCl and DMAP as previously described. PIH **7** contains a phenolic hydroxyl along with a primary alcohol, but the nucleophilicity of the phenol is greater than the primary alcohol and therefore using one equivalent of the aminocinnamic acid **50** during the coupling reaction was expected to only give a single acylated esterification product. The reactions proceeded as anticipated giving a 79% yield of the aminocinnamoyl-SIH CIC **51** and a 54% yield of the aminocinnamoyl-PIH CIC **52** (Scheme 18).

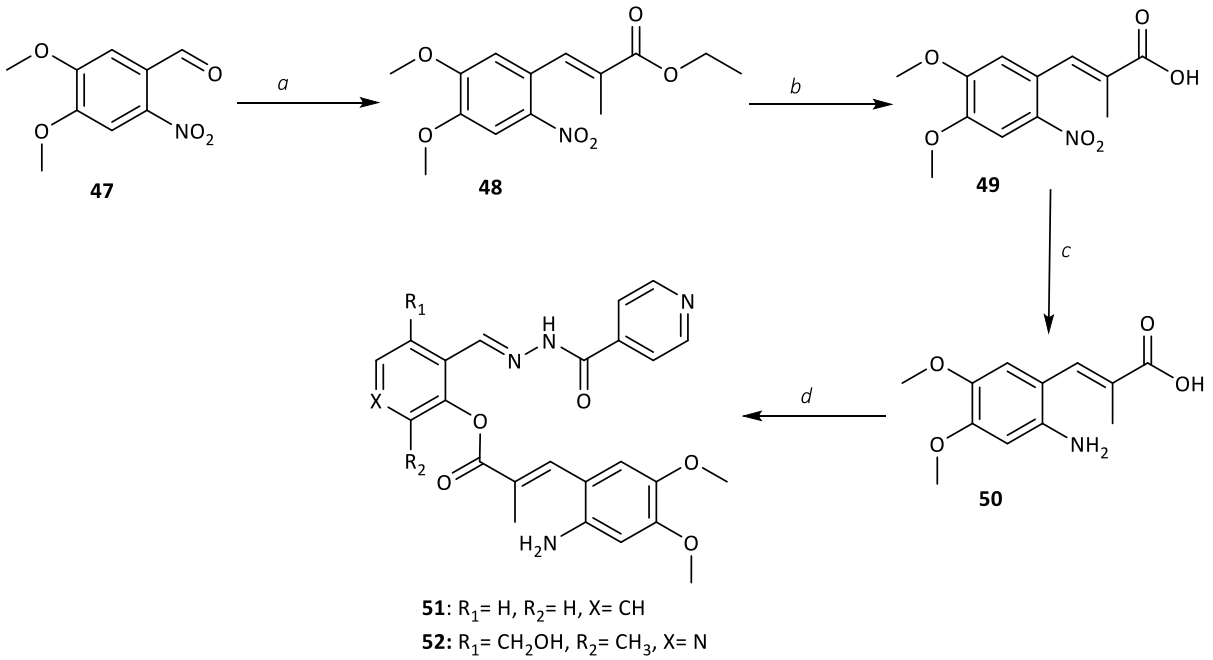

Scheme 18. Synthesis of 3,4-dimethoxy aminocinnamoyl CICs **51** and **52**. *Reagents and conditions:* **a.** ECETP, dry toluene, 85 ^{o}C, 36 h, 88%; **b.** 1M NaOH, 4:1 THF:EtOH, RT, 42 h, 99%; **c.** $FeSO_4.7H_2O$, water, aq. 35% NH_3, RT, 2 h, 91%; **d.** EDC.HCl, DMAP, **7** or **8**, dry DMF, 30 ^{o}C, O/N, 79% (**51**) and 54% (**52**).

As these coupling reactions proceeded well in good yields to give the desired CICs, the coupling of aminocinnamic acid **50** was tried with the deferasirox intermediate **32** as previously attempted with the hydroxycinnamoyl derivatives. Coupling of **50** to **32** proceeded in a 38% yield shown in Scheme 19. This intermediate was moisture-sensitive and quickly degraded, therefore it was transformed directly into the desired CIC **54** by treating with 4-hydrazinobenzoic acid and Et_3N in EtOH as per the synthesis of deferasirox **6**. The reaction proceeded well, however **54** also degraded during column chromatography and could only be characterised by mass spectrometry.

Kieler *et al.* reported the alkylation of deferasirox methyl ester **33** with complete regioselectivity for the phenol moiety attached to position 5 of the triazole ring, which was confirmed by X-ray crystallography of the alkylated structure.[100] Steinhauser *et al.* reported the crystal structure of deferasirox **6,** which indicated that the phenolic hydroxyl in position 3 of the triazole ring was rotated in order to form a stable intramolecular hydrogen bond with the triazole nitrogen in the 2-position.[98] This may be the explanation for the totally

regioselective alkylation of the other phenol group which is therefore more readily available for reaction with electrophilic reagents. Based on this premise, the esterification of deferasirox ester **33** with **50** was attempted (route c, Scheme 19). The reaction proceeded in a purified 28% yield with the formation of a single acylated CIC **55**. TLC and HPLC analysis also showed some unconverted acid **50** and deferasirox ester **33.**

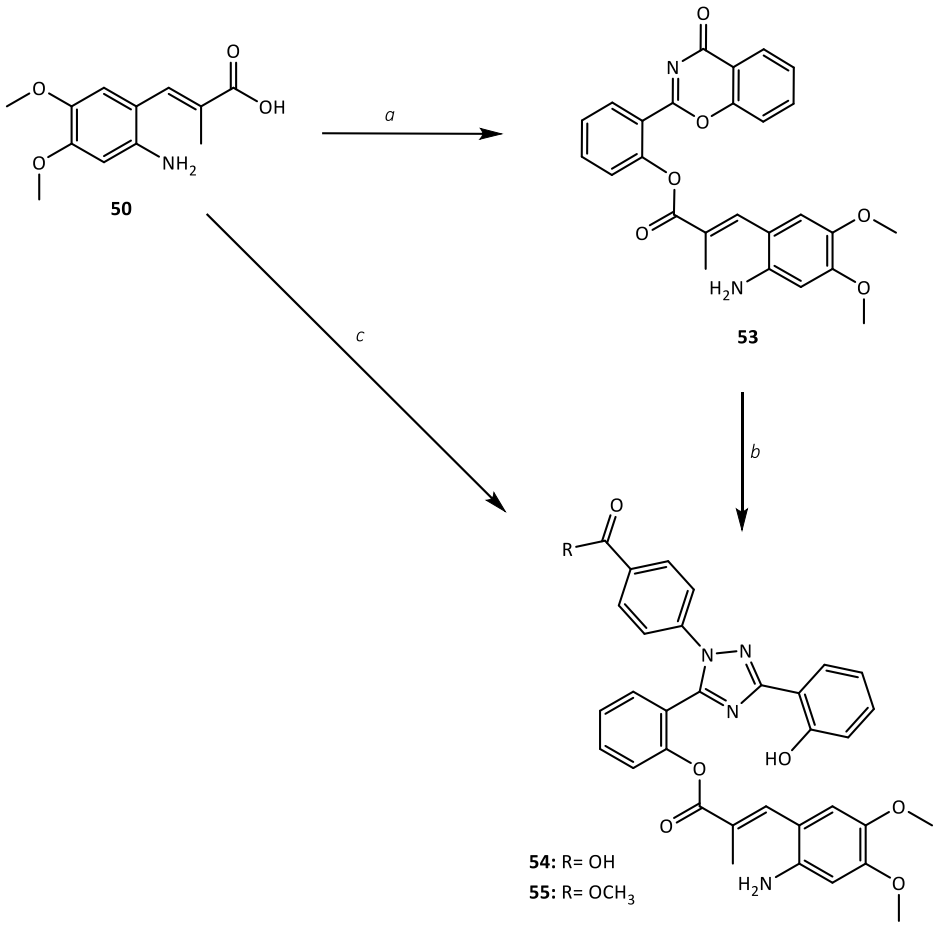

Scheme 19. Synthetic routes to 3,4-dimethoxy aminocinnamoyl-caged deferasirox derivatives **54** and **55**. *Reagents and conditions:* **a**. EDC.HCl, DMAP, **32**, DIPEA, dry DMF, RT, 40 h, 38%; **b.** 4-hydrazinobenzoic acid, NEt_3, EtOH, 60 ^oC, 48 h; **c.** EDC.HCl, DMAP, **33**, DIPEA, dry DMF, RT, 24 h, 28%.

As with the hydroxycinnamoyl CICs, the UV/Vis absorbance spectra of synthesised CICs **51**, **52** and **55** were recorded to ensure that the CICs absorbed in the relevant UVA wavelength range (320- 400 nm). Figure 26 shows that **51** absorbs maximally at 302 nm (in the UVB wavelength range) with a molar absorptivity of $Ɛ_{302}$= 2,870 L mol^{-1} cm^{-1}, and continues to absorb over the whole UVA range and into visible light up to 426 nm. The PIH-based CIC **52** has a maximal absorbance of 298 nm with a higher molar absorptivity of $Ɛ_{298}$= 9,250 L mol^{-1} cm^{-1}, and **52**

continues to absorb to over 450 nm, significantly into visible light, as shown in Figure 27. **55** absorbs maximally at 302 nm (molar absorptivity of ε_{302}= 7,640 L mol^{-1} cm^{-1}), but also has a significant absorbance peak at 380 nm in the UVA region (molar absorptivity of ε_{380}= 3,370 L mol^{-1} cm^{-1}) and also absorbs up to 450 nm, as shown in Figure 28.

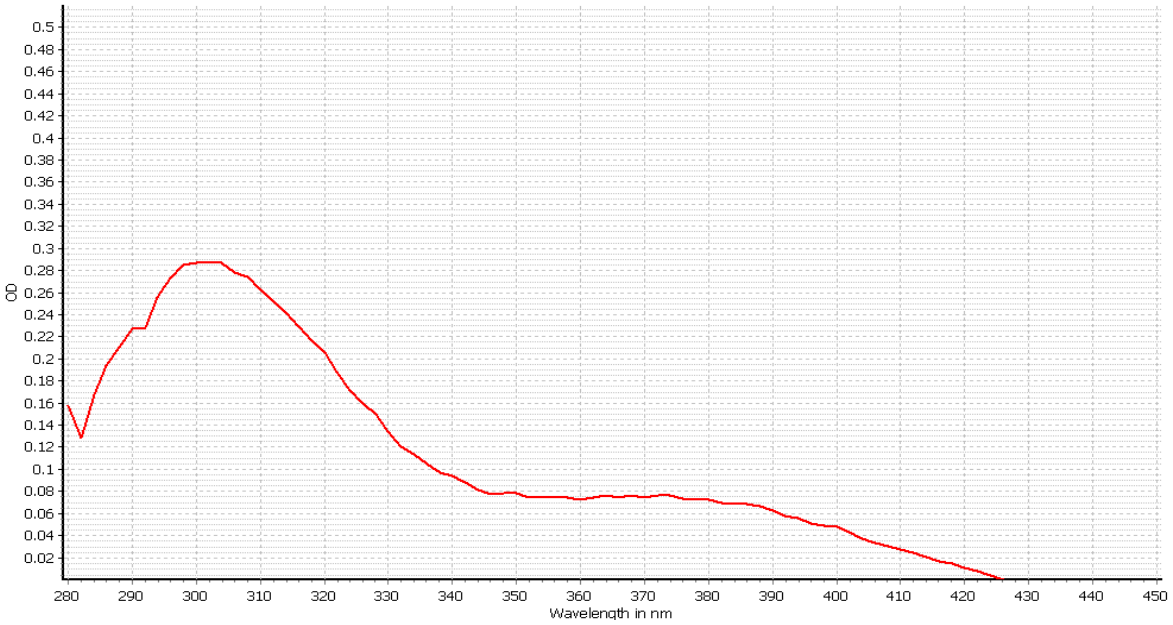

Figure 26. UV/Vis absorbance spectrum of CIC **51** in DMSO (100 μM).

Figure 27. UV/Vis absorbance spectrum of CIC **52** in DMSO (100 μM).

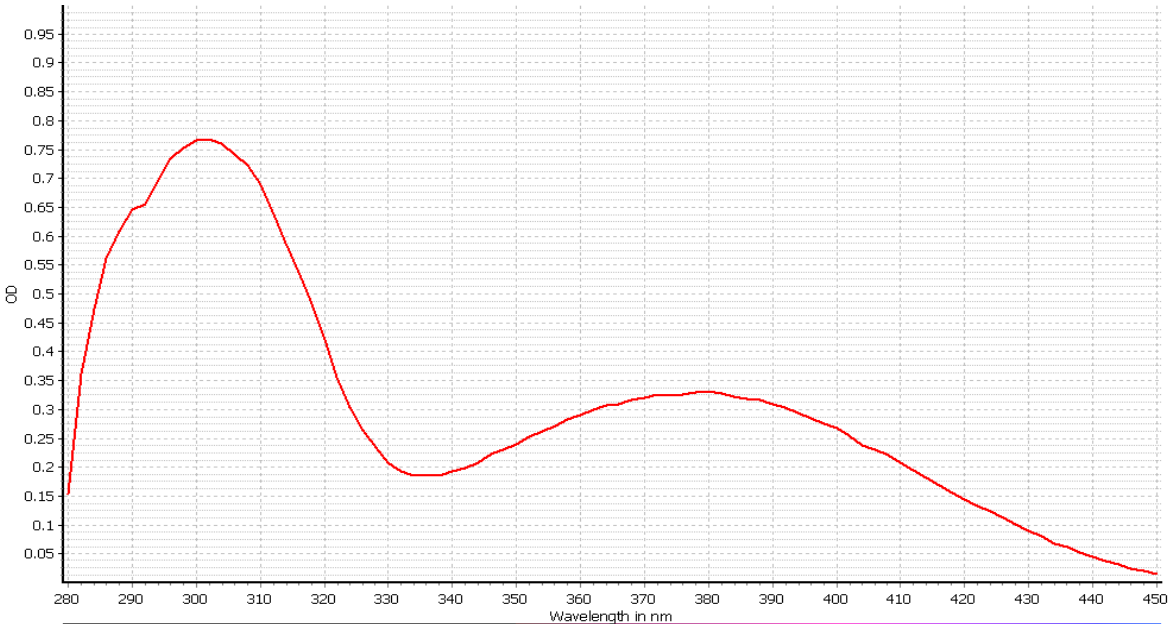

Figure 28. UV/Vis absorbance spectrum of CIC **55** in DMSO (100 μM).

Upon UVA irradiation of aminocinnamoyl photo-cleavable groups, a carbostyril photoproduct is released as opposed to the coumarin photoproducts seen with the hydroxycinnamoyl groups. Carbostyril structures have not been studied extensively and the photoproduct released from the 3,4-dimethoxy aminocinnamoyl CICs **51**, **52** and **55** is not commercially available. Therefore the synthesis of this photoproduct was important to act as a reference for HPLC analysis of the uncaging profiles. In 1981 Meth-Cohn *et al.* reported the use of Vilsmeier-Haack formylation with DMF and phosphoryl chloride to synthesise quinolones from acetanilides.[195] Following this synthetic approach, 3,4-dimethoxy aniline **56** was acetylated using acetyl chloride to give **57**, before performing a Vilsmeier-Haack reaction to give 2-chloro-6,7-dimethoxyquinoline-3-carbaldehyde **58** in a yield of 51% (Scheme 20). **58** was then treated with 70% aq. AcOH at reflux to give the quinolone aldehyde **59** in 50% yield. Reduction of the aldehyde of **59** with triethylsilane in the presence of TFA[196] gave the desired carbostyril product **60**, which would be released upon photo-cleavage of the corresponding CIC *via* the mechanism seen in Scheme 13.

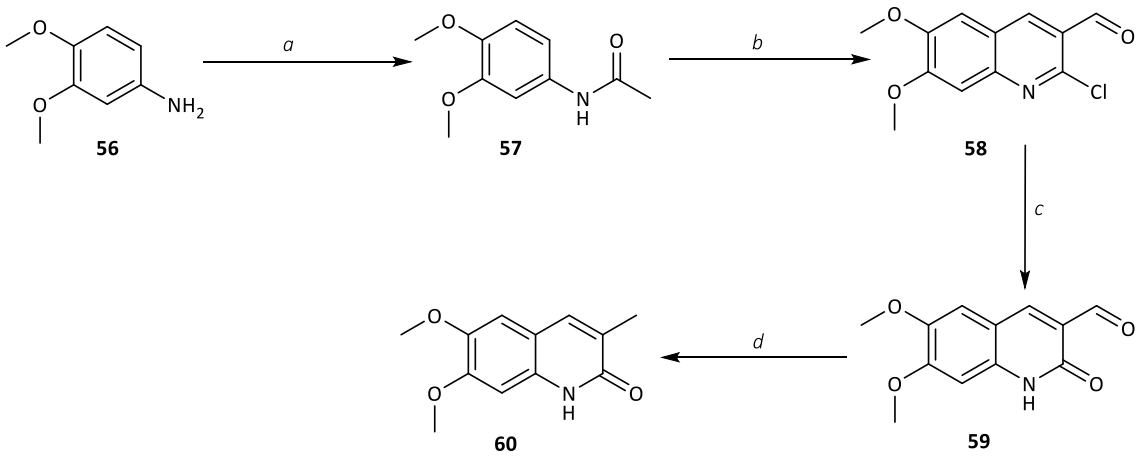

Scheme 20. Synthesis of 6,7-dimethoxy carbostyril **60**. *Reagents and conditions:* **a.** Et_3N, acetyl chloride, dry DCM, RT, 20 min, 75%; **b.** $POCl_3$, dry DMF, 85 ^oC, 3 h, 51%; **c.** 70% aq. AcOH, reflux, 16 h, 50%; **d.** TFA, Et_3SiH, RT, 2 h, 41%.

In the same manner as for the hydroxycinnamoyl CICs, the intact CICs **51**, **52** and **55** were irradiated at increasing doses of UVA and the extent of uncaging was followed on analytical HPLC. The HPLC chromatograms in Figure 29 correspond to the uncaging of SIH-based CIC **51.** Chromatogram **A** is a single peak at 6.10 min for pure **51** which disappears to form two new peaks at 5.72 min and 6.37 min respectively which correspond to SIH **8** and carbostyril **60**. These were both injected separately on the same gradient system of the analytical HPLC as references (chromatograms **E** and **F** respectively). **51** was completely uncaged upon 100 kJ/m^2 UVA irradiation (chromatogram **D**), equivalent to 500-1000 kJ/m^2 solar UVA irradiation or 1-2 MED.

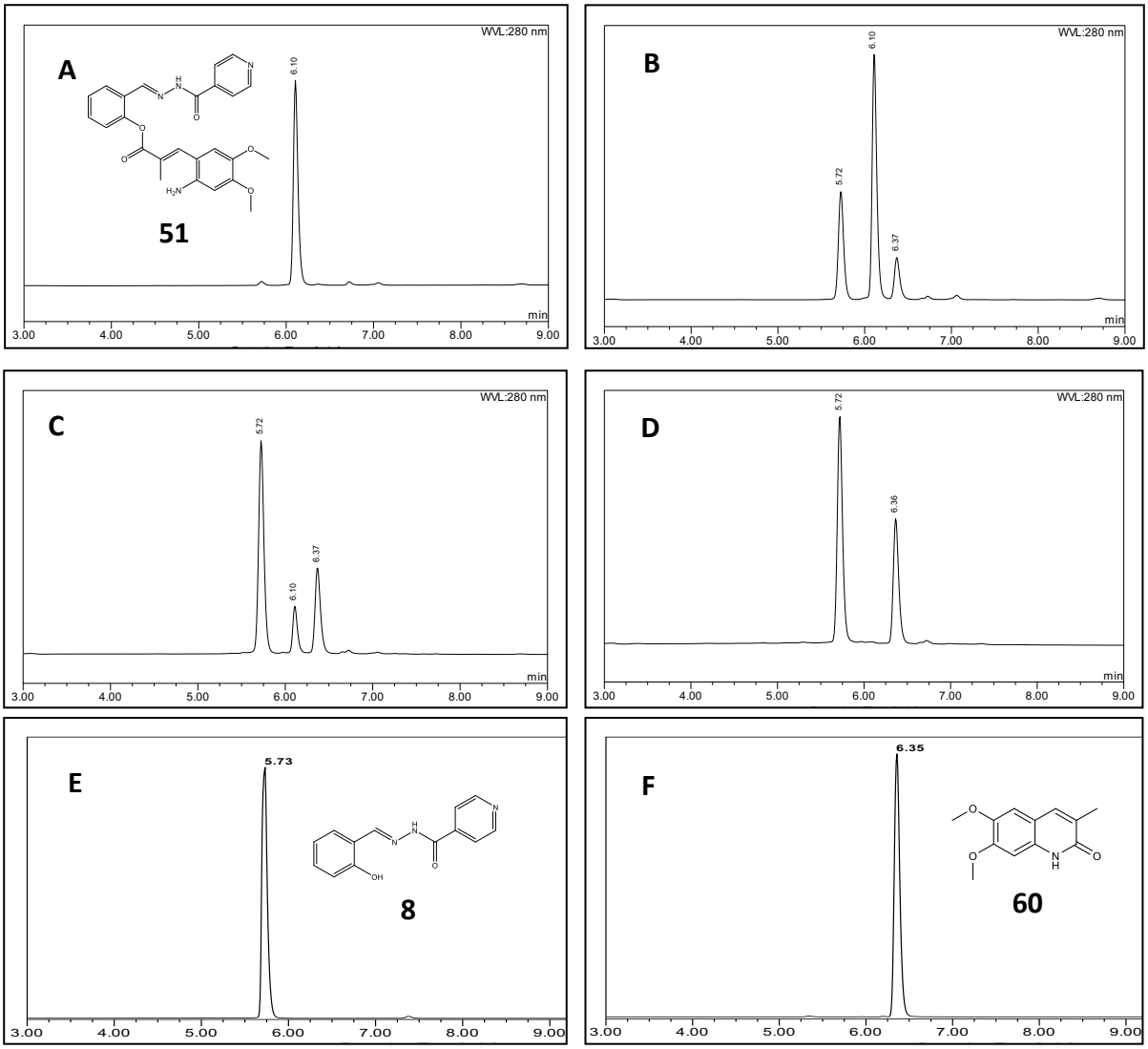

Figure 29. HPLC chromatograms of aminocinnamoyl-SIH ClC **51**: **A.** Non-irradiated control of 'intact' **51**; **B.** 25 kJ/m^2 irradiation; **C.** 50 kJ/m^2 irradiation; **D.** 100 kJ/m^2 irradiation showing complete uncaging; **E.** Reference SIH **8** injection; **F.** Reference carbostyril **60** injection. Samples in DMSO solution (1 mg/mL) were irradiated with a 4 kW broad spectrum UVA lamp (Sellas, Germany).

The chromatograms in Figure 30 show that the peak at 8.78 min for pure **52** (chromatogram **A**) disappears completely after 250 kJ/m^2 irradiation to form two new peaks at 4.28 min and 8.50 min, which correspond to PIH **7** and carbostyril **60** (reference chromatograms **E** and **F** respectively). The uncaging of **52** after 250 kJ/m^2 is equivalent to approximately 400 min of human skin sun exposure (~2500 kJ/m^2 physical dose) which is 5 MED. Therefore a severe amount of erythema would be reached before **52** exerted its full iron chelating activity. The

dose required for full uncaging of **52** is significantly higher than that required for **51,** despite CIC **52** absorbing more strongly at the principal wavelength of the UVA lamp output (360 nm). This indicates that PIH-based CICs have a slower mechanism of photo-release than SIH-based CICs. Considering the mechanism of photo-cleavage of cinnamic acids (shown in Scheme 13), the second step involving nucleophilic attack of the carbonyl is the more likely step to be affected by the ester group (*i.e* SIH or PIH) rather than the photoisomerization step. Therefore the extra *ortho* methyl group present in PIH may sterically hinder the nucleophilic attack and thus slow down the uncaging mechanism. Further investigations into the kinetics of the uncaging mechanism would be required to confirm this proposition.

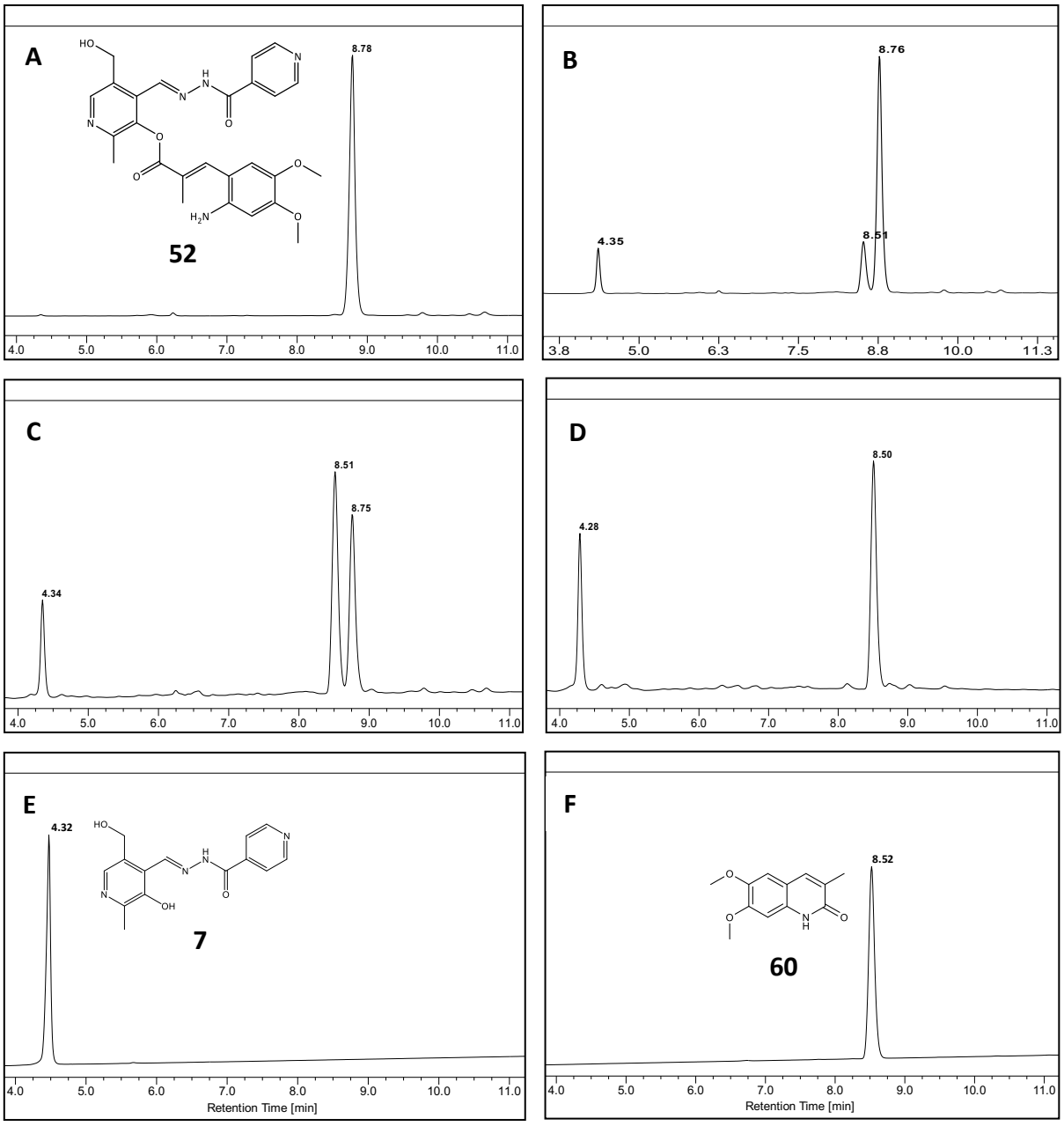

Figure 30. HPLC chromatograms of aminocinnamoyl-PIH CIC **52**: **A.** Non-irradiated control of 'intact' **52**; **B.** 50 kJ/m^2 irradiation; **C.** 100 kJ/m^2 irradiation; **D.** 250 kJ/m^2 irradiation showing complete uncaging; **E.** Reference PIH **7** injection; **F.** Reference carbostyril **60** injection. Samples in DMSO solution (1 mg/mL) were irradiated with a 4 kW broad spectrum UVA lamp (Sellas, Germany).

The HPLC chromatograms in Figure 31 correspond to the uncaging of deferasirox ester-based CIC **55.** Chromatogram **A** is a single peak at 9.51 min for pure **55** which disappears to form two new peaks at 6.37 min and 10.42 min which correspond to deferasirox ester **33** and carbostyril **60**. These were both injected separately on the same gradient system of the analytical HPLC as references (chromatograms **E** and **F** respectively). **55** was completely

uncaged upon 50 kJ/m^2 UVA irradiation (chromatogram **D**). This uncaging process proceeded faster than that of the SIH-based CIC **51** which may be due to **55** absorbing more strongly at 360 nm, the principal output of the UVA lamp, as well as over the entire UVA wavelength range.

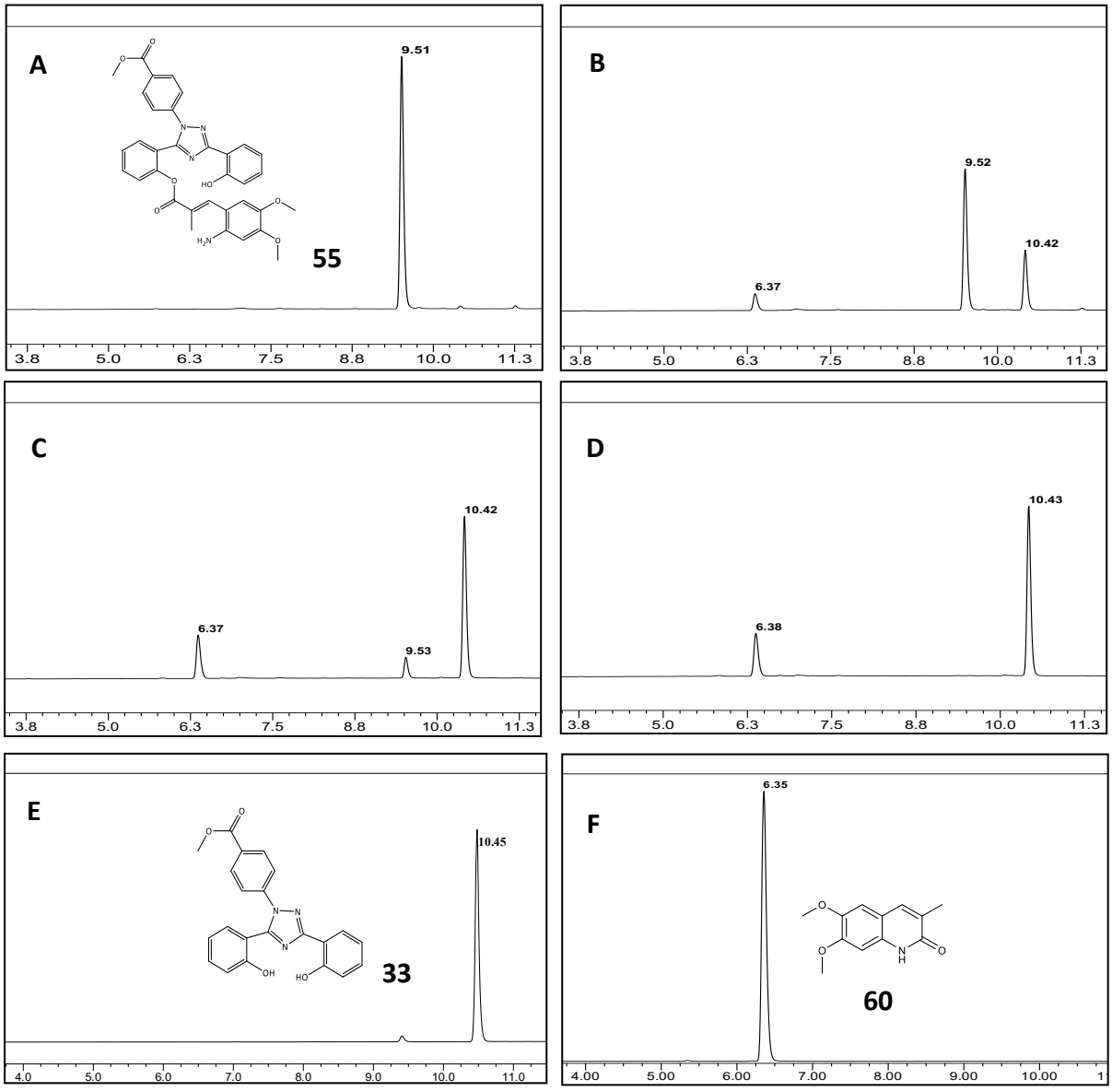

Figure 31. HPLC chromatograms of aminocinnamoyl-deferasirox ester CIC **55**: **A.** Non-irradiated control of 'intact' **55**; **B.** 10 kJ/m^2 irradiation; **C.** 25 kJ/m^2 irradiation; **D.** 50 kJ/m^2 irradiation showing complete uncaging; **E.** Reference deferasirox ester **33** injection; **F.** Reference carbostyril **60** injection. Samples in DMSO solution (1 mg/mL) were irradiated with a 4 kW broad spectrum UVA lamp (Sellas, Germany).

A respresentative comparison of the dose-dependent UVA uncaging of CICs **51, 52** and **55** is seen in Figure 32. The PIH-based CIC **52** required a considerably higher dose of UVA (250

kJ/m^2) to uncage in comparison to the SIH and deferasirox ester-based CICs **51** and **55**, which both uncaged between 50-100 kJ/m^2 UVA. Full uncaging of **52** (and thus photoprotection) would not be observed until several hours of human skin sun exposure and severe erythema, which may be not suitable for a photoprotective CIC which should uncage at relevant environmental levels of human sun exposure.

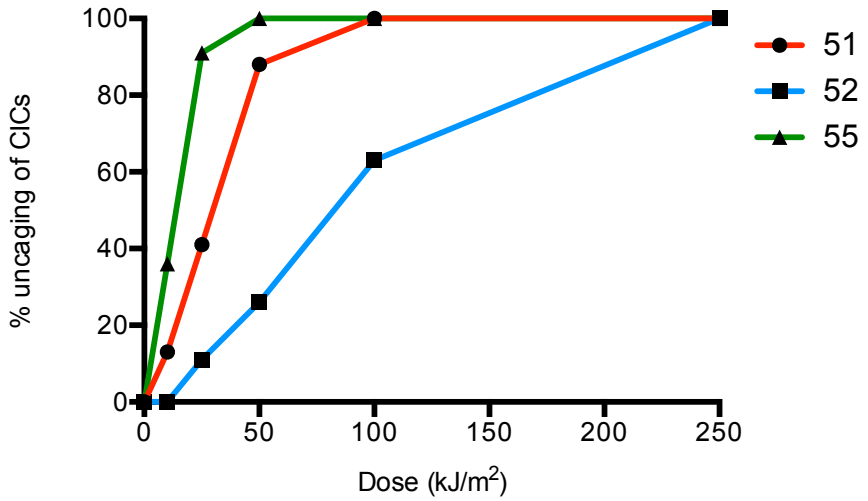

Figure 32. A representative comparison of the dose-dependent uncaging of the 3,4-dimethoxy aminocinnamoyl CICs **51**, **52** and **55**. Percentage uncaging calculated using the peak area of the remaining CIC compared to the peak area of the unirradiated sample. Samples in DMSO solution (1 mg/mL) were irradiated with a 4 kW broad spectrum UVA lamp (Sellas, Germany).

The MTT assay was used to assess the photoprotective properties of aminocinnamoyl CICs **51, 52** and **55**. In the same manner as for the hydroxycinnamoyl CICs, a final concentration of 20 µM of CICs was used, which was incubated with the cells for 18 h before irradiation of the monolayers of cells at 500 kJ/m^2 (Figure 33). Among the iron chelators, SIH **8** is a very good photoprotectant in its own right, significantly improving cell viability to 58% in comparison to the untreated control (36% enzymatic activity). Deferasirox ester **33** and PIH **7** increased cell viability to 46% and 43% respectively. The only aminocinnamoyl CIC to significantly improve the cell viability in comparison to the untreated irradiated control was the SIH-based CIC **51** (58%), which gave the same level of photoprotection as the parent iron chelator **8**, but was much less cytotoxic to unirradiated cells. Both **52** and **55** were less photoprotective than their parent iron chelators **7** and **33** and gave very little photoprotection in comparison to the

irradiated control (40% and 38% respectively). In the case of **52** this may be due to the afore-mentioned slow uncaging and therefore at a dose of 500 kJ/m^2 (equivalent to a dose of 50 kJ/m^2 in chemical irradiation) only approximately 25% of the active iron chelator would be released. CIC **55** has a relatively high molecular weight (MW=606.635) and therefore may also have a reduced ability to permeate the cell membrane and thus chelate labile iron in the cytosol upon UVA irradiation. This is consistent with the explanation provided by Glickstein *et al.* for the relative cell permeating efficiency of deferiprone **2** and deferasirox **6** compared to the larger DFO **1**.[150]

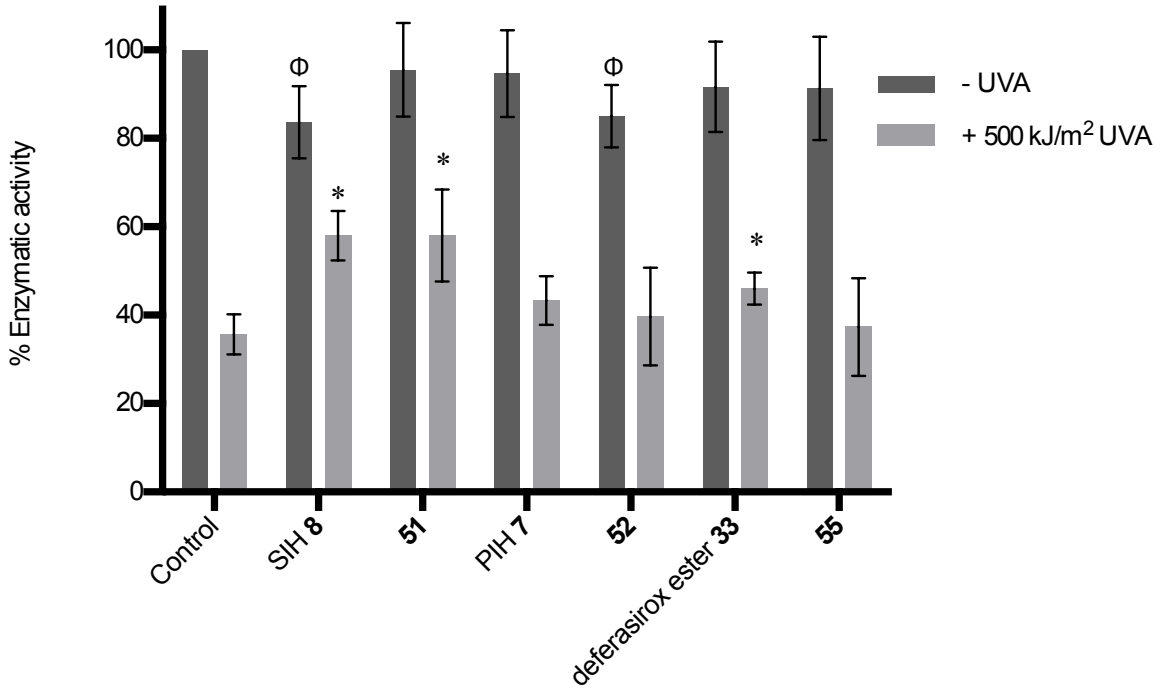

Figure 33. MTT assay evaluation of the photoprotection afforded by the aminocinnamoyl CICs **51, 52** and **55** along with their parent iron chelators SIH **8,** PIH **7** and deferasirox ester **33** in FEK4 fibroblasts. Cells were treated with the compounds (20 µM) overnight before ± 500 kJ/m^2 UVA irradiation followed by MTT analysis 24 h later. Data is expressed as the mean ± SD compared to the untreated unirradiated control, which was fixed at 100% enzymatic activity (n=3).

*= p< 0.05, significantly different from the untreated irradiated control.

Φ= *p* <0.05, significantly different from the untreated unirradiated control.

As already highlighted, the choice of using the 3,4-dimethoxy aminocinnamoyl caging group derived from **50** as a starting point was due to its previously reported use as a photo-cleavable group.[172] In comparison to the 2-hydroxy and 2,4-dihydroxy cinnamoyl PPGs studied above,

the 3,4-dimethoxy aminocinnamoyl group selected differs not only in its 2-amino group rather than 2-hydroxyl group, and different aromatic substituents, but it also has a methyl substituent on the olefinic bond. Coumarins are fluorescent molecules and Gagey *et al.* used this property to quantify the amount of coumarin produced upon two-photon uncaging of hydroxycinnamoyl-caged derivatives of ethanol. One series of compounds had methyl substitution on the olefinic bond whilst the other series did not, and Gagey *et al* reported that this substitution increased the quantum yield of coumarin.[166] The explanation for this outcome is that the presence of the methyl group increases the steric hindrance around the double bond which is thought to destabilize the *E* stereoisomer more than the *Z* isomer, thus giving rise to a larger proportion of the desired *Z* stereoisomer after one photocycle.

In order to investigate how the effect of methyl substitution affects the photostability of aminocinnamoyl CICs, the analogous 3,4-dimethoxy aminocinnamic acid without methyl substitution was synthesised. The synthesis began with 1-bromo-4,5-dimethoxy-2-nitrobenzene **61** which was converted into the ester **62** *via* a Heck reaction using the catalyst palladium(II) acetate with triphenylphosphine as the ligand to form the required reduced bis(triphenylphosphine)palladium(0) complex.[197] This palladium complex inserts into the aryl-Br bond *via* an oxidative addition step and then reacts with the activated alkene, ethyl acrylate, to give the desired ester **62** with *E* stereoselectivity.[197] The presence of the base Et_3N regenerates the catalyst. Saponification of the ester gave the carboxylic acid **63** which was then reduced with aqueous ferrous sulphate solution and concentrated aqueous ammonia[194] to give the desired 3,4-dimethoxy aminocinnamic acid **64,** as shown in Scheme 21. Coupling of **64** with SIH **8** and deferasirox ester **33** was attempted using the previously described coupling method. This gave CICs **65** and **66** in yields of 47% and 17% respectively (route d in Scheme 21). The relatively low yield obtained for **66** is similar to that obtained for the methylated 3,4-dimethoxy aminocinnamoyl CIC **55**, and once again unchanged iron chelator and aminocinnamic acid were observed upon TLC and HPLC analysis of the crude reaction mixture. This is consistent with the relatively hindered environment of the more reactive phenolic function of deferasirox, with the bulky *ortho* substituent apparently having a significant effect on the efficiency of esterification with different activated acids.

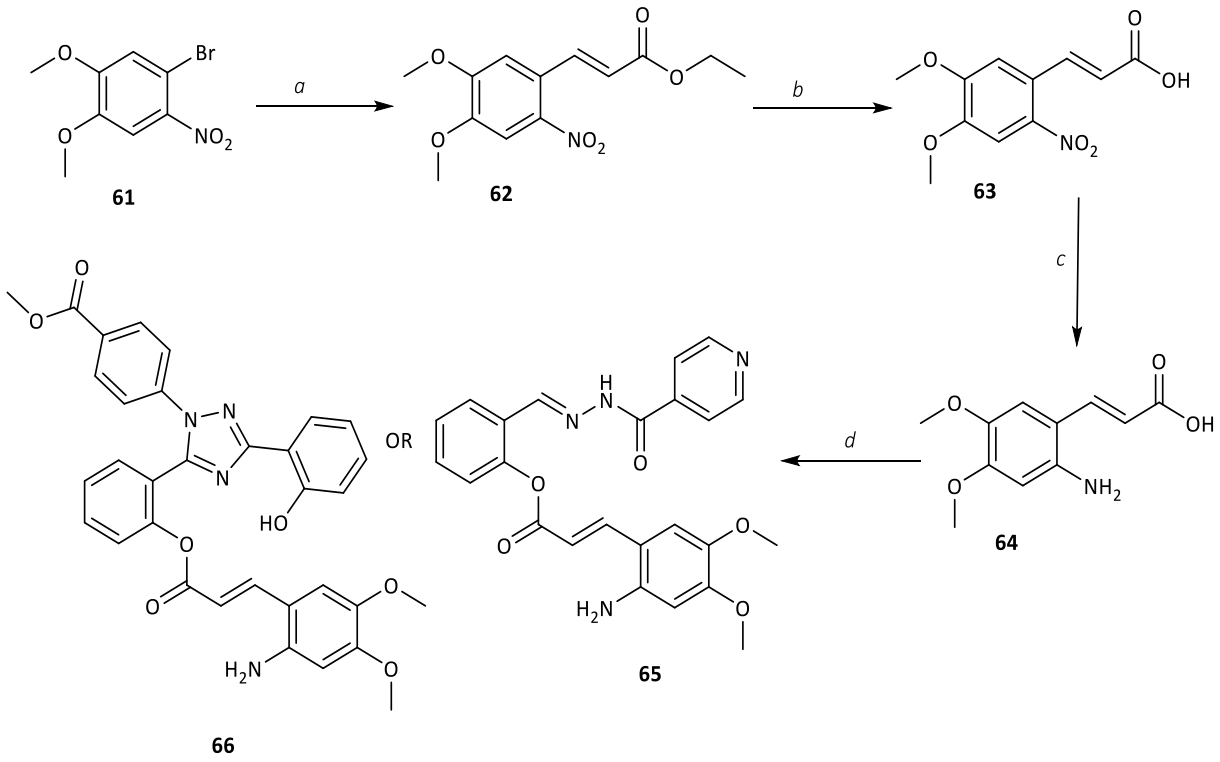

Scheme 21. Synthesis of 3,4-dimethoxy aminocinnamoyl CICs **65** and **66**. *Reagents and conditions:* **a.** $Pd(OAc)_2$, PPh_3, ethyl acrylate, Et_3N, dry DMF, 90 °C, O/N, 80%; **b.** 1M NaOH, 4:1 THF:EtOH, 40 °C, O/N, 88%; **c.** $FeSO_4.7H_2O$, water, aq. 35% NH_3, RT, 2 h, 81%; **d.** EDC.HCl, DMAP, **8** or **33**, dry DMF, 30 °C, 24 h, 47% (**65**) and 17% (**66**).

Synthesis of the carbostyril photoproduct released from irradiation of CICs **65** and **66** was required and the synthetic pathway by Park *et al.* was adopted.[198] 6-Nitroveratraldehyde **47** was reduced to the amine **67**, followed by acetylation with acetyl chloride to give **68** in good yield (Scheme 22). Base-catalysed intramolecular aldol-type condensation[198] was reported to give the final carbostyril **69**, however in our hands only a 10% yield of the desired product **69** was recovered. The main product instead appeared from ^{1}H NMR analysis to be the result of an intermolecular aldol condensation, as shown in Figure 34. Making the solution more dilute, adding the substrate more slowly and using a different base (NaH rather than Cs_2CO_3) were all alternative methods employed, however no improvement in yield was obtained. Finally, a much simpler route to **69** was discovered *via* a one-step acid-catalysed cyclization from the aminocinnamic acid **64**.[194] This reaction proceeded very well giving a 78% yield of the desired carbostyril **69** (route d, Scheme 22). Due to the ease and effectiveness of this method it was also used with the methyl-substituted aminocinnamic acid derivative **50**, which also proceeded very well giving an 83% yield of carbostyril **60**.

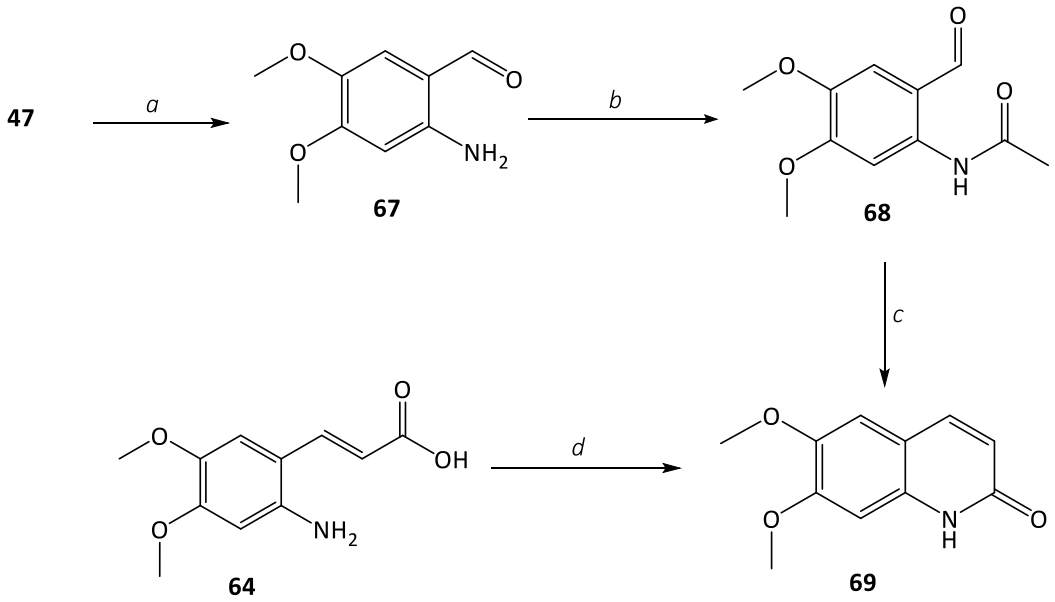

Scheme 22. Synthesis of carbostyril **69** along with alternative carbostyril synthesis. *Reagents and conditions:* **a.** $FeSO_4.7H_2O$, water, aq. 35% NH_3, RT, 2 h, 76%; **b.** Et_3N, acetyl chloride, dry DCM, RT, 30 min, 81%; **c.** Cs_2CO_3, dry DMF, 60 ^oC, 22 h, 10%; **d.** 1.4 M HCl, reflux, 2-4 h, 78%.

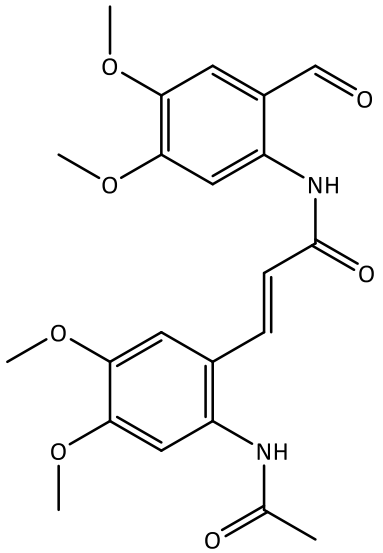

Figure 34. Predicted structure of the product of intermolecular aldol condensation of **68**.

The intact CICs **65** and **66** were irradiated at increasing doses of UVA (10-250 kJ/m^2) to monitor the extent of uncaging, which was followed on analytical HPLC. Upon irradiation a clean conversion to a single carbostyril photoproduct **69** was not observed. Instead three new

peaks appeared on each chromatogram, one of which corresponded to the parent iron chelator **8** or **33**, and one of which corresponded to the carbostyril **69.** A sample chromatogram of complete uncaging of CIC **66** at a dose of 100 kJ/m^2 is shown in Figure 35. The peak for the iron chelator **33** is seen at 10.5 min, carbostyril **69** is seen at 5.7 min and an unknown compound is at 6.8 min.

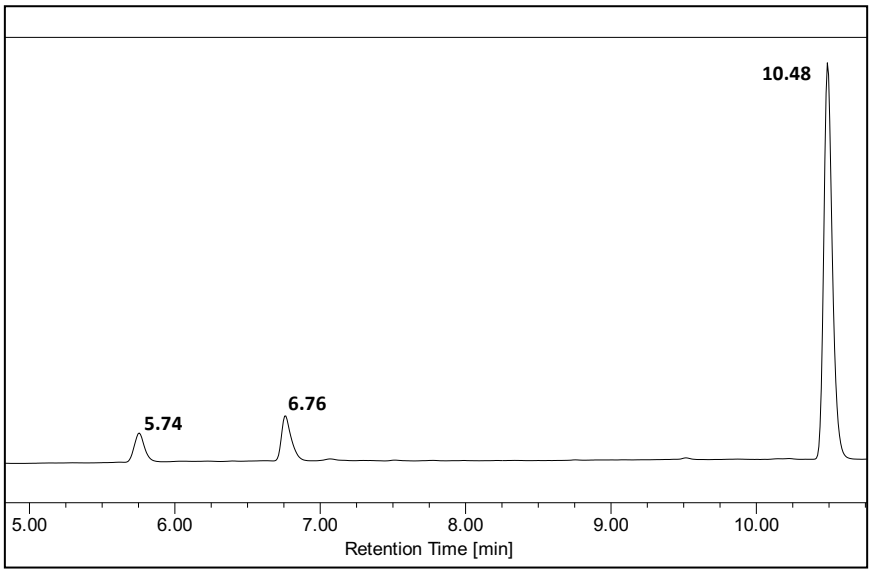

Figure 35. HPLC analysis of CIC **66** irradiated at a dose of 100 kJ/m^2 UVA. Sample in DMSO solution (1 mg/mL) were irradiated with a 4 kW broad spectrum UVA lamp (Sellas, Germany).

A representative comparison of the dose-dependent UVA uncaging of CICs **66** with the analogous CIC **55**, where deferasirox ester **33** is also masked is shown in Figure 36**.** The amount of cleavage of **66** at the lower doses of 10 and 25 kJ/m^2 is less than that of **55** which contains olefinic methyl substitution. However, once the dose of UVA increases to 50 kJ/m^2 the levels of cleavage are equal. This outcome is consistent with the work of Gagey *et al*.,[171] indicating that the presence of the olefinic methyl substituent increases the quantum yield of the reaction at lower UVA doses.

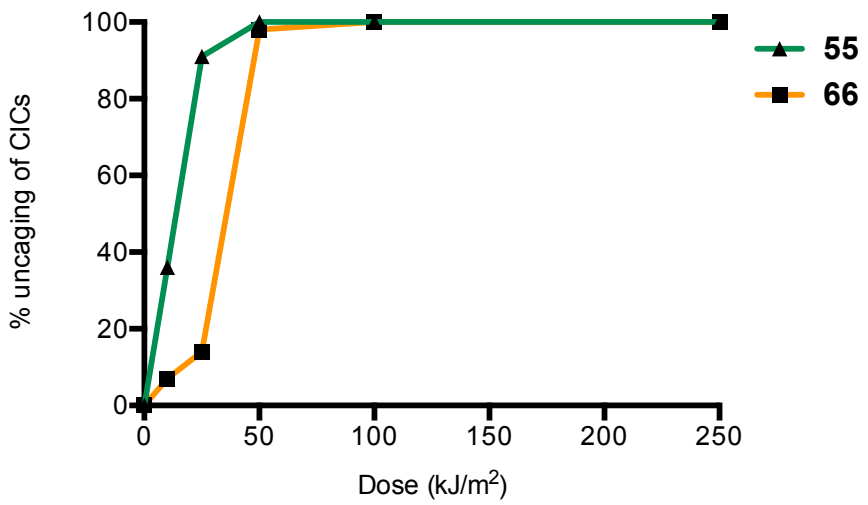

Figure 36. A representative comparison of the dose-dependent uncaging of the 3,4-dimethoxy aminocinnamoyl CICs **55** and **66**, with and without olefinic methyl substitution respectively. Percentage uncaging calculated using the peak area of the remaining CIC compared to the peak area of the unirradiated sample. Samples in DMSO solution (1 mg/mL) were irradiated with a 4 kW broad spectrum UVA lamp (Sellas, Germany).

It was postulated that the additional peak (6.8 min) was the product of a photoreaction of the carbostyril **69.** Therefore a solution of **69** in DMSO (1 mg/mL) was irradiated at a dose of 100 kJ/m^2 UVA and a sample in MeOH was injected on the analytical HPLC, and as hypothesised an additional peak at 6.8 min appeared, with a 45% relative peak area. This additional peak at 6.8 min was separated by HPLC and analysed using ^{1}H NMR which indicated the presence of a single compound, **69**. Tashima *et al.* have suggested that a carbostyril 2-quinolinone can undergo amide tautomerism to the 2-quinolinol derivative, as shown in Scheme 23.[199] To test whether the unknown compound observed could be a tautomer of **69**, a comparable solution of **69** in DMSO (1 mg/mL) was also left in the dark at room temperature for 3 days before analysis on HPLC. The appearance of the additional peak at 6.8 min was seen, however only in a 5% relative peak area. It therefore appears that in DMSO there is a low level of tautomerisation of **69**, which is intensified by UVA irradiation, however this does not occur with the methyl substituted carbostyril **60**. The biological activity of CICs **65** and **66** was not examined due to the apparently more complex uncaging of these CICs under UVA irradiation.

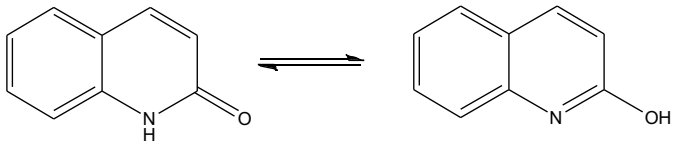

Scheme 23. Amide tautomerism of carbostyril **69** to 2-quinolinol.

5. Summary

In summary, the iron chelators PIH **7**, SIH **8**, and the methyl ester derivative of deferasirox **33** were all synthesised efficiently and their cytotoxicity in the human skin fibroblast model, FEK4 cells, was assessed. After 48 h of exposure, **7, 8** and **33** were all significantly cytotoxic at concentrations of 10-50 µM. This analysis confirmed the requirement for deactivated, or caged, iron chelators which can be dose-dependently activated upon UVA exposure to provide a photoprotective effect *via* chelation of intracellular labile iron. The well-documented 2-hydroxycinnamoyl PPG was chosen as the starting group to mask an iron chelator. Two hydroxycinnamoyl CICs **36** and **44** were synthesised and their chemical and photochemical properties were fully characterized and showed that both CICs absorb in the UVB and UVA wavelength range (280-400 nm). Although synthesis and purification of the CICs was achieved, the yields were rather low. The photoprotective capacity of both CICs was assessed in FEK4 cells exposed to an environmentally relevant dose of UVA radiation. **36** and **44** were analysed using the MTT assay and were shown to significantly increase the cell viability in comparison to the untreated irradiated control. However, neither CIC was more photoprotective than their parent iron chelator, SIH **8**. There are some concerns over the photosensitizing activity of coumarins which questions their utility in this project,[200] indeed the furanocoumarin psoralen is used as the photosensitizing drug in PUVA as described in the Introduction 1.4.1.

Subsequently the 2-aminocinnamoyl PPG was investigated as an appropriate alternative caging group for an iron chelator. A series of 3,4-dimethoxy aminocinnamoyl-caged iron chelators was efficiently synthesised (CICs **51**, **52** and **55**) and their chemical and photochemical properties were also fully characterized, revealing that CICs containing the

same caging group attached to a different iron chelator may uncage at significantly different rates. The UV/Vis absorbance spectra of CICs **51**, **52** and **55** showed that as well as covering the UVB-UVA wavelength range, the CICs also absorbed marginally into visible light. This may prove detrimental to the stability of the CICs in ambient lighting however it could also be a very interesting property due to the recent work by Lawrence *et al.* demonstrating that shortwave visible wavelengths (400-420 nm) induce photodamage including loss of cell viability and DNA damage.[201] In this 2-aminocinnamoyl CIC series the only CIC to significantly increase cell viability upon UVA irradiation when assessed in the MTT assay was the SIH-based CIC **51. 51** was equally as photoprotective as the parent iron chelator **8** and importantly was less cytotoxic than **8** after overnight incubation. Deferasirox ester **33** on its own also significantly increased cell viability.

These results show that CICs with the appropriate structure may be promising photoprotectants which can deliver a highly efficient iron chelator when activated. In order to exploit CICs to their full potential, the correct choice of iron chelator and caging group is needed. In particular, it would be interesting to incorporate additional protective properties into the photoproduct released upon uncaging, to provide a multi-functional CIC. To this end, as UVA irradiation delivers a highly oxidative environment it would be interesting to attempt to choose the caging group so as to co-deliver a novel antioxidant alongside the active iron chelator. The diversity and ease of synthesis of aminocinnamoyl-based CICs makes them more attractive as CICs, and thus the functionalisation of the carbostyril photoproduct could be advantageous. Carbostyrils are structurally similar to coumarins, some of which are known antioxidants. Therefore researching the properties of carbostyrils may provide a way to incorporate a pro-antioxidant function into CICs.

CHAPTER 3: RESULTS AND DISCUSSION

1. Introduction

The structure of carbostyrils (2-quinolones) mimics that of coumarins, whereby the ester is replaced with an amide. Therefore it would be reasonable to hypothesise that carbostyrils could also have an inherent antioxidant activity. Thuong *et al.* isolated 21 coumarins from medicinal plants and of these eight inhibited lipid peroxidation in rat liver mitochondria.[179] In all of the natural coumarins that had a positive effect, they contained one or more electron-donating hydroxyl or methoxy substituents. In particular, the compound that possessed considerable antioxidant activity contained a catechol group as seen in **34c**.[179] Sankaran *et al.* has highlighted the importance of nitrogen-containing heterocycles such as quinolones (carbostyrils) in medicinal chemistry research into compounds with antioxidant, antiproliferative, anti-inflammatory and anticancer biological activity.[202] For example, in a study by Chung *et al.* 4-carbomethoxy-6-hydroxy-2-quinolone **70** (Figure 37) was extracted from the purple-pigmented rice *Oryza sativa* cv. *Heugjinmi* and was shown to possess moderate antioxidant activity.[203] Similarly, a fused quinolone derivative **71** was found to be highly effective at free radical scavenging.[202] The free radical scavenging activity of the series of synthesised quinolone derivatives was thought to arise from either a phenolic hydroxyl group or from the imino function of the quinolone, which are both available sites for a free radical to undergo electron transfer or abstract a hydrogen atom.[202]

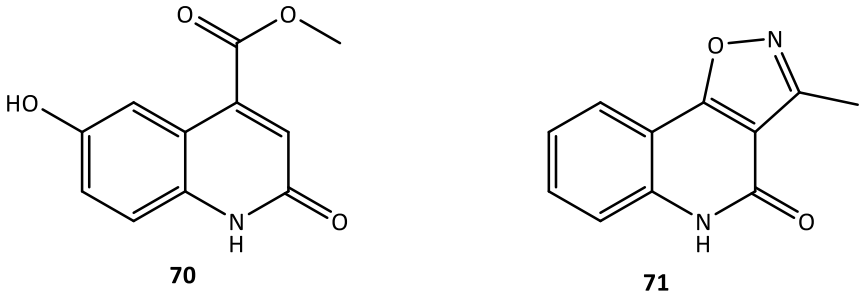

Figure 37. The structures of two quinolone derivatives **70** and **71** which have been investigated for their antioxidant activity.[202,203]

Upon UVA-induced photo-cleavage of an aminocinnamoyl caging group, a carbostyril photoproduct is released. This provides an opportunity to include a novel potentially antioxidant by-product as part of the release of an active iron chelator from a CIC. In order to investigate the antioxidant potential of carbostyril photoproducts, a 'retrosynthetic' approach was used, represented in Scheme 24. This process required the synthesis of a series of potential carbostyrils to find the photoproduct with the most biological potential. The corresponding caging group could then be synthesised and subsequently coupled to an iron chelator to provide a CIC with a multi-functional action.

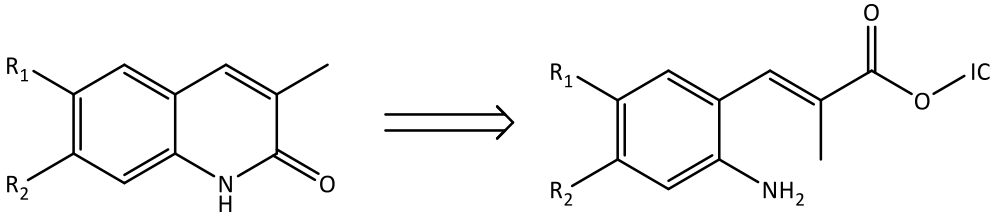

Scheme 24. 'Retrosynthetic' approach to synthesising a multi-functional CIC, beginning with the photoproduct that would be released upon UVA-cleavage.

2. Carbostyril photoproduct series: synthesis and antioxidant properties

To synthesise a series of carbostyrils, the route already developed in Chapter 2.4 for the synthesis of an aminocinnamic acid was used, followed by acid-catalysed cyclization to form the carbostyril (Scheme 22). Varying the electron-donating substituents on the aromatic ring of the starting materials would be expected to positively affect the ROS scavenging activity of the final carbostyril.[202,204] Synthesis of the series relied partially on the availability of starting materials containing suitable electron-donating groups such as methoxy and hydroxyl groups.

Table 4. The starting materials for the synthesis of a range of carbostyrils with varying aromatic substituents.

Starting material	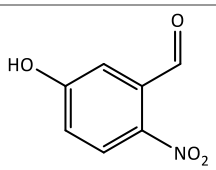	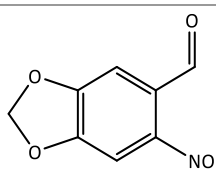	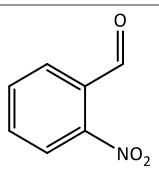	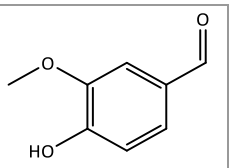
Compound number	**72**	**73**	**74**	**75**

All of the required nitrobenzaldehyde starting materials **72**-**74** were commercially available except for the 4-hydroxy-3-methoxybenzaldehyde derivative, 6-nitrovanillin, which was instead available as the aldehyde vanillin **75**, as shown in Table 4. Regiospecific nitration of vanillin *via* an electrophilic aromatic substitution reaction was required, however due to the deactivating *meta*-directing aldehyde, the product of direct nitration of **75** would be 5-nitrovanillin rather than the desired 6-nitrovanillin, as shown in Scheme 25.[205]

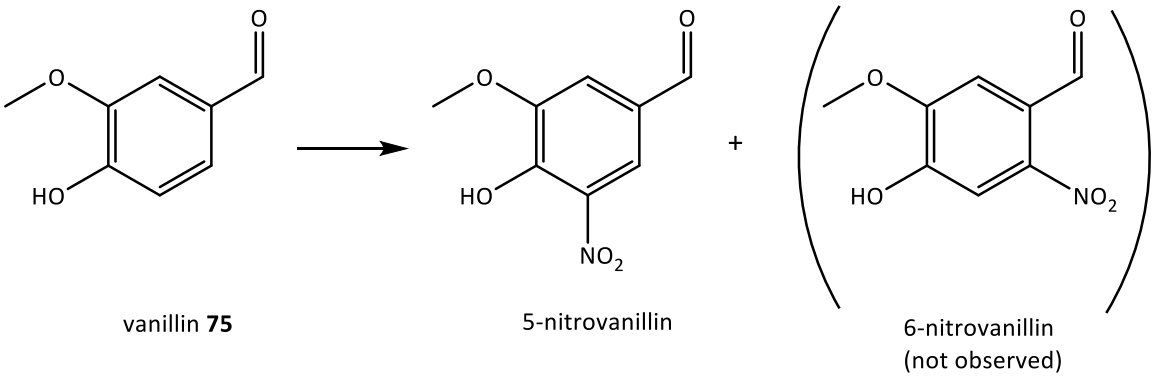

Scheme 25. The product of direct nitration of vanillin **75**: 5-nitrovanillin.

In order to change the regioselectivity of the nitration to give only 6-nitrovanillin, it was necessary to first protect the free 4-hydroxyl group of **75** as a benzyl ether. The steric hindrance from the benzyl group along with the *para*- directing potential of the electron-donating methoxy group has been used previously as a successful means to achieve selective nitration in the 6-position.[206-209] Benzyl protection of **75** using benzyl bromide and K_2CO_3 proceeded efficiently, and recrystallization from EtOH gave the protected vanillin derivative **76** in a 93% yield (Scheme 26). Regiospecific nitration was then carried out using 65% nitric acid at 0^{o}C to give **77** in a 60% yield after recrystallisation.

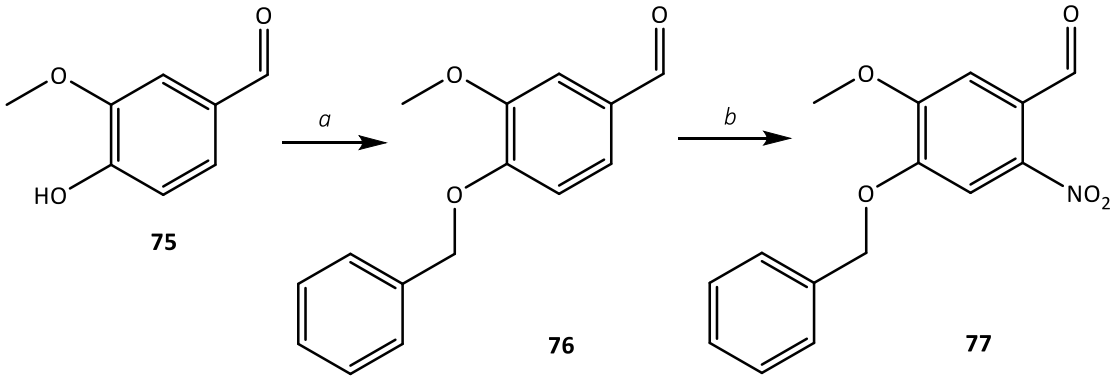

Scheme 26. Benzyl protection of vanillin **75** followed by regiospecific nitration to give the desired 6-nitrovanillin derivative **77.** *Reagents and conditions:* **a.** BnBr, K_2CO_3, MeOH, reflux, 4 h, 93%; **b.** aq. 65% nitric acid, 0^oC, 1 h, 60%.

Due to possible side reactions associated with the free nucleophilic hydroxyl group of 5-hydroxy-2-nitrobenzaldehyde **72** (Table 4) during the subsequent synthetic pathway, the hydroxyl group of this starting material was also protected with a benzyl ether. The reaction was carried out in the same manner as for vanillin **75** to give the protected derivative **78** in an 80% yield, as shown in Scheme 27. The addition of the benzyl group also was expected to improve the solubility of **78** in organic solvents and thus the ease of synthesis of subsequent intermediates.

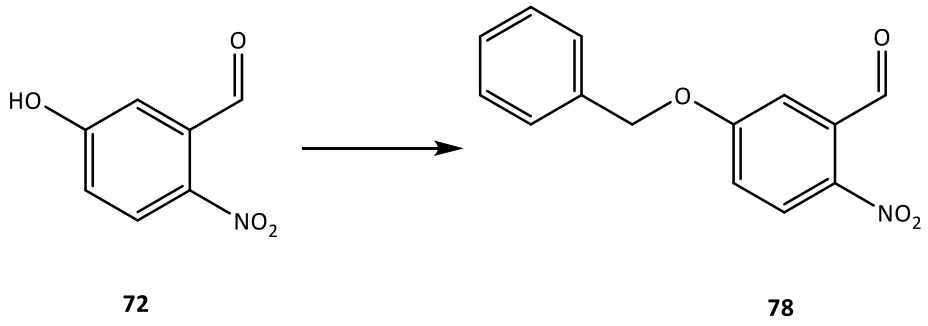

Scheme 27. Benzyl protection of 5-hydroxy-2-nitrobenzaldehyde **72** to give the desired protected derivative **78.** *Reagents and conditions:* BnBr, K_2CO_3, MeOH, reflux, 4 h, 80%.

All of the nitrobenzaldehydes **73, 74, 77** and **78** were then subjected to the same synthetic pathway as described in Chapter 2.4 to synthesise the aminocinnamic acids, as shown in Scheme 28. The Wittig reaction was carried out with ECETP in anhydrous toluene to give

esters **79-82** in excellent yields. Subsequent saponification of the esters to the carboxylic acids **83-86** also proceeded in high yields. Chemoselective reduction of the nitro group to an amino group using $FeSO_4$ and aqueous NH_3 to give aminocinnamic acids **87-90** then proceeded in good yields ranging from 59-80%. All of the aminocinnamic acids except for **88** were successfully cyclized to the respective carbostyril by refluxing in 4% HCl.[194] The acidic conditions also removed the benzyl protecting group of **89** and **90** to give the free hydroxyl group, and thus the desired carbostyrils **91, 93** and **94** were synthesised. In the case of **88**, there was no conversion of the starting material to the desired carbostyril **92** after refluxing in 4% HCl, as judged by TLC and HPLC. A different acid-catalyzed cyclization was therefore attempted using the alternative mineral acid, 70% H_2SO_4 instead. Under these conditions conversion of the starting material proceeded slowly, giving carbostyril **92** in a 25% yield after refluxing for 12 h.

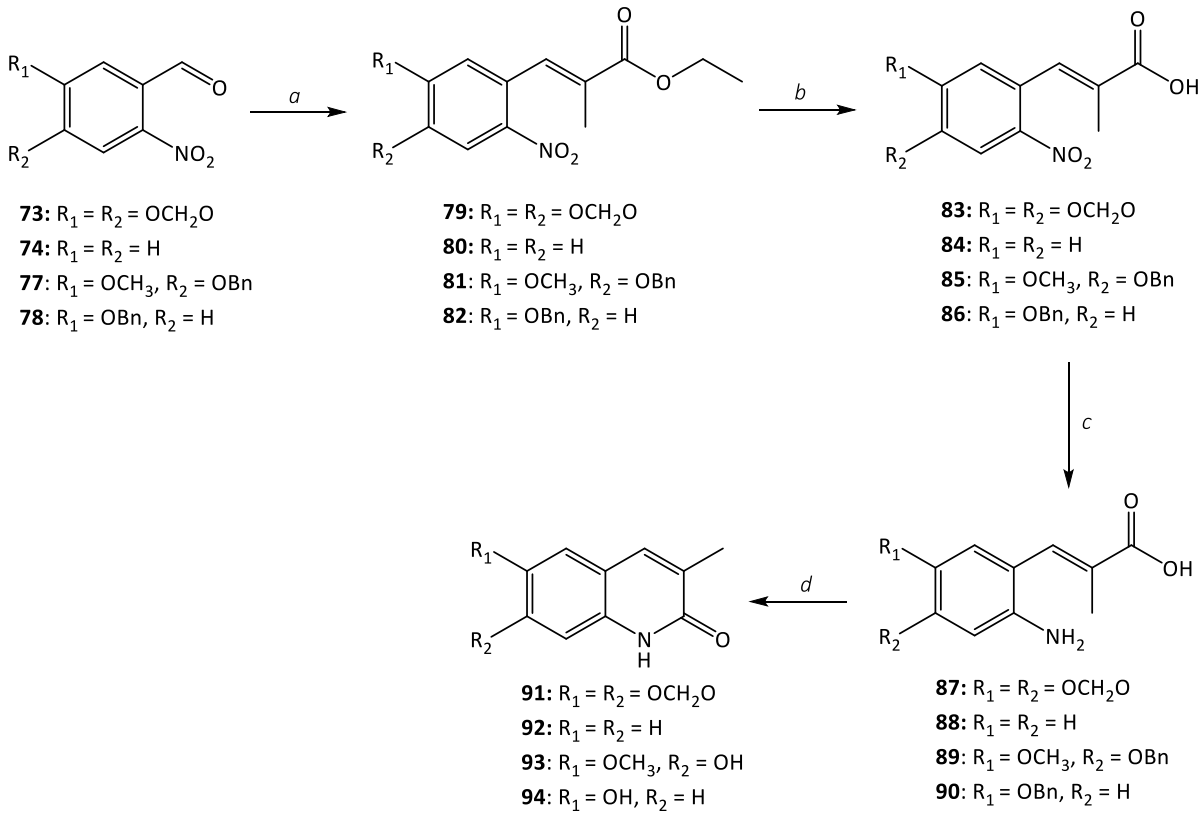

Scheme 28. The synthetic route to a series of carbostyril photoproducts **91-94**. *Reagents and conditions:* **a. b.** ECETP, dry toluene, 65°C, 98-99%; **c.** 1M NaOH, 4:1 THF:EtOH, RT- 40 °C, 90-99%; **d.** $FeSO_4.7H_2O$, water, aq. 35% NH_3, 80°C→ RT, 59-80%; **e.** 4% aq. HCl, reflux, 2-4 h, 57-95% or 70% aq. H_2SO_4, reflux, 12 h, 25%.

To complete the series of carbostyrils, the 6,7-dihydroxy derivative **95** was synthesised to compare its antioxidant activity to the strong free radical scavenging capabilities of the 6,7-dihydroxy coumarin, esculetin **34c**.[179,180] The easiest route of synthesis to the 6,7-dihydroxy carbostyril **95** was *via* cleavage of the 6,7-dimethoxy groups in the previously synthesised carbostyril **60** (Chapter 2.4). Methyl ether cleavage of coumarin derivatives using the strong Lewis acid boron tribromide has been described in the literature,[210,211] therefore this method was employed. A solution of **60** in anhydrous DCM was treated with a solution of 1M BBr_3 in DCM at 0°C under an argon atmosphere, giving the desired carbostyril **95** in an 82% yield, as shown in Scheme 29.

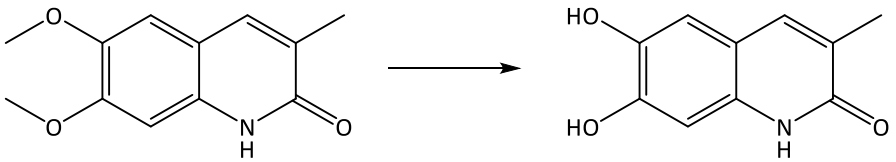

60 **95**

Scheme 29. Synthesis of a 6,7-dihydroxy carbostyril **95**. *Reagents and conditions:* 1M BBr_3, anhydrous DCM, 0°C→ RT, 18 h, 82%.

Seven synthesised carbostyrils (**60, 69** and **91-95**) were now available for analysis of their free radical scavenging capacity and potential photoprotective effects. All carbostyrils were fully characterised and their absorbance over the UVA/B range was recorded, as shown in Figure 38, with the absorption profiles compared in Table 5. The majority of carbostyrils exhibit a maximum absorption at 340-345 nm, except for **92** which is blue-shifted by approximately 20 nm. Li *et al.* reported a series of purified carbostyrils formed by UVA irradiation of the respective aminocinnamic acid.[172] This series had varying substituents on the aromatic ring as well as *N*-alkyl substitutions. The maximum absorption values reported in Li's study for carbostyrils which are comparable with those in our series ranged from 342-364 nm, in line with the maximum absorption values reported here. Likewise Li *et al.* also reported a blue-shift to 324 nm for carbostyril **92**. These results suggest that groups with a +M (mesomeric) effect may cause a red-shift in the maximum absorption of such compounds. However carbostyril **94** has a very different absorbance profile to the other carbostyrils, with a maximum absorbance at 203 nm. Carbostyril **95** absorbs quite significantly between 320-370

nm in the UVA wavelength range with a molar extinction coefficient, ε_{345}, of 10,130 L mol^{-1} cm^{-1} and has the highest maximum absorption which is explained by the presence of the two strongly electron-donating methoxy groups on the aromatic ring. This is also consistent with work by Fabian *et al.* who reported that donor substituents in the 6-position of carbostyrils produced substantial red-shifts in both absorption and fluorescence spectra.[212]

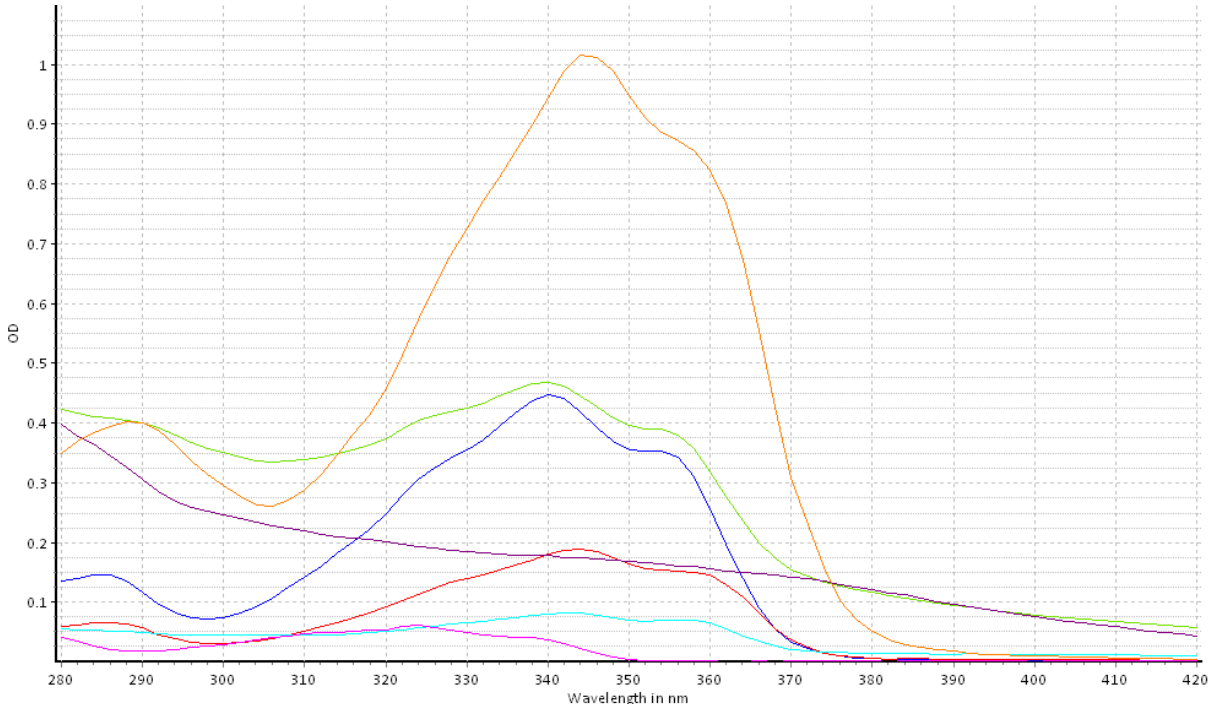

Figure 38. The UV/Vis absorbance spectra of all the synthesised carbostyrils **60, 69** and **91-95** in EtOH (100 µM).

Table 5. A comparison of the absorption profiles of carbostyrils **60, 69** and **91-95.**

Carbostyril	Spectrum colour	Absorption Maximum (nm)	Molar extinction coefficient, ε_{max} (L mol^{-1} cm^{-1})
60		341	4,500
69		344	1,890
91		343	930
92		323	566
93		341	4,710
94		203 (not shown)	9,070
95		345	10,130

A literature review was carried out to find the most suitable chemical assay to perform an initial screen of the antioxidant potential of the synthesised carbostyrils. The 2,2-diphenyl-1-picryl-hydrazyl-hydrate (DPPH) assay is widely used,[179,180,202,211,213-215] , and is a simple assay which can be carried out with minimal reagents and resources. The only drawback of this assay is that experimental procedures are not standardised and therefore results from different research groups cannot easily be compared. However, due to its simplicity, it was considered to be the most appropriate assay to screen the carbostyrils, alongside a positive antioxidant standard such as α-tocopherol or its water soluble derivative, trolox. DPPH itself is a stable free radical that can be reduced by an antioxidant molecule (A) *via* electron transfer. DPPH absorbs visible light at 520 nm giving a violet colour, and is converted to a colourless compound upon quenching, therefore disappearance of the violet colour reflects the presence of an active free radical-neutralising compound[213,215]:

$DPPH^{\cdot} + A\text{-}H \rightarrow DPPH\text{-}H + A^{\cdot}$

The DPPH assay was carried out on carbostyrils **60, 69** and **91-95,** coumarin **34a** and umbelliferone **34b** along with positive controls trolox and ascorbic acid as described in the Experimental Section 7.2.6. Three of the compounds tested (**93, 94** and **95**) showed antioxidant properties, the results of the DPPH assays for these compounds are summarised in Table 6. Figure 39 represents the percentage radical scavenging activity against concentration for the three active carbostyrils.

Table 6. The free radical scavenging activity of compounds **93**, **94** and **95**, along with the positive controls trolox and ascorbic acid. The straight line equation over the linear concentration range of activity is shown, and the calculated IC_{50} value is presented which represents the concentration at which 50% of the radicals are scavenged.

Compound	Linear range of activity (µM)	Line equation	IC_{50} (µM)
trolox	10-100	y = 0.9508x	52.3
ascorbic acid	10-100	y = 0.8682x	57.6
93	10-200	y = 0.4386x	114.0
94	10-100	y = 0.9151x	54.6
95	10-50	y = 1.979x	25.3

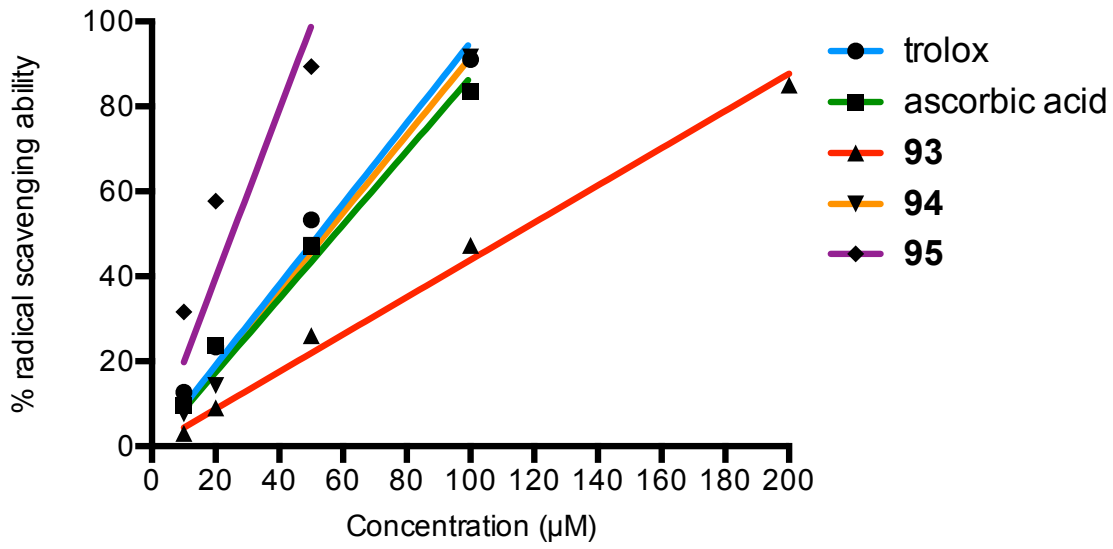

Figure 39. Plot of the percentage free radical scavenging activity against concentration of compounds **93-95** that were found to have a positive antioxidant effect, along with the positive controls trolox and ascorbic acid.

The DPPH assay confirmed the hypothesis that carbostyril **95** containing the catechol 6,7-dihydroxy motif should possess considerable antioxidant activity. In this assay **95** had an IC_{50} value (the concentration at which 50% of the radical was scavenged) of 25.3 µM, approximately twice as effective as the positive control, trolox (IC_{50} = 52.3 µM). The 6-hydroxy derivative **94** also performed well with an IC_{50} value of 54.6 µM, comparable to trolox and ascorbic acid (57.6 µM). Carbostyril **93** was a moderately good free radical scavenger with an IC_{50} value of 114.0 µM. All other carbostyrils and coumarins were inactive in this assay. The antioxidant power of **95** was proposed to be *via* the ability of the catechol group to neutralise two free radicals, such as the hydroxyl radical ·OH generated upon UVA irradiation, as represented in Scheme 30.[216]

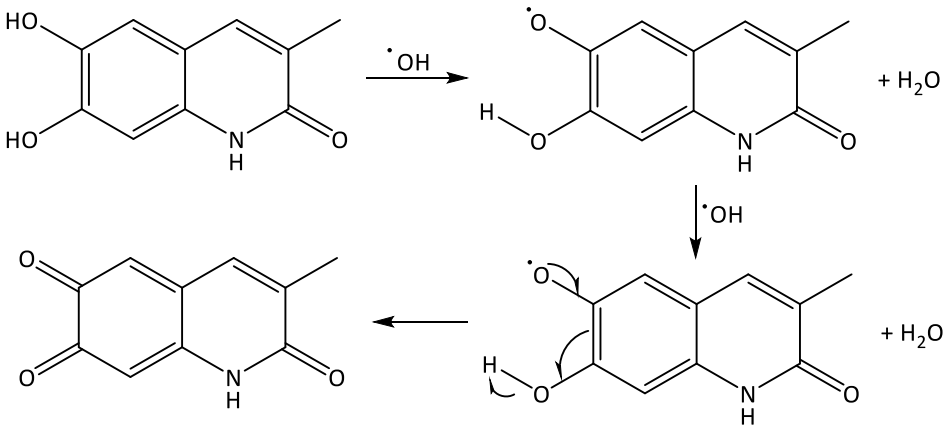

Scheme 30. Proposed free radical scavenging mechanism for carbostyril **95**.[216]

After determining the antioxidant potential of the series of carbostyrils in a chemical assay, the performance of the carbostyrils against UVA-generated ROS in a cellular assay was assessed. The two carbostyrils that displayed the most positive free radical scavenging activity (**94** and **95**) were taken forward to the DCFDA assay. CM-H_2DCFDA is the chloromethyl derivative of 2',7'-dichlorodihydrofluorescein diacetate (H_2DCFDA) which is a ROS indicator used in live cells. The chloromethyl derivative displays much better retention in live cells than H_2DCFDA. CM-H_2DCFDA passively diffuses into cells where the acetate groups are cleaved by intracellular esterases and the chloromethyl group reacts with intracellular glutathione and other thiols to trap the indicator inside the cell[217] (Scheme 31). Subsequent oxidation *via* an intracellular source of ROS yields the fluorescent adduct 2',7'-dichlorodihydrofluorescein, which absorbs at 492–495 nm and emits at 517–527 nm.

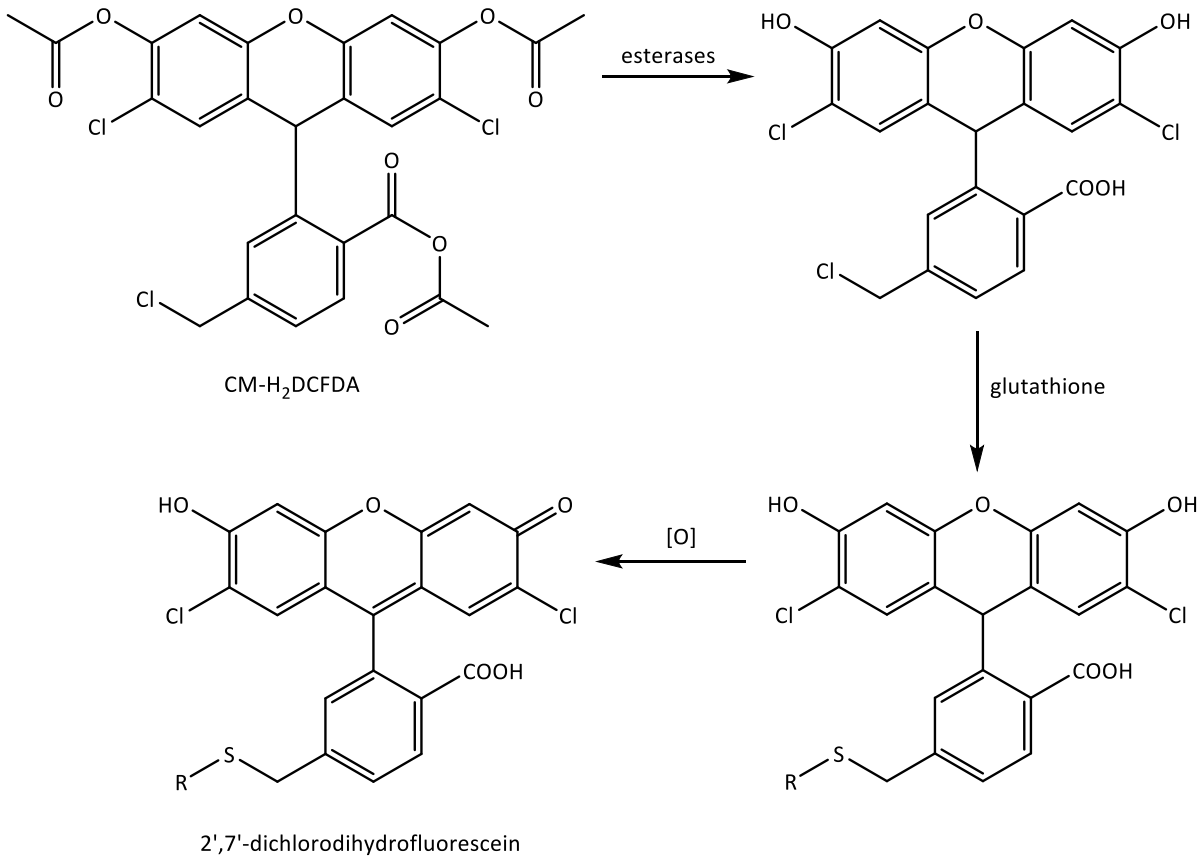

Scheme 31. Mechanisms of intracellular trapping and subsequent oxidation of the ROS probe CM-H_2DCFDA.

The level of fluorescence of 2',7'-dichlorodihydrofluorescein correlates directly to the level of intracellular ROS. In order to assess the photoprotective effects of the carbostyrils, FEK4 cells were treated with ± 20 µM of **94** and **95** for 18 h before exposure to ± 250 kJ/m^2 dose of UVA radiation. Cells were incubated with CM-H_2DCFDA after irradiation and the fluorescence was monitored by flow cytometry, with the results shown in Figure 40.

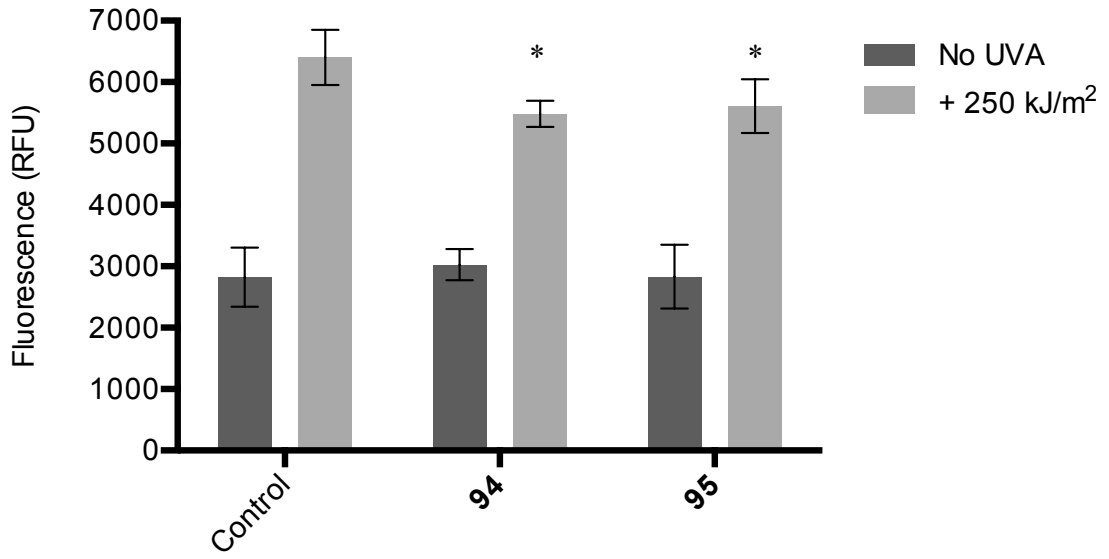

Figure 40. Evaluation of the free radical scavenging capacity of carbostyrils **94** and **95** against UVA-induced ROS in FEK4 fibroblasts. Cells were treated with ± compounds (20 µM) for 18 h before exposure to ± 250 kJ/m^2 dose of UVA radiation. The level of ROS was monitored by flow cytometry using the fluorescent CM-DCFDA dye. Data is expressed as the mean fluorescence ± SD (n=3–13). *= p <0.05, significantly different from untreated irradiated cells.

The addition of 20 µM **94** and **95** to FEK4 cells prior to UVA irradiation significantly reduced the level of fluorescence (therefore the amount of ROS present intracellularly) in comparison to the 250 kJ/m^2 UVA positive control. The positive control had a fluorescence of 6323 RFU which decreased to 5708 and 5787 RFU in the presence of carbostyrils **94** and **95** respectively.

To mimic the photoproducts released from UVA uncaging of a potential CIC, the combined free radical scavenging capacity of **94** and **95** was examined in the presence of an iron chelator at equivalent concentration (20 µM). Using this approach, the best combination of an iron chelator and carbostyril could potentially be found, and the CIC that corresponded to the identified photoproducts could then be synthesised. In Chapter 2.4 the photoprotective capacity of the iron chelators PIH **7**, SIH **8** and deferasirox ester **33** were compared using the MTT assay after 500 kJ/m^2 UVA irradiation. The results showed that whilst **8** and **33** were significantly photoprotective at a concentration of 20 µM, **7** was not. For this reason only iron chelators **8** and **33** were used in the following DCFDA assay. FEK4 cells were treated with ± 20 µM of either the iron chelator alone or the iron chelator plus **94** or **95.** After exposure to ±

250 kJ/m^2 UVA radiation, cells were incubated with CM-H_2DCFDA and the cell fluorescence was monitored by flow cytometry. The results of the assay using **33** combined with or without **94** or **95** are shown in Figure 41.

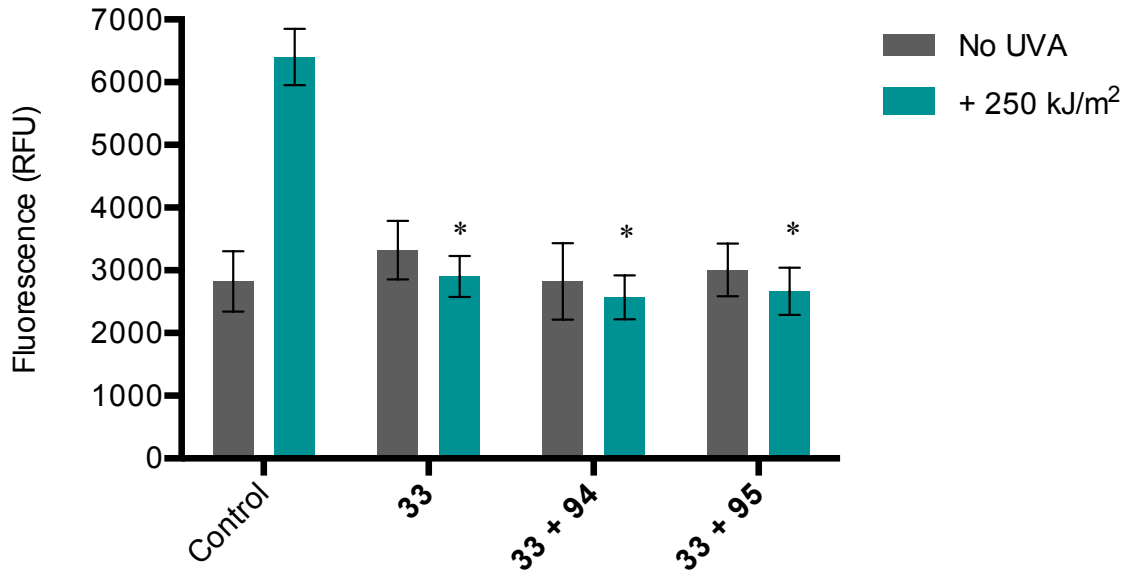

Figure 41. Evaluation of the combined free radical scavenging capacity of the iron chelator **33** and carbostyrils **94** and **95** against UVA-induced ROS in FEK4 fibroblasts. Cells were treated with ± compounds (20 µM) for 18 h before exposure to ± 250 kJ/m^2 dose of UVA radiation. The level of ROS was monitored by flow cytometry using the fluorescent CM-DCFDA dye. Data is expressed as the mean fluorescence ± SD (n=3–13). *= p <0.05, significantly different from irradiated untreated cells.

These results indicated that both deferasirox ester **33** alone and the combination of **33** and **94** or **95** all significantly reduced the level of intracellular ROS in comparison to the positive control. The combinations of iron chelator and carbostyrils reduced the free radicals slightly more than the iron chelator alone, with the fluorescence lower than that of the negative control without UVA irradiation. The same assay was repeated for SIH **8** along with carbostyrils **94** and **95**, and the results are shown in Figure 42.

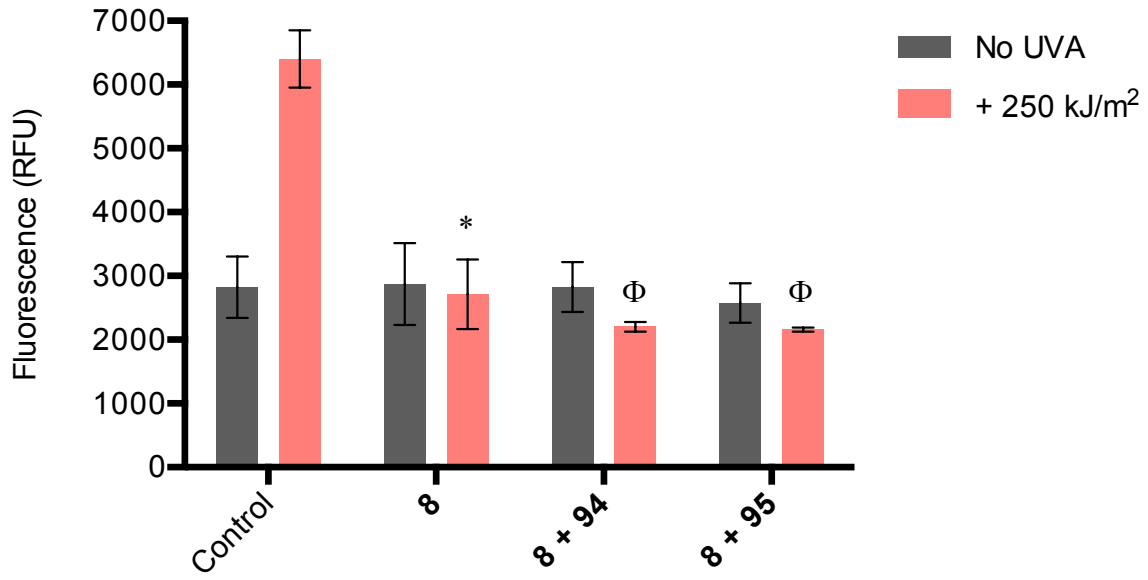

Figure 42. Evaluation of the combined free radical scavenging capacity of the iron chelator **8** and carbostyrils **94** and **95** against UVA-induced ROS in FEK4 fibroblasts. Cells were treated with ± compounds (20 µM) for 18 h before exposure to ± 250 kJ/m^2 dose of UVA radiation. The level of ROS was monitored by flow cytometry using the fluorescent CM-DCFDA dye. Data is expressed as the mean fluorescence ± SD (n=3–13). *= p <0.05, significantly different from irradiated untreated cells.

Φ= p <0.05, significantly different from both irradiated untreated cells and irradiated cells treated with **8** only.

Both SIH **8** alone and the combination of **8** and **94** or **95** all significantly reduced the level of intracellular ROS in comparison to the positive control. The combinations of **8** + **94** and **8** + **95** significantly reduced the UVA-induced ROS more than **8** alone (2202, 2157 and 2714 RFU respectively). The combined action of **8** + **94** and **8** + **95** also markedly lowered the fluorescence in comparison to the negative control without UVA irradiation. These results indicate that a multi-functional CIC combining the iron chelator SIH **8** and either carbostyril **94** or **95** should have the most favourable photoprotective and antioxidant potential. The combinations of deferasirox ester **33** and either carbostyril are also very promising.

3. Synthesis of multi-functional CICs

Carbostyrils **93, 94** and **95** showed the best antioxidant activity in the synthesised carbostyril series. Therefore the synthesis of the caging groups relating to carbostyrils **93, 94** and **95** was carried out in order to synthesise multi-functional CICs containing these photo-cleavable groups. The benzyl-protected aminocinnamic acids **89** and **90** were synthesised as part of the

synthetic route to carbostyrils **93** and **94** (Scheme 28). Removal of the benzyl protection would therefore give the required caging derivative for subsequent coupling to an iron chelator. Lai *et al.* reported the use of TFA to remove the benzyl group from protected 6-nitrovanillin,[218] therefore this method was attempted with aminocinnamic acid **89** at room temperature to give the desired product **96** (Scheme 32). The reaction effectively removed the benzyl group, but also catalysed the cyclization of **89** to give the carbostyril **93**.

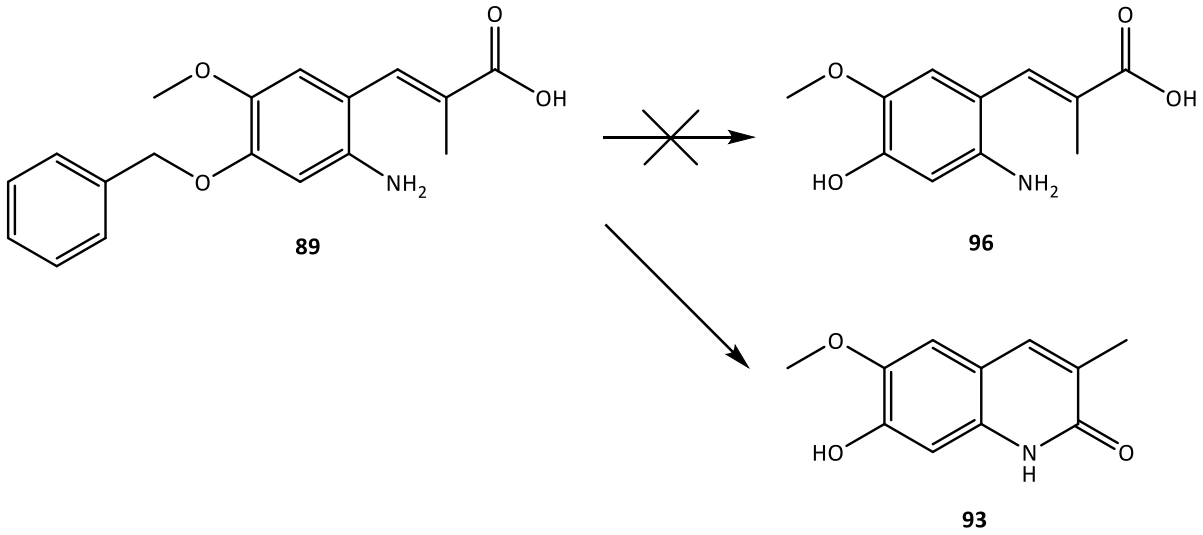

Scheme 32. Attempted removal of benzyl protecting group of **89** to give acid **96** generating carbostyril **93** instead**.** *Reagents and conditions:* TFA, RT, O/N, 74%.

Removal of benzyl ethers *via* palladium-catalyzed hydrogenolysis is another commonly used synthetic method.[183] Due to the presence of the reducible alkene unit in **89**, benzyl ether hydrogenation was first attempted with 10% Pd/C and H_2 in the moderately polar aprotic solvent EtOAc to slow the undesired reduction process.[219] However after 12h, there was no conversion of the starting material observable on TLC. The reaction was then repeated with the polar protic solvent AcOH. After 3 h the starting material was consumed, however the product was both debenzylated and the alkene function was saturated, as confirmed by ^{1}H NMR and mass spectrometry. Jung *et al.* have described the dealkylation of a large range of alkyl and aryl ethers using 1.3 equivalents of the Lewis acid, trimethylsilyl iodide (TMS-I).[220] This method was adopted and **89** was treated with TMS-I in anhydrous DCM under argon, but there was no consumption of starting material after 2 h at room temperature, so the reaction was heated to reflux. This also did not convert **89** to the desired product **96**. **89** was poorly

soluble in anhydrous DCM, which may have prevented the reaction from occurring, so the reaction was repeated in anhydrous MeCN at reflux as **89** was most soluble in this solvent. However **89** still did not convert to **96** in anhydrous MeCN.

As removal of benzyl protection in the aminocinnamic acid **89** to give **96** was difficult to achieve, debenzylation of the 6-nitro ester derivative **81** was attempted instead. Benzyl cleavage was carried out in TFA at 30^{o}C and proceeded cleanly in a 93% yield after column chromatography to give the debenzylated product **97** (route a in Scheme 33). Hydrolysis of the ester using the previously described method worked well to give **98** in an excellent yield. Reduction of **98** failed under the standard $FeSO_4$ conditions (previously used for a range of nitrocinnamic acids) giving a complex mixture of products on TLC. The reduction was also unsuccessful under conditions described for reduction of 6-nitrovanillin,[193] which has a free phenolic hydroxyl like **98** (step d in Scheme 33). This reaction also gave a complex mixture of products on TLC and a major product could not be identified by ^{1}H NMR analysis. Gowda *et al.* described the use of hydrazinium monoformate with zinc dust to selectively reduce nitro compounds in 2- 5 min in the presence of a range of reducible groups (*e.g* alkene, acid and ester groups).[221] This method was attempted, with hydrazinium monoformate being generated *in situ* by first neutralizing hydrazinium hydrate with equimolar formic acid, which was then added to **98** and zinc dust in MeOH. Under these conditions, there was no conversion of **98** to the desired reduced product after 2 h as judged by TLC.

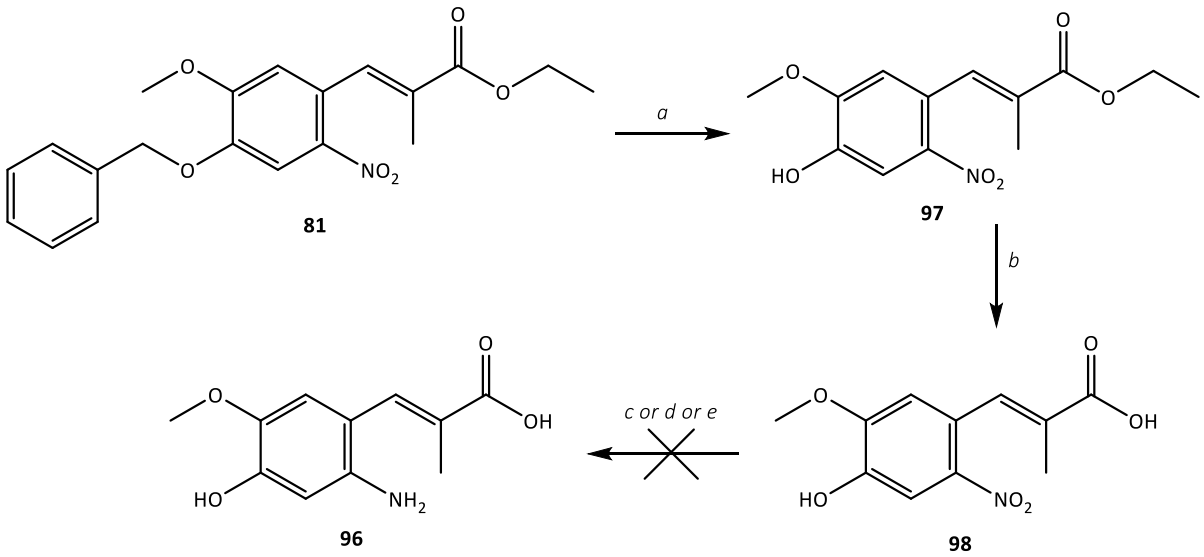

Scheme 33. Alternative attempted synthetic route to cinnamic acid **96**. *Reagents and conditions:* **a.** TFA, 30°C, O/N, 93%; **b.** 1M NaOH, 4:1 THF:EtOH, RT- 40 °C, 98%; **c.** $FeSO_4.7H_2O$, water, aq. 35% NH_3, 80°C→ RT; **d.** iron powder, NH_4Cl, 80% (aq.) EtOH, 80°C; **e.** hydrazinium monoformate, Zn dust, MeOH, 30°C**.**

In parallel, a similar synthetic pathway was attempted towards the synthesis of aminocinnamic acid **99** (Scheme 34). Benzyl ether cleavage of **82** with TFA at 30°C proceeded well to give a good yield of **100.** The ethyl ester was then hydrolysed to give **101** which was taken forward for reduction of the nitro group to give the desired aminocinnamic acid **99** using iron powder and NH_4Cl.[193] This reaction also gave a complex mixture of products on TLC.

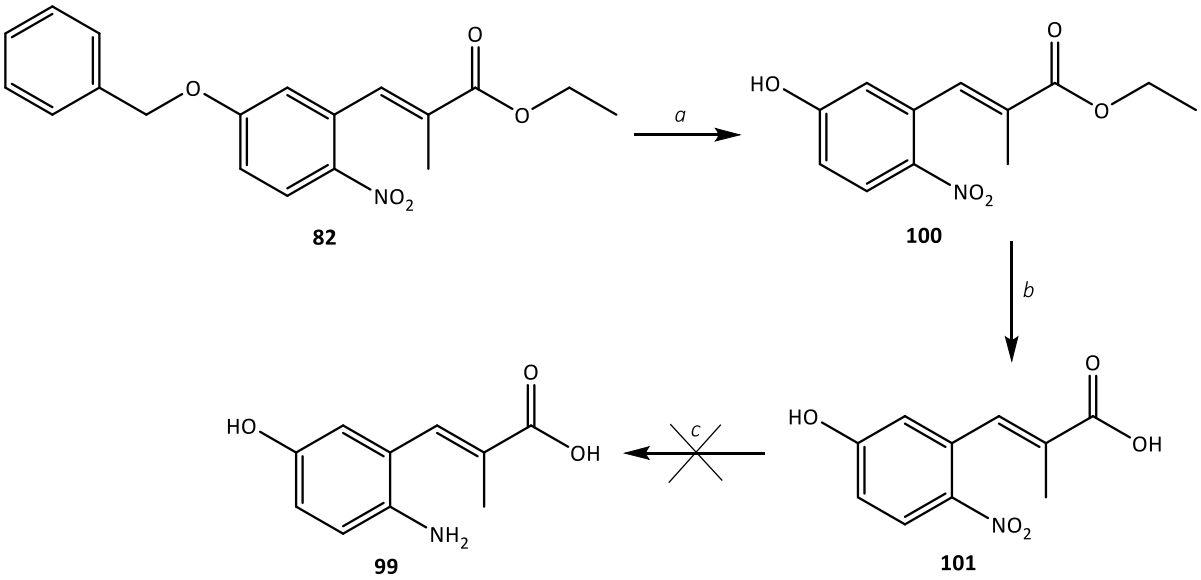

Scheme 34. Attempted synthetic route to cinnamic acid **99**. *Reagents and conditions:* **a.** TFA, 30°C, O/N, 93%; **b.** 1M NaOH, 4:1 THF:EtOH, 30 °C, 98%; **c.** iron powder, NH_4Cl, 80% (aq.) EtOH, 80°C.

These results indicated that either the presence of a phenolic hydroxyl in the 4-position (**98**) or the 3-position (**101**), or the carboxylic acid functional group in both **98** and **101** were affecting the reduction of the nitro group to the amine. Therefore to decipher which functional group was affecting the reaction, the deprotected nitro ester **97** was submitted to reduction using iron powder and NH_4Cl (Scheme 35). This reaction proceeded well to give pure **102** in a 92% yield, indicating that the presence of the phenolic hydroxyl did not affect the nitro group reduction under these conditions. Ethyl ester hydrolysis of **102** however gave a mixture of products, one of which was the carbostyril **93** which may have formed upon acidic work-up of the reaction.

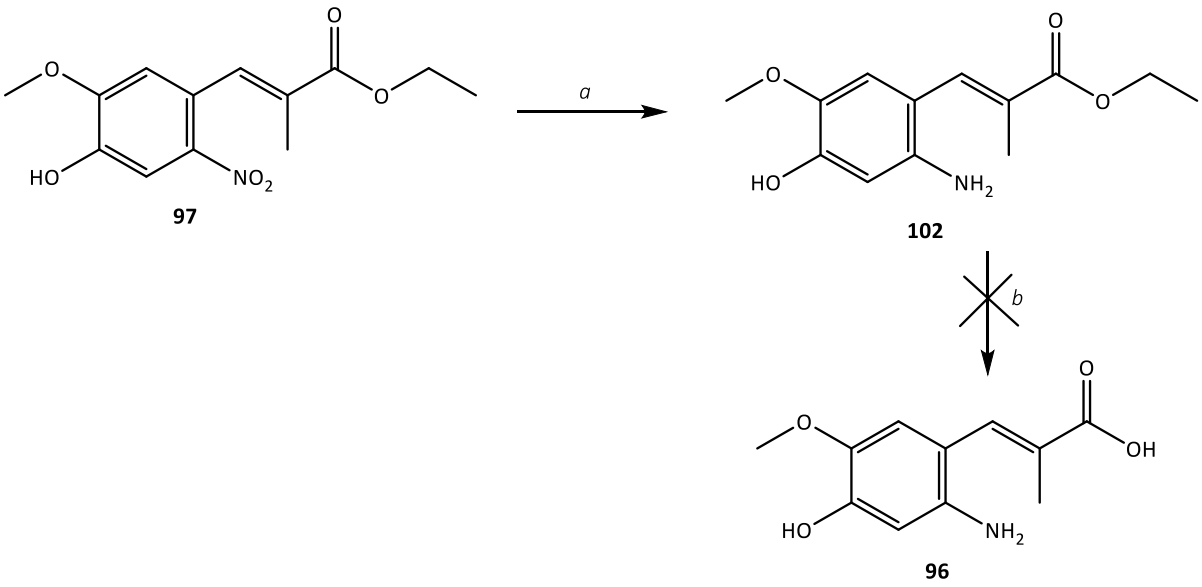

Scheme 35. Alternative synthetic route to aminocinnamic acid **96**. *Reagents and conditions:* **a.** iron powder, NH_4Cl, 80% (aq.) EtOH, 80°C, 2 h, 92%; **b.** 1M NaOH, 4:1 THF:EtOH, 30 °C.

So far all of the alternative routes to synthesise one of the desired aminocinnamic acids with a free hydroxyl function had proved unsuccessful. Cleavage of the benzyl protecting group with TFA proceeded well if the possibility of intramolecular cyclization to the carbostyril was not present (*e.g* route a in Scheme 33 and route a in Scheme 34). It was therefore proposed that the benzyl groups of the aminocinnamoyl unit could instead be cleaved after coupling with an iron chelator. The ester unit of a CIC is relatively sterically hindered and therefore acid-catalysed cyclization of the aminocinnamate group should be slower than for a simple ethyl ester. To test this hypothesis, a sample of one of the previously synthesised aminocinnamic acid CICs **51** was stirred in TFA at room temperature, and after 12 h the sample was analysed by HPLC which indicated that the CIC had not cleaved to the parent iron chelator and the carbostyril, but still remained as a single pure compound. Therefore the protected aminocinnamic acids could potentially be coupled with an iron chelator before cleavage of the benzyl groups with TFA.

The protected aminocinnamic acids that corresponded to the attractive carbostyrils **93** and **94** had already been synthesised (**89** and **90**). However the protected aminocinnamic acid that would release the most promising catechol-type carbostyril **95** was not yet available. The synthesis of this protected aminocinnamic acid began with 3,4-dihydroxybenzaldehyde and

proceeded *via* the previously used routes (Scheme 36). Protection of the catechol motif to give **103** was achieved using slightly more than two equivalents of benzyl chloride and K_2CO_3 in anhydrous DMF. Nitration of **103** was directed to the 6-position and proceeded in a 92% yield. The nitro ester **105** was generated using the Wittig reagent ECETP and was then hydrolysed to **106** in 1M NaOH and EtOH. Finally, reduction of the nitro group appeared to proceed efficiently by TLC and the desired protected aminocinnamic acid **107** was successfully isolated, although in a relatively low yield (16%)**.** Aqueous filtration of the reaction mixture through Celite may have been responsible for the loss of product due to the water insolubility of **107.**

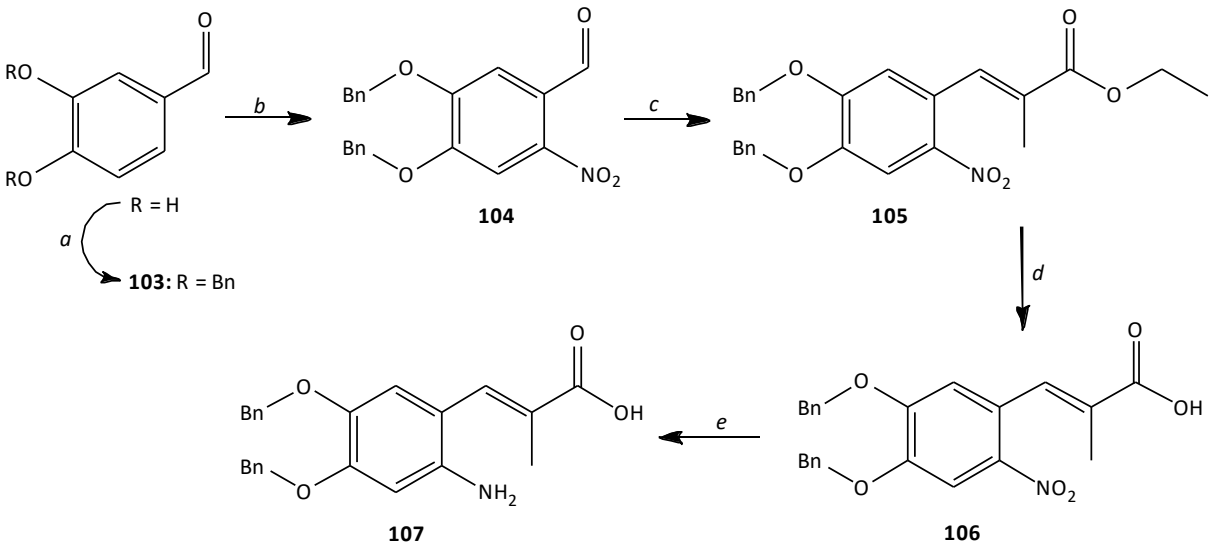

Scheme 36. Synthetic route to protected aminocinnamic acid **107**. *Reagents and conditions:* **a**. BnCl, K_2CO_3, anhydrous DMF, 80°C, 3 h, 96%; **b.** aq. 65% nitric acid, 0°C, 4 h, 92%; **c.** ECETP, dry toluene, 65°C, 24 h, 76%; **d.** 1M NaOH, 4:1 THF:EtOH, 40 °C, 92%; **e.** $FeSO_4.7H_2O$, water, aq. 35% NH_3, RT, 16%.

With the three protected aminocinnamic acids in hand (**89**, **90** and **107**), coupling to the iron chelators SIH **8** and deferasirox ester **33** was attempted using the coupling reagents EDC.HCl and DMAP (route a in Scheme 37). This gave three SIH-based protected CICs **108-110** in yields of 60-87% and deferasirox ester-based protected CICs **111-113** in yields of 19-39%. All of the coupling reactions with SIH **8** proceeded to completion with complete consumption of the phenolic component. In comparison, all of the deferasirox ester **33** coupling reactions failed to proceed to completion after 24 h with the presence of both the starting acid and phenol being detectable on TLC and HPLC analysis. The acid starting materials (**89, 90** and **107**) have

increased steric bulk due to the benzyl protecting groups in comparison to the 3,4-dimethoxy aminocinnamic acid **50** which could hinder the coupling reactions. The pKa of the phenol in **33** was predicted to be approximately 12.2 in comparison to the pKa of the phenol of **8** which was predicted to be 8.4, therefore the non-nucleophilic base diisopropylethylamine (DIPEA) was added to **33** before coupling to try and improve the effectiveness of the reaction, however no significant increase in yield was observed.

TFA cleavage of the benzyl protecting groups gave the final SIH-based CICs **114-116** and deferasirox ester-based final CICs **117-119** in yields ranging from 16% to 92%. The SIH-based CIC **116** and the deferasirox ester-based CIC **119** gave the lowest yields. These CICs both required cleavage of two benzyl groups, and TLC and HPLC analysis indicated the presence of the starting material after 24 h. The UV/Vis absorbance spectra of CICs **114-119** were recorded and are compared in terms of their caging groups in Figures 43-45.

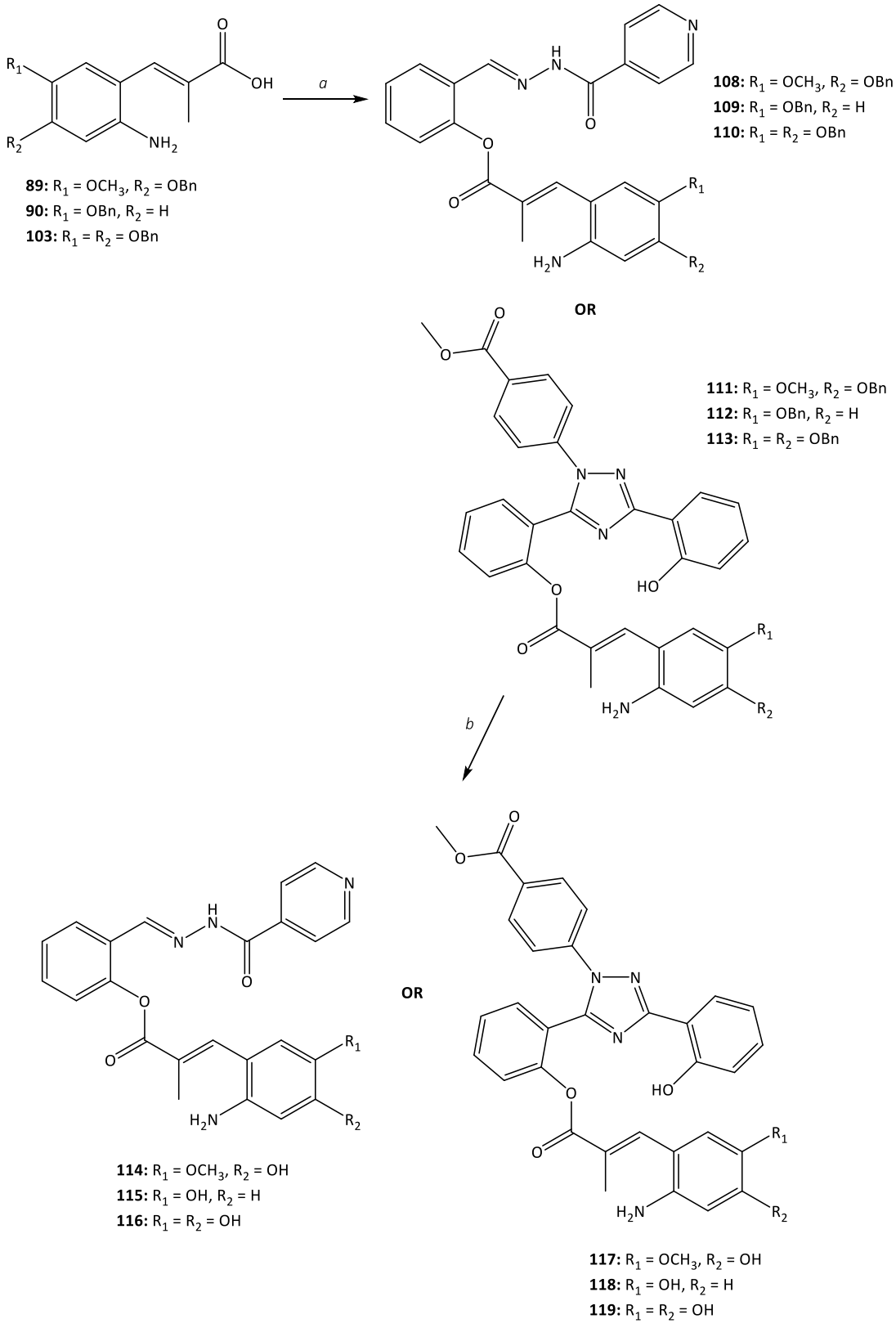

Scheme 37. Synthetic route to CICs **114-119**. *Reagents and conditions:* **a. 108-110:** EDC.HCl, DMAP, anhydrous DMF, RT, O/N, 87% (**108**), 84% (**109**), 60% (**110**), **111-113:** EDC.HCl, DMAP, DIPEA, anhydrous DMF, 30°C, 24 h, 39% (**111**), 32% (**112**), 19% (**113**); **b.** TFA, 30°C, O/N, 78% (**114**), 77% (**115**), 37% (**116**), 92% (**117**), 57% (**118**), 16% (**119**).

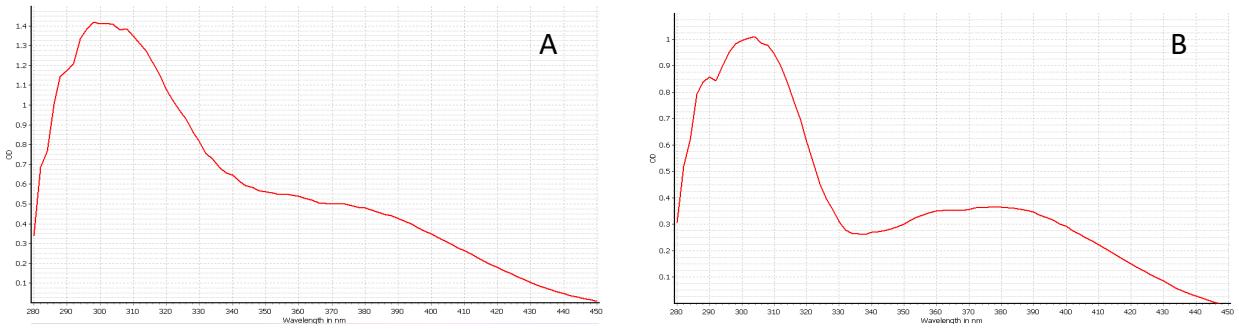

Figure 43. UV/Vis absorbance spectra of CICs **114** (A) and **117** (B) in EtOH (100 µM).

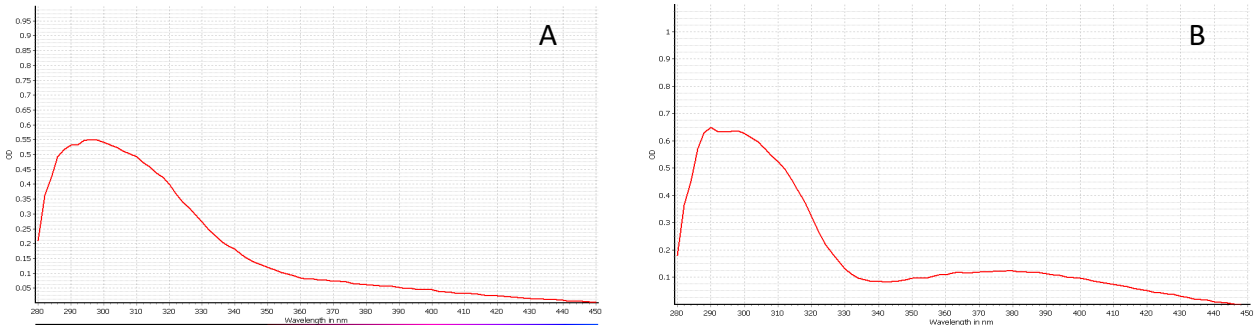

Figure 44. UV/Vis absorbance spectra of CICs **115** (A) and **118** (B) in EtOH (100 µM).

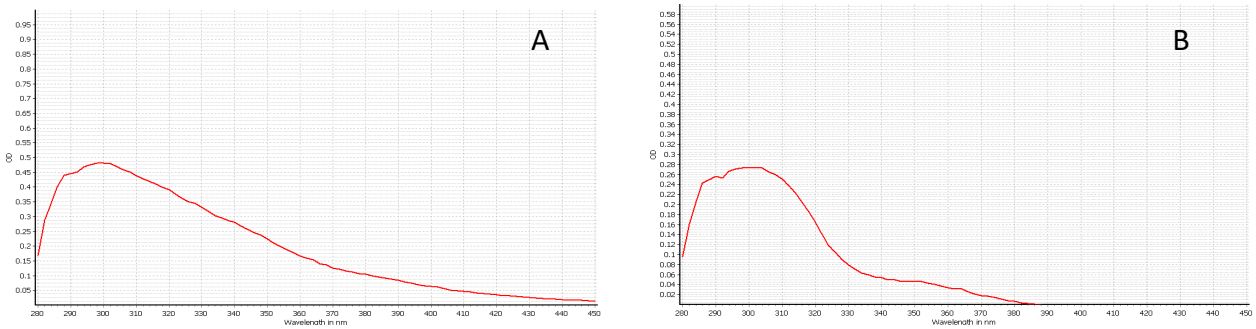

Figure 45. UV/Vis absorbance spectra of CICs **116** (A) and **119** (B) in EtOH (100 µM).

The two CICs containing the aminocinnamoyl group with the 4-hydroxy-3-methoxy substituents (**114** and **117**) have a strong maximum absorbance between 295-305 nm and absorb considerably up to 440 nm in visible light. **115** and **118** have a 3-hydroxy substituent on their caging group and have a maximum absorbance between 290-295 nm and absorb weakly to 440 nm. The presence of the 3,4-dihydroxy substituents in **116** and **119** reduces the absorptivity at the maximum absorbance (295- 305 nm). CIC **116** absorbs weakly to 440 nm, whereas **119** does not absorb higher than 380 nm.

The intact CICs **114-119** were irradiated at increasing doses of UVA (10-250 kJ/m^2) and the extent of uncaging was followed on analytical HPLC. The corresponding carbostyrils and iron chelators were injected on the HPLC as references for the uncaging process. The chromatograms for the uncaging of CICs **114-119** are shown in Appendix 1. Figures 46 and 47 compare the dose-dependent uncaging of CICs **114-119.**

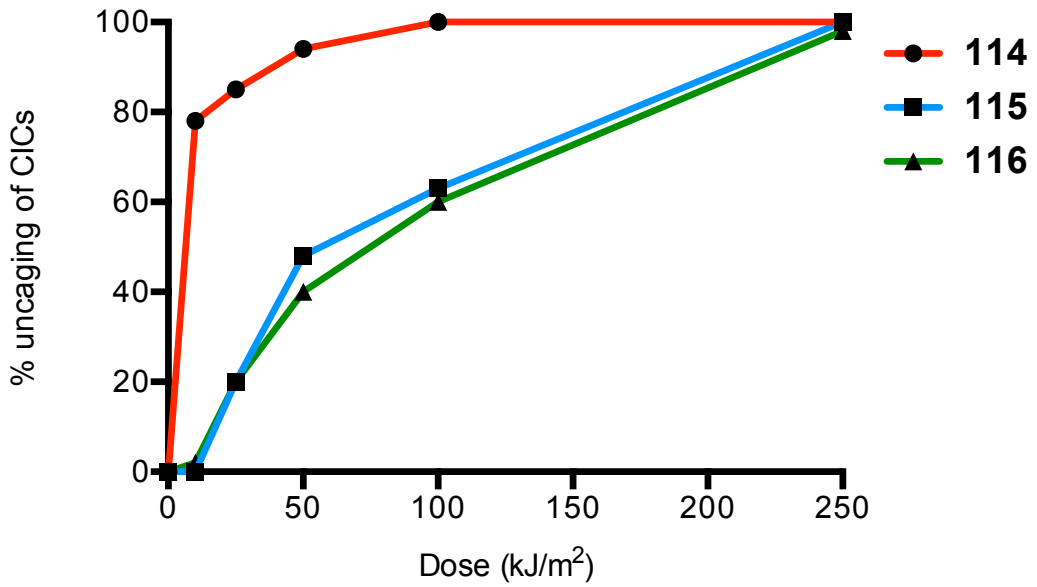

Figure 46. A representative comparison of the dose-dependent uncaging of the SIH-based CICs **114- 116**. Percentage uncaging calculated using the peak area of the remaining CIC compared to the peak area of the unirradiated sample. Samples in DMSO solution (1 mg/mL) were irradiated with a 4 kW broad spectrum UVA lamp (Sellas, Germany).

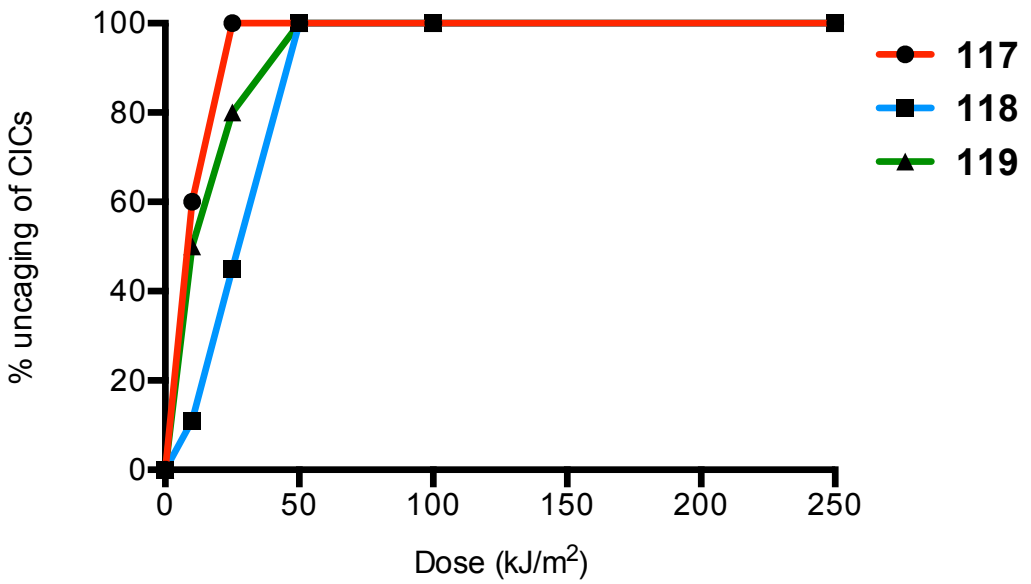

Figure 47. A representative comparison of the dose-dependent uncaging of the deferasirox ester-based CICs **117- 119**. Percentage uncaging calculated using the peak area of the remaining CIC compared to the peak area of the unirradiated sample. Samples in DMSO solution (1 mg/mL) were irradiated with a 4 kW broad spectrum UVA lamp (Sellas, Germany).

CICs **114** and **117** which contain the 4-hydroxy-3-methoxy caging group (red lines on Figures 46 and 47) both uncage the most efficiently. This is consistent with the absorbance profiles of **114** and **117,** as they displayed significant absorption over the UVA range (320- 400 nm). In general the SIH-based CICs **114-116** uncaged less effectively than the equivalent deferasirox ester- based CICs **117-119**. Both **115** and **116** did not fully uncage until a dose of 250 kJ/m^2 was delivered, thus photoprotection from these CICs would not be observed before several hours of human skin sun exposure and approximately 5 MED. This trend is consistent with the uncaging profiles observed in the first series of synthesised CICs. There are no striking differences between the absorption spectra of the equivalent SIH- and deferasirox ester-based compounds which suggests that intramolecular nucleophilic attack upon the ester carbonyl is the rate determining step here in the aminocinnamate photo-cleavage mechanism.

The MTT assay was used to assess the photoprotective capacity of CICs **114- 119.** A final concentration of 20 µM of CICs was used, which was incubated with FEK4 cells for 18 h before

irradiation of the monolayers of cells at 500 kJ/m^2. The results for the photoprotective ability of the SIH-based CICs **114-116** are displayed in Figure 48.

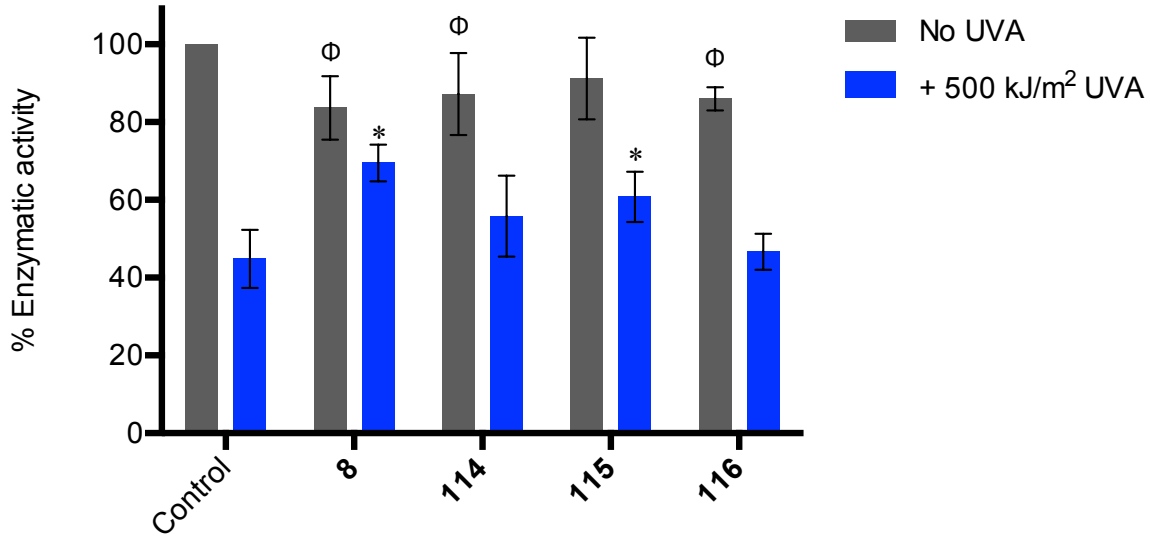

Figure 48. MTT assay evaluation of the photoprotection afforded by the SIH-based CICs **114-116** along with their parent iron chelator SIH **8** in FEK4 fibroblasts. Cells were treated with the compounds (20 µM) overnight before ± 500 kJ/m^2 UVA irradiation, followed by MTT analysis 24 h later. Data is expressed as the mean ± SD compared to the untreated unirradiated control, which was fixed at 100% enzymatic activity (n=3-7).

*= p< 0.05, significantly different from the untreated irradiated control.

Φ= *p* <0.05, significantly different from the untreated unirradiated control.

CICs **114** and **115** both improved the cell viability in comparison to the untreated irradiated control and CIC **115** significantly protected fibroblasts from UVA-induced loss of cell viability. Although none of the CICs improved cell viability more than the parent iron chelator **8** under UVA irradiation, CIC **115** was not cytotoxic without UVA irradiation in comparison to the significant cytotoxicity seen by **8**, **114** and **116** without UVA. CIC **116** did not display an increased photoprotective effect due to the antioxidant potential of the carbostyril **95** released, and this may be due to the aforementioned UVA absorbance profile of **116** and only partial uncaging at the applied dose of 500 kJ/m^2 (only 40% chemical uncaging was observed at a dose of 50 kJ/m^2 during chemical irradiation– see Figure 46). Figure 49 shows the photoprotective ability of the deferasirox ester-based CICs **117-119.** Unfortunately the presence of CICs **117** and **118** during UVA irradiation caused a higher loss of cell viability in comparison to the untreated irradiated control; they also induced a significant loss of cell viability without UVA irradiation, similar to the parent iron chelator **33**. CIC **119** with the 3,4-

dihydroxy motif improved cell viability in comparison to the untreated irradiated control but not significantly, however it was not cytotoxic without UVA irradiation.

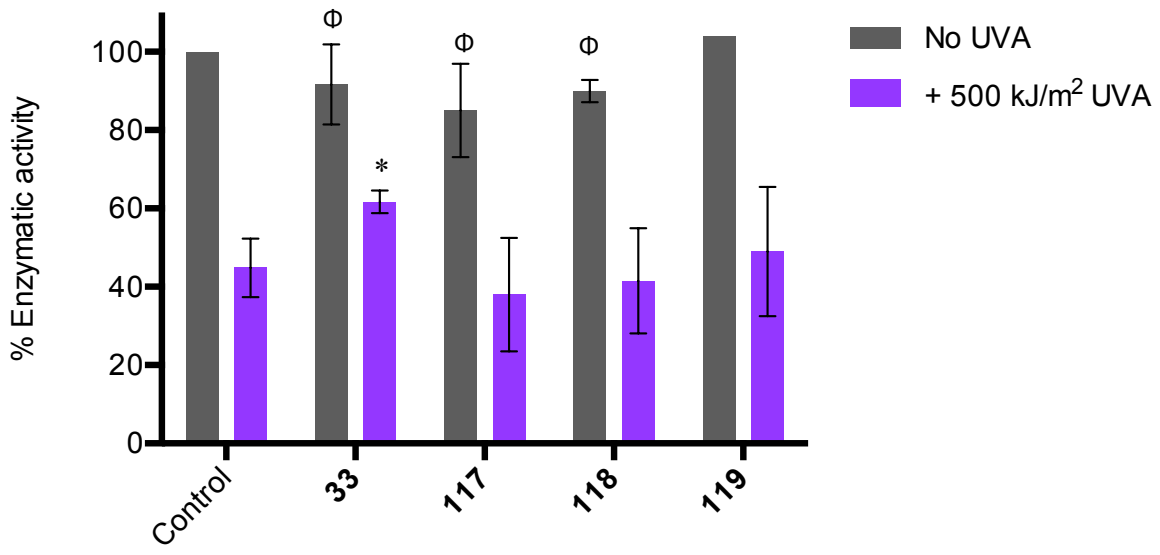

Figure 49. MTT assay evaluation of the photoprotection afforded by the deferasirox ester-based CICs **117-119** along with their parent iron chelator deferasirox ester **33** in FEK4 fibroblasts. Cells were treated with the compounds (20 µM) overnight before ± 500 kJ/m^2 UVA irradiation, followed by MTT analysis 24 h later. Data is expressed as the mean ± SD compared to the untreated unirradiated control, which was fixed at 100% enzymatic activity (n=3-7).

*= p< 0.05, significantly different from the untreated irradiated control.

Φ= *p* <0.05, significantly different from the untreated unirradiated control.

4. Summary

The synthetic route to a series of interesting carbostyrils with different substituents was developed to give carbostyrils **91-95**. This synthetic route has the potential to be used with a diverse range of starting benzaldehydes. Analysis of the antioxidant potential of the series of synthesised carbostyrils using the chemical DPPH assay showed that three of the carbostyrils **93**, **94** and **95** possessed a positive radical scavenging effect. Of these carbostyrils, **94** and **95** were analysed further in the cellular DCFDA assay and showed a significant antioxidant potential, especially combined with the iron chelator SIH **8.**

Synthesis of SIH and deferasirox ester-based CICs which would release the carbostyrils **93, 94** and **95** upon UVA-irradiation was achieved *via* coupling the iron chelators with benzyl-protected precursors of the caging groups. The benzyl protecting groups could then be easily

removed by stirring the protected CICs in TFA without compromising the stability of the CIC. This method afforded a series of six novel multi-functional CICs **114-119** which were fully characterised and their UV/Vis absorbance recorded. Out of these synthesised CICs, the 3-hydroxy aminocinnamic acid-caged SIH CIC **115** performed the best, significantly improving the cell viability of UVA- irradiated human fibroblasts. This result correlates with the significant antioxidant activity of the combination of SIH **8** and carbostyril **94** in the DCFDA assay. **115** delivers a significant photoprotective effect even though it is likely to be only partially uncaged under the experimental irradiation dose (500 kJ/m^2), thus **115** might provide more photoprotection upon longer environmental UVA exposure than **51.**

CHAPTER 4: RESULTS AND DISCUSSION

1. Abstract

The aim of this chapter was to assess the capacity of improperly applied UVR filters and sunscreen formulations to prevent UVA-induced cell death and labile iron release. Sunscreen application by consumers is usually far below the recommended application thickness of 2 mg/cm^2, and current formulations do not contain compounds that are designed specifically to trap harmful labile iron. As such the potential of CICs to augment the photoprotection afforded by sunscreen formulations was also investigated. The studies carried out and the underlying aim described above are represented graphically in Scheme 38.

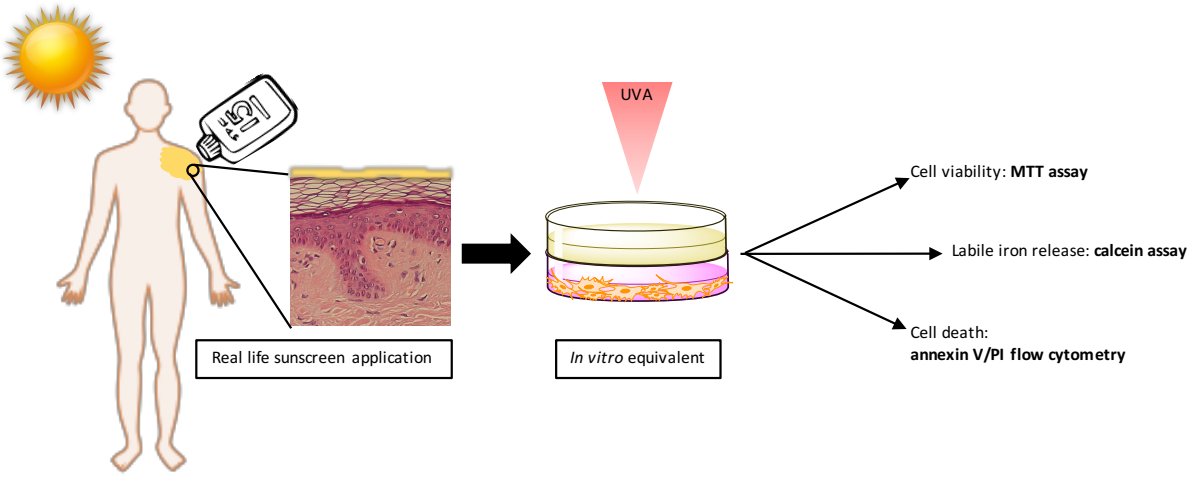

Scheme 38. Representation of the investigation into the protection afforded by UVR filters and sunscreen formulations against UVA exposure using an *in vitro* equivalent of real life sunscreen application.

2. Introduction

The SPF of a sunscreen formulation is determined using an application thickness of 2 mg/cm^2. It has been well documented that sunscreen application by consumers is usually far below 2 mg/cm^2 and is thought to range on average from 0.5- 1.3 mg/cm^2.[36,65,222-225] For example, in a study by Bech-Thomsen *et al.* in 1993, the average sunscreen application thickness used by 42 volunteers on a beach holiday was 0.5 mg/cm^2.[69] In another study by Autier *et al.*, the median application thickness applied by 124 European students was 0.39 mg/cm^2,[226] while

the median quantity of sunscreen applied in a trial by Neale *et al.* on randomly selected Australian residents was 0.79 mg/cm^2.[227] Sunscreen formulations are also applied rather haphazardly, leading to a non-uniform layer of protection. Rhodes *et al.* demonstrated the diversity of sunscreen application by the public by asking 5 patients to apply a quantity of sunscreen on their forearm 'as if they were on the beach'.[225] The sunscreen formulation applied was excited at 340 nm and gave a strong fluorescence emission at 400 nm, so that the sunscreen fluorescence could be quantified using a spectrometer. The results showed a significant variability in surface densities and most patients had some sites where no sunscreen had been applied.[225]

These factors greatly affect the actual SPF the consumer receives from a sunscreen formulation in comparison to their perceived photoprotection. Liu *et al.* compared the difference in actual SPF at different application thicknesses of low and high SPF formulations.[222] It was found that sunscreens with SPFs ranging from 4 to 15 showed a linear dose-response relationship with application thickness, for example an SPF 10 sunscreen applied at a thickness of 0.5 mg/cm^2 would give an actual SPF of 2.5. On the other hand, the relationship was exponential in high SPF (30+) sunscreens, therefore consumers may be receiving an even lower actual SPF when using high SPF products at sub-optimal application thicknesses.[222]

The fact that the general public is actually receiving a much lower level of sun protection than they believe is not only relevant to UVB mechanisms of photo-damage and skin cancer initiation (described in the Introduction 1.1.3), but also the level of UVA radiation experienced and thus oxidative stress and labile iron release in skin cells.

3. Analysis of common sunscreen filters

A range of filters was chosen for analysis of their UVA-photoprotection, based on their Food and Drug Administration (FDA) approval status along with market research of the most commonly found filters in popular sunscreen brands such as Neutrogena, Nivea, L'Oréal, La Roche-Posay, Banana Boat and Piz Buin. The organic filter avobenzone absorbs in the UVA

region (320-400 nm) and is the only chemical UVA absorber that has worldwide approval for use in sunscreen formulations, therefore it is the most popular UVA filter currently on the market despite its photo-instability.[75,78] For this reason, including avobenzone in this work was very important.

The other available UVR filters that have worldwide approval for use (including the sought after FDA approval) are all UVB filters.[75] Of these UVB filters, oxybenzone from the benzophenone class has the interesting property of also absorbing at 324 nm which is just inside the UVA2 range (320-340 nm). Oxybenzone is included in many sunscreen formulations as one of the UVB filters with an added UVA advantage, therefore it was also chosen for analysis. Octocrylene is a very popular UVB filter and has the added benefit of stabilising avobenzone against photodegradation, therefore it is usually included alongside avobenzone in a sunscreen formulation to provide a dual function.[79,80] The presence of 3.6% (w/v) octocrylene has been shown to increase the stability of avobenzone after a quantity of sun exposure from 23% avobenzone remaining to 90%, and likewise 5% (w/v) oxybenzone increased the amount of avobenzone remaining to 80%.[36] The UVA filter Meroxyl SX® (ecamsule) is patented by L'Oréal and has a very promising UVA photoprotection profile,[81,82] along with being photo-stable.[228] However, it has not been approved for use in the USA, except *via* a new drug application by L'Oréal in 2006 which allowed it to be used in concentrations up to 3% (w/v), solely in their products.[36] Meroxyl is approved for use in Europe and Australia, and as the newest organic UVA filter on the market it was included in this selection of organic filters.

The inorganic class of UVR-blocking sunscreen products contain either ZnO or TiO_2. These products have lower consumer compliance due the likelihood of leaving a white opaque film on the skin.[65] On the other hand, these inorganic materials are popular UVR filters as they provide broad spectrum photoprotection and they are marketed as 'natural' and 'hypoallergenic',[228] although they are often chemically treated in order to formulate them into a sunscreen product.[75] In order to combat the unappealing application of ZnO or TiO_2-based formulations, the use of nanoparticle forms of the oxides has become widespread since the 1990s, leading to creams that are lighter textured on the skin.[76] Nanoparticle formulations of TiO_2 are approved worldwide, however ZnO is not approved for nano grade in Europe.[36]

Due to the broad spectrum protection that these inorganic blockers provide, these were also included in the selection for this work. Nanoparticle sizes of 21 nm and 18 nm for TiO_2 and ZnO respectively were chosen. This was based on a study by Osmond-McLeod *et al*. into the biological impact of commercially available sunscreen formulations containing TiO_2 and ZnO nanoparticles. The ZnO and TiO_2 nanoparticles in the chosen formulations were characterised by transmission electron microscopy (TEM) and found to have average diameters of 18.2 ± 0.4 nm and 21.5 ± 0.6 nm respectively.[76]

To have a clear picture of the UVR photoprotection profile of all of the selected sunscreen filters, the UVR absorbance spectra of each was recorded in EtOH (10 μg/mL). The spectra are shown in Table 7 along with the experimentally determined maximum absorbance (nm). All experimentally determined absorption profiles compared well with the reported values for each filter,[36,229] except for ZnO which did not absorb well above 340 nm (UVA1 region). This may have been due to the nanoparticle size, as decreasing the size of the particle leads to protection at shorter wavelengths, or the formation of UVR-inactive agglomerates despite attempts to make a uniform suspension in EtOH.[230]

Table 7. The sunscreen filters chosen for analysis of their photoprotective effect along with their experimentally determined UVR absorbance spectra and their maximum absorbance wavelength in EtOH (10 μg/mL).

Name	Absorbance Spectrum	Determined Maximum Absorbance (nm)
Avobenzone	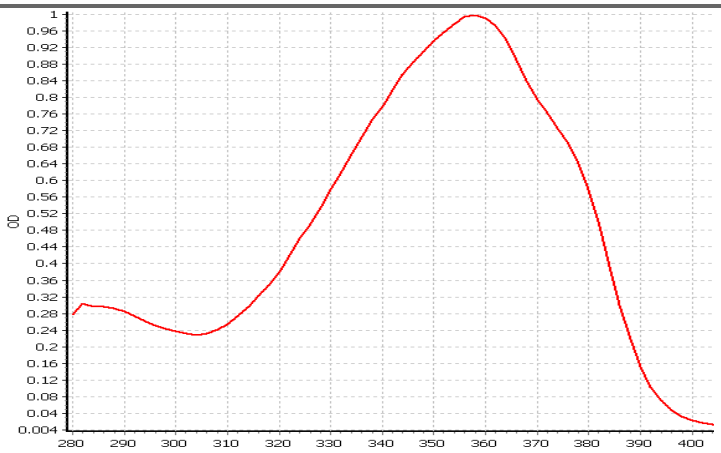	358
Mexoryl SX	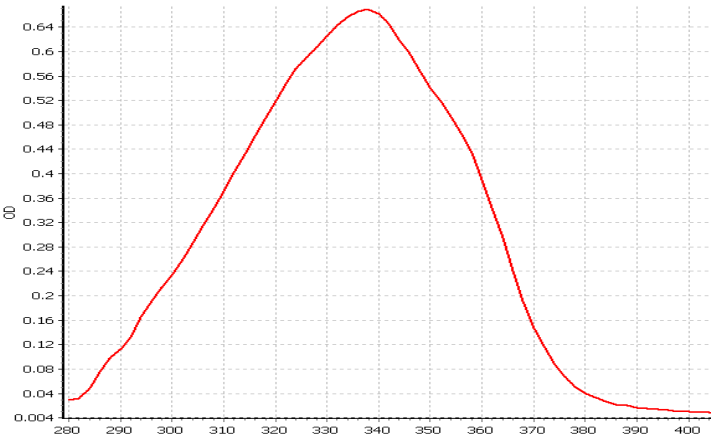	337
Octocrylene	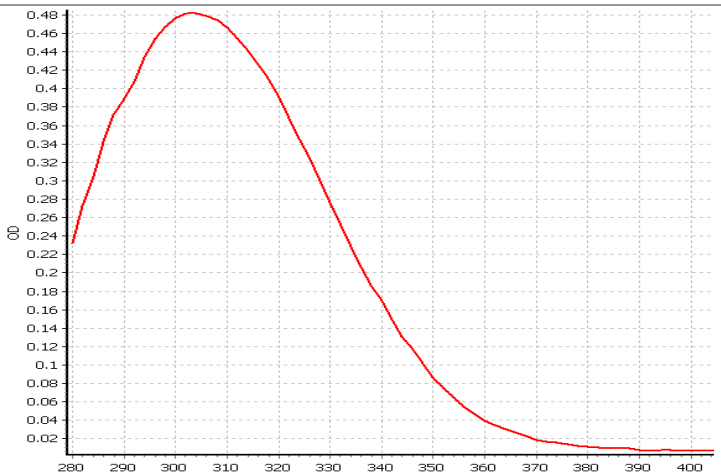	304

Oxybenzone	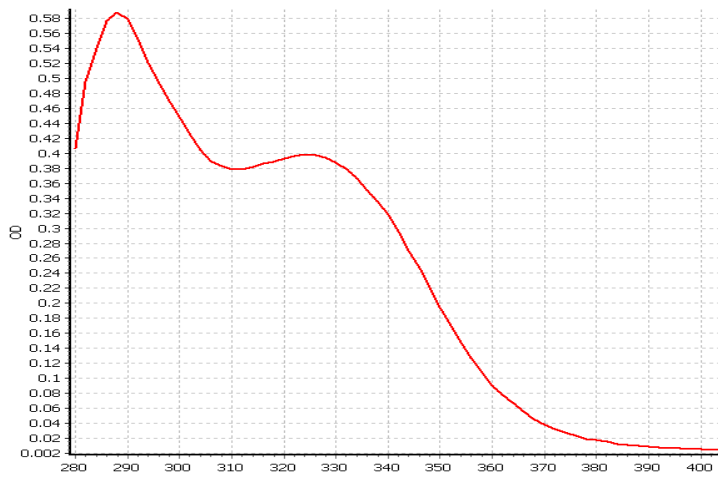	287, 324
TiO_2	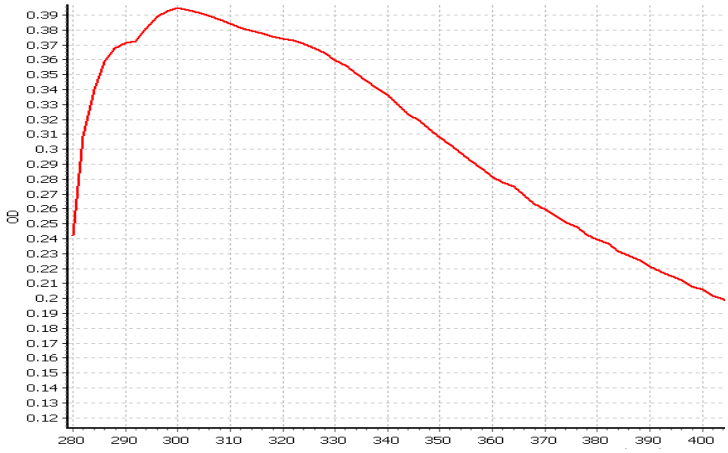	300
ZnO	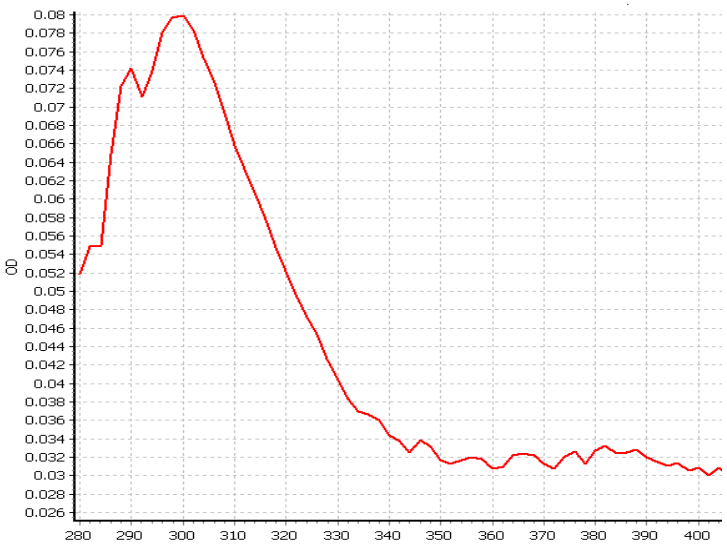	300

The reported photo-instability of avobenzone occurs due to conversion of the UVA-absorbing enol form to the UVC-absorbing keto form upon irradiation at 357 nm[75] (Scheme 4, Introduction 1.2.2). This significantly decreases the ability of the filter to absorb damaging solar radiation. Cantrell *et al.* examined the kinetic decay of the enol form of avobenzone in different solvents using the change in UVR absorbance. The results showed that protic solvents such as butanol and ethanol accelerated the transition to the keto form of avobenzone, as did the presence of water.[79] In a study by Mturi *et al.*, the photostability of avobenzone was examined using HPLC. A method was found whereby the enol form of avobenzone eluted as a distinct peak at a longer retention time than the keto form, thus allowing the relative concentrations of each form (relative peak areas) to be examined after irradiation. The HPLC analysis (monitored at a wavelength of 272 nm) confirmed that before irradiation avobenzone exists predominantly in the enol form in a variety of solvents, indicating that the keto-enol equilibrium of avobenzone lies towards the enol form.[78]

As the irradiation of avobenzone was central to our work, these findings were checked using our broad spectrum UVA lamp and HPLC analysis at a detection wavelength of 280 nm, which is very similar to the detection wavelength used by Mturi *et al*. Figure 50 shows the HPLC chromatogram of avobenzone in DMSO before irradiation, along with the retention time of the two peaks and their relative areas. Based on the study by Mturi *et al.* it was assumed that the peak with the longer retention time of 12.13 min was the enol form, and the peak at 10.58 min corresponded to the keto form. The chromatogram obtained before irradiation would then be consistent with the tendency of avobenzone to exist in the enol form in unirradiated solution, as the relative area of the peak at 12.13 min (75%) was significantly greater in comparison to the peak at 10.58 min.

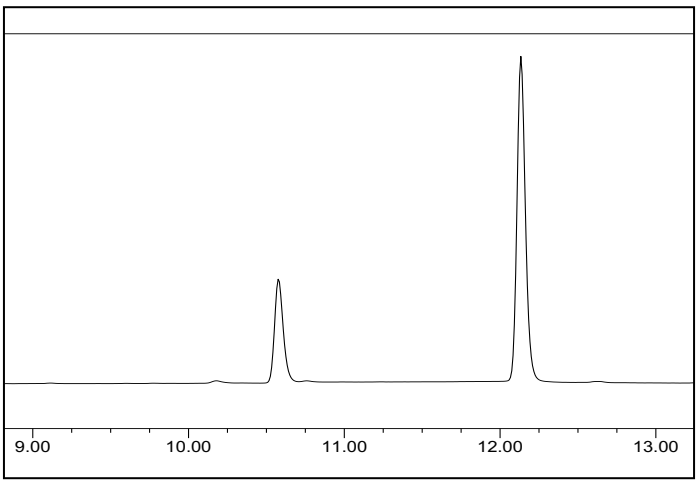

Retention Time min	Relative Area %
10.58	24.59
12.13	75.41

Figure 50. HPLC chromatogram at a detection wavelength of 280 nm of unirradiated avobenzone in DMSO (1 mg/mL) diluted 1 in 10 with MeOH before injection onto the HPLC. The keto form is assumed to be at 10.58 min and the enol form is at 12.13 min.[78]

Mturi *et al.* reported that the irradiation of avobenzone in DMSO for 15 h (a dose was not given but a significant amount of time), decreased the proportion of the enol form of avobenzone by 75% according to HPLC analysis. The spectral output of the irradiation source used by Mturi *et al.* was at wavelengths higher than 300 nm, with a maximum output in the UVA range of 360 nm. In order to verify the observation in this work, a solution of avobenzone in DMSO was irradiated with increasing doses of UVA from 100- 1000 kJ/m^2, as this range of radiation was relevant to the typical doses used in our cellular experiments. In our hands, HPLC analysis at 280 nm showed that even the dose of 1000 kJ/m^2 UVA did not decrease the percentage relative peak area of the enol form below that of the unirradiated control (shown in Table 8). This was consistent across the other 3 detection wavelengths of the HPLC (214, 220 and 254 nm). This finding indicated that a 1 mg/mL solution of avobenzone in DMSO would be photostable at all doses required for our cellular experiments without the addition of a photostabilizer. However, in order to closely represent a typical sunscreen filter combination, avobenzone was used in conjunction with octocrylene during the latter cellular experiments subsequently described here.

Table 8. The relative peak areas (percentage) of the keto and enol forms of avobenzone after UVA irradiation at doses 100-1000 kJ/m^2, established by HPLC analysis at a detection wavelength of 280 nm to analyse the photostability of avobenzone in DMSO.

UVA dose (kJ/m^2)	Relative peak area (%)		% of control
	Keto	Enol	
0	25	75	-
100	25	75	100
250	25	75	100
500	26	74	99
750	27	73	97
1000	26	74	99

4. UVA photoprotection of FEK4 cells by sunscreen filters

In order to test the UVA photoprotection afforded by the chosen sunscreen filters, a suitable assay method was required. Previous studies analysing the photoprotection afforded by various sunscreens have mostly been carried out by applying a layer of sunscreen or an individual filter to a patient or to porcine epidermis,[71,231-234] with the amount of sunscreen or filter applied being typically calculated from the difference in sunscreen weight before and after application. This method was a good starting point for assay development in this study, however a more accurate way of applying the filters at exact thicknesses (*e.g* 0.5 mg/cm^2) was required. The procedure that was established (described in the Experimental section 7.2.5) involved using a 'reservoir' of filter in DMSO at the correct concentration corresponding to the required thickness for the experiment. The reservoir was placed over the top of the Petri dish containing a monolayer of FEK4 cells during UVA irradiation. Controls cells were covered with a Petri dish containing only DMSO so that transmission of light through the dish and the carrier were accounted for.

The FDA stipulates a maximum concentration of filter which can be formulated into a sunscreen product (shown in Table 9). Using these concentrations as a starting point, a

comparison of publicly available common sunscreen products was carried out and the experimental concentrations shown in Table 9 were chosen.

Table 9. The FDA-approved sunscreen filters chosen for this work along with their approved maximum concentrations in a sunscreen formulation**.**

***** This concentration is approved by the FDA solely for L'Oréal products.[235]

Filter name	FDA approved maximum concentration in a sunscreen formulation (% w/v)	Concentration used in these experiments (% w/v)
Avobenzone	3	3
Mexoryl SX	3*	3
Octocrylene	10	5
Oxybenzone	6	6
TiO_2	25	20
ZnO	25	20

The amount of filter required to correspond to the chosen concentration of filter at different sunscreen thicknesses was calculated as shown in the following worked example for avobenzone:

Area of the reservoir used in the experiment= 9.6 cm^2

Amount of sunscreen for a thickness of 2 mg/cm^2= 19.2 mg/reservoir

Concentration of filter in sunscreen formulation= 3% w/v

Amount of filter required for reservoir= 0.03*19.2= 0.576 mg

Amount of filter required for reservoir for a thickness of 0.5 mg/cm^2= 0.576/4= 0.144 mg

The correct amount of filter required per reservoir was made up into 500 μL DMSO in every experiment. Using this method, FEK4 cells were irradiated at 500 kJ/m^2 UVA covered by a reservoir of sunscreen filter at thicknesses of 2 mg/cm^2 and 0.5 mg/cm^2. The thickness of 2 mg/cm^2 is the amount used for the SPF calculation of a sunscreen,[100] therefore this thickness was chosen as a control along with the thickness of 0.5 mg/cm^2, which is closer to the thickness of sunscreen that a consumer commonly applies. MTT assay analysis was carried out 24 h after UVA exposure, and the results of the assays for the four chosen organic filters avobenzone, Mexoryl SX®, oxybenzone and octocrylene are shown in Figure 51.

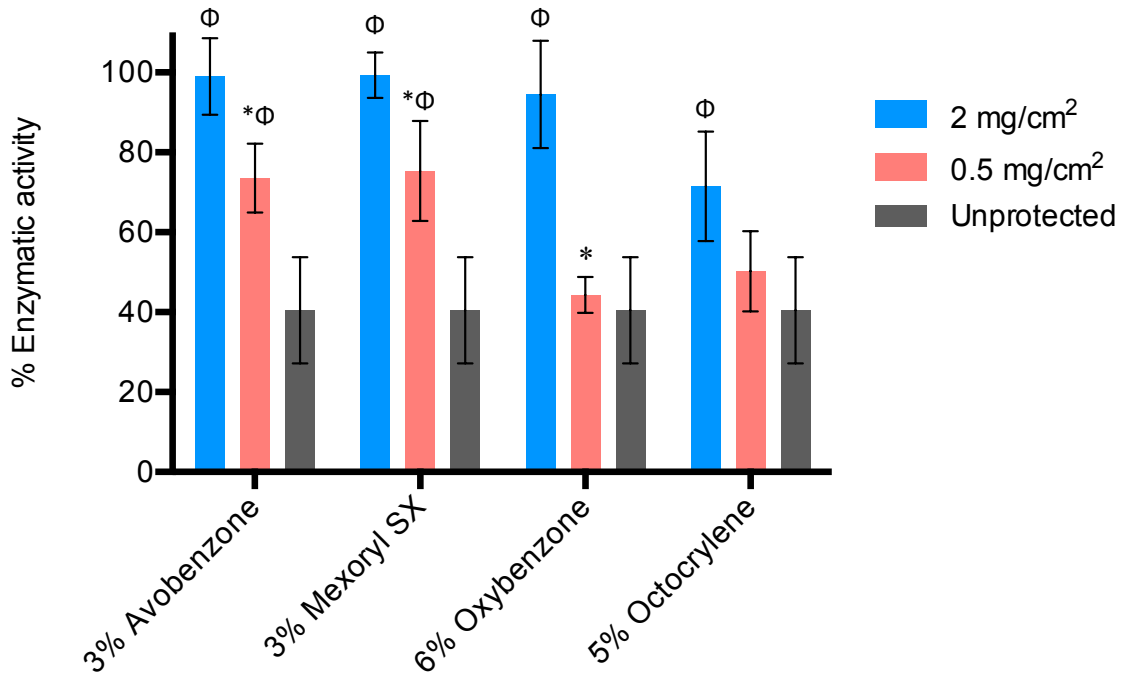

Figure 51. MTT assay evaluation of the UVA photoprotection afforded by four popular organic sunscreen filters in FEK4 fibroblasts. Cells were ± covered with a reservoir of the sunscreen filter at thicknesses of 0.5 mg/cm^2 or 2 mg/cm^2 and then exposed to a 500 kJ/m^2 dose of UVA radiation followed by MTT analysis 24 h later. Data is expressed as the mean ± SD compared to the unirradiated control, which was fixed at 100% enzymatic activity (n=3-5).

* = p <0.05, significantly different from cells covered by 2 mg/cm^2 of the same filter.

Φ = p <0.05, significantly different from the unprotected cells.

The results of this assay show that at the recommended sunscreen thickness of 2 mg/cm^2 there is no significant loss of enzymatic activity for the three organic filters that absorb in the UVA region (avobenzone, Mexoryl SX and oxybenzone), as expected. The enzymatic activity for 5% (w/v) octocrylene decreased to 72% at 2 mg/cm^2 which is consistent with octocrylene being primarily a UVB filter, but which has some absorption between 320-360 nm in the UVA region (absorbance spectrum shown in Table 7). At a sunscreen thickness of 0.5 mg/cm^2, the two predominantly UVA filters, avobenzone and Mexoryl SX®, both afforded significantly less photoprotection (74% and 75% enzymatic activity respectively) compared to the 2 mg/cm^2 control. The photoprotective capacity of oxybenzone was also significantly reduced to a similar level to that of the unprotected control, indicating that at the reduced concentration (thickness) the UVA-absorbing capacity of the filter was exceeded. These results suggest that at the thickness of sunscreen that a consumer usually applies, the level of UVA

photoprotection afforded by the specific filters investigated is markedly reduced. The same assay was carried out with the two inorganic filters TiO_2 and ZnO in suspensions in DMSO to the required concentrations for 2 mg/cm^2 and 0.5 mg/cm^2 sunscreen thicknesses, and the results are shown in Figure 52.

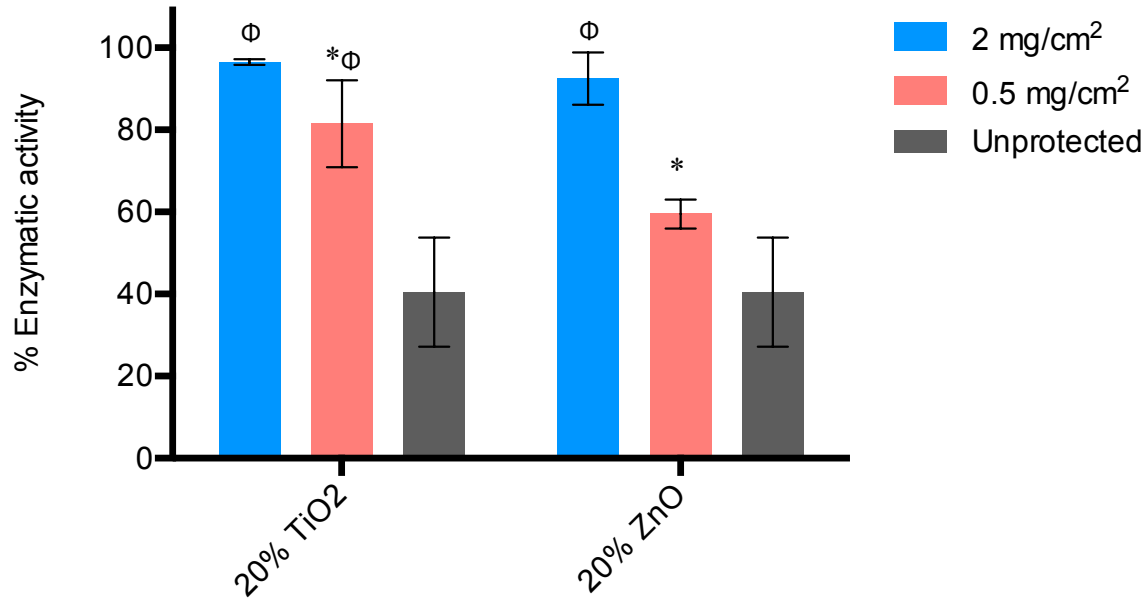

Figure 52. MTT assay evaluation of the UVA photoprotection afforded by the two inorganic sunscreen filters in FEK4 fibroblasts. Cells were ± covered with a reservoir of the sunscreen filter at thicknesses of 0.5 mg/cm^2 or 2 mg/cm^2 and then exposed to a 500 kJ/m^2 dose of UVA radiation followed by MTT analysis 24 h later. Data is expressed as the mean ± SD compared to the unirradiated control, which was fixed at 100% enzymatic activity (n=3-5).

* = p <0.05, significantly different from cells covered by 2 mg/cm^2 of the same filter.

Φ = p <0.05, significantly different from the unprotected cells.

These results indicate that at 0.5 mg/cm^2 the broad spectrum UVB/UVA filter TiO_2 (20% w/v) provided the best photoprotection (82% enzymatic activity) out of all the individual filters tested. At a sunscreen thickness of 0.5 mg/cm^2 the photoprotective capacity of ZnO (20% w/v) was markedly less, with a reduction to 60% enzymatic activity, consistent with the lack of absorption above 340 nm that was observed previously (spectrum shown in Table 7) and hence inadequate UVA photoprotection.

Figure 53 presents photographic evidence to support the loss of enzymatic activity upon photoprotection by 3% (w/v) avobenzone in a sunscreen thickness of 0.5 mg/cm^2. The images

were taken 24 h post-UVA irradiation before the MTT assay was carried out. Panel A shows the characteristic morphology of healthy FEK4 fibroblasts, with elongated flattened cells growing in an irregular manner. Panel B is after a dose of 500 kJ/m^2 UVA irradiation (1 MED), where many of the cells have become rounded and raised as they detach from the surface of the dish. Blebbing of the plasma membrane occurs, characterized by the spherical bulky morphology of the cells. The photoprotection afforded by 3% (w/v) avobenzone at a sunscreen thickness of 0.5 mg/cm^2 is seen in panel C. Here, there is smaller percentage of blebbing cells relative to the number of healthy fibroblasts which have remained elongated and attached to the dish surface.

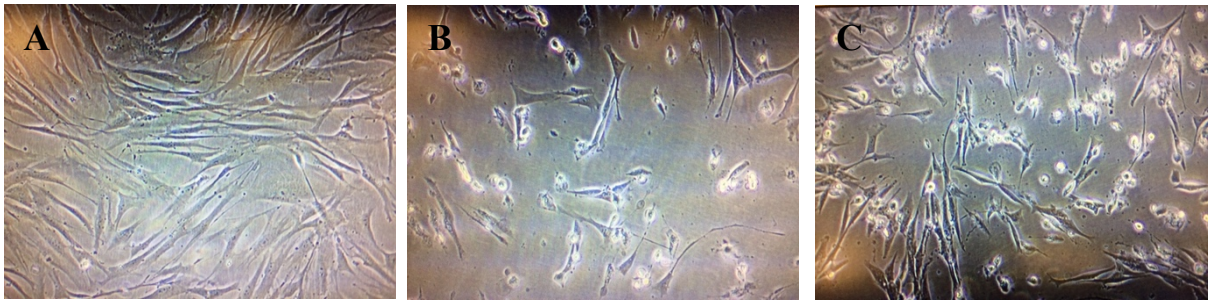

Figure 53. Images of FEK4 fibroblasts taken 24 h post UVA irradiation. **A**. Negative control, cells were not irradiated; **B**. Positive control, cells irradiated with 500 kJ/m^2 UVA; **C.** Cells protected with 3% (w/v) avobenzone at a sunscreen thickness of 0.5 mg/cm^2 and irradiated with 500 kJ/m^2 UVA. Images captured on a Motic AE2000 inverted microscope (Motic Deutschland GmbH, Wetzlar, Germany) via a Moticam 580 digital camera.

5. Intracellular labile iron release in UVA irradiated cells

As described in the Introduction 1.1.4, the release of labile iron in the cell cytosol through UVA-induced oxidative damage is a significant mechanism of cell death. To determine the extent of UVA-induced labile iron release in FEK4 fibroblasts, the fluorescent divalent metal probe calcein (CA) was employed. Calcein acetoxymethyl (CA-AM) is a non-fluorescent compound which is readily loaded into live cells. Intracellular esterases then convert CA-AM into the green-fluorescent CA *via* cleavage of the acetoxymethyl groups, as shown in Scheme 39. Fluorescent CA is excited at 490 nm and emits at 517 nm.

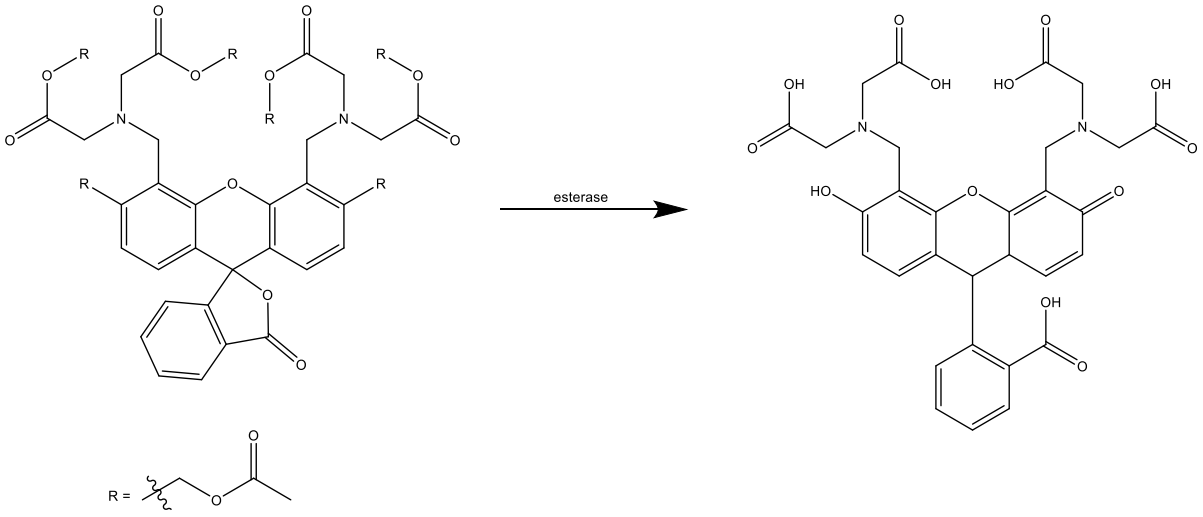

Scheme 39. Conversion of CA-AM to the fluorescent CA in the cytosol of cells by intracellular esterases.

CA can act as a metal-sensitive probe in solution and has been shown to bind iron with a 1:1 stoichiometry.[236,237] When CA is bound to iron [CA-Fe], the fluorescence of CA is quenched. It is considered that not all CA will be bound to iron in the cytosol, but instead is in equilibrium with free iron that is loosely bound to endogenous ligands (e.g ATP, glutathione)[238] as follows:

$$[CA]^* + [Fe] \rightleftharpoons [CA\text{-}Fe]$$

The quenching of CA by iron can be reversed by the addition of an excess of the lipophilic cell membrane-permeant iron chelator SIH **8**, which has a very high affinity for ferric iron (pFe^{3+} = 24.6)[105]. The unquenched CA gives rise to an increase in fluorescence (ΔF) which is equivalent to the available chelatable labile iron (Fe^{2+}) in the cytosol, [CA-Fe]. UVA-induced labile iron release is overlooked in conventional commercially available sunscreen products, therefore when a consumer applies a typical amount of sunscreen formulation (0.5 mg/cm^2) there is a possibility that they are compromised in terms of the detrimental effects of labile iron generated within skin cells. In order to analyse the hypothesis that the application of a sub-optimal thickness of sunscreen before UVA exposure could lead to intracellular labile iron release, FEK4 cells were ± protected by 3% (w/v) avobenzone + 5% (w/v) octocrylene at 0.5 mg/cm^2 prior to irradiation at a dose of 250 kJ/m^2 and analysed using the calcein assay *via* the spectrofluorimeter method as described in the Experimental Section 7.2.10.1.

Following UVA-irradiation, FEK4 cells were incubated with CA-AM (0.05 μM) and the cell suspension was transferred to a cuvette. The fluorescence of the cell suspension was recorded on the F-4500 (Hitachi High-Technologies), and then SIH **8** (40 μM) was used to elicit a change in fluorescence due to displacement of CA by the iron chelator, giving the free [CA]* as a function of the original [CA-Fe]=

$$[CA\text{-}Fe] \rightarrow [SIH\text{-}Fe] + [CA]^*$$

A schematic to explain this change in fluorescence as described above is represented in Figure 54. Table 10 presents the results from a typical assay showing the calculation of the change in fluorescence per 10^6 cells and the fold- increase in intracellular chelatable labile iron upon 250 kJ/m^2 UVA irradiation ± 3% (w/v) avobenzone + 5% (w/v) octocrylene at 0.5 mg/cm^2 in comparison to the level of intracellular chelatable labile iron in the control.

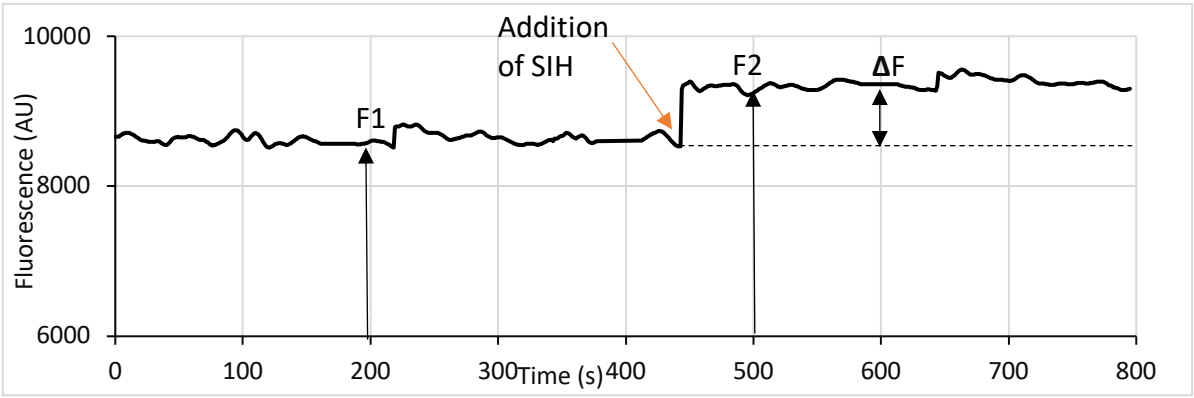

Figure 54. Diagram representing the fluorescence signal of a cell suspension before and after addition of SIH **8** (40 μM). The average fluorescence is indicated by F1 and F2, which were used to calculate the change in fluorescence (*Δ*F).

Table 10. Example assay results and the respective calculations to find the fold-increase in chelatable labile iron per 10^6 FEK4 cells.

	Control		250 kJ/m² UVA		0.5 mg/cm² filters + 250 kJ/m² UVA	
	no SIH (F1)	SIH (F2)	no SIH (F1)	SIH (F2)	no SIH (F1)	SIH (F2)
Average fluorescence (AU)	8640	9142	8348	9042	7074	7638
Cell count (x10^6)	0.413		0.378		0.401	
ΔF	0.055		0.077		0.074	
ΔF/ 10^6	0.133		0.203		0.185	
Fold increase	**1**		**1.53**		**1.39**	

This experiment was repeated to n=8 to give the average fold-increase in chelatable labile iron in comparison to the unirradiated control, and the results are displayed in Figure 55. The average fold-change in fluorescence for the cells irradiated with 250 kJ/m^2 UVA was 1.92 ± 0.42, whereas the corresponding increase for irradiated cells protected with 0.5 mg/cm^2 3% (w/v) avobenzone + 5% (w/v) octocrylene was 1.31 ± 0.18. The fold-change in intracellular labile iron with 0.5 mg/cm^2 3% (w/v) avobenzone + 5% (w/v) octocrylene was significant compared to the control unirradiated cells, indicating that using a sub-optimal sunscreen thickness of the filter avobenzone stabilized with octocrylene does indeed lead to release of detrimental intracellular labile iron which can cause severe oxidative damage within the cell. This is consistent with the loss of enzymatic activity seen in the MTT assays. These results confirmed that this version of the calcein assay could be used to reproducibly monitor changes in the level of intracellular labile iron upon UVA irradiation. Although a highly valuable assay, the single cuvette format does not allow sufficiently high throughput. This is due to the timescale of the experiment: stabilisation of the base-line fluorescence plus stabilisation of the fluorescence after addition of SIH takes approximately 15 min per cuvette sample. Zhong *et al.* demonstrated that FEK4 cells irradiated at 250 kJ/m^2 UVA returned to the basal level of intracellular labile iron 6 h post UVA irradiation.[151] Consequently, this is the amount of time required for the intracellular homeostasis of iron to return to normal. In order to minimise the time-sensitive loss of labile iron, it was therefore practical to translate the assay to a microplate format to achieve greater throughput in the subsequent studies.

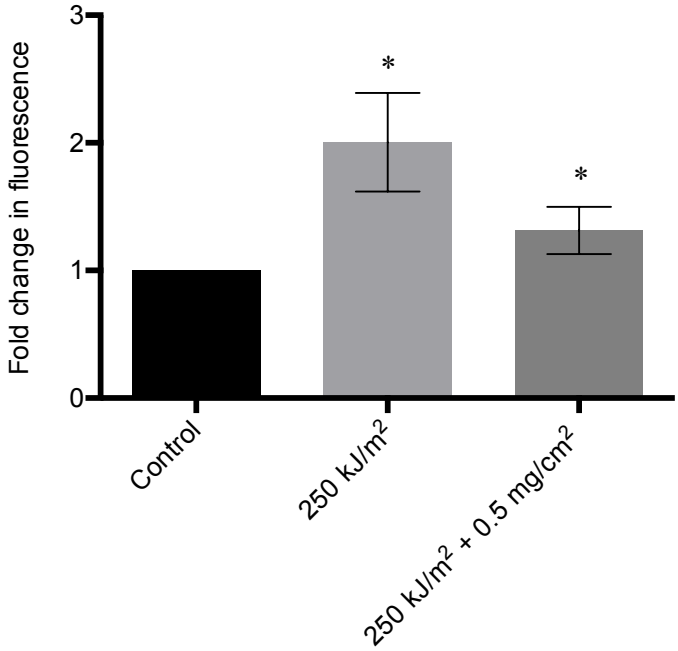

Figure 55. Calcein assay for FEK4 cells protected by ± 3% avobenzone + 5% (w/v) octocrylene at 0.5 mg/cm^2, showing the fold-changes in intracellular labile iron upon irradiation with a dose of 250 kJ/m^2 UVA. (n= 8)
* = p <0.05, significantly different from unirradiated control cells.

6. Combination of sunscreen filters and CICs

The results of the MTT assays revealed that in all cases the photoprotection provided by a 0.5 mg/cm^2 sunscreen thickness of individual common UVR filters was significantly lower than the photoprotection afforded by the recommended 2 mg/cm^2 of the same filter. Alongside these results was the observation that a 0.5 mg/cm^2 sunscreen thickness of 3% (w/v) avobenzone + 5% (w/v) octocrylene (the FDA maximum concentration) results in a 1.31 fold increase in intracellular labile iron upon UVA irradiation. Together these data build the argument that implementing a CIC into a sunscreen formulation could lead to improved protection against UVA-induced oxidative damage and enhanced cell survival when sunscreens are applied at sub-optimal thicknesses. In order to investigate this hypothesis, two commercially available sunscreen formulations from well-known brands were chosen. The sunscreen formulations were selected because they contained either avobenzone or Mexoryl SX® or both as their primary UVA filter, however the concentrations are unknown as formulation information is not disclosed in the UK:

Formulation 1

Name: Nivea Sun Protect & Moisture Lotion SPF30

Active UVR filters: avobenzone (UVA), homosalate (UVB), octocrylene (UVB), octisalate (UVB), nanoparticle TiO_2 (UVA/B).

Contains vitamin E as an antioxidant.

Formulation 2

Name: La Roche-Posay Anthelios XL Ultra Light Fluid SPF50+

Active UVR filters: avobenzone (UVA), Mexoryl SX (UVA), octocrylene (UVB), ethylhexyl triazone (UVB-not FDA approved), Mexoryl XL (UVA/B-not FDA approved), bis-ethylhexyloxyphenol methoxyphenyl triazine (UVA/B- not FDA approved).

In order to assess whether CICs had a positive photoprotective effect when used in conjunction with a sunscreen formulation applied at a thickness of 0.5 mg/cm^2, the dual staining annexin V and propidium iodide (PI) assay was employed to assess necrotic cell death rather than enzymatic activity as per the MTT assay. The translocation of phosphatidylserine (PS) from the cytoplasmic surface of the plasma cell membrane (as per normal viable cells) to the outer cell membrane, is a well-known hallmark of cell apoptosis.[239] The Ca^{2+}-dependent phospholipid-binding protein, annexin V, has a high affinity for PS, therefore exposure of PS to the external cellular environment allows it to be detected by annexin V. Conjugation of annexin V with the dye, Alexa Fluor 488, provides a highly fluorescent probe that can reliably detect cell apoptosis in a cell suspension, with excitation at 495 nm and emission at 519 nm. Apoptosis is a normal process of programmed cell death which is required for the maintenance of tissue under pathological conditions. In apoptosis, the cell actively participates in its own destruction, and annexin V-positive staining can therefore provide an indication of early apoptosis of cells as they perform their natural function.

PI is a DNA base intercalator with limited sequence preference, and as it does not permeate live cells, it is a popular fluorescent stain for the detection of dead or damaged cells (necrotic cells). PI is excited at 535 nm and emits at 617 nm.[239] Dual positive staining of cells with both annexin V and PI indicates a loss of membrane integrity which accompanies late apoptotic or necrotic 'unprogrammed' cell death due to external factors. This assay therefore allows one

to distinguish between the two forms of cell death.[239] It has previously been reported that necrosis is the primary mode of fibroblast cell death induced by UVA irradiation, and therefore this end point is commonly used to analyse the impact of UVA radiation.[151] However due to the highly oxidative environment induced by UVA radiation and the potentital of the ROS generated to damage DNA, repair processes such as the tumour suppressor protein p53 may be activated. Apoptosis is regulated by p53 and therefore may be induced if repair processes fail, as such it is possible for some UVA-induced apoptosis to occur as well as necrosis under UVA irradiation.[240] The ability to stain for both of these cell death procedures in the annexin V/PI assay enables analysis of the amount of live cells remaining after UVA irradiation which is more reliable than analysing the presence of necrotic cells.

The assay was carried out as described in the Experimental 7.2.9, and the photoprotective capacity of 0.5 mg/cm^2 of the sunscreen formulations along with 3% (w/v) avobenzone + 5% (w/v) octocrylene were first tested independently. The outdoor radiometer readings that were reported in Chapter 2.3 indicated that on a British summer's day, a dose of 500 kJ/m^2 UVA would equate to 80 min of sun exposure. The mean daily sun exposure ranges from 2.6-3.1 h depending on the SPF of the sunscreen applied,[241] therefore UVA doses of 500 kJ/m^2 and 750 kJ/m^2 (2 h of sun exposure or 1-1.5 MED) were used in the initial experiments. FEK4 cells were covered with ± 0.5 mg/cm^2 of an appropriate sunscreen/filter before irradiation, and then 24 h post-irradiation, the assay was carried out and analysis was performed on the flow cytometer. 10,000 events were recorded which were gated to separate intact cells from cell debris. This population was split into quadrants Q1-4, where Q1= PI-positive cells only; Q2= dual stained annexin V/PI-positive cells; Q3= cells negative for both stains; Q4= annexin V-positive cells only. A representative example of the gating for the negative control, 750 kJ/m^2 UVA and 0.5 mg/cm^2 formulation 1 + 750 kJ/m^2 UVA conditions is shown in Figure 56. The average percentage live cells (percentage of Q3) for each condition were used to create Figure 57.

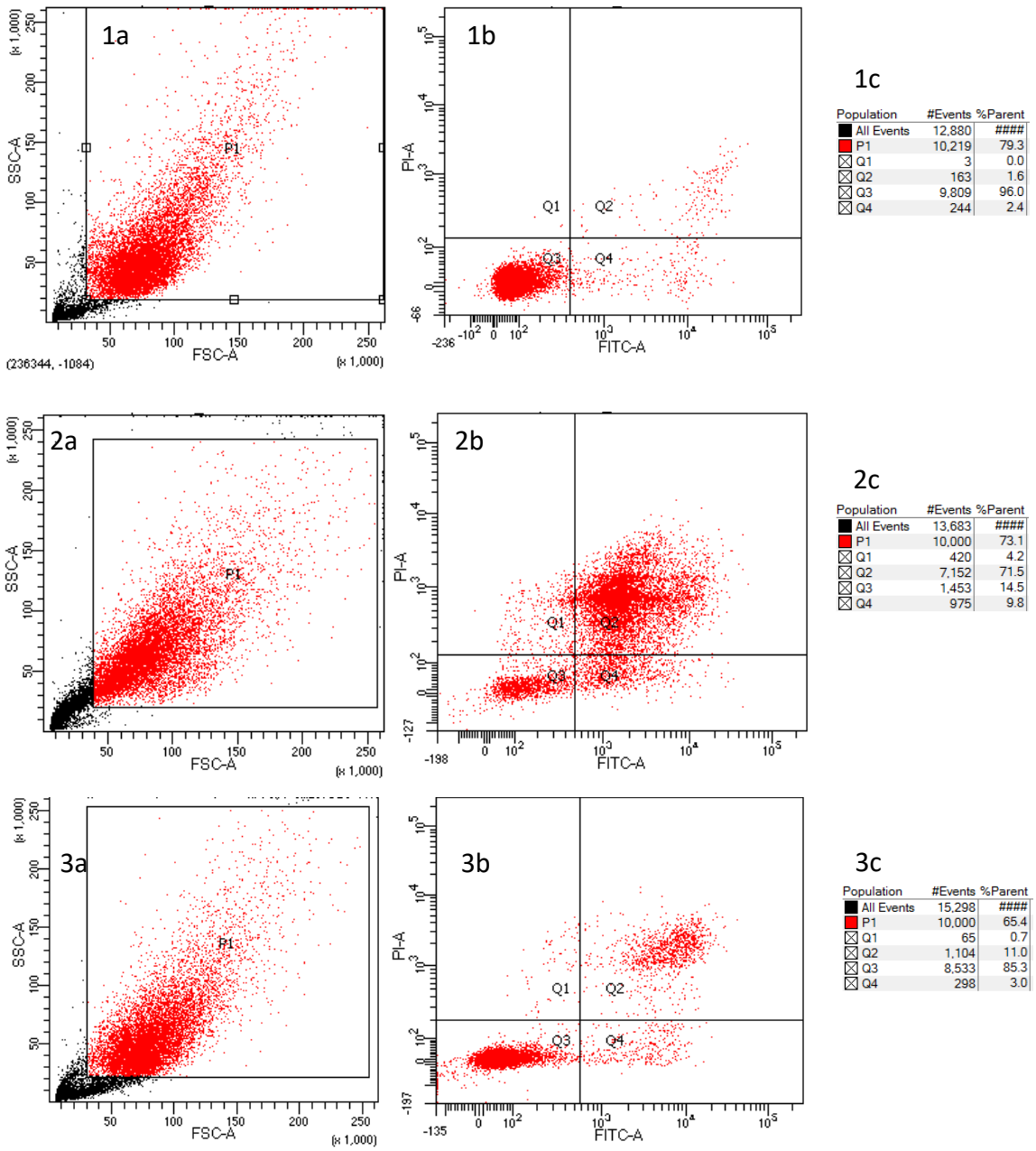

Figure 56. Representative example of the gating in an annexin V/PI assay. **Panel 1.** Control unirradiated cells; **Panel 2.** Cells irradiated with 750 kJ/m^2 dose of UVA; **Panel 3.** Cells covered with 0.5 mg/cm^2 of formulation 1 and irradiated with 750 kJ/m^2 dose of UVA. **a.** Initial gating of cells to exclude cell debris to give P1; **b.** Splitting of P1 into quadrants Q1-4 with the annexin V stain on the x axis and PI stain on the y axis; **c.** Table showing the percentage of events in each quadrant of P1.

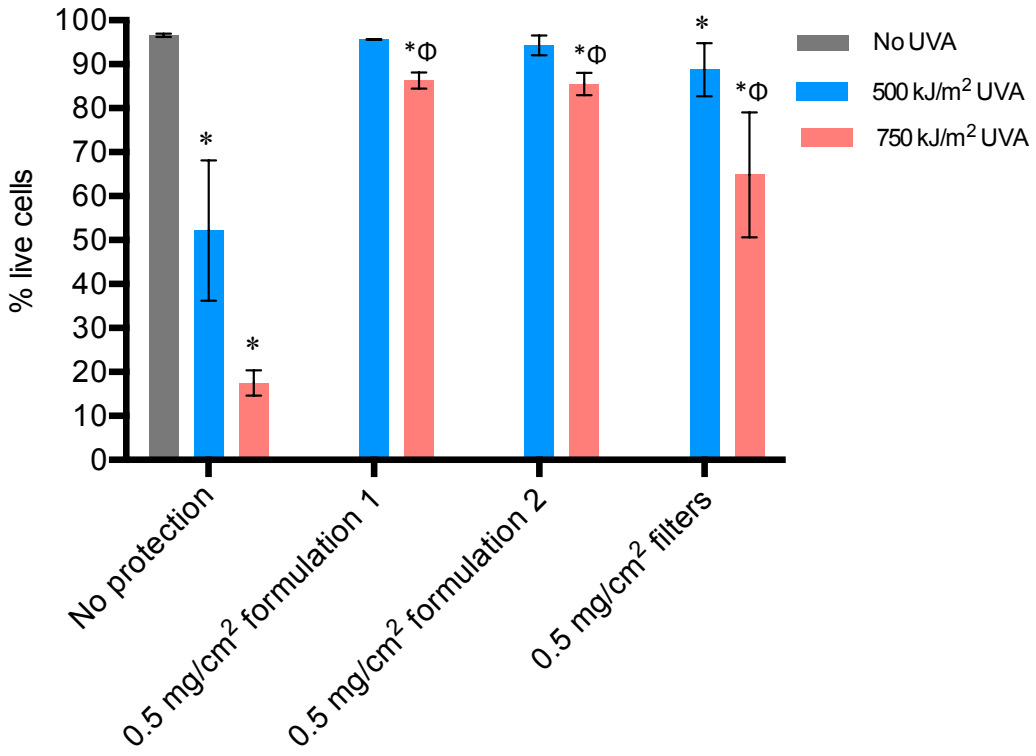

Figure 57. Flow cytometry analysis of UVA photoprotection of FEK4 cells, showing the average percentage of live cells. Cells were irradiated with a UVA dose of either 500 kJ/m^2 or 750 kJ/m^2 and covered with 0.5 mg/cm^2 of either formulation 1, formulation 2, or filters (3% (w/v) avobenzone + 5% (w/v) octocrylene). The assay was carried out 24 h post irradiation (n= 4).

* = p <0.05, significantly different from unirradiated control cells.

Φ = p <0.05, significantly different from cells protected with the same formulation irradiated at 500 kJ/m^2.

The results of the assays reveal that both of the commercial sunscreen formulations protect human skin fibroblasts against UVA-induced cell death at an application thickness of 0.5 mg/cm^2 for 80 min on a British summer day (500 kJ/m^2 UVA or 1 MED). Without any photoprotection, the 500 kJ/m^2 irradiated control has an average of 52.2 % live cells. Protection with 3% (w/v) avobenzone + 5% (w/v) octocrylene is significantly different from the unirradiated control at a dose of 500 kJ/m^2 which indicates the increased UVA protection afforded by the additional active UVA filters in the sunscreen formulations. When the dose was increased to 2 h (750 kJ/m^2), all three conditions were significantly different to the unirradiated control which indicates that the UVA radiation protection afforded by an application thickness of 0.5 mg/cm^2 sunscreen only lasts between 80-120 min.

The photoprotection afforded by CICs is expected to be through their quenching of labile iron generated by UVA rather than by acting as UVA filters. CICs **51** and **115** were evaluated independently in the annexin V/PI assay for their photoprotective capacity as they had been observed to be the best-performing compounds in the MTT assays (Chapter 2.4 and Chapter 3.3). This assay also allowed the lack of cytotoxicity of **51** and **115** without irradiation to be confirmed. FEK4 cells were treated with ± CICs **51** and **115** (20 μM) before irradiation with 500 kJ/m^2 or 750 kJ/m^2 UVA, and the results are shown in Figure 58.

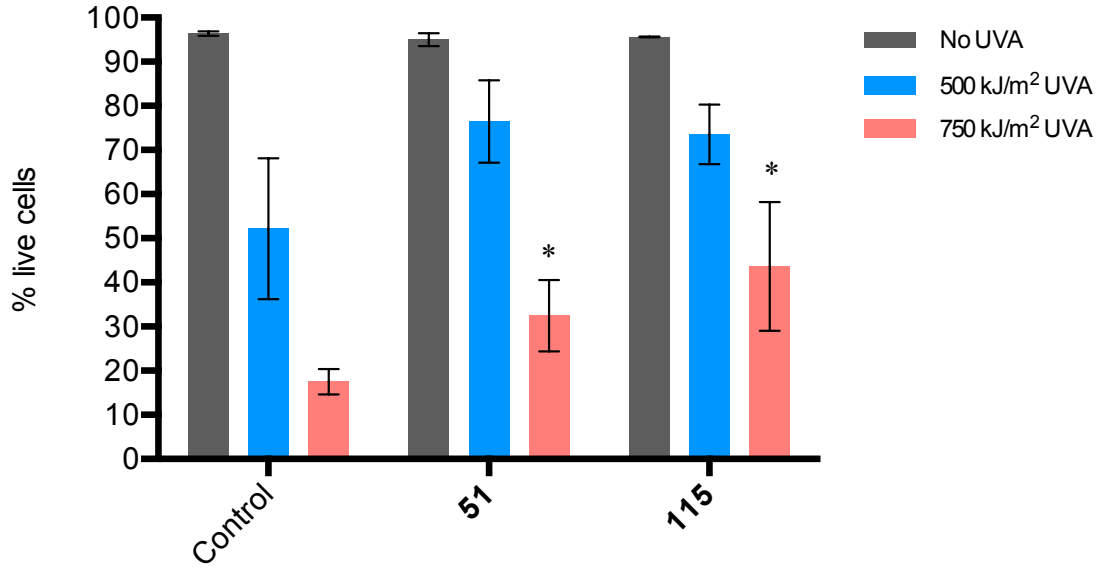

Figure 58. Flow cytometry analysis of UVA photoprotection of FEK4 cells, showing the average percentage of live cells. Cell were incubated overnight with CICs **51** and **115** (20 μM) before irradiation with a UVA dose of either 500 kJ/m^2 or 750 kJ/m^2 UVA. The assay was carried out 24 h post irradiation (n= 4).

* = p <0.05, significantly different from untreated control cells irradiated with a dose of 750 kJ/m^2.

Both CICs **51** and **115** were found to be effective in protecting human skin cells against UVA-induced cell death. At a dose of 500 kJ/m^2, the control irradiated cells have an average of 52.2% live cells, which is markedly increased by CICs **51** and **115** to 76.4% and 73.6% live cells respectively. At a dose of 750 kJ/m^2, the presence of CICs **51** and **97** significantly increases the percentage of live cells compared to the irradiated control from 17.5% to 32.5% and 43.6% live cells respectively.

Finally, we tested whether CICs such as **51** and **115** are able to act as a secondary line of defence once the full photoprotective capacity of a sunscreen applied at sub-optimal thickness is exceeded. A dose of 750 kJ/m^2 was chosen for these assays since at this dose it had been observed that the photoprotection afforded by the sunscreen formulations had diminished and the CICs also provided the most significant increases in protection. FEK4 cells were incubated overnight with CICs **51** and **115** (20 μM) and then covered with 0.5 mg/cm^2 sunscreen formulation or filter combination before irradiation. The assay was carried out 24 h later and the results are displayed in Figure 59.

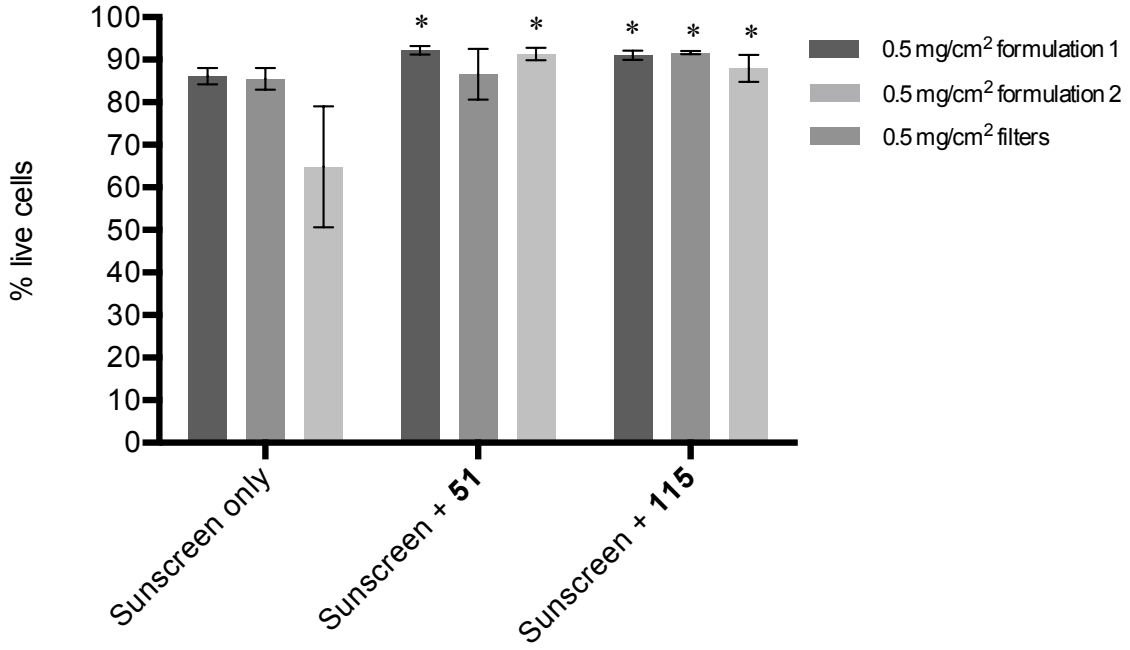

Figure 59. Flow cytometry analysis of UVA photoprotection of FEK4 cells, showing the average percentage of live cells. Cell were incubated overnight with CICs **51** and **115** (20 μM) before irradiation with a UVA dose of 750 kJ/m^2 UVA whilst covered with 0.5 mg/cm^2 of sunscreen formulation or filters (3% (w/v) avobenzone + 5% (w/v) octocrylene). The assay was carried out 24 h post irradiation (n= 3).

* = p <0.05, significantly different from cells only protected by the respective sunscreen/filter.

The combined photoprotective effect of CICs with 0.5 mg/cm^2 sunscreen formulation or filters when irradiated at 750 kJ/m^2 was found to be significant in comparison to the sunscreen formulation/filter alone in all cases except for CIC **51** with formulation 2. CIC **115** performed very well, restoring the percentage of live cells of formulation 1, formulation 2 and 3% (w/v) avobenzone + 5% (w/v) octocrylene to 91.0%, 91.4% and 88.0% respectively. Conducting a comparison of the levels of uncaging of CICs **51** and **115** with increasing doses of UVA (shown

in Figures 32 and 46 respectively) suggests that the superior photoprotection observed for CIC **115** at the higher dose of 750 kJ/m^2 UVA may be due to its slower uncaging profile, with respect to CIC **51**. Thus **115** exerts more powerful photoprotection at higher UVA doses where uncaging of the CIC also delivers an antioxidant moiety.

These data are important as they suggest that the presence of an iron chelator that is activated upon UVA irradiation provides increased photoprotection compared to a sunscreen alone. As seen in Chapter 3.2, the presence of an iron chelator alone has a more substantial effect on reducing intracellular ROS than the presence of a carbostyril alone. This indicates that the increase in photoprotection seen here is primarily through the mechanism of labile iron chelation, with the release of a secondary antioxidant molecule playing a more minor role. The real impact of these results however, is that CICs do provide extra photoprotection that is relevant to a real-world setting and thus may help prevent skin cancer in consumers who apply sunscreen formulations too thinly, unevenly or infrequently.

To confirm that the increased photoprotection observed with these CICs was by chelation of UVA-induced labile iron, the calcein assay was performed on FEK4 cells ± incubated with CIC **51** (20 μM) before irradiation with 500 kJ/m^2 UVA. The following calcein assays were performed in microplate format on the CLARIOstar microplate reader rather than in the cuvette format, due to the greater throughput that could be achieved with this equipment for these time-sensitive experiments. The results are shown in Figure 60 as a fold-change in fluorescence per 10^6 cells in comparison to the unirradiated, untreated control cells.

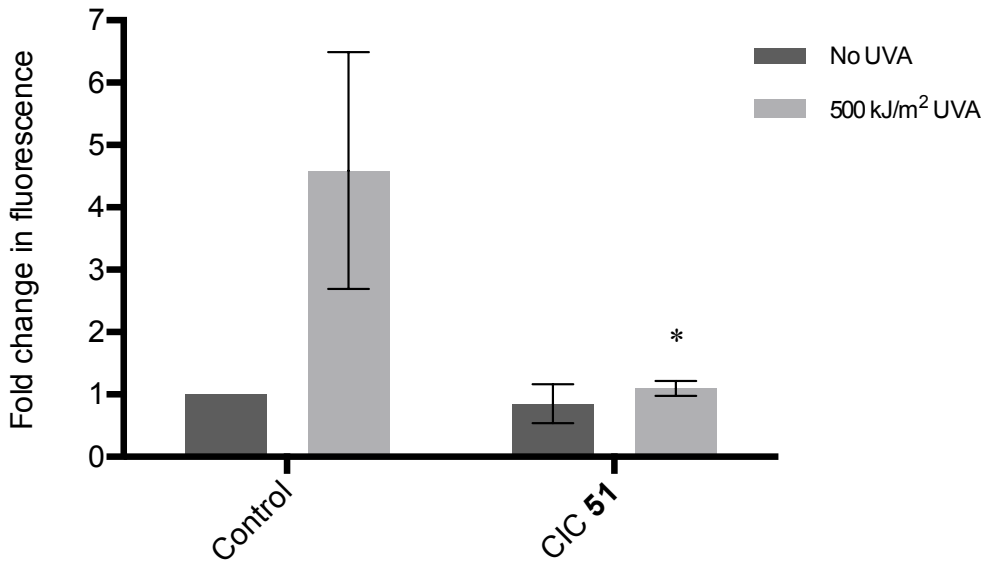

Figure 60. Calcein assay analysis of the change in intracellular labile iron upon irradiation with 500 kJ/m^2 UVA ± CIC **51** (20 μM). Data is represented as a fold- change in fluorescence (Δ*F*) per 10^6 cells of FEK4 cells, compared to the untreated unirradiated control which was set to 1. (n= 3)

* = p <0.05, significantly different from the respective control cells.

Irradiation at 500 kJ/m^2 UVA increased the fluorescence per 10^6 cells by an average fold-change of 4.59 compared to the unirradiated control cells. Cells that were incubated with CIC **51** (20 μM) prior to UVA irradiation reduced the fold-increase in fluorescence to an average of 1.10, indicating a positive uncaging of the iron chelator SIH **8** to yield a UVA-induced labile iron quenching effect. The assay was then repeated by incubating cells with ± CIC **51** overnight and then covering cells with 0.5 mg/cm^2 sunscreen formulation 1, 2 or filter combination (3% (w/v) avobenzone + 5% (w/v) octocrylene) during irradiation at 500 kJ/m^2 UVA. These results are represented in Figure 61.

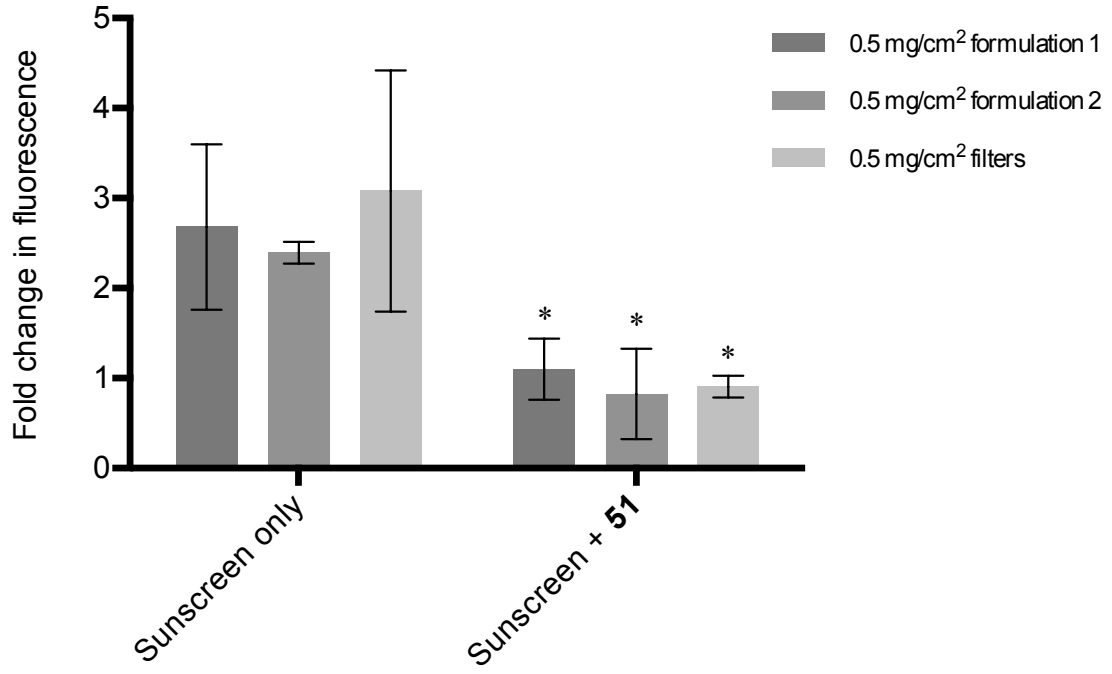

Figure 61. Calcein assay analysis of the change in intracellular labile iron upon irradiation of FEK4 cells protected by 0.5 mg/cm^2 of formulation 1, formulation 2 or combined filters (3% (w/v) avobenzone + 5% (w/v) octocrylene) with 500 kJ/m^2 UVA ± CIC 51 (20 μM). Data is represented as a fold- change in fluorescence (Δ*F*) per 10^6 cells of FEK4 cells, compared to the untreated unirradiated control which was set to 1. (n= 3)

* = p <0.05, significantly different from the respective cells protected solely by the sunscreen formulation or filter.

The results of this assay show average fold-changes in fluorescence in comparison to the untreated unirradiated control of 2.68, 2.40 and 3.08 for 0.5 mg/cm^2 of formulation 1, formulation 2 and the filter combination respectively, after a dose of 500 kJ/m^2 UVA irradiation. This data is consistent with the significant cell death observed under the same conditions in the flow cytometry assays, using a dose of 750 kJ/m^2. However, after overnight incubation of the cells with CIC **51** (20 μM) the fold-change in fluorescence is significantly decreased to a similar level as the untreated, unirradiated control in all three conditions. This result is also consistent with the observed recovery of live cells seen in the flow cytometry analysis upon addition of a CIC to cells covered by 0.5 mg/cm^2 of a sunscreen formulation or filter. This indicates that a sub-optimal thickness of a commercial sunscreen formulation does not prevent UVA-induced labile iron release and that the presence of an activatable strong iron chelator, such as SIH **8**, can be very beneficial in quenching the immediate onset of free intracellular iron. The annexin V/PI assays were carried out 24 h post-irradiation, hence the presence of apoptotic and necrotic cells were due to immediate cell death initiated by acute

UVA irradiation, however this does not account for the accumulation of damage caused by severe labile iron-induced oxidative stress which is demonstrated by these calcein assays.

The fluorescence of the supernatant from the final centrifugation step of the 500 kJ/m^2 UVA condition was also recorded during the calcein assays. This allowed the calculation of the fluorescence leakage of CA out of the cells due to loss of membrane integrity during irradiation. The average fluorescence leakage calculated as a percentage of the total fluorescence from the 500 kJ/m^2 sample was 11.6%, therefore all fluorescence data for these calcein assays has an error of ± 11.6%.

Understanding the significance of a change in fluorescence of CA (*Δ*F) within the FEK4 fibroblast cell system in terms of the concentration of chelatable labile iron rather than just the fold-change in fluorescence compared to the unirradiated control would enable the qualitative data displayed in Figures 60 and 61 to be converted into quantitative data. To achieve this, a titration was carried out whereby the *Δ*F of CA was monitored by quenching with Fe^{2+} in the form of ferrous ammonium sulphate (FAS). The titration was performed in microplate format on the CLARIOstar microplate reader to be consistent with the calcein assays performed for Figures 60 and 61. FEK4 cells were cultured and prepared for the titration as explained in the Experimental Section 7.2.10.3, and the ionophore A23187 (5 μM) was first added to the cells in suspension as described by Breuer *et al.* to permeabilise the cell membranes towards divalent metal ions.[236] The first fluorescence reading was recorded and then deoxygenated FAS was added in 0.5 μM increments as a source of Fe^{2+} ions to elicit step decreases in fluorescence.[238] The results of the average of three repeats of the titration are shown in Figure 62, with the fluorescence being normalised against the initial fluorescence reading before addition of FAS. The results indicate that CA forms a non-fluorescent [CA-Fe] adduct with Fe^{2+} permeabilised to the cytosol, assuming that the concentrations of Fe^{2+} in the buffer and the cytosol are equivalent. In the presence of physiological levels of glutathione, Fe^{2+} is scavenged by SIH as Fe^{3+}, therefore the Fe^{2+} delivered by FAS corresponds to the labile iron that would be released upon UVA exposure and is suitable for quantification of cytosolic labile iron in the calcein assay.[105]

Figure 63 was generated by converting the normalised fluorescence into the change in fluorescence (ΔF) upon addition of increasing concentrations of FAS, and a cell count was performed after the assay and the change in fluorescence was adjusted per 10^6 cells. The line of best fit was obtained using linear least-squares regression, with an R^2 value of 0.9753 indicating a good fit of the data. The line equation (y = 0.8057x – 0.05286) could then be used to calculate the concentration of chelatable labile iron in the cytosol, [Ca-Fe], that was associated with an experimentally determined change in fluorescence.

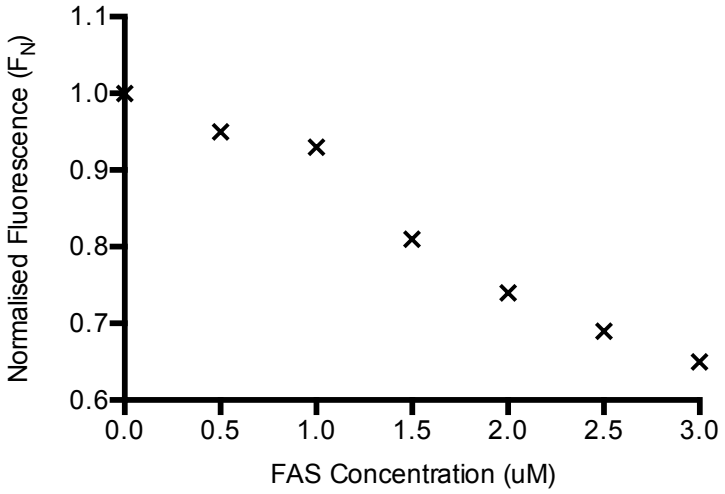

Figure 62. Titration of CA-AM (0.05 μM) with 0.5 μM increments of ferrous ammonium sulphate (FAS) in FEK4 fibroblasts, represented as the change in fluorescence normalised to the control (0 μM FAS) against FAS concentration.

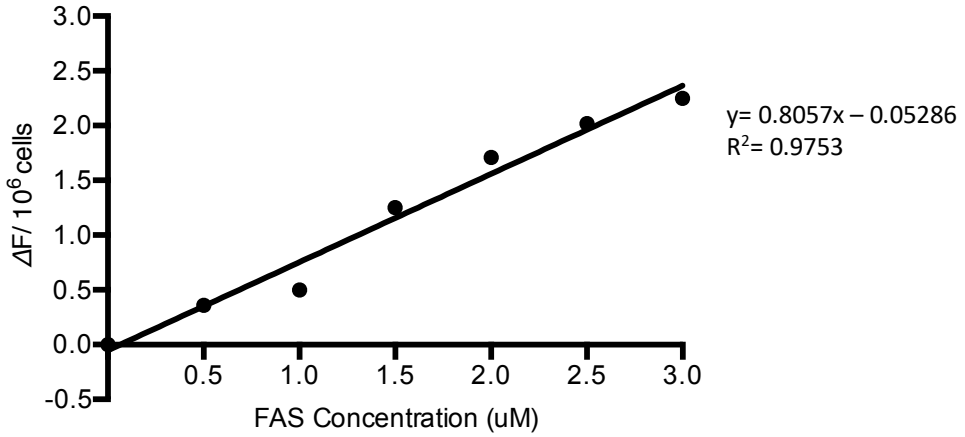

Figure 63. Change in fluorescence (ΔF) per 10^6 cells upon addition of increasing concentrations of FAS. The line of best fit was obtained using linear least-squares regression.

An estimate of the concentration of chelatable intracellular labile iron was made using the FAS titration and the equation of the line from Figure 63, and the data is shown in Table 11. This transformed data gives a more comprehensive representation of the calcein assay data than Figures 60 and 61.

Table 11. Estimation of the concentration of intracellular chelatable labile iron (μM) in FEK4 cells under different conditions, calculated using FAS titration of CA giving the line equation y=0.8057x – 0.05286, represented as the mean ±SD. The fold-change in average concentration compared to the untreated unirradiated control is also shown. (n=3)

* = p <0.05, significantly different from the respective cells protected solely by the sunscreen formulation or filter.

Condition	Concentration intracellular labile iron (μM)	Fold change in concentration
No UVA	0.39 ±0.32	1.00
500 kJ/m^2 UVA	1.39 ±0.53	3.56
CIC **51** - UVA	0.42 ±0.23	1.08
CIC **51** + UVA	0.64 ±0.33	1.64
formulation 1 + UVA	0.81 ±0.45	2.08
formulation 1/CIC **51** + UVA	0.42 ±0.06	1.08
formulation 2 + UVA	0.69 ±0.17	1.77
formulation 2/CIC **51** + UVA	0.41 ±0.10 *	1.05
3% (w/v) avobenzone + 5% (w/v) octocrylene + UVA	0.64 ±0.11	1.63
3% (w/v) avobenzone + 5% (w/v) octocrylene /CIC **51** + UVA	0.43 ±0.10 *	1.10

The fold-changes (in comparison to the untreated unirradiated control) were calculated using the average estimated concentrations of intracellular chelatable labile iron rather than the differences in fluorescence. Calibrating the change in fluorescence using the FAS concentration titration curve gives more accurate data which follows the same trend as Figures 60 and 61. Table 11 indicates that the fold-change in chelatable labile iron concentration is 3.56 for the condition irradiated with 500 kJ/m^2 UVA, while overnight incubation with CIC **51** (20 μM) reduces the chelatable labile iron to 1.64-fold. The presence

of the CIC after overnight incubation in unirradiated cells does not seem to cause a reduction in the chelatable labile iron in comparison to the control (1.08), indicating that the CIC is stable and does not chelate iron using the two available coordination sites. When sunscreen formulation 2 or the filter combination was irradiated with 500 kJ/m^2 UVA in the presence of CIC **51,** there was a significant reduction in the chelatable labile iron compared to the sunscreen alone, for example formulation 2 under irradiation gives a fold-increase in chelatable iron concentration of 1.77 which is decreased to 1.05 with overnight incubation of CIC **51**.

7. Summary

The results of both the annexin V/PI flow cytometry and the calcein assays suggest that the use of a CIC in conjunction with a sunscreen formulation can be beneficial in increasing the cell survival of human skin cells through quenching of UVA-generated labile iron, which may have noteworthy impact in preventing skin photoaging or cancer. A CIC as an additive in a sunscreen formulation could act as a second line of defence when a sub-optimal thickness of sunscreen is applied to the skin (0.5 mg/cm^2). The annexin V/PI assays were carried out using a dose of 750 kJ/m^2 which elicited a reduction in percentage live cells in cells protected by 0.5 mg/cm^2 sunscreen, however this dose (2 h sun exposure or 1.5 MED) is still lower than the suggested average time of sun exposure (2.6- 3.1 h). With this in mind if the trend in reduction of percentage live cells continued in the same manner as it did between the doses of 500-750 kJ/m^2, it could be hypothesised that at the higher doses there would be considerably fewer live cells and therefore the presence of a CIC would be more important and would have the potential to significantly bridge the gap in sun photoprotection. This has the impact of a sunscreen formulation potentially being awarded a higher UVA-PF rating thus improving the level of photoprotection consumers would receive. The calcein assays were carried out immediately post-500 kJ/m^2 UVA irradiation and as such demonstrate the presence of intracellular chelatable iron immediately after 80 min of sun exposure. At this time the endogenous antioxidant defences of the cell (described in the Introduction 1.1.4) are overcome with the highly oxidative environment induced by UVA, and intracellular iron homeostasis is disturbed.

CHAPTER 5: RESULTS AND DISCUSSION

1. Introduction

In 1908 Beijerinck made the observation that the yeast *Candida pulcherrima* formed a red pigment when grown in media containing iron salts, conversely if the yeast was grown on iron- deficient media the pigment was not produced. The addition of a ferric salt solution to yeast growing on iron-deficient media caused the colonies and the surrounding media to turn red.[242] It was postulated in this study that *C. pulcherrima* produces a colourless precursor that reacts in the presence of iron and oxygen to form the pigment. In 1946, Roberts further investigated the factors affecting the production of this pigment and found that strongly pigmented cells were non-viable. This finding indicated that pigment production by the yeast was a pathological defence reaction against a toxic concentration of iron in the media.[243]

The pigment was named pulcherrimin by Van Der Walt and the chemical structure was subsequently investigated.[244] Kluyver *et al.* isolated pulcherrimin from *C. pulcherrima* in 1953 and reported some of its chemical properties. It was shown that the iron content of the pigment was 12.4% or higher, and that it was very resistant to hydrolysis by relatively strong acid. Even after boiling in 50% concentrated HCl in EtOH for 6-10 h, some of the pigment remained undissolved.[245] Notwithstanding its high acid resistance, the resulting liquid produced from hydrolysis was tested for the presence of amino acids and the only amino acid found in a significant amount was leucine. Pyrolysis of the pulcherrimin pigment was carried out using zinc dust under vacuum at 220^{o}C, which allowed elemental analysis of the white needles which formed. The molecular formula from pyrolysis in this way was reported as $C_{12}H_{18}N_2O_2$. At a similar time, parallel work was being undertaken by Dutcher into the structure of aspergillic acid (shown in Figure 64), an antibiotic compound excreted by the fungus *Aspergillus flavus*.[246] Research into aspergillic acid gave the same basic molecular formula $C_{12}H_{18}N_2O_2$ as that obtained for the product of pyrolysis of pulcherriminic acid. The elucidation of the structure of aspergillic acid along with further similarities in the UV spectra of both products led to the proposal of a diketo-pyrazine nucleus (Figure 65), with the

remaining C_8H_{18} attributed to aliphatic side chains.[245] Hydrogenation of pulcherrimin gave a diketopiperazine product, also shown in Figure 65.

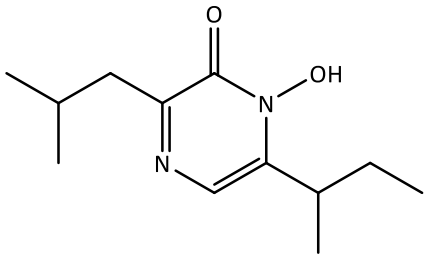

Figure 64. The structure of aspergillic acid, an antibiotic excreted by *Aspergillus flavus,* elucidated by Dutcher.[246]

Based on this evidence, a symmetrical structure for the pulcherrimin nucleus was suggested (i.e related to a 2,5-diketopiperazine) and the final structure for the precursor pulcherriminic acid **14** was presented as shown in the Introduction Section 1.3.3, Figure 14. Dutcher proposed that the formation of a red iron complex in the presence of aspergillic acid was *via* the hydroxamic acid moiety of the molecule.[246] Due to the similarities in structure and the formation of a red pigment, it was strongly suggested that the binding of ferric iron in pulcherrimin is also *via* a hydroxamate-like moiety in a 3:1 complex,[245] shown in Figure 66. However, the exact chemical structure of this complex has yet to be elucidated by X-ray crystallography.

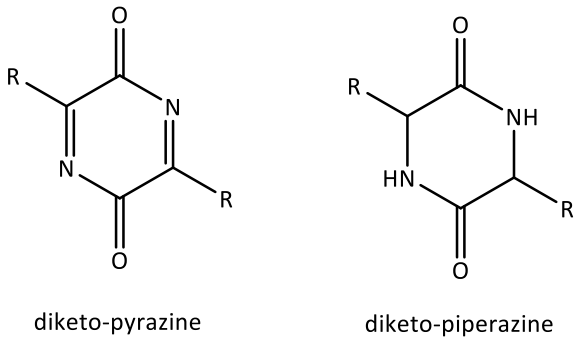

Figure 65. The structures proposed by Kluyver *et al.* of the product of pyrolysis of pulcherrimin (diketopyrazine) and the product of hydrogenation of pulcherrimin (diketopiperazine).[245]

Pulcherrimin production has also been found to occur in the yeast *Metschnikowia pulcherrima* (found on wine grapes)[132] and is not limited to yeasts; it is also excreted by *Bacillus subtilis* and *Bacillus cereus*[244] along with *Bacillus licheniformis.*[126] As described in the Introduction Section 1.3.3, siderophores such as DFO **1** (produced by *Streptomyces pilosus*)

are naturally occurring iron chelators which are part of a pathogen's mechanism for scavenging iron from the environment or during host invasion. The scavenged iron:siderophore complex is internalized by the pathogen and the ferric iron is reduced to ferrous iron which triggers release from the complex in order for the Fe^{2+} to be used intracellularly.[126] Pulcherriminic acid has similarities to siderophores through its tautomeric N-oxide iron chelating group which is similar to the DFO hydroxamic acid iron-binding motif. However, the insoluble pulcherrimin complex cannot act as an iron carrier as siderophores do.[126,132] The excretion of pulcherriminic acid only performs a 'biocontrol' mechanism, for example in the case of pulcherriminic acid production by *M. pulcherrima*, the iron chelator protects grapes, apples and peaches from rot caused by post-harvest pathogens, which is particularly important in the wine-making industry.[132]

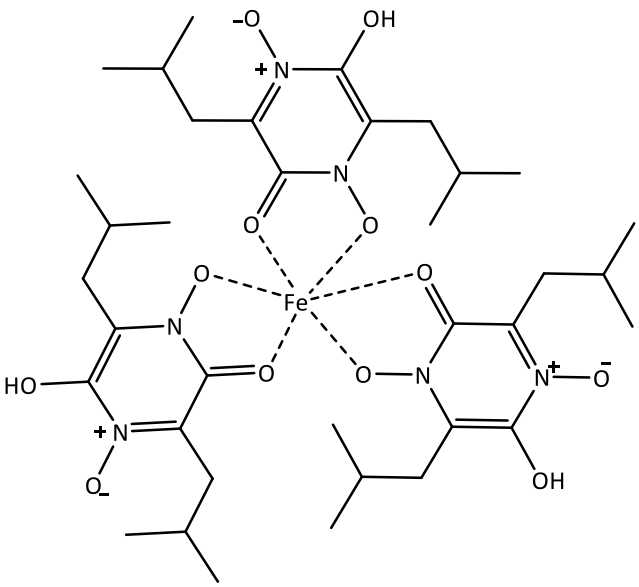

Figure 66. Pulcherrimin, the red pigment produced on binding of pulcherriminic acid with ferric iron in a 3:1 complex through the hydroxamate-like moiety of pulcherriminic acid, as proposed by Kluyver *et al.*[245]

Pulcherriminic acid **14** is of great interest as a naturally occurring high affinity iron chelator as consumers move towards more 'natural' and 'eco-friendly' ingredients in cosmetics (including sunscreen formulations). A considerable amount of **14** is generated as a by-product in bioreactor processes producing high value materials such as lipids, monosaccharides, and 2-phenylethanol, which shows its potential as a sustainable natural reagent.[247] For these

reasons, the chemical synthesis of **14** was attempted to allow its chemical and biological analysis as a potent natural iron chelator.

2. Synthesis of pulcherriminic acid

The structure of pulcherriminic acid **14** was determined by Kluyver and later further investigated by Cook *et al.*[133] and Macdonald.[248] Combining all of the evidence including functional group analysis by ^{1}H NMR of purified **14** from *C. pulcherrima* gave **14** the empirical formula $C_{12}H_{20}N_2O_4$, which as noted above may be related to an oxidised 2,5-diketopiperazines (2,5-DKP). 2,5-DKPs are attractive chemical scaffolds as they are small and conformationally constrained heterocycles. Structural diversity can be introduced in six positions and stereochemical control is available at four positions. 2,5-DKPs are abundant in nature and as such are interesting candidates for drug discovery and for medicinal chemistry.[249] For example tryprostatin B, shown in Figure 67, is isolated from *A. fumigatus* and has gained interest for development as an anti-cancer drug due to its ability to inhibit growth of human breast, prostate and lung cancer cell lines in the G2/M phase of the cell cycle.[250] Many drugs have been synthesised by chemists through structure-activity relationship (SAR) analysis of a 2,5-diketopiperazine core. For example, a spirodiketopiperazine derivative (shown in Figure 67) was found to be a potent cytotoxic compound in kidney, melanoma and cervical adenocarcinoma cancer cell lines that were resistant to the anti-cancer drug doxorubicin.[251]

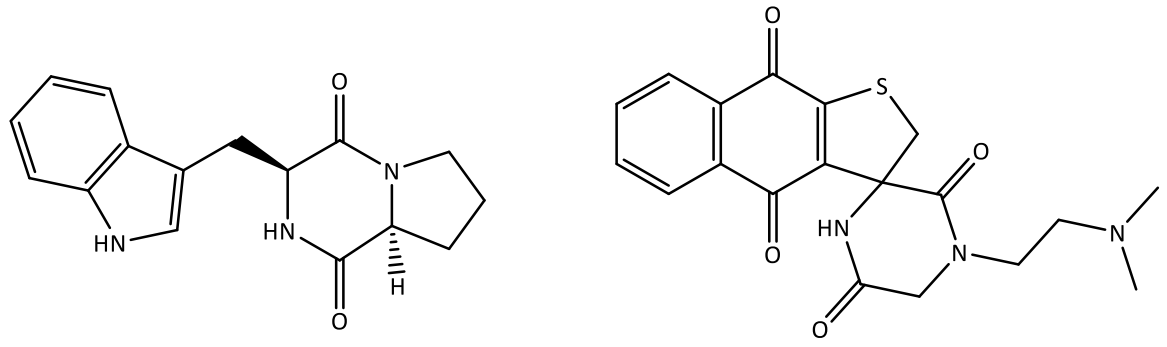

tryprostatin B

4'-(2-(dimethylamino)ethyl)-2*H*-spiro[naphtho[2,3-*b*]thiophene-3,2'-piperazine]-3',4,6',9-tetraone

Figure 67. The structures of two drug candidates containing a 2,5-diketopiperazine core which have shown potential in cellular studies.

The 2,5-DKP core is a cyclic dipeptide (CDP). CDPs are generated by the coupling and end-to-end cyclization of two amino acids, and thus are the simplest of cyclic peptides. In natural organisms (ranging from bacteria to humans), CDPs are biosynthesised through the action of cyclodipeptide synthases and non-ribosomal peptide synthetases.[252] Kluyver *et al.* confirmed that the only amino acid present in pulcherriminic acid is L-leucine. The molecular formula from pyrolysis of pulcherriminic acid was reported as $C_{12}H_{18}N_2O_2$ which indicates that the two identical R groups attached to the DKP structure (Figure 65) would consist of a C_4H_9 unit, consistent with the side chain of L-leucine. In order to chemically synthesise the starting CDP core of pulcherriminic acid, two units of L-leucine would need to be cyclized *via* formation of two amide bonds. A preparation of pulcherriminic acid *via* pulcherrimin was reported by Ohta[253] in 1964, starting from racemic *cyclo*(leucyl-leucine), however very limited experimental detail was reported and no spectroscopic characterisation was presented.[253,254] In 1992 Cook *et al.* reported the synthesis of the CDP *cyclo*(L-isoleucyl-L-isoleucine) through a self-condensation reaction of two units of L-isoleucine by refluxing in ethane-1,2-diol.[255] Although efficient, the drawback of this method is that the stereochemistry of the chiral centres is compromised, which in Cook's report led to a mixture of *cis*-(3*S*, 6*S*), *trans*- and *cis*-(3*R*, 6*R*) products. In view of this, a more controlled, classical peptide synthesis approach was employed in this work to stereoselectively synthesise a leucine-derived CDP intermediate. This approach had the advantage of more simple NMR analysis due to the generation of a

single stereoisomer, and the progress of subsequent reaction steps might also be different using a single CDP stereoisomer compared to a mixture of 3 stereoisomers.

Cyclic dipeptide synthesis is typically achieved by first forming a protected linear precursor *via* an amide bond between an N-protected amino acid (carboxy component) and an amino acid alkyl ester (amino component).[249] The synthesis is then completed by removal of the N-terminal protecting group and cyclisation via direct intramolecular nucleophilic attack upon the C-terminal ester carbonyl.

In order to couple the two amino acid starting materials together, the carboxylic acid function of the carboxy component requires activation. As described in Chapter 2.3, carbodiimides are extensively used coupling reagents for ester and amide bond formation and therefore EDC.HCl was once again employed as a coupling reagent (see Scheme 39), together with 1-hydroxy-1*H*-benzotriazole (HOBt), which is an additive that is commonly used in amide bond formation to prevent formation of an unreactive dialkylurea by-product.[256] HOBt reacts with the *O*-acylurea (shown in Chapter 2.3, Scheme 14) to give an activated ester in a similar manner to DMAP. Using HOBt as a reaction catalyst has also been shown to reduce epimerisation during coupling, which is a potential problem for the activation of certain amino acids during amide bond formation.[256]

Furukawa *et al.* synthesised 20 CDPs containing L-leucine in high yields using the general synthetic route: dipeptide formation with an N-protected amino acid and an amino acid methyl ester, cleavage of the N-protecting group and cyclization. This general route was therefore employed here to synthesise *cyclo*(L-leucyl-L-leucine) **124** starting with the commercially available *t*-butyl carbamate (Boc)-protected L-leucine **120** and L-leucine methyl ester hydrochloride **121**, as shown in Scheme 40. The Boc protecting group in **120** is stable towards nucleophilic attack and therefore effectively prevents polypeptide formation, whereas it can also be easily removed using a strong acid such as TFA, generating isobutylene and CO_2 as by-products.[183] A solution of **120** in anhydrous DMF was cooled to 0^{o}C and treated with 1.5 equivalents of HOBt followed by 1.5 equivalents of EDC.HCl. After stirring for 30 min, a solution of **121** in anhydrous DMF with 3 equivalents of DIPEA was added. A single stereoisomer (*cis*-3*S*, 6*S*) of the desired dipeptide **122** was obtained as a white powder in a 74% yield. Treatment of **122** with TFA at RT for 1.5 h then gave the N-deprotected dipeptide

123 as the trifluoroacetic salt in 99% yield. Cyclization by forming a second amide bond to give the CDP **124** was then achieved by a modification of the method of Suzuki *et al.*[257] This method involved acetic acid-catalyzed cyclization of the dipeptide under reflux in the presence of one equivalent of the tertiary amine base N-methylmorpholine (NMM).[257] The yield of CDP achieved using this method was reported to surpass that of base-catalyzed or autoaminolysis reactions.[257-259] Therefore **123** was refluxed in 0.1 M acetic acid in butanol with one equivalent of DIPEA as an alternate tertiary amine to NMM, in order to neutralize the TFA released in solution. This gave the desired *cis*-3*S*, 6*S* CDP **124** in a 93% yield.

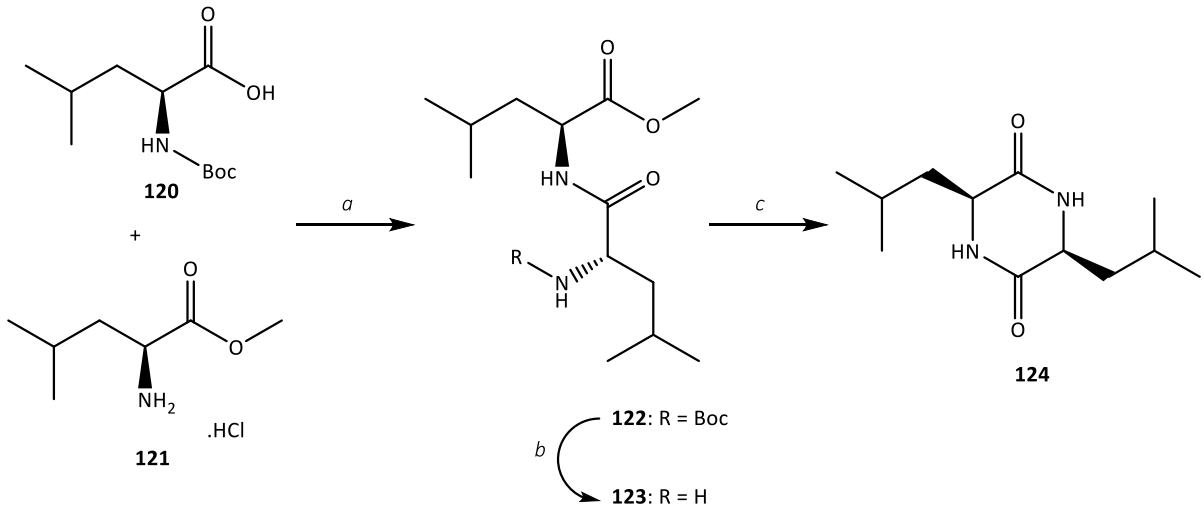

Scheme 40. Synthetic route to *cyclo*(L-leucyl-L-leucine) **124**. *Reagents and conditions:* **a.** HOBt, EDC.HCl, DIPEA, anhydrous DMF, RT, 24 h, 74%; **b.** TFA, DCM, RT, 1.5 h, 99%; **c.** 0.1 M acetic acid in butanol, DIPEA, reflux, O/N, 93%.

The next steps in the synthesis of **14** required the conversion of the DKP nucleus to a pyrazine system and the oxidation of both nitrogen atoms. In 1982 Göktürk *et al.* investigated pyrazine N-oxides related to the synthesis of mycelianamide, wherein one of the synthesised intermediates **125** (shown in Figure 68) has a very similar structure to pulcherriminic acid **14**.[260] More recently Usui *et al.* reported the total synthesis of phellodonin, a complex alkaloid isolated from the fungus *Phellodon niger*, whose structure contains an embedded DKP-like component.[261] This synthetic pathway involved the preparation of an L-isoleucine CDP which was manipulated to give the intermediate **126** shown in Figure 68, which also has an analogous structure to a 2-trimethylsilyl ether derivative of pulcherriminic acid. Both of the described papers carried out chlorination of the respective CDP to give a 2,5-dichloropyrazine

derivative which was then subjected to N-oxidation to give a pyrazine-*bis*-N-oxide, followed by displacement of the chloro groups with an oxygen nucleophile.

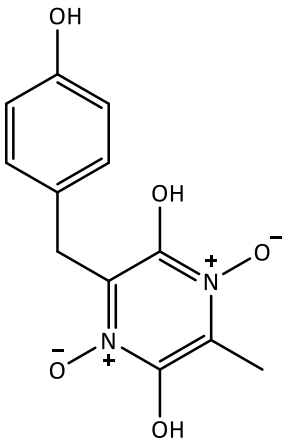

125

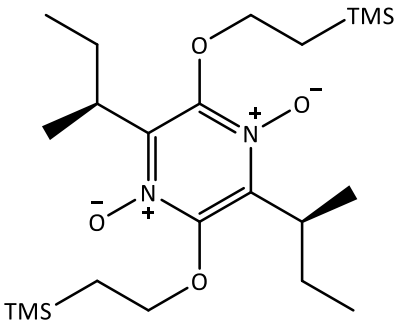

126

Figure 68. Intermediates **125** and **126** in the synthesis of mycelianamide and phellodonin respectively, which have structural similarities to pulcherriminic acid **14**.

The first steps of Ohta's original synthesis are shown in Scheme 41. *Cyclo*(leucinyl-leucine) was reacted with a mixture of chlorinating reagents, phosphorous oxychloride ($POCl_3$) and phosphorous pentachloride (PCl_5), which gave a mixture of products that were then subjected to further oxidation and chlorination *via* a series of steps[253] to give the 2,5-dichloropyrazine derivative **127**.

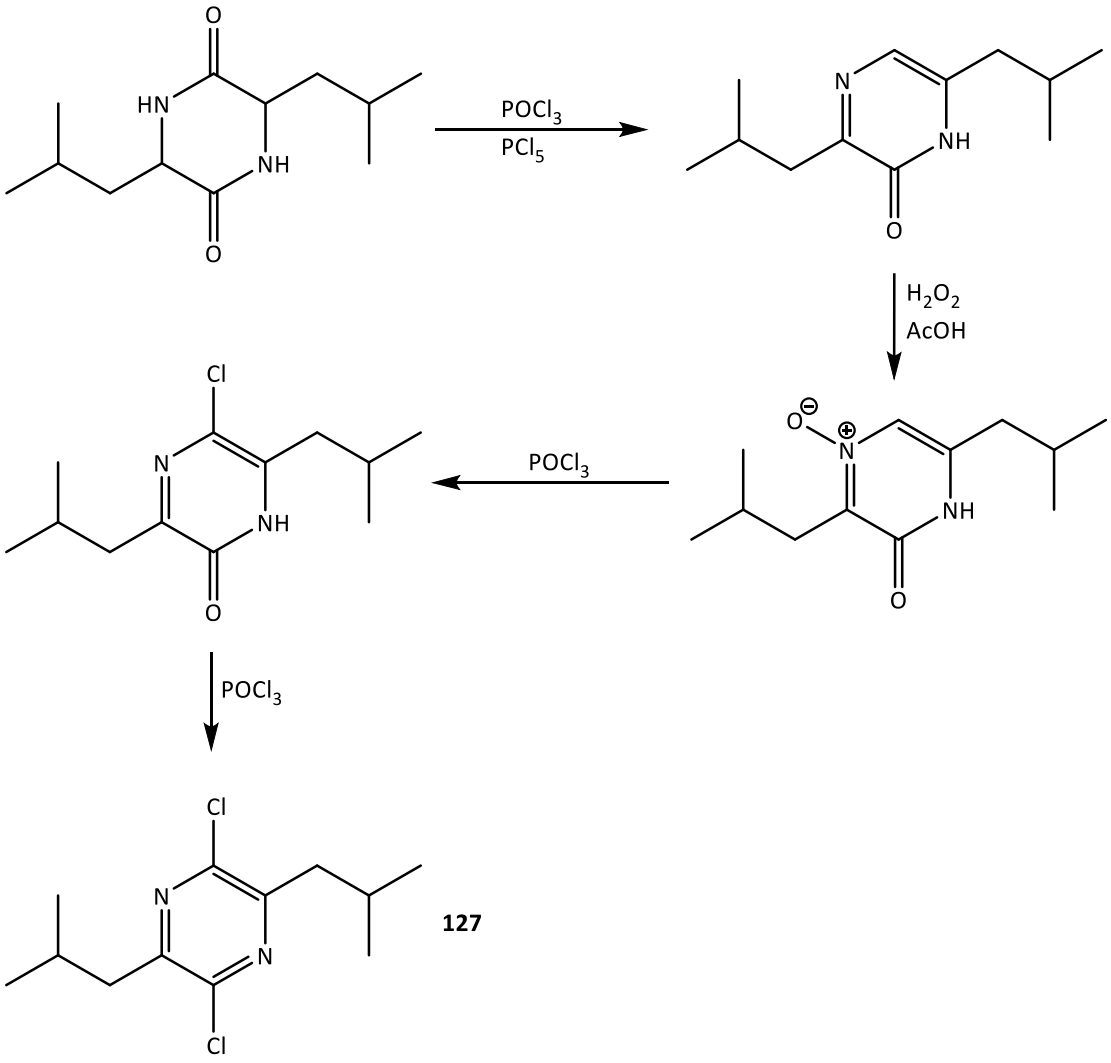

Scheme 41. Synthetic pathway reported by Ohta for the synthesis of the 2,5-dichloropyrazine intermediate **127** from a racemic mixture of *cyclo*(leucinyl-leucine).[253]

For this work, the well-described synthetic pathways elucidated by Göktürk *et al.* and Usui *et al.* were instead applied, and with **124** (the required core structure of pulcherriminic acid) in hand, the synthesis of the 2,5-dichloropyrazine intermediate **127** was attempted. Usui *et al.* reported the attempted generation of a dichloropyrazine derivative *via* Vilsmeier-Haack-type chemistry using an excess of the chlorinating reagent $POCl_3$ at 100°C. However, rather than producing the desired dichloropyrazine, it was reported that the principal product was instead the monochloropyrazine (shown in Scheme 42).

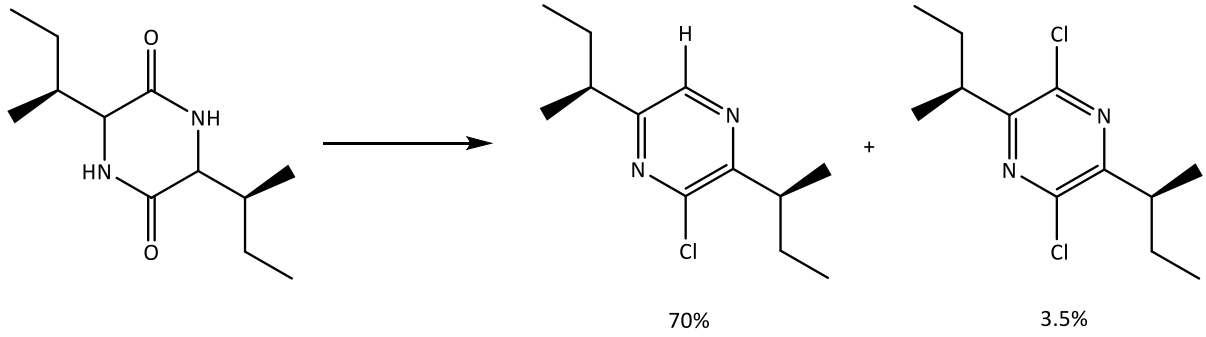

Scheme 42. The two products generated from chlorination of *cyclo*(L-isoleucyl-L-isoleucine) reported by Usui *et al.* The major product (70%) was the monochloropyrazine derivative.[261]

These conditions were nonetheless applied using the CDP **124** in an excess of $POCl_3$, which was heated to 100°C in a sealed pressure tube overnight (route a in Scheme 43). As anticipated, both mono and dichlorinated products were obtained which were easily separated by column chromatography. Unlike Usui's synthesis from an isoleucine CDP starting material, the reaction here gave a higher proportion of dichlorination, however the desired dichloropyrazine **127** was still the minor product (17%) in comparison to the monochloropyrazine **128** (39%).

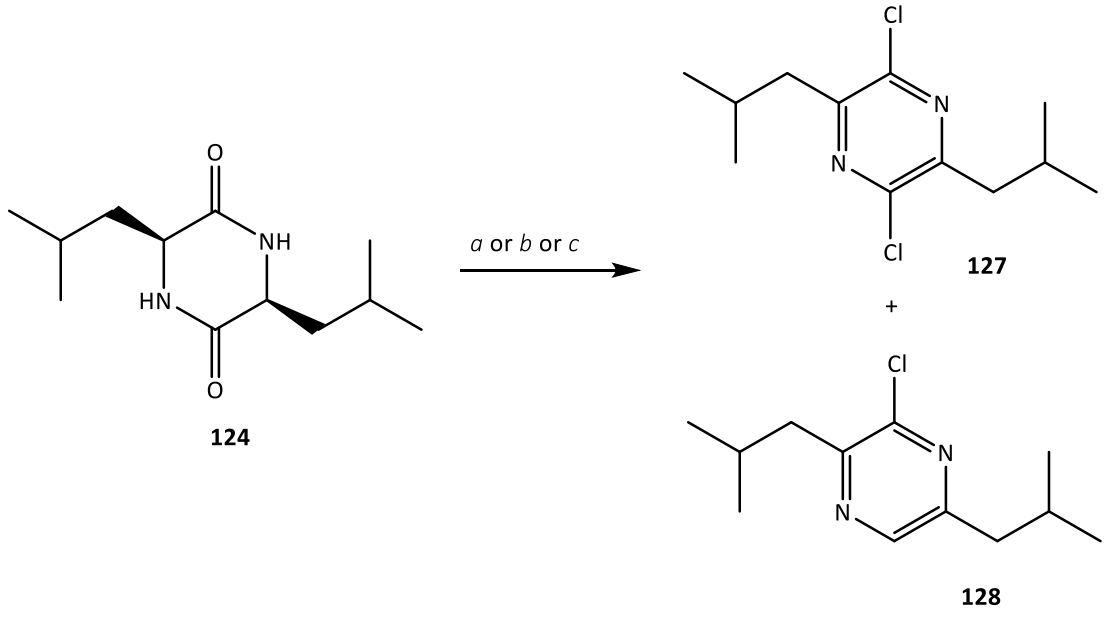

Scheme 43. Attempted synthesis of 2,5-dichloro-3,6-diisobutyl pyrazine **127** along with the major monochlorinated side product **128**. *Reagents and conditions:* **a.** excess $POCl_3$, 100°C , O/N; **b.** excess $POCl_3$, RT, O/N; **c.** 2 eq. $POCl_3$, 1 eq. pyridine, 160°C, 2 h.

Göktürk *et al.* reported that reacting a CDP containing one benzyl and one methyl side chain with an excess of $POCl_3$ at RT for 20 h formed the dichloropyrazine as the principal product with a trace of monochloropyrazine.[260] The chlorination reaction of **124** was therefore repeated with an excess of $POCl_3$ at RT, however this was found to give the opposite result, and only the monochloropyrazine **128** was generated in a 30% yield (route b in Scheme 43). It would appear that the disparity in yields of products compared to the reports of Usui *et al.* and Göktürk *et al.* may be due to the difference in steric bulk of the amino acid side chains in the DKP starting materials. A suggested mechanism for the generation of the mono and dichloropyrazines is presented in Scheme 44. With increased steric bulk of the substituents, R, the intermediate formed upon activation with a second equivalent of $POCl_3$ may undergo rearrangement and elimination of $OPOCl_2$ rather than addition of the chloride nucleophile, thus leading to a monochloropyrazine rather than the desired dichloropyrazine. It is noteworthy that Ohta *et al.* reported that chlorination of a racemic mixture of *cyclo*(alanyl-alanine), R= CH_3, with excess $POCl_3$ at reflux led to a similar ratio of mono and dichlorinated products to that observed for **124** in this work (R= $CH_2CH(CH_3)_2$).[262]

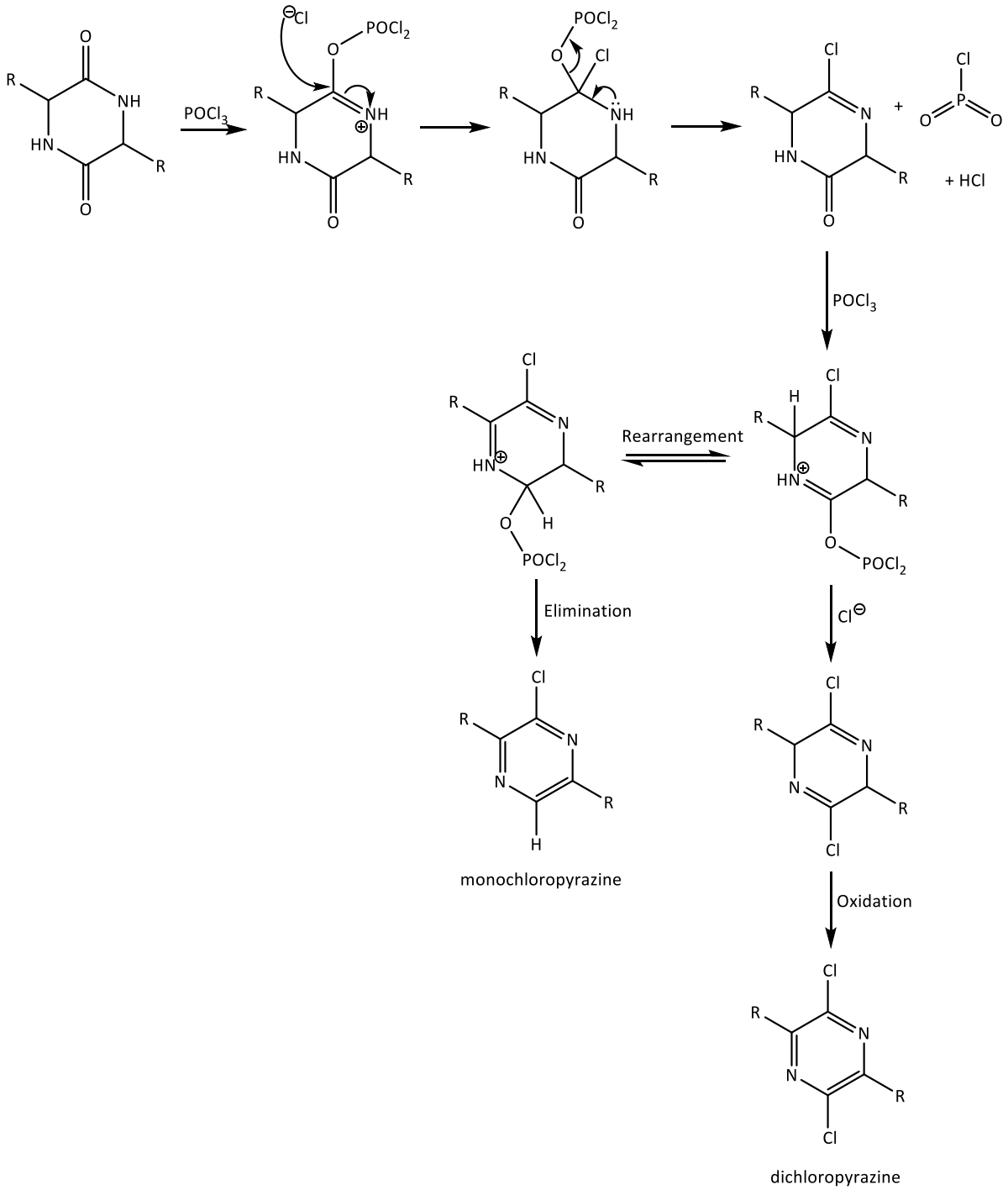

Scheme 44. Proposed reaction mechanism of the chlorination reaction with $POCl_3$ generating either the monochloropyrazine or the dichloropyrazine derivative.

Wang *et al.* have reported the chlorination of a wide range of compounds including hydroxy pyrimidines, pyrazines and amides using one equivalent of $POCl_3$ per reactive OH or amide group, and one equivalent of pyridine at 160°C for 2 h.[263] With this reaction method 72% and

76% yields respectively were obtained of the dichloropyrazines derived from *cyclo*(alanyl-alanine) and *cyclo*(phenylalanyl-phenylalanine), as shown in Figure 69.

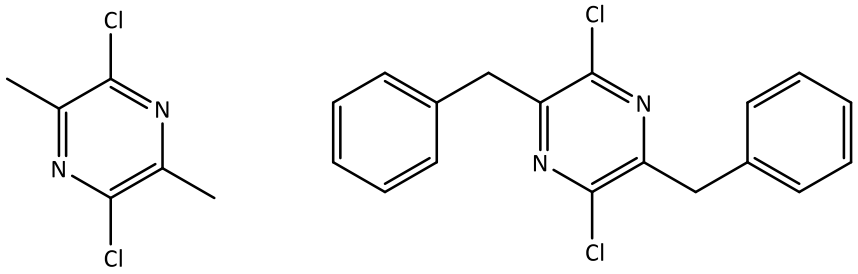

72% 76%

Figure 69. The structures of two dichloropyrazines synthesised in good yields *via* an alternative $POCl_3$ method proposed by Wang *et al.*[263]

As the 3,6-dimethyl and 3,6-dibenzyl substituents of these CDP starting materials have quite different steric demands, it was considered that it might be suitable for the preparation of **127**. Wang's method was therefore employed and **124** was treated with two equivalents of $POCl_3$ and one equivalent of pyridine and heated to 160°C for 2 h (route c in Scheme 43). Under these conditions, the main product was still the monochloro derivative **128** in a 56% yield with **127** being obtained in a 4% yield, however this reaction had a slightly higher overall conversion to either **127** or **128** than the previous two methods, with the starting material being fully consumed in all cases. The results of the various chlorination reactions attempted are collated in Table 12.

Table 12. Comparison of reaction conditions and yields of di and mono chlorination products **127** and **128** from reaction of CDP **124** with $POCl_3$.

Method	Yield of **127** (%)	Yield of **128** (%)	Total conversion (%)
a[261]	17	39	56
b[260]	0	30	30
c[263]	4	56	60

All three chlorination methods were unsuccessful in generating a good yield of the desired dichloropyrazine **127**, therefore an extra synthetic step was employed to make use of the monochloropyrazine side-product **128**. Usui *et al.* demonstrated that it was possible to drive

the formation of the dichloropyrazine derivative through N-oxidation of the monochloropyrazine.[261] The nucleophilicity of the N-oxide promotes the reaction with $POCl_3$ to encourage a second chlorination. As per the methodology of Usui *et al.*, the monochloropyrazine **128** was treated with three equivalents of *m*-CPBA (*meta*-chloroperoxybenzoic acid) in DCM and stirred at 40 °C overnight. This reaction gave a yellow oil which was a 4:1 mixture of mono **129** and di-N-oxides **130** respectively (route a in Scheme 45). The structure of **129** was verified using ^{1}H- ^{15}N HMBC and ^{13}C NMR. The mixture of **129** and **130** was then treated with excess $POCl_3$ and stirred at 100°C overnight[261] to give the desired dichloropyrazine **127** in a 59% yield.

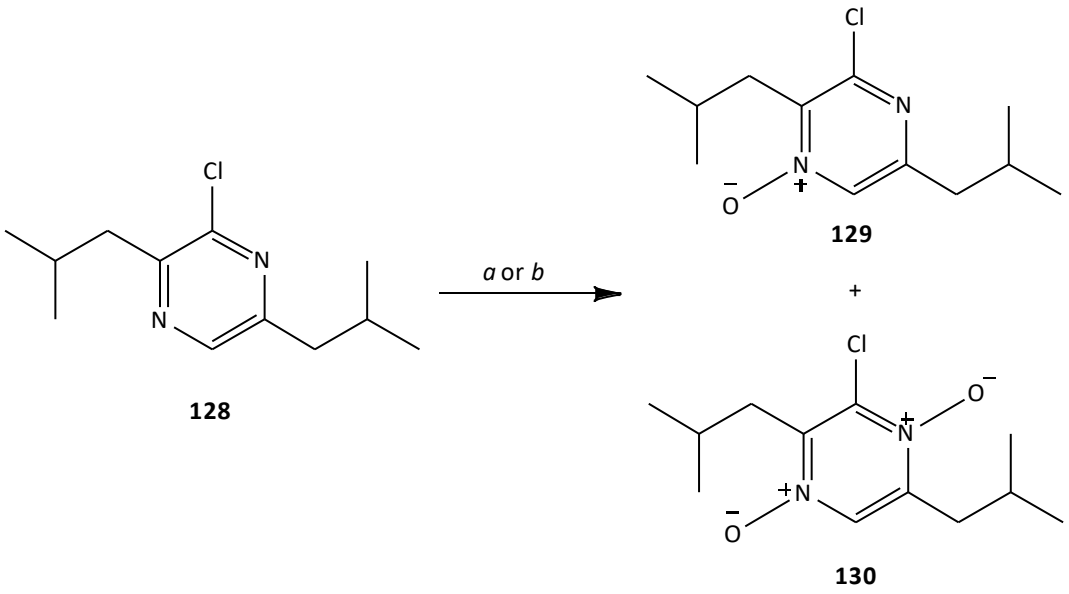

Scheme 45. Synthesis of N-oxide derivatives **129** and **130** of the monochloropyrazine **128**. *Reagents and conditions:* **a.** 3 eq. *m*-CPBA, DCM, 40°C, O/N; **b.** 3 eq. *m*-CPBA, DCM, 40°C , 3 h, 98% of **129** only.

The presence of the di-N-oxide derivative **130** in the mixture taken forward for the next chlorination step lowers the yield of the desired dichloropyrazine **127** by generating a dichloro mono-N-oxide derivative. With this in mind, the oxidation of **128** was repeated using Usui's conditions (route b, Scheme 45), however the reaction was stopped as soon as complete consumption of the starting material was observed on TLC (3 h). This gave pure mono-N-oxide **129** in a 98% yield, which was reacted with excess $POCl_3$ at 100°C[261] (shown in Scheme 46) to give an 84% yield of the desired dichloropyrazine **127**, thus providing a practical synthetic route to **127** from **124** in a good overall yield with minimal side-product formation.

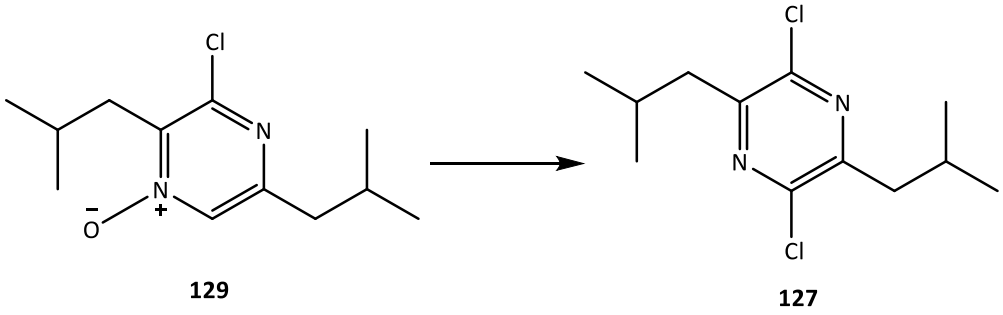

129 **127**

Scheme 46. Synthesis of dichloropyrazine **127** from pure mono-N-oxide derivative **129**. *Reagents and conditions:* excess $POCl_3$, 100°C, O/N, 84%.

In order to transform the dichloropyrazine **127** into the di-N-oxide derivative **131** (shown in Scheme 48), the synthetic route used by Usui *et al.* was applied once again. Usui reported that it was necessary to use vigorous oxidation to convert the pyrazine to the di-N-oxide and two rounds of the oxidation reaction were necessary to achieve a 52% overall yield with respect to recovered starting material (Scheme 47).[261]

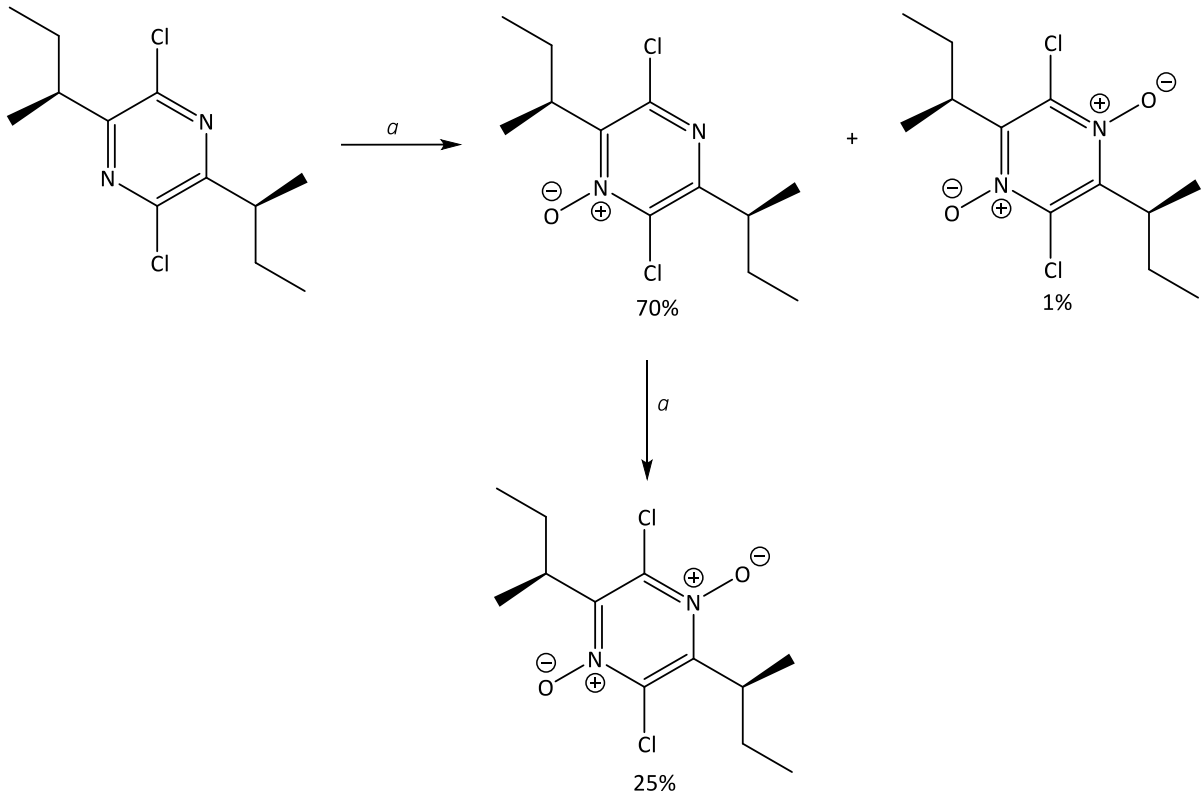

Scheme 47. The synthetic method reported by Usui *et al.* to generate a di-N-oxide derivative over two steps, resulting in a 52% overall yield with respect to recovered starting material. *Reagents and conditions:* **a.** TFA, 50% H_2O_2, 50°C, 3 h.

The conditions of Usui *et al.* were nonetheless applied and as such **127** was dissolved in TFA and treated dropwise with 50% H_2O_2 (see Scheme 48). The reaction was stirred at 50°C for 3 h before the peroxides were neutralised with ice-cold sat. $Na_2S_2O_5$. In our hands this reaction gave a 67% isolated yield of the desired di-N-oxide product **131** along with a 20% yield of the mono-N-oxide **132,** which is vastly different to the outcome seen by Usui *et al.* It was therefore unnecessary to carry out a further oxidation to recycle the mono-N-oxide **132**, in an analogous fashion to the approach of Usui *et al*. Once again, the significant difference in behaviour compared to the corresponding isoleucine derivative probably reflects a change in steric bulk of the side chain; the α-methyl group of the Ile-derived side chain may hinder the approach of the electrophilic oxidant leading to a much less effective di-oxidation. Previous reports by Ohta also support this proposal; oxidation of **127** with other less practical reagents, *i.e* permaleic acid (generated *in situ* using 90% H_2O_2)[253] or potassium persulphate ($K_2S_2O_8$) in concentrated sulphuric acid,[254] gave similar proportions of **131** and **132**.

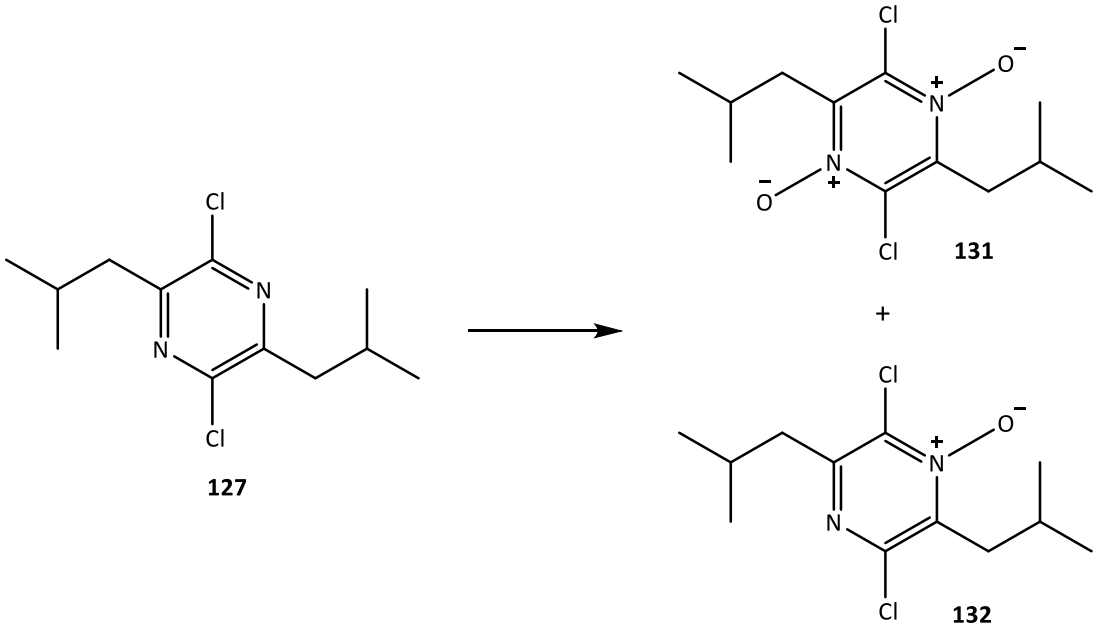

Scheme 48. Synthesis of di-N-oxide **131** from dichloropyrazine **127**. *Reagents and conditions:* TFA, 50% H_2O_2, 50°C, 3 h, 67% (**131**), 20% (**132**).

Intermediate **131** could now be converted to pulcherriminic acid **14** through displacement of the chloro groups with an alkoxy nucleophile *via* nucleophilic aromatic substitution,[253] followed by cleavage of the alkyl fragment in the resulting product to yield the final 2,5-

dihydroxy structure of **14**. Usui *et al.* carried out nucleophilic displacement of the dichloro groups of the di-N-oxide derivative (shown in Scheme 47) using TMS-ethanol with NaO^{t}Bu as the base to form the oxyanion,[261] while Göktürk *et al.* used sodium benzyloxide, generated *in situ* from benzyl alcohol and sodium hydride. [260] Both methods were attempted on the di-N-oxide **131**, and it was anticipated that the presence of the positive N atom adjacent to the chloro carbon would facilitate nucleophilic attack and substitution. However, the reaction of **131** with TMS-ethanol in the presence of the base KO^{t}Bu did not proceed as expected giving a mixture of products. ^{1}H NMR and mass spectrometry analysis were not consistent with the formation of a TMS-ethyl-protected structure, although all of the starting material had been consumed (assessed by TLC). On the other hand, the reaction with benzyl alcohol in the presence of KO^{t}Bu proceeded well on TLC giving conversion to a single new spot. The crude product was purified by column chromatography to give compound **133** in a 46% yield (route a in Scheme 49).

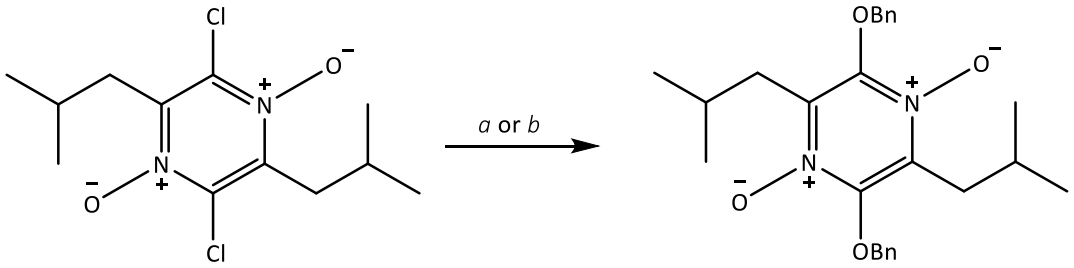

131 **133**

Scheme 49. Synthesis of a benzyl-protected compound **133** *via* nucleophilic displacement of the chloro groups in **131.** *Reagents and conditions:* **a.** benzyl alcohol, KO^{t}Bu, anhydrous THF, RT, O/N, 46%; **b.** benzyl alcohol, NaO^{t}Bu, anhydrous THF, RT, O/N, 44%.

HPLC analysis of **133** showed a single peak, however upon ^{1}H NMR analysis it was evident that another product was present. Göktürk *et al.* described the formation of a new product upon attempts to recrystallise their benzyl-protected compound, or when it was left standing at room temperature for several days. The new compound was identified as an N-benzyloxypyrazinone, where the benzyl group had migrated onto the N-oxide group.[260] Applying this knowledge allowed the ^{1}H NMR spectrum obtained to be rationalised; the desired symmetrical product **133** gave one set of signals for the CH_3, CH_2, CH and OCH_2 groups, while for the unsymmetrical rearranged product **134** all of the ^{1}H signals are duplicated. The

^{1}H NMR spectrum obtained is shown in Figure 70 and the structure of **134** is shown in Scheme 49.

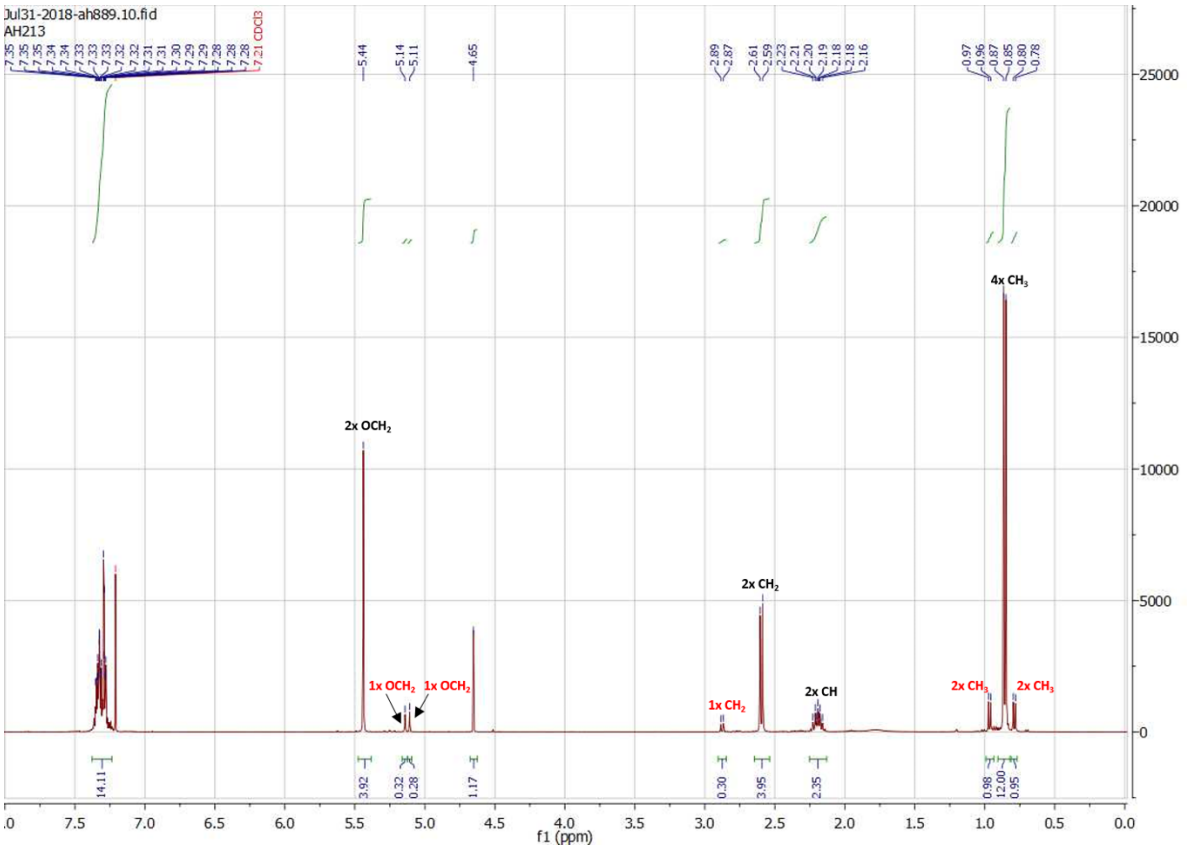

Figure 70. ^{1}H NMR spectrum of isolated symmetrical benzyl-protected pulcherriminic acid **133** showing the presence of unsymmetrical rearranged product **134** in a 6:1 ratio. Key signals are labelled in black for **133** and red for **134**. The signal at 4.65 ppm corresponds to the CH_2 signal for trace benzyl alcohol.

In our hands, the rearrangement of **133** appeared to occur very quickly rather than after a few days of standing. ^{1}H NMR analysis was carried out on the crude reaction mixture immediately after work-up and the presence of more than one compound was already visible, in a 6:1 ratio of **133** to **134** respectively (Figure 70). The mechanism of rearrangement of **133** to the new unsymmetrical compound **134** is presented in Scheme 50. The reaction was repeated using NaO^{t}Bu as the base, in line with the method of Göktürk *et al.*, but under these conditions only the rearrangement product **134** was seen in the crude ^{1}H NMR. Infrared analysis of the isolated product was also carried out and a strong absorption at 1644 cm^{-1} was observed, corresponding to an amide C=O stretch, again consistent with the structure of **134**. The chemical shifts for the pure rearrangement product **134** obtained in the reaction using

NaO^{t}Bu were slightly different to those seen in the ^{1}H NMR for the KO^{t}Bu reaction. This is presumably due to intermolecular interactions between the two distinct components in the mixture of **133** and **134** which results in a displacement of chemical shifts compared to **134** alone.

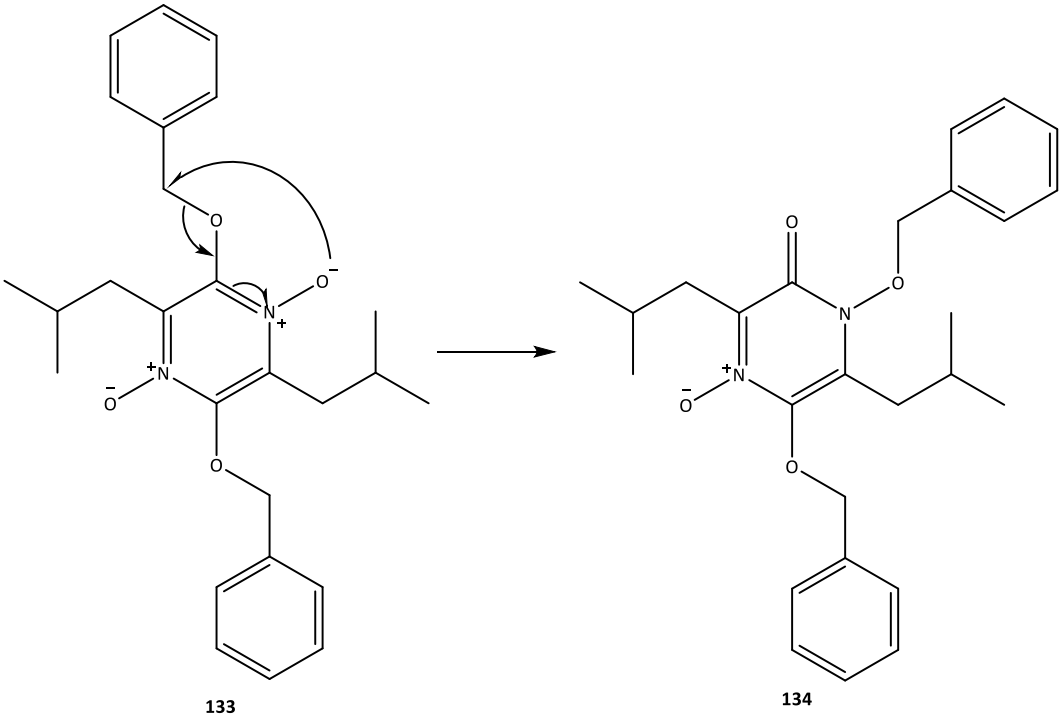

Scheme 50. Mechanism for the migration rearrangement of the O-benzyl group in **133** to a N-benzyloxy isomer **134**.

Cleavage of the benzyl groups was required in order to generate the desired pulcherriminic acid **14**. Göktürk *et al.* demonstrated that treatment of either the O-benzyl compound or the N-benzyloxy rearrangement compound with TFA and anisole yielded the desired product. The mixture of **133** and **134** was therefore treated with 1:1 anisole:TFA (1:1) and stirred at RT under an inert atmosphere for 2.5 h (Scheme 51). This gave pure pulcherriminic acid **14** as a pale yellow solid, which corresponded with the description of **14** isolated by Macdonald and Kupfer *et al*.[244,248] Chemical analysis by mass spectrometry, ^{1}H and ^{13}C NMR, and melting point confirmed the structure of **14**.

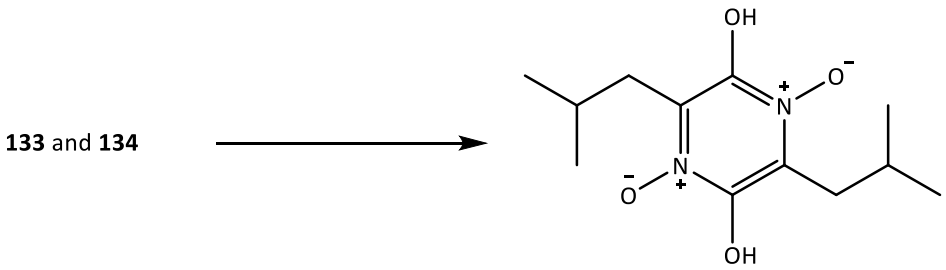

14

Scheme 51. Conversion of a mixture of N-oxides **133** and **134** to pulcherriminic acid **14.** *Reagents and conditions:* TFA, anisole, RT, 2.5 h, 75%.

3. Activity of pulcherriminic acid

With the sought after pulcherriminic acid **14** in hand, its solubility and stability were tested. **14** was found to be insoluble in a range of organic solvents (MeOH, chloroform, DCM, MeCN, and THF) and was sparingly soluble in DMSO (soluble to a concentration of 2 mM). This lack of solubility is consistent with the report by Kluyver *et al.* where 30 different solvents were tested to dissolve the pulcherrimin pigment. However, **14** was completely soluble and stable in pure TFA and formic acid. A solution of **14** in TFA (1 mg/mL) was left in the dark for 24 h, after which time HPLC analysis showed that there was no apparent change or degradation. Conversely, when **14** was added to 1M NaOH, the compound converted immediately to a new peak on HPLC. **14** was also found to be sensitive to visible light. When a solution of **14** in TFA (1 mg/mL) was left under ambient laboratory lighting, HPLC analysis showed that complete degradation had occurred after 5 h.

In order to compare the photoprotective capacity of **14** to the other iron chelators used in this project, a solution of **14** in DMSO (20 µM) was incubated in FEK4 cells overnight prior to UVA irradiation at doses of 250 kJ/m^2 and 500 kJ/m^2. MTT assay analysis was carried out 24 h post-UVA irradiation, and the results from these assays are presented in Figure 71.

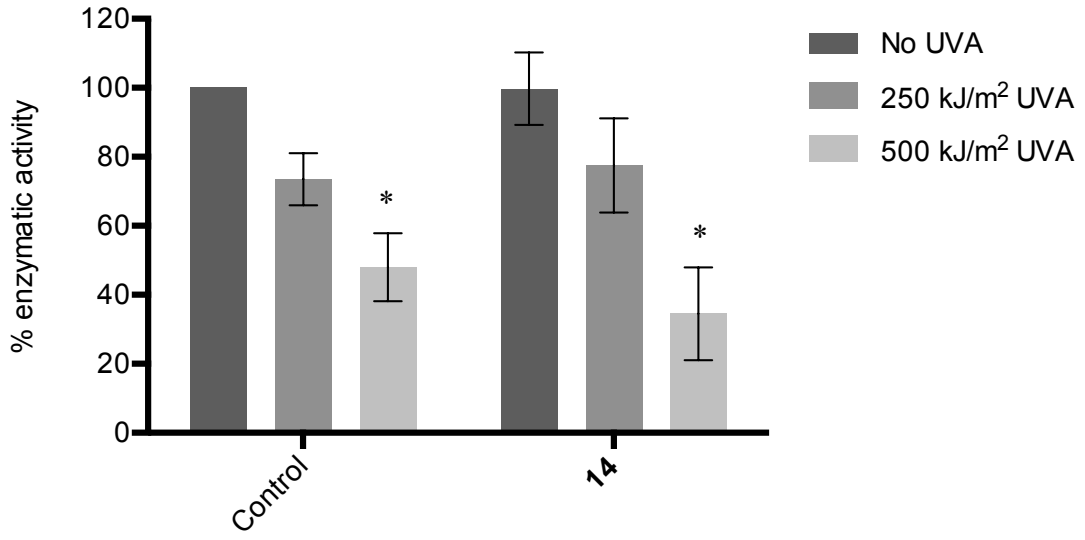

Figure 71. MTT assay analysis of the photoprotective capacity of **14** (20 µM) in FEK4 cells after 250 or 500 kJ/m^2 UVA irradiation. Data is represented as percentage enzymatic activity of the untreated unirradiated control, which was set to 100% enzymatic activity. (n=4)

* p <0.05, significant decrease compared to the respective 250 kJ/m^2 UVA irradiated cells.

MTT analysis showed that pulcherriminic acid **14** was not cytotoxic to cells at a concentration of 20 µM, however it did not provide any photoprotection in comparison to the untreated irradiated cells at a dose of 250 kJ/m^2 UVA. Moreover **14** seemed to be cytotoxic to cells in comparison to the untreated cells irradiated at a dose of 500 kJ/m^2 UVA. This outcome may have been due to the observed instability of **14** under visible light.

Furukawa *et al.* examined the hydroxyl radical scavenging activity of 20 L-leucine based CDPs by using electron spin resonance (ESR). Although they reported that *cyclo*(L-leucyl-L-leucine) had a lower scavenging effect than the control vitamin E, it was decided to investigate whether pulcherriminic acid **14** derived from this CDP nucleus possessed any antioxidant activity. Manchineella *et al.* reported the synthesis of 5 CDPs from alternative L-amino acids that were tested for their radical scavenging activity in the DPPH assay. Therefore **14** was analysed in the DPPH assay method developed in Chapter 3.2, alongside the positive control, trolox. Figure 72 shows the percentage radical scavenging activity of **14** and trolox over the range of concentrations required to give a linear relationship.

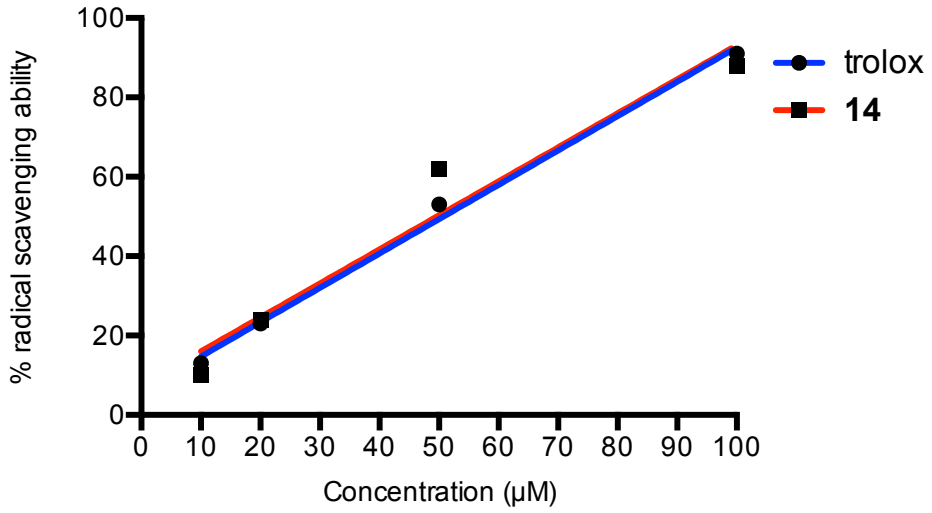

Figure 72. DPPH assay analysis of **14** along with the positive antioxidant control, trolox, showing the percentage free radical scavenging activity against concentration. Each concentration point represents an average of n=3.

The DPPH assay demonstrates for the first time a free radical scavenging activity for pulcherriminic acid **14**. The percentage radical scavenging profiles of **14** and trolox are very similar, and the line equation of **14** is y=0.8571*x + 7.429 which gives an IC_{50} value of 49.7 µM. This IC_{50} value is comparable to the IC_{50} value of **94** (54.6 µM), a lead carbostyril which performed well in the DCFDA assay in reducing the level of UVA-induced intracellular free radicals and was incorporated into CIC **115**, the best photoprotectant in annexinV/PI flow cytometry assays.

4. Attempted caging of pulcherriminic acid

The instability of **14** to ambient light undoubtedly affects its ability to act as an iron-chelating photoprotective agent. We hypothesised that a photo-cleavable group would protect **14** against ambient light for long enough for it to be localised within the cytosol and therefore be in a suitable location to exert its iron-chelating effect upon UVA irradiation. Therefore as a proof of concept for future investigations, caging of the phenolic groups of **14** was attempted with the simple and well-known photo-labile group 2-NPE (discussed in the Introduction 1.4.4) This was attempted by nucleophilic displacement of the chloro groups of

the di-N-oxide intermediate **131** using the alkoxide generated from 1-(2-nitrophenyl)ethan-1-ol. The reaction was carried out using NaO^tBu as the base and using the same reaction conditions as the previous nucleophilic aromatic substitution reactions, as shown in Scheme 52. After overnight reaction, the starting material had been converted to two new products on TLC. Mass spectrometry analysis of the crude reaction mixture after aqueous work-up indicated the presence of both the mono- and di-NPE caged pulcherriminic acid derivatives **135** and **136** which could not however be separated by column chromatography.

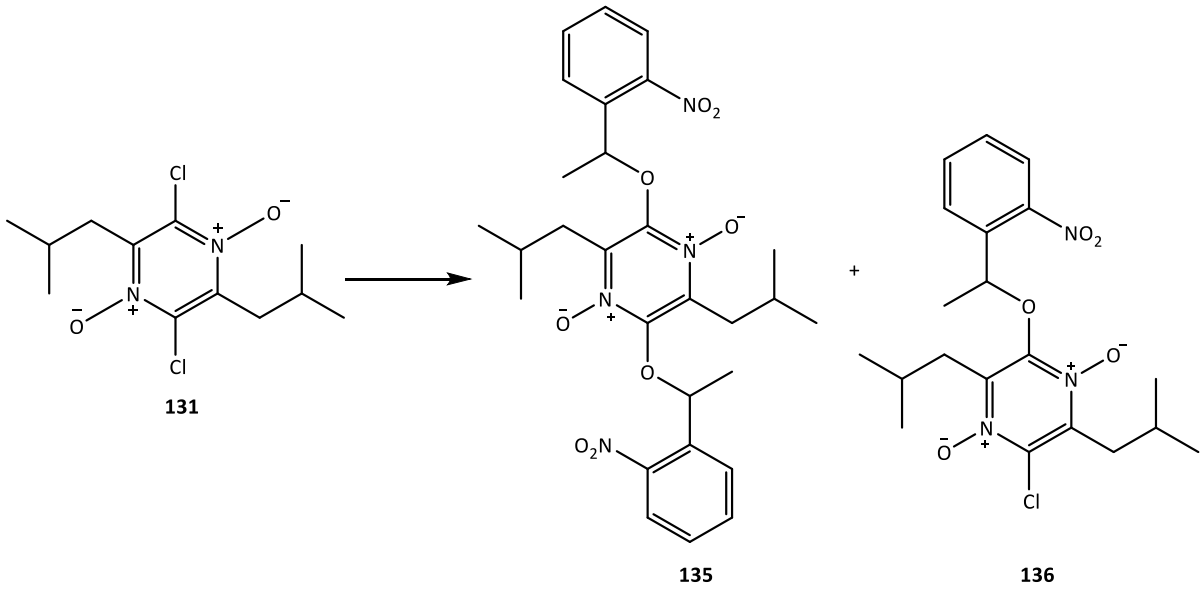

Scheme 52. Synthesis of mono- and di-NPE protected compounds **135** and **136** *via* nucleophilic displacement of the chloro groups in **131.** *Reagents and conditions:* 2-NPE, NaO^tBu, anhydrous THF, RT, O/N.

5. Summary

A 9-step synthesis of pulcherriminic acid **14** has been developed and all intermediates investigated have been fully characterised. The synthetic route was optimised to give the highest yields and to limit the by-products generated at each step. The examination of this pathway enables the scale-up of the synthesis of **14**, a natural product iron chelator that may have potential as a protective agent against UVA-induced iron release and ROS. **14** was found to be quite insoluble in a range of organic solvents and unstable under ambient light and in basic solutions in agreement with previous reports. Further investigation into

derivatives of this natural product may provide an opportunity to create related iron chelators with better bioavailability and physicochemical properties. DPPH assay analysis demonstrated that **14** has a promising free radical scavenging activity which could provide an extra benefit alongside its inherent iron-chelating activity.

CHAPTER 6: FINAL CONCLUSIONS AND FUTURE WORK

This project was directed towards the synthesis and biological evaluation of novel caged iron chelators (CICs) as potential agents for use in skin photoprotection.

Chapter 2 focussed on the development of synthetic routes to hydroxycinnamoyl and aminocinnamoyl derivatives of iron chelators with known clinical potential which have a phenolic iron-binding motif that can be caged. For this purpose, two aroylhydrazone iron chelators PIH **7** and SIH **8** were synthesised as well as the methyl ester derivative of the clinically used iron chelator deferasirox **33**. Hydroxycinnamoyl caging groups were investigated as photo-cleavable groups and two TBS-protected SIH derivatives **38a** and **42a** were synthesised, exploiting a novel approach for the generation of selectively protected hydroxycinnamic acids *via* selective cleavage of a silyl ester group over a silyl ether (using 0.3% TFA in MeCN). Hydroxycinnamoyl caged CIC derivatives of SIH could be successfully prepared using acid chloride coupling chemistry, however the yields were modest due to the steric hindrance introduced by the silyl protecting groups. Neither of the SIH-derived CICs **36** and **44** were more UVA photoprotective than the parent iron chelator SIH **8** towards FEK4 human skin fibroblasts as assessed by the MTT assay. Aminocinnamoyl caging groups were also investigated for the development of CICs. A three-step optimised synthetic route to the known 3,4-dimethoxyaminocinnamic acid **50** was achieved and the three iron chelators **7**, **8** and **33** were esterified with this derivative to produce prototype aminocinnamoyl CICs. The photoprotective ability of the respective CICs **51**, **52** and **55** under UVA irradiation was analysed using the MTT assay, and the SIH-based CIC **51** was significantly photoprotective compared to the untreated irradiated control. A simple synthetic route was also elaborated for the carbostyril photo-products that are generated upon UVA uncaging of aminocinnamoyl CICs, by stirring the respective carboxylic acid in 4% HCl at reflux. This allowed detailed analysis of the photoproducts of CIC cleavage upon UVA irradiation.

In Chapter 3 the route discovered for the generation of the carbostyril photoproducts was exploited. A retrosynthetic approach was taken to identify and synthesise a series of CICs with the potential to release an antioxidant photoproduct by first synthesising a series of

carbostyrils with varying substituents in the aromatic ring. Three novel carbostyrils **93**, **94** and **95** tested positive for free radical scavenging activity in the chemical colorimetric DPPH assay, with IC_{50} values of 114.0, 54.6 and 25.3 μM respectively compared to the IC_{50} value of the positive control trolox (52.3 μM). The antioxidant effects of the two carbostyrils with the best potential, **94** and **95,** were also tested in the cellular DCFDA assay with FEK4 fibroblasts post-UVA irradiation. Carbostyril **94** on its own and in combination with equimolar SIH **8** was the most exciting prospect, markedly reducing the intracellular UVA-induced ROS present. The use of electron spin resonance spectroscopy (ESR) in future investigations of antioxidant compounds such as **94** would give more insight into the type of free radical scavenged, potentially allowing for further structural fine-tuning. This technique is also particularly relevant as it is used to measure the radical skin protection factor (RSF) of sunscreen formulations.[63,64]

The aminocinnamic acids corresponding to carbostyrils **93, 94** and **95** were integrated into a series of SIH- and deferasirox ester-based CICs, **114-119**. MTT assay analysis of these CICs indicated that CIC **115** which releases carbostyril **94** and SIH **8** upon UVA irradiation was the best photoprotectant, significantly improving the cell viability of UVA-irradiated human skin fibroblasts. These results suggest that the design of a novel multi-functional CIC with the best photoprotective properties is a balance between incorporating motifs which provide an antioxidant effect (through alteration of substituents on the photo-cleavable group), whilst sustaining high maximum absorption over the target UVA wavelength window (320-400 nm). These properties alongside clean and efficient photo-cleavage at environmentally relevant doses of UVA are very desirable for a multi-functional CIC. Therefore to develop a more effective aminocinnamoyl CIC, a two-pronged exploration as follows would be valuable. Firstly, an investigation into the kinetics of the photo-release mechanism would clarify the role of steric hindrance in the nucleophilic attack of the ester carbonyl and subsequent cyclization. Synthesising derivatives of iron chelators **7**, **8** and **33** containing additional groups *ortho* to the ester bond present upon caging would be beneficial in this respect. Secondly, it would be useful to expand the series of aminocinnamic acids to include derivatives containing electron-donating groups in alternative positions around the aromatic ring, not only to fine-tune the antioxidant potential of the corresponding carbostyrils, but also the UVR absorption maxima of resulting CICs. Consistent with the results discussed in Chapter 3.2, the presence

of electron-donating or +M groups should cause a red-shift in the absorption maximum. Similarly Li *et al.* reported that N-alkylation of aminocinnamates causes a red-shift in the spectrum, and this would be an interesting principle to investigate.[172] Deferasirox ester also has the potential to be masked by two photo-cleavable groups through its two phenolic hydroxyls, providing a synthetic opportunity to create a multi-functional CIC which could release two molecules of antioxidant per iron chelator.

Following on from the work of the previous chapter, Chapter 4 investigated the detrimental effects of applying a sub-optimal thickness of sunscreen formulation (0.5 mg/cm^2), and how this might be compensated using CICs. An assay was developed which involved the addition of a reservoir of filter, at the desired concentration to equate to specified thicknesses of sunscreen formulation, sitting above the dish containing a monolayer of cells. Using this format during UVA irradiation followed by the MTT assay, the photoprotective capacity of a range of sunscreen filters could be analysed. Both of the two chosen UVA filters, avobenzone and Mexoryl SX®, provided full protection at the recommended thickness of 2 mg/cm^2, but the protection provided by them significantly reduced at a thickness of 0.5 mg/cm^2. Similarly, the UVA protection afforded by two broad spectrum inorganic blockers, ZnO and TiO_2, was significantly reduced at 0.5 mg/cm^2 formulation thickness. The capacity of a sub-optimal thickness of an individual filter or commercial sunscreen formulation to prevent against UVA-induced intracellular labile iron release was analysed using the calcein assay. The key outcome of this chapter was the finding that two commercial sunscreen formulations as well as 3% (w/v) avobenzone + 5% (w/v) octocrylene at a concentration equating to a sunscreen thickness of 0.5 mg/cm^2 did not prevent the release of intracellular labile iron upon UVA irradiation. Building on this, the addition of CIC **51** (20 μM) prior to UVA irradiation significantly reduced the concentration of chelatable labile iron produced with protection by 3% (w/v) avobenzone + 5% (w/v) octocrylene or a typical commercial formulation. Flow cytometry analysis using annexin V/PI staining was carried out on cells protected with 0.5 mg/cm^2 sunscreen ± CIC **51** or **115.** The results of these assays confirmed the conclusions of the calcein assays showing that the presence of a CIC leads to a decrease in UVA-induced cell death, in comparison to the cells where the protection is not supplemented with a CIC. Analysis of the percentages of apoptotic and necrotic cell death under different conditions,

rather than live cells, in the future could give more insight into the mode of cell death induced by UVA radiation and the release of labile iron.

To build on the work carried out in Chapter 4, it would be useful to modify the experimental design to use poly (methyl methacrylate) (PMMA) plates rather than Petri dishes as the sunscreen 'reservoir'. Although a simple and easily reproducible method, the limitation of using Petri dishes for the experiments in Chapter 4 is that their smooth and even surface is not typical of the peak and troughs found naturally on the surface of the human stratum corneum. PMMA plates are sand-blasted to give a rough texture which mimics the stratum corneum and have been indicated in the European Cosmetic and Perfumery Association (COLIPA) guidelines as the substrate of choice for the UVA-PF sunscreen testing method.[264] However work by Ferrero *et al.* and Sohn *et al.* has demonstrated the difficulties associated with experiments using PMMA plates in terms of reproducibility of results due to variation in plate roughness.[265,266]

It would also be very interesting to repeat the photoprotection experiments using SSR rather than UVA radiation, this would give an idea how the CICs would perform in a 'real world' format and would be essential before CICs could be implemented into a sunscreen formulation. Using SSR as a solar mimic of exposing the CICs to direct sunlight would enable the full benefits of CICs to be quantified. For example the absorption spectra for all CICs synthesised in Chapters 2 and 3 show that the CICs absorb in the UVB wavelength region as well as the UVA region. Therefore, although not their primary purpose, CICs may also exhibit a UVR filtering effect which would provide protection against the effects of UVB radiation as well. In order to asess the UVR filtering potential of CICs, the same experimental procedure used for testing the sunscreen formulations could be used. A reservoir of a CIC in solution could be placed over untreated cells before irradiation, this method would separate the iron-chelating mechanism from the UVR absorption mechanism. It is also important to point out that the uncaging profiles of all synthesised CICs may be different under SSR or real sunlight conditions. From analysing the absorption spectra of the CICs one could hypothesise that they would uncage faster when a broader spectrum of radiation is used (SSR) as they also absorb UVB radiation, this would be a key experiment to advance the CICs into potential sunscreen ingredients. Work by Lawrence *et al.* demonstrated the photodamaging effects of short

wavelength visible radiation (400 -420 nm) on keratinocytes,[201] a selection of synthesised CICs also absorbed over these visible wavelengths (CICs **51**, **51**, **55**, **114** and **117**). So in a similar sense to CICs exhibiting a beneficial UVB radiation absorbing profile, these CICs may also provide 'real world' protection against the potentially damaging visible radiation that is part of solar radiation.

The ability of a multi-functional CIC to provide skin photoprotection through chelation of UVA-induced labile iron and quenching of harmful free radical species is the primary purpose of CICs, and as such should only be required as a second line of defence behind the UVR absorbing/blocking profile of sunscreen filters and not as a sole photoprotectant. The potential real-life impact of this research is that the presence of a CIC in a sunscreen formulation may help to bridge the gap in sun protection that frequently exists due to ineffective application of current sunscreens, and ultimately help prevent skin cancer and other consequences of exposure to harmful levels of UVA. In order to investigate the full potential of CICs, it would be necessary to conduct research into their penetration through the *stratum corneum* to reach the epidermis and the dermis. Current methodologies for assessing the transdermal delivery of drugs include *stratum corneum* tape-stripping where a topical formulation is applied to the skin and after an established amount of time the *stratum corneum* is collected using adhesive tapes. The amount of drug in each tape is then quantified to give the clearance of the drug.[267] This method is often used alongside *in vitro* skin permeation tests using porcine skin where the topical drug formulation is applied to the *stratum corneum* and the dermal side is in contact with a physiological buffer. Time-course HPLC analysis of the buffer can then be used to quantify the transdermal clearance of the drug.[267] Certain coumarin photoproducts have the additional benefit of being fluorescent, indeed the fluorescence of 3,5-dibromo-4-hydroxy coumarin has been exploited as an 'optical syringe' by Gagey *et al.*[171] This property of coumarins and carbostyrils has the potential to be used to identify the transdermal location of a CIC upon UVA irradiation.

Chapter 5 examined the synthetic pathway towards the natural iron chelator pulcherriminic acid **14**, which has been previously studied for its ability to form an iron-containing pigment, pulcherrimin.[133,244,245] A 9-step synthesis of pulcherriminic acid **14** was developed, with all intermediates fully characterised. A study of the desired reaction at each stage led to

optimised conditions to give the highest yields and to limit the by-products generated. The developed synthetic pathway allows the opportunity to scale-up the synthesis starting with easily accessible amino acid derivatives. The final step of the synthesis gave **14** in 75% yield from a benzyl ether-protected derivative. In order to further probe the disparity in yields seen in the key dichlorination step between this work and other studies with related CDPs[260,261,263] (Schemes 41 and 42, and Figure 69) a systematic approach would need to be taken. Synthesising a series of CDPs with varying side chains (either symmetrical or using two different amino acids) should be straightforward using the synthetic pathway developed here. This series could then be subjected to the $POCl_3$ chlorination reaction to investigate how the nature and size of the R-groups may affect the relative yields of the mono- and dichloropyrazine products. A further advantage of generating a series of CDPs with varying side chains is exemplified in two studies by Manchineella *et al.* and Furukawa *et al*.[252,268] . In these studies amino acids whose side chains have potential ROS scavenging activity, for example L-serine, L-lysine, L-tyrosine and L-DOPA, were incorporated into CDPs. The free radical scavenging capacity of these CDPs was assessed in the DPPH assay, with some derivatives giving very promising results. As pulcherriminic acid **14** was shown for the first time in this project to have some inherent antioxidant activity (DPPH IC_{50} = 49.7 μM), it would be interesting to generate derivatives of pulcherriminic acid using different amino acids which would allow it to act not only as a potent iron chelator but also as a highly effective antioxidant. Variation of the amino acid side chains may also improve the problematic bioavailability and physicochemical properties observed for **14** itself. The preliminary investigation into the conversion of the dichloro di-N-oxide intermediate **131** to a derivative of **14** that is caged with the photo-cleavable group 2-NPE was promising, and continuation of this research to drive the reaction to completion would provide a basis for subsequent UVA-activated uncaging experiments and further investigation into applying a range of suitable photo-cleavable groups.[162] This could then lead to the synthesis of a new generation of natural product-inspired light-activated CICs as potential UVA photoprotectants.

CHAPTER 7: EXPERIMENTAL

1.Chemistry

1.1 General

Solvents, chemical reagents and starting materials were purchased from Sigma Aldrich, Alfa Aesar, VWR and Fisher Scientific. Analytical thin layer chromatography was performed on Merck silica gel 60 aluminium plates F254. Column chromatography was carried out using Sigma Aldrich Silica gel 60Å (particle size 40-63 µm).

^{1}H, ^{13}C and ^{15}N NMR were obtained using Bruker Avance III 400 MHz and 500 MHz instruments, ^{13}C NMR data was either at 100 MHz or 125 MHz, and ^{15}N NMR data was at 50 MHz. Chemical shift values stated are in parts per million (ppm) and coupling constant values (J) are given in Hertz (Hz). Routine mass spectrometry was carried out using a Bruker Daltonics micrOTOF instrument with electrospray ionisation (ESI). Atmospheric pressure chemical ionisation (APCI) quadrupole time-of-flight (QTOF) analysis was conducted using a Bruker Daltonics MaXis HD mass spectrometer operated in ESI mode. The QTOF was equipped with an APCI source and direct analysis probe. Melting points were determined using an Electrothermal IA9000 series digital melting point apparatus. Infrared spectra were recorded on a Perkin-Elmer 782 infrared spectrometer using a KBr disk, and values are given in cm^{-1} as either strong (s), medium (m) or weak (w) intensity. UV absorbance spectra were obtained on either a Perkin-Elmer Lambda 35 UV/Vis spectrometer or a BMG LABTECH CLARIOstar microplate reader; λ_{max} values are reported in nm, extinction coefficients are in L mol^{-1} cm^{-1}.

Analytical HPLC was performed on a Dionex Ultimate 3000 system using a Phenomenex Gemini 5µm C-18 110A column with a flow rate of 1 mL/min at 35°C, and UV detection of 214, 220, 254 and 280 nm. For solvent system A; the mobile phase A was 0.1% CF_3CO_2H in water and mobile phase B was 0.1% CF_3CO_2H in acetonitrile. For solvent system B; the mobile phase A was 0.1% HCO_2H in water, mobile phase B was 0.1% HCO_2H in acetonitrile. Gradient: t = 0, %B = 5; t = 10, %B = 95; t = 15, %B = 95; t = 15.1, %B = 5.

1.2 Compound synthesis

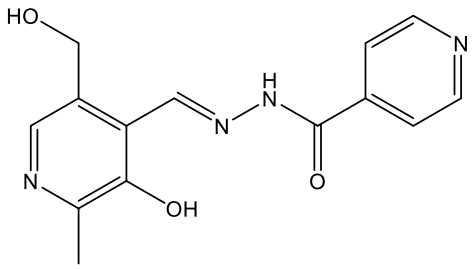

(*E*)-N'-((3-hydroxy-5-(hydroxymethyl)-2-methylpyridin-4-yl)methylene)isonicotinohydrazide (PIH, 7)[176]

A solution of INH (1.37 g, 9.99 mmol) in EtOH (100 mL) was treated with pyridoxal. HCl (2.03 g, 9.99 mmol) followed by a solution of NaOAc (820 mg, 9.99 mmol) in H_2O (100 mL). The reaction was stirred at reflux for 1.5 h, concentrated by 50% and then cooled overnight. The resulting orange precipitate was collected under suction filtration. Drying under vacuum at 40°C gave **7** as a bright orange powder (2.43 g, 85%). R_f = 0.62 (30% acetone: DCM); R_t= 5.7 min (solvent system A); mp = 263-265°C (lit.[269] 261-262°C); ^{1}H NMR (DMSO-d_6, 400 MHz) δ 2.43 (3H, s, CH_3), 4.28 (1H, s, OH), 4.74 (2H, d, J = 6.4, C$\underline{H_2}$OH), 6.91 – 6.95 (2H, m, Ar), 7.32 (1H, td, J = 7.7, 1.8, Ar), 7.61 (1H, dd, J = 7.6, 1.6, Ar), 7.85 (2H, dd, J = 4.4, 1.6, Pyr), 8.68 (1H, s, HC=N), 8.80 (2H, dd, J = 4.6, 1.8, Pyr), 11.08 (1H, s, OH), 12.29 (1H, s, NH); ^{13}C NMR (DMSO-d_6, 100 MHz) δ 18.53 (CH_3), 58.86 (CH_2), 120.60 (Pyr), 121.52 (Pyr), 132.82 (Pyr), 137.97 (Pyr), 139.13 (Pyr), 147.33 (Pyr), 147.51 (C=N), 150.47 (Pyr), 150.90 (Pyr), 161.59 (C=O).

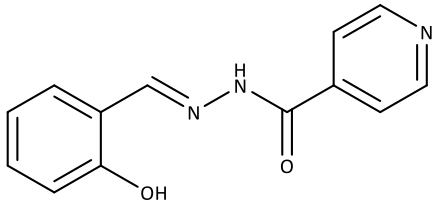

(*E*)-N-(2-Hydroxybenzylidene)isonicotinohydrazide (SIH, 8)[176]

A solution of salicylaldehyde (1.00 g, 8.19 mmol) and INH (1.12 g, 8.19 mmol) in EtOH (25 mL) was heated at reflux for 3 h, when a solid white precipitate had formed. The reaction mixture

was cooled and the precipitate was collected under suction filtration. Drying under vacuum at 40°C gave **8** as a white powder (1.88 g, 95%). R_f = 0.48 (10% MeOH in DCM); R_t= 5.7 min (solvent system A); mp = 249- 252°C (lit.[269] 253-255°C); ^{1}H NMR (DMSO-d_6, 400 MHz) δ 2.50 (3H, s, CH_3), 4.69 (2H, s, CH_2), 5.50 (1H, br s, OH), 7.95 (2H, d, J = 6.4, Pyr), 8.05 (1H, s, Pyr), 8.89 (2H, d, J = 5.2, Pyr), 9.06 (1H, s, HC=N), 12.24 (1H, s, OH), 12.92 (1H, s, NH); ^{13}C NMR (DMSO-d_6, 100 MHz) δ 116.41 (Ar), 118.69 (Ar), 119.42 (Ar), 121.49 (Pyr), 129.12 (Ar), 131.73 (Ar), 139.96 (Ar), 148.83 (C=N), 150.38 (Pyr), 157.43 (Ar), 161.30 (C=O).

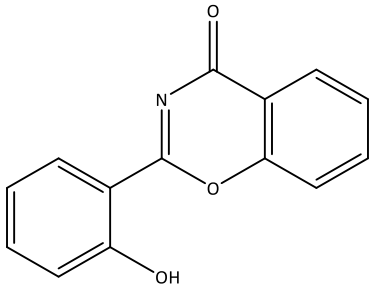

2-(2-Hydroxyphenyl)-4H-benzo[e][1,3]oxazin-4-one (32)[98]

A mixture of salicylic acid (2.10 g, 15.2 mmol), salicylamide (1.90 g, 13.9 mmol) and pyridine (150 µL) was heated to reflux in *p*-xylene (6 mL). The solution was then treated with thionyl chloride (2.1 mL, 29 mmol), added dropwise over 1 h. The evolution of HCl and SO_2 gas was absorbed using a H_2O scrubber. The reaction was allowed to reflux for a further 2.5 h and then the heat was removed. The solvent was evaporated to give a yellow solid. This was resuspended in EtOH (20 mL) and acetic acid (200 µL) and heated gently, then allowed to cool to RT and placed at -20 °C overnight. The precipitate which formed was filtered off under suction then dried under vacuum at 50 °C to give **32** as a pale yellow solid (2.16 g, 65%). R_f = 0.45 (20% EtOAc: petroleum ether); R_t = 9.1 min (solvent system A); mp = 204-206 °C (lit.[270] 200- 201 °C); ^{1}H NMR (DMSO-d_6, 400 MHz) δ 7.12-7.17 (2H, m, Ar), 7.64-7.71 (2H, m, Ar), 7.84 (1H, dd, J = 8.4, 0.4, Ar), 8.00 (1H, td, J = 8.0, 1.6, Ar), 8.12 (1H,dd, J = 7.6, 1.6, Ar), 8.26 (1H, dd, J = 7.6, 1.6 Ar), 12.97 (1H, s, OH); ^{13}C NMR (DMSO-d_6, 100 MHz) δ 111.51 (Ar), 117.49 (Ar), 117.80 (Ar), 117.99 (Ar), 119.59 (Ar), 126.78 (Ar), 127.21 (Ar), 129.01 (Ar), 136.02 (Ar), 136.72 (Ar), 153.91 (Ar), 161.85 (C=N), 163.44 (Ar), 164.83 (C=O); [Found (ESI+) 240.0657 $[M+H]^+$, $C_{14}H_9NO_3$ requires 240.0661].

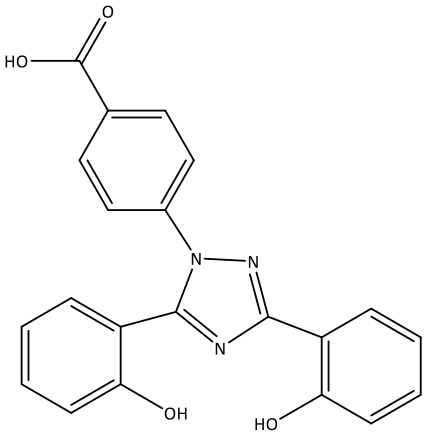

4-(3,5-Bis(2-hydroxyphenyl)-1H-1,2,4-triazol-1-yl)benzoic acid (deferasirox, 6)[98]

4-Hydrazinobenzoic acid (100 mg, 0.657 mmol) and NEt_3 (92 µL, 0.66 mmol) were dissolved in boiling EtOH (10 mL) under stirring. This solution was treated with **32** (142 mg, 0.594 mmol) and the reaction was stirred at reflux for 2.5 h then allowed to cool to RT. H_2O (75 mL) was added until the first sign of precipitation then the mixture was concentrated by 50% and 6M HCl was added (10 mL). The resulting precipitate was collected by suction filtration and dried under high vacuum to give **6** as a beige solid (186 mg, 85%). R_f = 0.4 (5% MeOH: DCM); R_t = 9.4 min (solvent system A); mp = 260-263 °C (lit[270] 261-163 °C); ^{1}H NMR (DMSO-d_6, 400 MHz) δ 6.93 (1H, d, J = 8.4, Ar), 7.05 (3H, m, Ar), 7.44 (2H, m, Ar), 7.61 (3H, m, Ar), 8.05 (2H, m, Ar), 8.11 (1H, dd, J = 8.0, 1.6, Ar), 10.08 (1H, s, OH), 10.84 (1H, s, OH), 13.20 (1H, s, CO_2H); ^{13}C NMR (DMSO-d_6, 100 MHz) δ 113.65 (Ar, C_q), 114.41 (Ar, C_q), 116.14 (Ar), 117.05 (Ar), 119.44 (Ar), 119.67 (Ar), 123.33 (Ar), 126.77 (Ar), 130.27 (Ar), 130.55 (Ar, C_q), 131.04 (Ar), 131.44 (Ar), 132.53 (Ar, C_q), 141.17 (Ar), 152.04 (Ar, C_q), 155.18 (Ar, C_q), 156.33 (Tri), 159.88 (Tri), 166.39 (C=O).

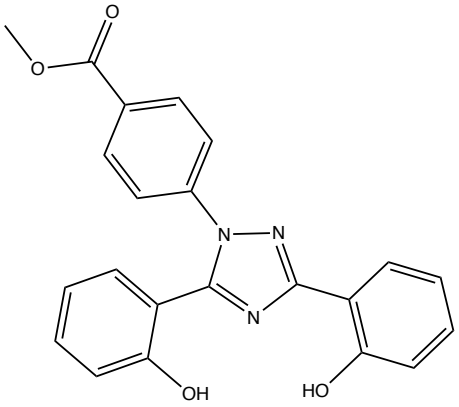

Methyl 4-(3,5-bis(2-hydroxyphenyl)-1*H*-1,2,4-triazol-1-yl)benzoate (deferasirox ester, 33)

A solution of **6** (190 mg, 0.51 mmol) in MeOH (10 mL) was treated slowly with H_2SO_4 (50 µL) then heated to reflux overnight with stirring. The solvent was evaporated and the residue was dried to give a pale brown solid (170 mg, 86%). R_f = 0.9 (4% acetone:DCM); R_t = 10.4 min (solvent system A); mp = 170-173 °C (lit[271] 172-175 °C); ^{1}H NMR (DMSO-d_6, 400 MHz) δ 3.92 (3H, s, CH_3), 6.92 (1H, dd, J = 8.0, 0.8, Ar), 7.02- 7.10 (3H, m, Ar), 7.41-7.48 (2H, m, Ar), 7.61 (1H, dd, J = 7.6, 1.6, Ar), 7.64 (2H, d, J = 8.8, Ar), 8.07 (2H, d, J = 8.8, Ar), 8.10 (1H, dd, J = 8.0, 1.6, Ar); ^{13}C NMR (DMSO-d_6, 100 MHz) δ 48.57 (CH_3), 113.45 (Ar), 114.02 (Ar), 116.11 (Ar), 117.03 (Ar), 119.45 (Ar), 119.69 (Ar), 123.45 (Ar), 126.88 (Ar), 129.31 (Ar), 130.19 (Ar), 131.06 (Ar), 131.57 (Ar), 132.67 (Ar), 141.38 (Ar), 151.96 (Ar), 155.11 (Ar), 156.27 (Tri), 159.58 (Tri), 165.33 (C=O).

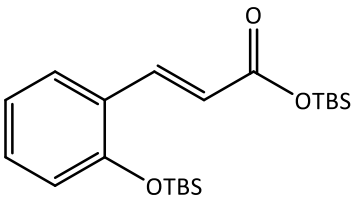

***tert*-Butyldimethylsilyl (*E)*-3-(2-((*tert*-butyldimethylsilyl)oxy)phenyl)acrylate (37)[272]**

trans-2-Hydroxycinnamic acid (1.5 g, 9.1 mmol), imidazole (1.25 g, 18.4 mmol) and TBDMS-Cl (2.82 g, 18.7 mmol) were added to a N_2 purged flask. Anhydrous DMF (20 mL) was added and the solution was stirred at RT under N_2 overnight, then for 2 h at 60 °C. The solvent was evaporated to give a beige oil which was dissolved in DCM (60 mL) and extracted with brine

(3 x 50mL). The organic phase was dried over $MgSO_4$, filtered, and the solvent was evaporated. Purification by column chromatography eluting with 0-2% MeOH in DCM + 0.1% pyridine gave **37** as a colourless oil (2.95 g, 83%). R_f = 0.75 (5% EtOAc: petroleum ether); R_t = 14.3 min (solvent system A); ^{1}H NMR ($CDCl_3$, 400 MHz) δ 0.25 (6H, s, $Si(CH_3)_2$), 0.33 (6H, s, $Si(CH_3)_2$), 0.99 (9H, s, Si^tBu), 1.02 (9H, s, Si^tBu), 6.38 (1H, d, J = 16.0, HC=C), 6. 83 (1H, dd, J = 8.2, 1.0, Ar), 6.95 (1H, t, J = 7.4, Ar), 7.24 (1H, t, J = 7.4, Ar), 7.53 (1H, dd, J = 8.0, 1.6, Ar), 7.97 (1H, d, J = 16.0, HC=C);); ^{13}C NMR ($CDCl_3$, 100 MHz) δ -9.43 ($Si(CH_3)_2$), -8.95 ($Si(CH_3)_2$), 12. 69 ($\underline{C}(CH_3)_3$), 13.05 ($\underline{C}(CH_3)_3$), 20.34 (($CH_3)_3$), 20.59 (($CH_3)_3$), 114.54 (Ar), 114.88 (Ar), 116.32 (Ar), 120.80 (C=C), 122.54 (Ar), 125.90 (Ar), 135.02 (Ar), 149.48 (C=C), 161.91 (C=O).

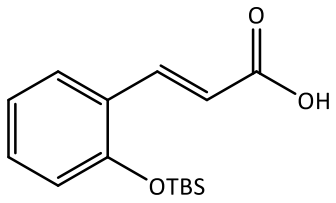

(*E*)-3-(2-((*tert*-Butyldimethylsilyl)oxy)phenyl)acrylic acid (38a)

Method A[187]:

A solution of **37** (1.0 g, 2.6 mmol) in 2:1 THF and MeOH (6 mL) was treated with K_2CO_3 (0.90 g, 6.5 mmol) in H_2O (2 mL). The reaction was stirred for 1 h then diluted with Et_2O (15 mL) and extracted with 10% HCl (3 x 30 mL) and water (3 x 30 mL). The organic phase was dried over $MgSO_4$, filtered, and the solvent was evaporated. The crude product was purified by column chromatography eluting with 10% acetone in DCM to give a colourless oil (256 mg, 35%) which was found to be a mixture of desilylated products by ^{1}H NMR.

Method B:

A solution of **37** (400 mg, 1.78 mmol) in 0.3% TFA in MeCN (10 mL) was stirred at RT overnight, after which the solvent was evaporated and the residue was co-evaporated with MeCN to remove traces of TFA. The crude material was purified by column chromatography eluting with 2-10% acetone in DCM +0.1% pyridine and dried under high vacuum to give **38a** as a

white solid (280 mg, 98%). R_f = 0.5 (10% acetone: DCM); R_t = 10.6 min (solvent system A); mp = 80-84 °C (lit.[187] 127- 129 °C); IR (KBr) 3441s (O-H), 1681s (C=O); ^{1}H NMR ($CDCl_3$, 400 MHz) δ 0.24 (6H, s, $Si(CH_3)_2$), 1.04 (9H, s, Si^tBu), 6.41 (1H, d, J = 16, HC=C), 6. 85 (1H, dd, J = 8.2, 1.0, Ar), 6.97 (1H, t, J = 7.4, Ar), 7.28 (1H, t, J = 7.4, Ar), 7.55 (1H, J = 8, 1.6, Ar), 8.17 (1H, d, J = 16, HC=C); ^{13}C NMR ($CDCl_3$, 100 MHz) δ -4.30 ($Si(CH_3)_2$), 18.27 ($\underline{C}(CH_3)_3$), 25.70 ($(CH_3)_3$), 116.98 (Ar), 120.03 (Ar), 121.55 (Ar), 122.81 (C=C), 127.79 (Ar), 131.69 (Ar), 142.44 (Ar), 154.88 (C=C), 172.79 (C=O).

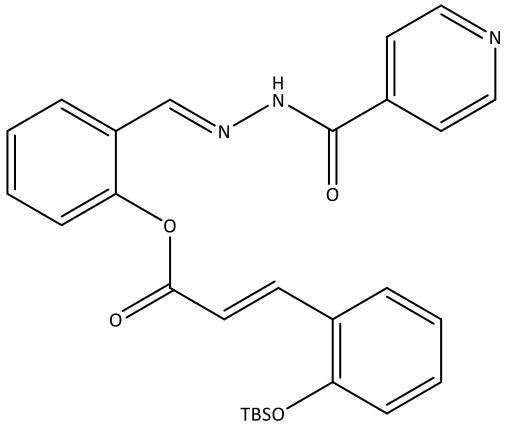

2-((*E*)-(2-Isonicotinoylhydrazono)methyl)phenyl (*E*)-3-(2-((*tert*-butyldimethylsilyl)oxy)phenyl)acrylate (39)

Method A:

Acid chloride formation via the cinnamic acid[187]:

A solution of **38a** (0.20 g, 0.72 mmol) in anhydrous DCM (2 mL) was treated with $SOCl_2$ (500 µL, 6.89 mmol) and stirred under N_2 at reflux for 4 h. The volatiles were evaporated and the yellow residue was co-evaporated with DCM to remove traces of $SOCl_2$.

Coupling:

The crude acid chloride **38b** was treated with a solution of **8** (157 mg, 0.651 mmol), DMAP (9 mg, 0.1 mmol) and anhydrous pyridine (53 µL, 0.72 mmol) in anhydrous DMF (3 mL). The

solution was stirred at 30 °C under N_2 for 24 h. The solvent was evaporated to give an orange oil which was dissolved in DCM (20 mL) and extracted with H_2O (3 x 20 mL) and brine (3 x 20 mL). The organic phase was dried over $MgSO_4$, filtered and the solvent was evaporated to give a residue which was purified by column chromatography, eluting with 10- 20% acetone in DCM + 0.1% pyridine. This gave unchanged **38a** (60 mg, 24%) and **39** as a colourless oil (108 mg, 27%; 36% based on recovered **38a**). R_f = 0.30 (10% acetone: DCM); R_t = 9.7 min (solvent system A); ^{1}H NMR (CD_3OD, 400 MHz) δ 0.33 (6H, s, $Si(CH_3)_2$), 1.09 (9H, s, Si^tBu), 6.84 (1H, d, J = 16.4, HC=C), 7.02 (1H, dd, J = 8.4, 0.8, Ar), 7.13 (1H, t, J = 7.8, Ar), 7.29 (1H, dd, J = 8.0, 0.8, Ar), 7.45 (2H, m, Ar), 7.60 (1H, td, J = 7.8, 1.6, Ar), 7.84 (1H, dd, J = 7.8, 1.4, Ar), 7.92 (2H, d, J = 6, Pyr), 8.33 (1H, dd, J = 8.0, 1.6, Ar), 8.44 (1H, d, J = 16.4, HC=C), 8.63 (1H, s, HC=N), 8.78 (2H, d, J = 5.6, Pyr); ^{13}C NMR (CD_3OD, 100 MHz) δ -4.08 ($Si(CH_3)_2$), 19.26 ($\underline{C}(CH_3)_3$), 26.30 ($(CH_3)_3$), 116.78 (Ar), 121.33 (Ar), 123.12 (Pyr), 124.14 (Ar), 126.60 (Ar), 127.51 (Ar), 127.80 (Ar), 128.13 (Ar), 128.79 (Ar), 129.26 (Ar), 132.92 (Ar), 133.57 (Ar), 142.26 (Pyr), 143.96 (C=C), 146.23 (C=N), 151.11 (Pyr), 151.65 (Ar), 156.37 (Ar), 164.53 (C=O), 166.97 (C=O); [Found (ESI+) 502.2131 $[M+H]^+$, $C_{28}H_{31}N_3O_4Si$ requires 502.2162].

Repeating the preparation on a similar scale but with anhydrous DCM as the coupling solvent gave unchanged **38a** (45 mg, 20%) and **39** (88 mg, 20%; 34% based on recovered **38a**).

Method B:

Acid chloride formation via the TBS-ester[188]:

A solution of **37** (153 mg, 0.390 mmol) and catalytic DMF (2 drops) was treated with 2M oxalyl chloride in DCM (0.25 mL, 0.98 mmol) at 0°C and the mixture was stirred under N_2 for 4 h. The volatiles were evaporated and the residue was co-evaporated with DCM.

Coupling:

This crude acid chloride **38b** was treated with a solution of SIH (75 mg, 0.31 mmol), DMAP (5 mg, 0.04 mmol) and anhydrous pyridine (29 µL, 0.39 mmol) in anhydrous DMF (1 mL). The solution was stirred at 30 °C under N_2 for 24 h. The solvent was evaporated to give an orange

oil which was dissolved in DCM (20 mL) and extracted with H_2O (3 x 20 mL) and brine (3 x 20 mL). The organic phase was dried over $MgSO_4$, filtered and the solvent was evaporated to give a residue which was purified by column chromatography, eluting with 10- 20% acetone in DCM + 0.1% pyridine. This gave unchanged **38a** (40 mg, 37%) and **39** as a colourless oil (34 mg, 27%; 35% yield based on recovered **38a**).

Repeating the preparation on a similar scale but with anhydrous DCM as the coupling solvent gave unchanged **38a** (30 mg, 20%) and **39** (55 mg, 25%; 31% based on recovered **38a**).

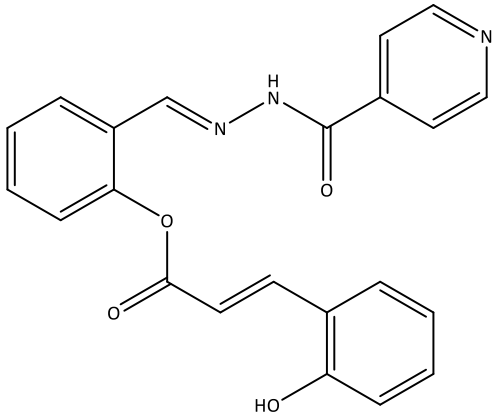

2-((*E*)-(2-Isonicotinoylhydrazono)methyl)phenyl (*E*)-3-(2-hydroxyphenyl)acrylate (36)

Method A:

A stirred solution of *trans*-2-hydroxy cinnamic acid (121 mg, 0.74 mmol) in anhydrous DMF (20 mL) under N_2 was cooled to 0 ^oC and DMAP (90 mg, 0.74 mmol) was added, followed by EDC.HCl (142 mg, 0.74 mmol). The solution was allowed to stir for 15 min, then a solution of **8** (99 mg, 0.41 mmol) and DIPEA (71 µL, 0.41 mmol) in anhydrous DMF (5 mL) was added and the temperature was increased to 30 ^oC. The reaction was stirred under N_2 overnight, after which time the solvent was evaporated to give an orange oil. This oil was dissolved in DCM (20 mL) and extracted with sat. NH_4Cl (3 x 20 mL) and brine (1 x 20 mL). The organic phase was dried over $MgSO_4$, filtered and the solvent evaporated. Mass spectrometry indicated the presence of **36**, however all attempts to separate it from coumarin **34a** by column chromatography failed.

Method B:

A stirred solution of **38a** (150 mg, 0.54 mmol) in anhydrous DMF (20 mL) under N_2 was cooled to 0 ^oC and DMAP (66 mg, 0.54 mmol) was added, followed by EDC.HCl (104 mg, 0.54 mmol). The solution was allowed to stir for 30 min, then a solution of **8** (92 mg, 0.38 mmol) and DIPEA (66 µL, 0.38 mmol) in anhydrous DMF (5 mL) was added and the temperature was increased to 30 ^oC. The reaction was stirred under N_2 for 3 days, after which time there was no conversion of the starting material observed on TLC.

Method C:

A solution of TBAF trihydrate (125 mg, 0.441 mmol) and acetic acid (25 µL) in anhydrous DMF (2 mL) was stirred under N_2 at 0 ^oC for 30 min. This was treated dropwise with a solution of **39** (63 mg, 0.13 mmol) in anhydrous DMF (2 mL) and stirred at 0 ^oC for a further 30 min. The reaction mixture was diluted with H_2O (40 mL) and extracted with Et_2O (3 x 40 mL) and EtOAc (1 x 40 mL). The combined organic phases were dried over $MgSO_4$, filtered and the solvent was evaporated to give a yellow oil. Purification by column chromatography eluting with 4% MeOH in DCM + 0.1% pyridine gave **36** as an off-white solid (43 mg, 86%). R_f = 0.6 (10% MeOH: DCM); R_t = 7.0 min (solvent system A); mp = 145- 148 ^oC; UV (EtOH) λ_{max} 290 (15200); ^1H NMR (DMSO-d_6, 400 MHz) δ 6.95 (1H, t, J = 7.6, Ar), 7.02 (1H, d, J = 16.0, HC=C), 7.02 (1H, d, J = 8.4, Ar), 7.36 (2H, m, Ar), 7.47 (1H, t, J = 7.6, Ar), 7.60 (1H, td, J = 7.8, 1.6, Ar), 7.79 (1H, d, J = 7.2, Ar), 7.85 (2H, d, J = 6, Pyr), 8.10 (1H, dd, J = 7.8, 1.4, Ar), 8.17 (1H, d, J = 16.0, HC=C), 8.60 (1H, s, HC=N), 8.81 (2H, d, J = 3.6, Pyr), 10.49 (1H, s, OH), 12.17 (1H, s, NH); ^{13}C NMR (CD_3OD, 100 MHz) δ 115.56 (Ar), 121.76 (Ar), 123.34 (Pyr), 124.76 (Ar), 126.43 (Ar), 126.98 (Ar), 127.54 (Ar), 127.87 (Ar), 128.56 (Ar), 129.23 (Ar), 132.45 (Ar), 133.21 (Ar), 141.67 (Pyr), 143.42 (C=C), 145.87 (C=N), 149.91 (Pyr), 151.03 (Ar), 156.29 (Ar), 163.79 (C=O), 166.17 (C=O); [Found (ESI+) 410.1105 $[M+H]^+$, $C_{22}H_{17}N_3O_4Na$ requires 410.1117].

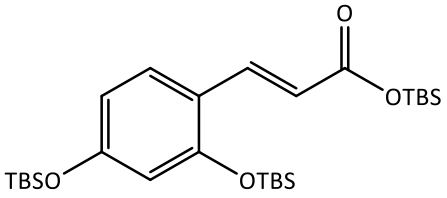

tert-Butyldimethylsilyl (_E_)-3-(2,4-bis((_tert_-butyldimethylsilyl)oxy)phenyl)acrylate (41)[272]

trans-2,4-Dihydroxycinnamic acid (1.5 g, 8.3 mmol), imidazole (1.77 g, 26 mmol) and TBDMS-Cl (3.92 g, 26 mmol) were added to an N_2 purged flask. Anhydrous DMF (30 mL) was added and the solution was stirred at 60 ^oC under N_2 overnight. The solvent was evaporated to give an oil which was dissolved in DCM (80 mL) and extracted with brine (3 x 80 mL). The organic phase was dried over $MgSO_4$, filtered and the solvent was evaporated. Purification by column chromatography eluting with 1% MeOH in DCM + 0.1% pyridine gave **41** as a colourless oil (3.17 g, 73%). R_f = 0.80 (5% acetone: DCM); R_t = 15.0 min (solvent system A); ^1H NMR ($CDCl_3$, 400 MHz) δ 0.21 (6H, s, $Si(CH_3)_2$), 0.24 (6H, s, $Si(CH_3)_2$), 0.31 (6H, s, $Si(CH_3)_2$), 0.97 (9H, s, Si^tBu), 0.98 (9H, s, Si^tBu), 1.01 (9H, s, Si^tBu), 6.26 (1H, d, J = 16.0, HC=C), 6. 32 (1H, d, J = 2.4, Ar), 6.46 (1H, dd, J = 8.6, 2.4, Ar), 7.41 (1H, d, J = 8.6, Ar), 7.89 (1H, d, J = 16.0, HC=C); ^{13}C NMR ($CDCl_3$, 100 MHz) δ -4.66 ($Si(CH_3)_2$), -4.42 ($Si(CH_3)_2$), -4.21 ($Si(CH_3)_2$), 17.80 ($\underline{C}(CH_3)_3$), 18.19 ($\underline{C}(CH_3)_3$), 18.31 ($\underline{C}(CH_3)_3$), 25.55 (($CH_3)_3$), 25.73 (($CH_3)_3$), 25.78 (($CH_3)_3$), 111.24 (Ar), 114.03 (Ar), 117.64 (Ar), 119.53 (C=C), 128.49 (Ar), 139.96 (Ar), 155.68 (Ar), 158.51 (C=C), 167.41 (C=O).

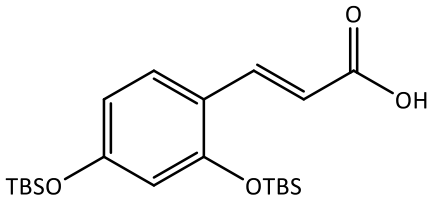

(_E_)-3-(2,4-Bis((_tert_-butyldimethylsilyl)oxy)phenyl)acrylic acid (42a)

A solution of **41** (0.63 g, 0.62 mmol) in 0.3% TFA in MeCN (10 mL) was stirred at RT overnight, after which the solvent was evaporated and the residue was co-evaporated with MeCN to remove traces of TFA. The crude product was purified by column chromatography, eluting

with 2-10% acetone in DCM +0.1% pyridine, then dried under high vacuum to give **42a** as a white solid (467 mg, 95%). R_f = 0.6 (10% acetone: DCM); R_t = 12.8 min (solvent system A); mp = 130-134 ^oC; ^1H NMR ($CDCl_3$, 400 MHz) δ 0.22 (6H, s, $Si(CH_3)_2$), 0.24 (6H, s, $Si(CH_3)_2$), 0.98 (9H, s, Si^tBu), 1.03 (9H, s, Si^tBu), 6.28 (1H, d, J = 16.4, HC=C), 6. 33 (1H, d, J = 2.4, Ar), 6.49 (1H, dd, J = 8.4, 2.4, Ar), 7.43 (1H, d, J = 8.4, Ar), 8.08 (1H, d, J = 16.0, HC=C); ^{13}C NMR ($CDCl_3$, 100 MHz) δ -4.41 ($Si(CH_3)_2$), -4.30 ($Si(CH_3)_2$), 18.20 ($\underline{C}(CH_3)_3$), 18.28 ($\underline{C}(CH_3)_3$), 25.55 ($(CH_3)_3$), 25.70 ($(CH_3)_3$), 111.49 (Ar), 114.20 (Ar), 114.47 (Ar), 119.27 (C=C), 128.68 (Ar), 142.16 (Ar), 156.18 (Ar), 159.07 (C=C), 173.12 (C=O).

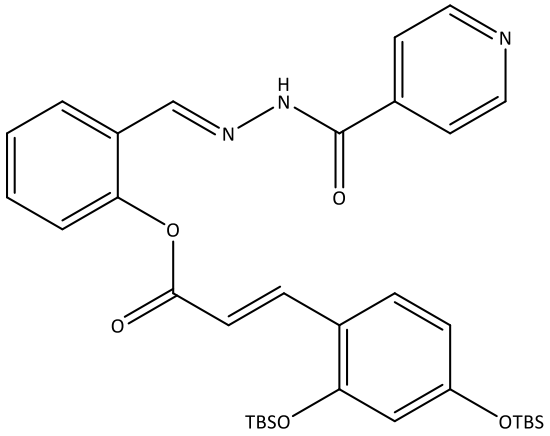

2-((*E*)-(2-Isonicotinoylhydrazono)methyl)phenyl (*E*)-3-(2,4-bis((*tert*-butyldimethylsilyl)oxy)phenyl)acrylate (43)

Method A:

Acid chloride formation via the cinnamic acid[187]:

A solution of **42a** (0.30 g, 0.73 mmol) in anhydrous DCM (3 mL) was treated with $SOCl_2$ (0.60 mL, 8.27 mmol) and the mixture was stirred under N_2 at reflux for 4.5 h. The volatiles were evaporated and the residue was co-evaporated with DCM to remove traces of $SOCl_2$.

Coupling:

The acid chloride **42b** was treated with a solution of **8** (159 mg, 0.659 mmol), DMAP (10 mg, 0.08 mmol) and anhydrous pyridine (53 µL, 0.73 mmol) in anhydrous DMF (3 mL). The solution was stirred at 30 ^{o}C under N_2 for 48 h. The solvent was evaporated to give an orange oil which was dissolved in DCM (20 mL) and extracted with H_2O (3 x 20 mL) and brine (3 x 20 mL). The organic phase was dried over $MgSO_4$, filtered and the solvent was evaporated to give a residue which was purified by column chromatography, eluting with 0- 2% MeOH in DCM + 0.1% pyridine. This gave unchanged **42a** (180 mg, 60%), and **43** as a colourless oil (16 mg, 4%; 10% based on recovered **42a**). R_f = 0.45 (10% acetone: DCM); R_t = 11.6 min (solvent system A); ^{1}H NMR (CD_3OD, 400 MHz) δ 0.32 (6H, s, $Si(CH_3)_2$), 0.32 (6H, s, $Si(CH_3)_2$), 1.07 (9H, s, $Si^{t}Bu$), 1.08 (9H, s, $Si^{t}Bu$), 6.46 (1H, d, J = 2.4, Ar), 6.65 (1H, dd, J = 8.4, 2.4, Ar), 6.70 (1H, d, J = 16.0, HC=C), 7.26 (1H, dd, J = 8.4, 0.8, Ar), 7.43 (1H, t, J = 7.6, Ar), 7.80 (1H, td, J = 7.8, 1.2, Ar), 7.74 (1H, d, J = 8.4, Ar), 7.91 (2H, d, J = 6.0, Pyr), 8.32 (1H, dd, J = 8.0, 1.6, Ar), 8.35 (1H, d, J = 16.4, HC=C), 8.62 (1H, s, HC=N), 8.77 (2H, br s, Pyr); ^{13}C NMR (CD_3OD, 100 MHz) δ -4.15 ($Si(CH_3)_2$), -4.02 ($Si(CH_3)_2$), 19.20 ($\underline{C}(CH_3)_3$), 19.28 ($\underline{C}(CH_3)_3$), 26.11 (($CH_3)_3$), 26.26 (($CH_3)_3$), 112.53 (Ar), 114.29 (Ar), 115.77 (Ar), 120.44 (Pyr), 123.19 (Ar), 124.17 (Ar), 127.42 (Ar), 127.85 (Ar), 128.08 (Ar), 130.03 (Pyr), 132.89 (Pyr), 142.32 (Ar), 143.76 (C=C), 146.24 (C=C), 151.13 (C=N), 151.76 (Ar), 157.74 (Ar), 161.01 (Ar), 164.57 (C=O), 167.35 (C=O); [Found (ESI+) 654.2790 $[M+H]^{+}$, $C_{34}H_{45}N_3O_5Si_2$ requires 654.2795].

Repeating the preparation on a similar scale but with anhydrous DCM as the coupling solvent gave unchanged **42a** (91 mg, 45%) and **43** (28 mg, 10%; 18% based on recovered **42a**).

Method B:

Acid chloride formation via the TBS-ester[188]:

A solution of **41** (307 mg, 0.586 mmol) and catalytic DMF (2 drops) was treated with 2M oxalyl chloride in DCM (880 µL, 1.76 mmol) at 0^{o}C and the mixture was stirred under N_2 for 4 h. The volatiles were evaporated and the residue was co-evaporated with DCM.

Coupling:

The acid chloride **42b** was treated with a solution of **8** (114 mg, 0.473 mmol), DMAP (7 mg, 0.06 mmol) and anhydrous pyridine (130 µL, 1.78 mmol) in anhydrous DMF (1 mL). The solution was stirred at 30 ^{o}C under N_2 for 45 h. The solvent was evaporated to give an orange oil which was dissolved in DCM (20 mL) and extracted with H_2O (3 x 20 mL) and brine (3 x 20 mL). The organic phase was dried over $MgSO_4$, filtered and the solvent was evaporated to give a residue which was purified by column chromatography, eluting with 0- 2% MeOH in DCM + 0.1% pyridine. This gave unchanged **42a** (170 mg, 71%) and **43** as a colourless oil (27 mg, 9%; 31% yield based on recovered **42a**).

***Method C**:*

Acid chloride formation via the cinnamic acid[187]:

A solution of **42a** (180 g, 0.440 mmol) in anhydrous DCM (3 mL) was treated with $SOCl_2$ (0.30 mL, 4.14 mmol) and the mixture was stirred under N_2 at reflux for 4.5 h. The volatiles were evaporated and the residue was co-evaporated with DCM to remove traces of $SOCl_2$.

Coupling:

The acid chloride **42b** was treated with a solution of salicylaldehyde (43 µL, 0.40 mmol), DMAP (5 mg, 0.04 mmol) and anhydrous pyridine (32 µL, 0.44 mmol) in anhydrous DCM (5 mL). The solution was stirred at 30 ^{o}C under N_2 for 48 h. The solvent was evaporated to give an orange oil which was dissolved in DCM (20 mL) and extracted with H_2O (3 x 20 mL) and brine (3 x 20 mL). The organic phase was dried over $MgSO_4$, filtered and the solvent was evaporated to give a residue which was purified by column chromatography, eluting with 0- 6% EtOAc in petroleum ether + 0.1% pyridine. This gave the desired product **45** (67 mg, 33%) which was immediately used in the next step.

Condensation:

A solution of **45** (67 mg, 0.13 mmol) and INH (18 mg, 0.13 mmol) in EtOH (5 mL) was heated at reflux for 3 h. The solvent was evaporated to give a yellow oil which was purified by column chromatography, eluting with 0-2% MeOH in DCM + 0.1% pyridine. This gave **43** as a colourless oil (17 mg, 21%).

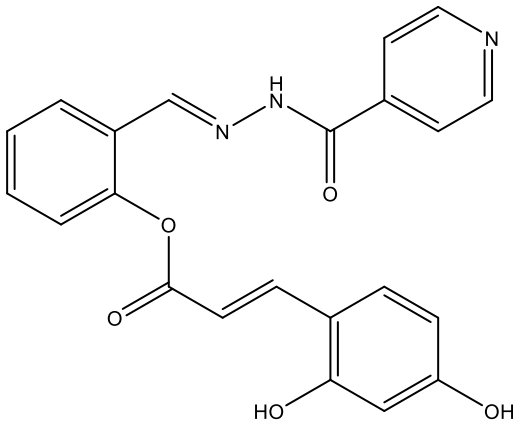

2-((*E*)-(2-isonicotinoylhydrazineylidene)methyl)phenyl (*E*)-3-(2,4-dihydroxyphenyl)acrylate (44)

A solution of TBAF trihydrate (142 mg, 0.45 mmol) and acetic acid (100 µL) in anhydrous DMF (2 mL) was stirred under N_2 at 0 ^oC for 30 min. A solution of **43** (63 mg, 0.10 mmol) in anhydrous DMF (2 mL) was added dropwise and the mixture was stirred at 0 ^oC for 45 min, then H_2O (20 mL) was added and the mixture was extracted with EtOAc (3 x 20 mL). The combined organic phases were dried over $MgSO_4$, filtered and the solvent was evaporated to give a yellow oil. Purification by column chromatography eluting with 5-10% MeOH in DCM + 0.1% pyridine gave the product as a yellow oil (6 mg, 15%). R_f = 0.20 (10% MeOH: DCM); R_t = 6.57 min (solvent system A); UV (EtOH) λ_{max} 304 (7500); ^{1}H NMR (DMSO-d_6, 500 MHz) δ 6.33 (1H, dd, J = 8.5, 2.5, Ar), 6.41 (1H, d, J = 2.5, Ar), 6.72 (1H, d, J = 15.5, HC=C), 7.26 (1H, dd, J = 8.5, 1.5, Ar), 7.39 (1H, td, J= 8.0, 1.0, Ar), 7.54 (1H, td, J = 8.0, 2.0, Ar), 7.55 (1H, d, J = 9.0, Ar), 7.80 (2H, d, J = 6.0, Pyr), 8.01 (1H, d, J = 15.5, HC=C), 8.04 (1H, dd, J = 7.5, 1.2, Ar), 8.54 (1H, s, HC=N), 8.77 (2H, br s, Pyr), 10.05 (1H, s, OH), 10.37 (1H, s, OH), 12.15 (1H, s, NH); ^{13}C NMR (DMSO-d_6, 125 MHz) δ 102.45 (Ar), 108.06 (Ar), 110.96 (C=C), 112.39 (Ar), 121.48 (Pyr), 123.43 (Ar), 125.79 (Ar), 126.19 (Ar), 126.68 (Ar), 127.91 (Ar), 131.18 (Ar), 131.37 (Pyr), 140.35 (Ar),

143.03 (C=C), 143.38 (C=N), 149.78 (Ar), 150.26 (Pyr), 159.16 (Ar), 161.66 (C=O), 165.91 (C=O); [Found (ESI+) 404.1243 $[M+H]^+$, $C_{22}H_{18}N_3O_5$ requires 404.1241].

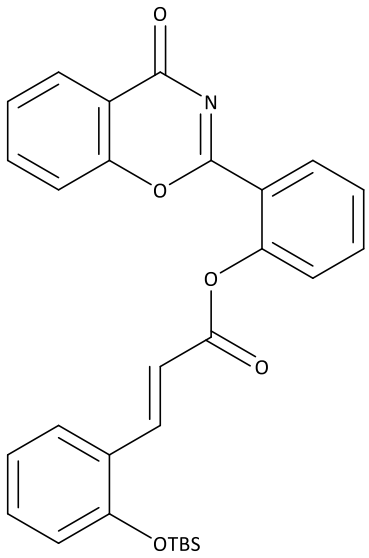

2-(4-Oxo-4H-benzo[e][1,3]oxazin-2-yl)phenyl (*E*)-3-(2-((*tert*-butyldimethylsilyl)oxy)phenyl)acrylate (46)

Acid chloride formation via the cinnamic acid[187]:

A solution of **38a** (70 mg, 0.25 mmol) in anhydrous DCM (2 mL) was treated with $SOCl_2$ (0.2 mL, 2.5 mmol) and stirred under N_2 at reflux for 4 h. The volatiles were evaporated and the residue was co-evaporated with DCM to remove traces of $SOCl_2$.

Coupling:

The acid chloride **38b** from the previous step was treated with a solution of **32** (55 mg, 0.23 mmol), DMAP (4 mg, 0.03 mmol) and anhydrous pyridine (20 µL, 0.25 mmol) in anhydrous DMF (3 mL). The solution was stirred at 30 ^oC under N_2 for 48 h after which time there was no conversion of the starting materials.

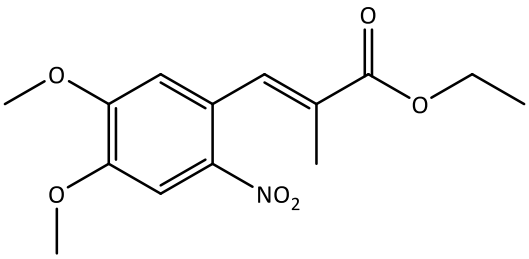

Ethyl-(*E*)-3-(4,5-dimethoxy-2-nitrophenyl)-2-methylacrylate (48)[172]

A solution of 6-nitroveratraldehyde (2.00 g, 9.48 mmol) and ECETP (5.15 g, 14.22 mmol) in anhydrous toluene (85 mL) was heated overnight at 65°C under N_2. The solvent was evaporated and the residue was purified by column chromatography eluting with DCM to give **48** as a yellow solid (2.46 g, 88%). R_f = 0.63 (DCM); R_t= 9.53 min (solvent system A); mp = 147-148°C (lit.[172] 146-147 °C); ^{1}H NMR ($CDCl_3$, 400 MHz) δ 1.34 (3H, t, J = 7.2, $CH_2C\underline{H}_3$), 1.90 (3H, s, $C=CCH_3$), 3.95 (3H, s, OCH_3), 3.98 (3H, s, OCH_3), 4.29 (2H, q, J = 7.2, $C\underline{H}_2CH_3$), 6.71 (1H, s, Ar), 7.74 (1H, s, Ar), 7.92 (1H, s, C=CH); ^{13}C NMR ($CDCl_3$, 100 MHz) δ 14.08 (CH_3), 14.24 (CH_3), 56.39 (OCH_3), 56.47 (OCH_3), 61.04 (CH_2), 107.72 (Ar), 112.23 (Ar), 126.60 (Ar), 129.32 (C=C), 136.48 (C=C), 140.21 (Ar), 148.21 (Ar), 152.90 (Ar), 167.76 (C=O).

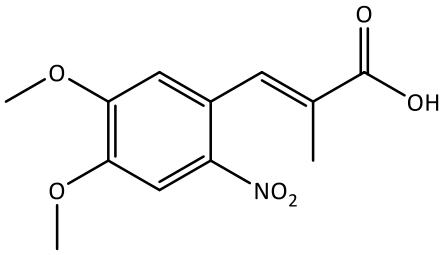

(*E*)-3-(4,5-Dimethoxy-2-nitrophenyl)-2-methylacrylic acid (49)

A solution of **48** (1.06 g, 3.59 mmol) in THF (40 mL) was treated with 1M NaOH (17 mL) and EtOH (10 mL) and stirred at RT overnight. The organic solvents were removed under reduced pressure and the remaining aqueous solution was diluted with H_2O (20 mL) and the pH was adjusted to 3 with with 6M HCl. The resulting suspension was extracted with EtOAc (3 × 40 mL) and the organic phases were dried over $MgSO_4$, filtered, and the solvent was evaporated. This gave **49** as a yellow solid (950 mg, 99%). R_f = 0.63 (10% MeOH: DCM); R_t = 7.78 min (solvent system A); mp = 236- 237 °C; ^{1}H NMR (acetone-d_6, 400 MHz) δ 1.98 (3H, s, $C=CCH_3$),

4.05 (3H, s, OCH_3), 4.07 (3H, s, OCH_3), 7.08 (1H, s, Ar), 7.83 (1H, s, Ar), 7.99 (1H, s, C=CH); ^{13}C NMR (acetone-d_6, 100 MHz) δ 14.18 (CH_3), 56.67 (OCH_3), 56.92 (OCH_3), 108.73 (Ar), 113.66 (Ar), 126.95 (Ar), 130.07 (C=C), 137.33 (C=C), 141.27 (Ar), 149.91 (Ar), 154.41 (Ar), 169.02 (C=O).

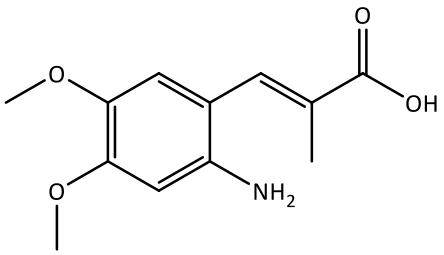

(*E*)-3-(2-Amino-4,5-dimethoxyphenyl)-2-methylacrylic acid (50)

Method A[193]:

A solution of **49** (80 mg, 0.30 mmol), iron powder (100 mg, 1.79 mmol) and AcOH (2 mL) in EtOH (2 mL) and H_2O (1 mL) was heated for 2 h at reflux under N_2. The reaction mixture was filtered through celite and the volatiles were evaporated. The resulting suspension was diluted with H_2O (20 mL) and extracted with EtOAc (4 × 30 mL). The organic phases were dried over $MgSO_4$, filtered, and the solvent was evaporated. The resulting residue was co-evaporated with MeCN, toluene and $CHCl_3$ to give **50** as a dark yellow solid (60 mg, 85%).

Method B[194]:

A suspension of **49** (900 mg, 3.79 mmol) and $FeSO_4.7H_2O$ (10.6 g, 38.0 mmol) in H_2O (30 mL) was heated to 80 ^oC. 35% (aq.) NH_3 solution (10 mL) was added to the orange solution which immediately turned black. After stirring for 5 min, the heat was removed and the solution was allowed to stir for a further 2 h at RT. The reaction mixture was filtered through celite and acidified to pH 4 using 1M HCl, then it was extracted with EtOAc (9 x 50 mL). The organic phases were dried over Na_2SO_4, filtered, and the solvent was evaporated to give **50** as a dark yellow solid (725 mg, 91%). R_f = 0.45 (10% ^{i}PrOH: DCM); R_t = 4.9 min (solvent system A); mp = 154-156 ^oC; ^1H NMR (DMSO-d_6, 400 MHz) δ 2.02 (3H, s, $C=CCH_3$), 3.69 (3H, s, OCH_3), 3.76 (3H, s, OCH_3), 4.91 (2H, s, NH_2), 6.46 (1H, s, Ar), 6.75 (1H, s, Ar), 7.55 (1H, s, C=CH), 12.15 (1H, s,

OH); ^{13}C NMR (DMSO-d_6, 100 MHz) δ 14.31 (CH_3), 55.15 (OCH_3), 56.56 (OCH_3), 100.13 (Ar), 111.01 (Ar), 114.41 (Ar), 125.14 (C=C), 134.70 (C=C), 139.83 (Ar), 142.68 (Ar), 150.73 (Ar), 169.64 (C=O). [Found (ESI-) 236.0924 $[M-H]^-$, $C_{12}H_{14}NO_4$ requires 236.0923].

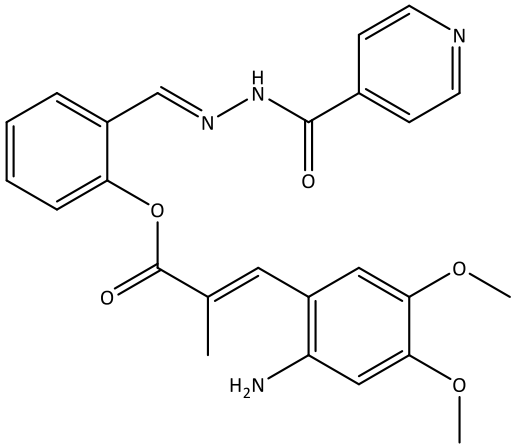

2-((*E*)-(2-Isonicotinoylhydrazono)methyl)phenyl (*E*)-3-(2-Amino-4,5-dimethoxyphenyl)-2-methylacrylate (51)

A stirred solution of **50** (700 mg, 2.95 mmol) in anhydrous DMF (20 mL) under N_2 was cooled to 0 °C and DMAP (360 mg, 2.95 mmol) was added, followed by EDC.HCl (566 mg, 2.95 mmol). The solution was allowed to stir for 10 min, then a solution of **8** (499 mg, 2.07 mmol) and DIPEA (360 µL, 2.07 mmol) in anhydrous DMF (5 mL) was added and the temperature was increased to 30 °C. The reaction was stirred under N_2 overnight, after which time the solvent was evaporated to give an orange oil. This oil was dissolved in DCM (100 mL) and extracted with sat. NH_4Cl (3 x 100 mL) and brine (3 x 100mL). The organic phase was dried over $MgSO_4$, filtered and the solvent evaporated. Purification by column chromatography eluting with 2-6% MeOH in DCM + 0.1% pyridine gave **51** as a bright orange solid (750 mg, 79%). R_f = 0.5 (10% MeOH: DCM); R_t = 6.1 min (solvent system A); mp = 114-117 °C; IR (KBr) 3430m (N-H), 1657s (C=O), 1607s (C=O); UV (EtOH) λ_{max} 302 (2870); ^{1}H NMR (DMSO-d_6, 400 MHz) δ 2.26 (3H, d, J = 0.8, CH_3), 3.73 (3H, s, OCH_3), 3.79 (3H, s, OCH_3), 5. 22 (2H, s, NH_2), 6.50 (1H, s, Ar), 6.88 (1H, s, Ar), 7.33 (1H, d, J = 7.6, Ar), 7.45 (1H, t, J = 7.6, Ar), 7.60 (1H, td, J = 7.7, 1.8, Ar), 7.86 (2H, dd, J = 4.4, 1.6, Pyr), 7.94 (1H, d, J = 0.8, HC=C), 8.07 (1H, dd, J = 8.0, 1.6, Ar), 8.62 (1H, s, HC=N), 8.83 (2H, d, J = 5.6, Pyr), 12.16 (1H, s, NH); ^{13}C NMR (DMSO-d_6, 500 MHz) δ 14.64 (CH_3), 55.15 (OCH_3), 56.43 (OCH_3), 99.92 (Ar), 110.03 (Ar), 113.96 (Ar), 121.97 (Ar), 123.54 (Ar), 126.22 (Ar), 126.32 (C=C), 126.69 (Ar), 131.32 (Ar), 137.88 (Ar), 139.55 (Pyr),

139.89 (Pyr), 140.41 (Pyr), 143.55 (C=C), 143.79 (C=N), 150.09 (Ar), 150.34 (Ar), 151.60 (Ar), 161.71 (C=O), 166.95 (C=O); [Found (ESI+) 461.1819 $[M+H]^+$, $C_{25}H_{24}N_4O_5$ requires 461.1819].

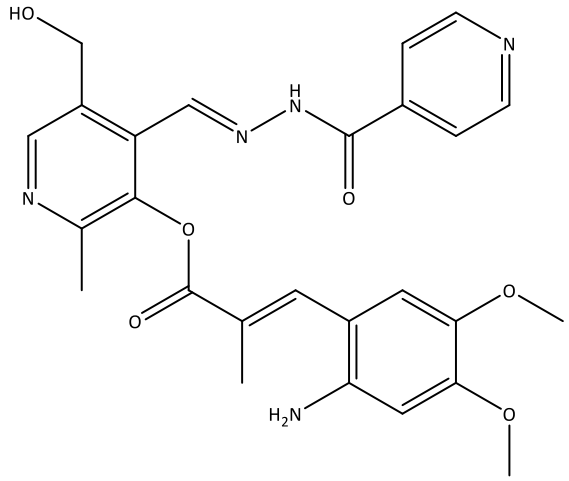

5-(hydroxymethyl)-4-((*E*)-(2-isonicotinoylhydrazineylidene)methyl)-2-methylpyridin-3-yl (*E*)-3-(2-amino-4,5-dimethoxyphenyl)-2-methylacrylate (52)

A stirred solution of **50** (195 mg, 0.82 mmol) in anhydrous DMF (5 mL) under N_2 was cooled to 0 ^oC and treated with DMAP (100 mg, 0.82 mmol) and EDC.HCl (157 mg, 0.82 mmol). The solution was allowed to stir for 10 min before a solution of **7** (129 mg, 0.45 mmol) and DIPEA (78 µL, 0.45 mmol) in anhydrous DMF (2 mL) was added. The temperature was increased to 30^oC and the reaction was stirred overnight. The solvent was then evaporated and the remaining residue was dissolved in DCM (20 mL) and extracted with sat. NH_4Cl (3 x 20 mL) and brine (1 x 20 mL). The organic phase was dried over $MgSO_4$, filtered and the solvent was evaporated to give an oil which was purified by column chromatography, eluting with 0-15% MeOH in DCM + 0.1% pyridine. This gave **52** as an orange oil (126 mg, 53%). R_f = 0.2 (5% MeOH: DCM) ;R_t = 5.18 min (solvent system A); UV (EtOH) λ_{max} 298 (9250); ^{1}H NMR (DMSO-d_6, 400 MHz) δ 2.23 (3H, d, J = 1.2, CH_3), 2.41 (3H, s, CH_3), 3.68 (3H, s, OCH_3), 3.75 (3H, s, OCH_3), 4.78 (2H, d, J = 6.4, $C\underline{H}_2OH$), 5.18 (2H, s, NH_2), 5.41 (1H, t, J = 6.4, OH), 6.46 (1H, s, Ar), 6.87 (1H, s, Ar), 7.84 (2H, d, J = 6.0, Pyr), 7.92 (1H, d, J = 1.6, C=CH), 8.57 (1H, s, Pyr), 8.64 (1H, s, N=CH), 8.81 (2H, br s, Pyr), 12.49 (1H, br s, NH); ^{13}C NMR (DMSO-d_6, 100 MHz) δ 14.47 (CH_3), 18.85 (CH_3), 55.16 (OCH_3), 56.20 (OCH_3), 59.68 (CH_2), 99.96 (Ar), 110.21 (Ar), 113.62 (Ar), 121.60 (Pyr), 122.05 (C=C), 131.81 (Pyr), 133.86 (Ar), 138.03 (C=C), 139.75 (Ar), 139.94 (Pyr),

142.82 (Pyr), 143.25 (Pyr), 143.78 (C=N), 145.84 (Pyr), 150.22 (Pyr), 151.39 (Pyr), 151.66 (Ar), 162.39 (C=O), 166.45 (C=O); [Found (ESI+) 528.1866 $[M+H]^+$, $C_{26}H_{27}N_5O_7Na$ requires 528.1854].

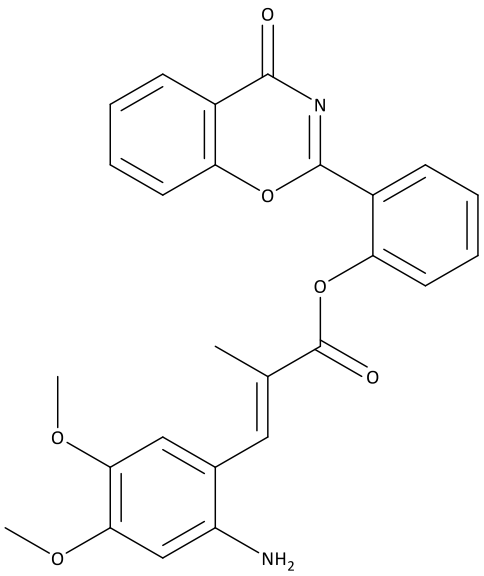

2-(4-oxo-4H-benzo[e][1,3]oxazin-2-yl)phenyl (*E*)-3-(2-amino-4,5-dimethoxyphenyl)-2-methylacrylate (53)

A stirred solution of **50** (85 mg, 0.36 mmol) in anhydrous DMF (2 mL) under N_2 was cooled to 0 ^oC and treated with EDC.HCl (69 mg, 0.36 mmol) and DMAP (44 mg, 0.36 mmol). The mixture was allowed to stir for 10 min before a solution of **32** (60 mg, 0.25 mmol) and DIPEA (44 µL, 0.25 mmol) in anhydrous DMF (2 mL) was added. The temperature was allowed to increase to RT and the reaction stirred for 40 h after which time the solvent was evaporated and the remaining residue was dissolved in DCM (20 mL) and then extracted with sat. NH_4Cl (3 x 20 mL) and brine (3 x 20 mL). The organic phase was dried over $MgSO_4$, filtered and the solvent was evaporated to give a residue which was purified by column chromatography, eluting with 2-6% acetone in DCM + 0.1% pyridine. This gave **53** as a yellow oil (43 mg, 38%) which decomposed on standing. R_f = 0.4 (6% acetone: DCM); R_t = 7.7 min (solvent system A); ^1H NMR (DMSO-d_6, 400 MHz) δ 2.19 (3H, d, J = 1.6, CH_3), 3.83 (3H, s, OCH_3), 3.88 (3H, s, OCH_3), 6.32 (1H, s, Ar), 6.80 (1H, s, Ar), 7.31 (1H, dd, J = 8.0, 0.8, Ar), 7.38 (1H, dd, J = 8.4 ,0.8, Ar), 7.47 (2H, m, Ar), 7.70 (2H, m, Ar), 8.03 (1H, d, J = 0.8, HC=C), 8.14 (1H, dd, J = 7.8, 1.4, Ar), 8.31 (1H, dd, J = 8.0, 1.6, Ar); [Found (ESI+) 481.1375 $[M+H]^+$, $C_{26}H_{22}N_2O_6Na$ requires 481.1376].

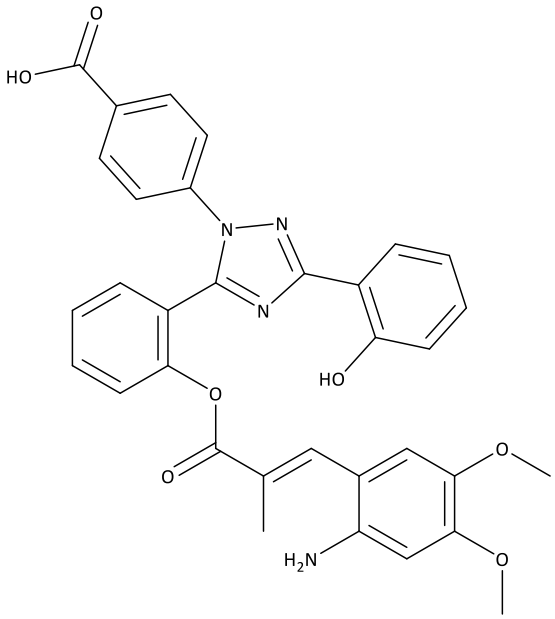

(*E*)-4-(5-(2-((3-(2-Amino-4,5-dimethoxyphenyl)-2-methylacryloyl)oxy)phenyl)-3-(2-hydroxyphenyl)-1H-1,2,4-triazol-1-yl)benzoic acid (54)[98]

4-Hydrazinobenzoic acid (17 mg, 0.11 mmol) and NEt_3 (15 µL, 0.11 mmol) were dissolved in boiling EtOH (5 mL) under stirring. This solution was added to **53** (42 mg, 0.09 mmol) and the reaction was stirred at 60 ^oC for 48 h then allowed to cool to RT. The reaction was diluted with H_2O (10 mL) and concentrated by 50%. 6M HCl was added (1 mL) and the solution was extracted with DCM (3 x 20 mL) and then brine (3 x 20 mL), dried over $MgSO_4$, filtered and the solvent evaporated to give an orange residue. Purification by column chromatography (1-6% MeOH in DCM + 0.1% pyridine) gave **54** as a yellow residue (14 mg, 26%) which decomposed readily under ambient lighting. R_f = 0.4 (6% MeOH: DCM); R_t = 8.1 min (solvent system A); [Found (ESI+) 615.1854 $[M+H]^+$, $C_{33}H_{27}N_4O_7Na$ requires 615.1856].

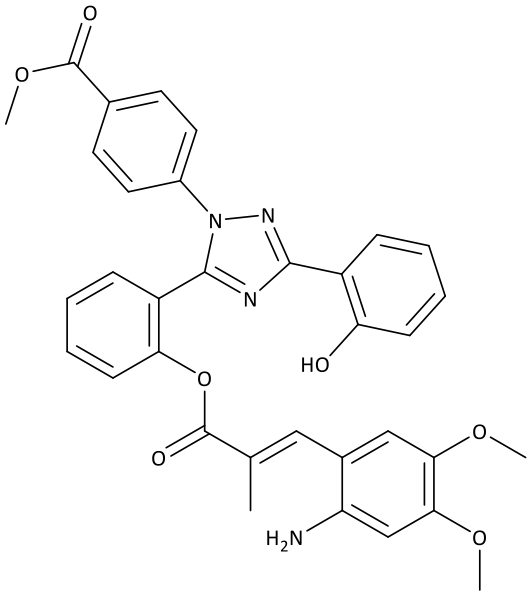

Methyl (*E*)-4-(5-(2-((3-(2-amino-4,5-dimethoxyphenyl)-2-methylacryloyl)oxy)phenyl)-3-(2-hydroxyphenyl)-1H-1,2,4-triazol-1-yl)benzoate (55)[100]

A stirred solution of **50** (63 mg, 0.27 mmol) in anhydrous DMF (2 mL) under N_2 was cooled to 0 ^oC and was treated with DMAP (33 mg, 0.27 mmol) and EDC.HCl (52 mg, 0.27 mmol). The mixture was allowed to stir for 10 min before a solution of **33** (93 mg, 0.24 mmol) and DIPEA (42 µL, 0.24 mmol) in anhydrous DMF (1 mL) was added. The temperature was increased to 30^oC and the mixture was stirred overnight. The solvent was then evaporated and the remaining residue was dissolved in DCM (10 mL) and extracted with sat. NH_4Cl (3 x 10 mL) and brine (3 x 10 mL). The organic phase was dried over $MgSO_4$, filtered and the solvent was evaporated to give a residue which was purified by column chromatography, eluting with 0-2% acetone in DCM + 0.1% pyridine. This gave **55** as an orange oil (41 mg, 28%). R_f = 0.45 (2% acetone: DCM); R_t = 9.67 min (solvent system A); UV (EtOH) λ_{max} 302 (7640), 380 (3370); ^1H NMR ($CDCl_3$, 400 MHz) δ 1.92 (3H, d, J = 1.2, CH_3), 3.70 (3H, s, OCH_3), 3.78 (3H, s, OCH_3), 3.88 (3H, s, CO_2CH_3), 6.20 (1H, s, Ar), 6.60 (1H, s, Ar), 6.89 (1H, td, J = 8.8, 1.2, Ar), 6.94 (1H, dd, J = 8.4, 1.2, Ar), 7.19- 7.21 (2H, m, Ar), 7.26 (1H, td, J = 8.0, 1.6, Ar), 7.31 (1H, d, J = 8.0, Ar), 7.49-7.57 (3H, m, Ar), 7.62 (1H, d, J = 1.2, C=CH), 8.01 (2H, d, J = 8.8, Ar), 8.07 (1H, dd, J = 7.6, 1.6, Ar), 10.92 (1H, br s, OH); ^{13}C NMR (DMSO-d_6, 100 MHz) δ 14.21 (CH_3), 52.38 (OCH_3), 55.15 (OCH_3), 56.36 ($CO_2\underline{C}H_3$), 99.49 (Ar), 110.01 (Ar), 113.32 (Ar), 113.87 (Ar), 117.07 (Ar), 119.71 (Ar), 120.41 (Ar), 122.01 (C=C), 123.73 (Ar), 124.47 (Ar), 126.08 (Ar), 126.80 (Ar), 129.81 (Ar),

130.34 (Ar), 131.31 (Ar), 131.59 (Ar), 132.43 (Ar), 138.07 (C=C), 139.90 (Ar), 140.44 (Ar), 143.32 (Ar), 149.01 (Ar), 150.22 (Ar), 151.47 (Tri), 156.27 (Ar), 160.07 (Tri), 165.23 (C=O), 166.16 (C=O); [Found (ESI+) 607.2192 $[M+H]^+$, $C_{34}H_{30}N_4O_7$ requires 607.2193].

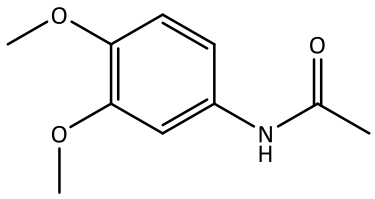

N-(3,4-Dimethoxyphenyl)acetamide (57)[273]

A solution of 3,4- dimethoxyaniline (500 mg, 3.26 mmol) and Et_3N (545 µL, 3. 91 mmol) in anhydrous DCM (4 mL) was treated dropwise with acetyl chloride (280 µL, 3.91 mmol). The mixture was stirred under N_2 at RT for 20 min and then extracted with sat. NH_4Cl (3 x 10 mL) and brine (3 x 10 mL). The organic phase was dried over Na_2SO_4, filtered and the solvent was evaporated to give **57** as a dark purple solid (478 mg, 75%). R_f = 0.35 (80% EtOAc: pet. ether); R_t = 5.7 min (solvent system A), mp = 128-129 ^oC (lit[274] 128 -130 ^oC); ^1H NMR ($CDCl_3$, 400 MHz) δ 2.15 (3H, s, CH_3), 3.84 (3H, s, OCH_3), 3.85 (3H, OCH_3), 6.78 (1H, s, Ar), 6.85 (1H, d, J = 2.4, Ar), 7. 29 (1H, d, J = 2.4, Ar); ^{13}C NMR ($CDCl_3$, 100 MHz) δ 24.29 (CH_3), 55.85 (OCH_3), 56.06 (OCH_3), 105.16 (Ar), 111.33 (Ar), 111.99 (Ar), 131.40 (Ar), 145.93 (Ar), 149.03 (Ar), 168.26 (C=O).

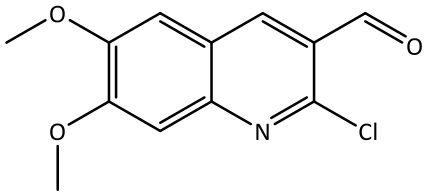

2-Chloro-6,7-dimethoxyquinoline-3-carbaldehyde (58)[195]

A mixture of **57** (470 mg, 2.41 mmol) and anhydrous DMF (740 µL, 9.64 mmol) under N_2 was cooled to 0^oC and treated dropwise with $POCl_3$ (2.7 mL, 29.0 mmol). The temperature was increased to 85^oC and the mixture was stirred for 3 h. The reaction mixture was poured onto ice-cold water and stirred for 30 min. The resulting precipitate was collected by suction

filtration and washed with H_2O before being recrystallized from MeCN to give **29** as beige needles (308 mg, 51%). R_f = 0.80 (80% EtOAc: pet. ether); R_t = 8.4 min (solvent system A); mp = 215- 218 ^oC (lit[195] 215 ^oC); ^1H NMR ($CDCl_3$, 400 MHz) δ 4.02 (3H, s, OCH_3), 4.05 (3H, s, OCH_3), 7.13 (1H, s, Ar), 7.37 (1H, s, Ar), 8.56 (1H, s, Ar), 10.49 (1H, s, HC=O); ^{13}C NMR ($CDCl_3$, 400 MHz) δ 56.21 (OCH_3), 56.45 (OCH_3), 106.19 (Ar), 107.20 (Ar), 122.29 (Ar), 124.58 (Ar), 137.54 (Ar), 147.51 (Ar), 148.65 (Ar), 150.85 (Ar), 155.92 (Ar), 189.18 (HC=O).

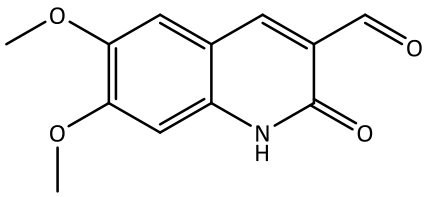

6,7-Dimethoxy-2-oxo-1,2-dihydroquinoline-3-carbaldehyde (59)[195]

A stirred solution of **58** (300 mg, 1.19 mmol) and 70% AcOH (12 mL) was heated to reflux under N_2 for 16 h. The solution was allowed to cool to RT then poured into ice-cold water (20 mL). The resulting precipitate was collected by suction filtration and washed with H_2O and EtOAc, then dried under high vacuum to give **59** as a bright yellow solid (140 mg, 50%). R_f = 0.40 (20% acetone: DCM); R_t = 5.9 min (solvent system A); mp = >280 ^oC; ^1H NMR (DMSO-d_6, 400 MHz) δ 3.86 (3H, s, OCH_3), 3.93 (3H, s, OCH_3), 6.93 (1H, s, Ar), 7.48 (1H, s, Ar), 8.43 (1H, s, Ar), 10.24 (1H, s, HC=O), 12.09 (1H, s, NH); ^{13}C NMR (DMSO-d_6, 100 MHz) δ 55.78 (OCH_3), 55.88 (OCH_3), 97.29 (Ar), 110.40 (Ar), 111.67 (Ar), 122.55 (Ar), 138.45 (Ar), 141.46 (Ar), 145.58 (Ar), 155.13 (Ar), 161.50 (C=O), 189.30 (HC=O); [Found (ESI+) 256.0597 $[M+H]^+$, $C_{12}H_{10}NO_4Na$ requires 256.0586].

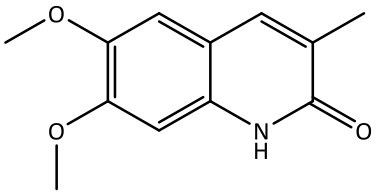

6,7-Dimethoxy-3-methylquinolin-2(1H)-one (60)

Method A[196]:

A solution of **59** (130 mg, 0.56 mmol) in TFA (3 mL) under N_2 was cooled to 0^oC and treated with Et_3SiH (270 µL, 1.68 mmol), the temperature was increased to RT and the mixture was stirred for 2 h. The reaction mixture was poured into ice-cold water (20 mL) and extracted with DCM (3 x 15 mL) and brine (3 x 15 mL). The organic phases were combined and dried over $MgSO_4$, filtered and the solvent was evaporated to give the crude product which was purified by column chromatography eluting with 2% MeOH in DCM. This gave **60** as a white solid (50 mg, 41%). R_f = 0.40 (5% MeOH:DCM); R_t = 6.3 min (solvent system A); mp = 236- 238 ^oC; UV (EtOH) λ_{max} 214 (29928), 234 (18082), 341 (4500); ^1H NMR ($CDCl_3$, 400 MHz) δ 2.26 (3H, d, J = 0.8, CH_3), 3.91 (3H, s, OCH_3), 3.98 (3H, s, OCH_3), 6.81 (1H, s, Ar), 6.89 (1H, s, Ar), 7.55 (1H, s, Ar), 11.56 (1H, s, NH); ^{13}C NMR ($CDCl_3$, 100 MHz) δ 16.33 (CH_3), 56.13 (OCH_3), 56.26 (OCH_3), 98.24 (Ar), 107.14 (Ar), 114.29 (Ar), 125.98 (Ar), 132.73 (Ar), 138.02 (Ar), 146.24 (Ar), 151.98 (Ar), 163.61 (C=O); [Found (ESI+) 220.0984 $[M+H]^+$, $C_{12}H_{13}NO_3$ requires 220.0974].

Method B[194]:

A solution of **50** (25 mg, 0.11 mmol) and 4% HCl (2 mL) was heated to reflux and stirred for 3 h. The reaction was cooled in an ice bath and 1% (aq.) NH_3 solution (5 mL) was added, then extracted with DCM (3 x 10 mL). The organic phases were combined and extracted with brine (2 x 30 mL), then dried over Na_2SO_4, filtered and the solvent was evaporated to give **60** as a pale yellow solid (20 mg, 83%).

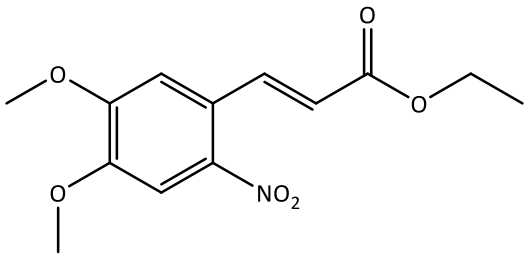

Ethyl (*E*)-3-(4,5-dimethoxy-2-nitrophenyl)acrylate (62)

1-Bromo-4,5-dimethoxy-2-nitrobenzene (1.00 g, 3.82 mmol), $Pd(OAc)_2$ (85 mg, 0.38 mmol) and PPh_3 (199 mg, 0.76 mmol) were dissolved in anhydrous DMF (30 mL). The solution was treated with ethyl acrylate (2.0 mL, 18.8 mmol) and Et_3N (1.1 mL, 7.89 mmol) and stirred under a N_2 atmosphere at 90°C overnight. The solvent was evaporated and the resulting residue was dissolved in DCM and extracted with 1M HCl (3 x 50 mL) and brine (1 x 50 mL). The organic phase was evaporated and the residue was purified by column chromatography (DCM) to give **62** as a bright yellow powder (1.07 g, 80%). R_f = 0.45 (DCM); R_t = 9.3 min (solvent system A); mp = 148 -150°C (lit.[275] 148°C); ^{1}H NMR ($CDCl_3$, 400 MHz) δ 1.35 (3H, t, J = 7.2, $CH_2C\underline{H}_3$), 3.98 (3H, s, OCH_3), 3.99 (3H, s, OCH_3), 4.29 (2H, q, J = 7.2, $C\underline{H}_2CH_3$), 6.29 (1H, d, J = 16.0, HC=C), 6.97 (1H, s, Ar), 7.63 (1H, s, Ar), 8.21 (1H, d, J = 16.0, HC=C); ^{13}C NMR ($CDCl_3$, 100 MHz) δ 14.21 (CH_3), 56.45 (OCH_3), 56.46 (OCH_3), 60.77 (CH_2), 107.88 (Ar), 109.92 (Ar), 121.99 (C=C), 125.20 (Ar), 140.64 (C=C), 141.14 (Ar), 149.83 (Ar), 153.10 (Ar), 165.90 (C=O).

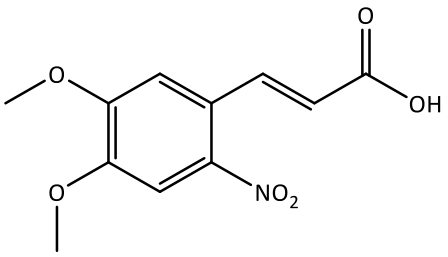

(*E*)-3-(4,5-Dimethoxy-2-nitrophenyl)acrylic acid (63)

A solution of **62** (850 mg, 3.02 mmol) in THF (16 mL) was treated with 1M NaOH (11 mL) and EtOH (4 mL) and the mixture was stirred at 40°C overnight. The organic solvents were evaporated and the remaining solution was diluted with H_2O (30 mL), the pH was adjusted to 2 with 6M HCl and the yellow precipitate that formed was filtered and dried to give **63** (675

mg, 88%). R_f = 0.39 (5% MeOH:DCM); R_t = 7.5 min (solvent system A); mp = 270-273°C (lit.[194] 286°C); ^{1}H NMR (DMSO-d_6, 400 MHz) δ 3.90 (3H, s, OCH_3), 3.97 (3H, s, OCH_3), 6.62 (1H, d, J = 16.0, HC=C), 7.36 (1H, s, Ar), 7.65 (1H, s, Ar), 7.93 (1H, d, J = 16.0, HC=C), 12.59 (1H, s, CO_2H); ^{13}C NMR (DMSO-d_6, 100 MHz) δ 56.24 (OCH_3), 56.49 (OCH_3), 107.83 (Ar), 110.38 (Ar), 122.70 (C=C), 123.67 (Ar), 138.94 (C=C), 141.20 (Ar), 149.56 (Ar), 152.78 (Ar), 167.14 (C=O).

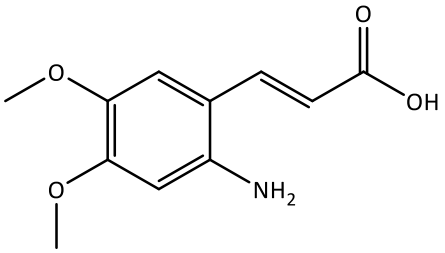

(*E*)-3-(2-Amino-4,5-dimethoxyphenyl)acrylic acid (64)[194]

A suspension of **63** (210 mg, 0.829 mmol) and $FeSO_4.7H_2O$ (2.38 g, 8.56 mmol) in H_2O (10 mL) was heated to 80 °C under stirring. 35% (aq.) NH_3 solution (3 mL) was added to the orange solution which immediately turned black. After stirring for 5 min, the heat was removed and the solution was allowed to stir for a further 2 h at RT. The reaction mixture was filtered through celite and acidified to pH 4 using 1M HCl, then extracted with EtOAc (4 x 30 mL). The organic phases were dried over Na_2SO_4, filtered, and the solvent was evaporated to give **64** as a dark yellow solid (150 mg, 81%). R_f = 0.60 (20% MeOH: DCM); R_t = 4.7 min (solvent system A); mp = 156-158 °C (lit.[194] 175- 177 °C); ^{1}H NMR (DMSO-d_6, 400 MHz) δ 3.73 (3H, s, OCH_3), 3.76 (3H, s, OCH_3), 5.33 (2H, s, NH_2), 6.20 (1H, d, J = 15.6, C=CH), 6.40 (1H, s, Ar), 7.01 (1H, s, Ar), 7.81 (1H, d, J = 15.6, C=CH), 11.89 (1H, s, OH); ^{13}C NMR (DMSO-d_6, 100 MHz) δ 55.14 (OCH_3), 56.12 (OCH_3), 100.33 (Ar), 109.20 (Ar), 110.14 (Ar), 112.92 (C=C), 139.88 (C=C), 140.99 (Ar), 144.11 (Ar), 152.53 (Ar), 168.37 (C=O).

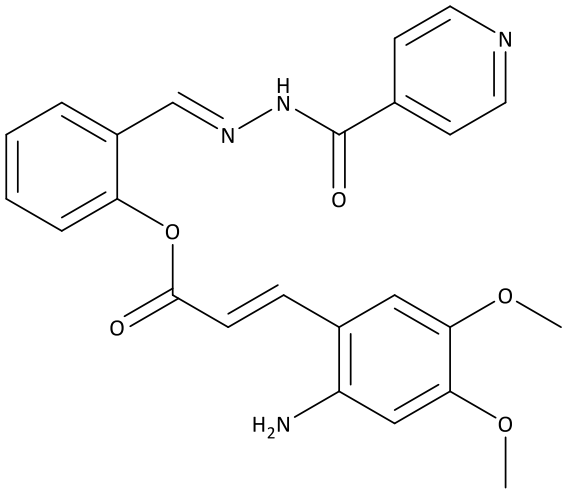

2-((*E*)-(2-Isonicotinoylhydrazono)methyl)phenyl (*E*)-3-(2-amino-4,5-dimethoxyphenyl) acrylate (65)

A stirred solution of **63** (50 mg, 0.22 mmol) in anhydrous DMF (2 mL) under N_2 was cooled to 0 ^oC and treated with DMAP (27 mg, 0.22 mmol) and EDC.HCl (42 mg, 0.22 mmol). The solution was allowed to stir for 10 min before a solution of **8** (48 mg, 0.20 mmol) and DIPEA (35 µL, 0.20 mmol) in anhydrous DMF (1 mL) was added. The temperature was increased to 30 ^oC and the reaction was stirred for 24 h. The solvent was then evaporated and the remaining residue was dissolved in DCM (10 mL) and extracted with sat. NH_4Cl (3 x 10 mL) and brine (3 x 10 mL). The organic phase was dried over $MgSO_4$, filtered and the solvent was evaporated to give a yellow residue. Purification by column chromatography, eluting with 2-8% MeOH in DCM + 0.1% pyridine gave a mixture of **8** and **65** as an orange solid which was dissolved in DCM (20 mL) and extracted with 2M aq. $FeSO_4.7H_2O$ (3 x 20 mL) and brine (3 x 20 mL). The solvent was evaporated to give **65** as a dark yellow solid (40 mg, 47%). R_f = 0.8 (5% MeOH: DCM); R_t = 6.2 min (solvent system A); mp = 110-115 ^oC; ^1H NMR (DMSO-d_6, 400 MHz) δ 3.78 (3H, s, OCH_3), 3.86 (3H, s, OCH_3), 5. 65 (2H, s, NH_2), 6.42 (1H, s, Ar), 6.62 (1H, d, J = 15.6, HC=C) 7.17 (1H, s, Ar), 7.30 (1H, d, J = 8.0, Ar), 7.44 (1H, t, J = 7.4, Ar), 7.59 (1H, t, J = 7.2, Ar), 7.86 (2H, d, J = 5.2, Pyr), 8.09 (1H, d, J = 7.2, Ar), 8.16 (1H, d, J = 15.6, HC=C), 8.63 (1H, s, HC=N), 8.82 (2H, br s, Pyr), 12.21 (1H, s, NH); ^{13}C NMR (DMSO-d_6, 125 MHz) δ 54.17 (OCH_3), 55.73 (OCH_3), 100.25 (Ar), 109.09 (Ar), 113.45 (Ar), 120.76 (Ar), 123.24 (Ar), 126.42 (Ar), 126.75 (C=C), 127.19 (Ar), 131.345 (Ar), 137.98 (Ar), 139.76 (Pyr), 140.09 (Pyr), 141.87 (Pyr), 143.35 (C=C), 143.95 (C=N), 149. 78 (Ar), 150.24 (Ar), 151.45 (Ar), 161.98 (C=O), 167.04 (C=O); [Found (ESI+) 469.1484 $[M+H]^+$, $C_{24}H_{23}N_4O_5Na$ requires 469.1488].

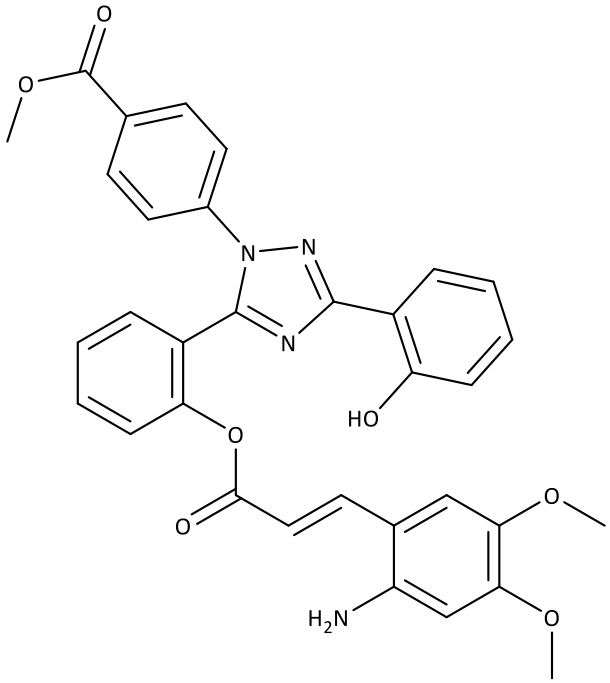

Methyl (*E*)-4-(5-(2-((3-(2-Amino-4,5-dimethoxyphenyl)acryloyl)oxy)phenyl)-3-(2-hydroxyphenyl)-1H-1,2,4-triazol-1-yl)benzoate (66)[100]

A stirred solution of **63** (38 mg, 0.17 mmol) in anhydrous DMF (2 mL) under N_2 was cooled to 0 ^oC and treated with DMAP (21 mg, 0.17 mmol) and EDC.HCl (33 mg, 0.17 mmol). The mixture was allowed to stir for 10 min before a solution of **33** (66 mg, 0.17 mmol) and DIPEA (30 µL, 0.17 mmol) in anhydrous DMF (1 mL) was added. The temperature was increased to 30 ^oC and the mixture was stirred for 24 h. The solvent was then evaporated and the remaining residue was dissolved in DCM (10 mL) and extracted with sat. NH_4Cl (3 x 10 mL) and brine (3 x 10 mL). The organic phase was dried over $MgSO_4$, filtered and the solvent was evaporated to give a residue which was purified by column chromatography, eluting with 0-4% acetone in DCM + 0.1% pyridine. This gave unchanged deferasirox methyl ester (27 mg, 41%) and **25** as a yellow residue (17 mg, 17%, 28% yield based on recovered deferasirox methyl ester). R_f = 0.85 (5% MeOH: DCM); R_t = 10.1 min (solvent system A); ^1H NMR ($CDCl_3$, 400 MHz) δ 3.80 (3H, s, OCH_3), 3.85 (3H, s, OCH_3), 3.93 (3H, s, CH_3), 6.07 (1H, d, J = 15.6, HC=C), 6.19 (1H, s, Ar), 6.92 (1H, td, J = 7.3, 1.2, Ar), 6.98 (1H, dd, J = 8.4, 0.8, Ar), 7.32 (4H, m, Ar), 7.57 (3H, m, Ar), 7.77 (1H, d, J = 15.6, HC=C), 8.06 (2H, d, J = 8.8, Ar), 8.12 (1H, dd, J = 7.6, 1.6, Ar), 11.00 (1H, s, OH). ^{13}C NMR ($CDCl_3$, 100 MHz) δ 52.33 (OCH_3), 55.79 (OCH_3), 56.30 ($CO_2\underline{C}H_3$), 100.60 (Ar), 110.09 (Ar), 110.91 (Ar), 112.00 (Ar), 113.51 (Ar), 117.21 (Ar), 119.53 (Ar), 120.87 (Ar), 123.71

(Ar), 124.04 (C=C), 125.83 (Ar), 126.85 (Ar), 130.20 (Ar), 130.73 (C=C), 130.88 (Ar), 131.41 (Ar), 132.09 (Ar), 140.93 (Ar), 142.16 (Ar), 142.37 (Ar), 142.66 (Ar), 149.20 (Ar), 150.04 (Ar), 153.20 (Tri), 156.98 (Ar), 161.24 (Tri), 165.08 (C=O), 165.96 (C=O); [Found (ESI+) 615.1837 $[M+H]^+$, $C_{33}H_{28}N_4O_7Na$ requires 615.1856].

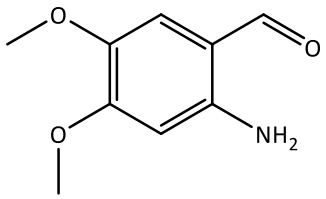

2-Amino-4,5-dimethoxybenzaldehyde (67)[194]

A suspension of 6-nitroveratraldehyde (500 mg, 2.37 mmol) and $FeSO_4.7H_2O$ (6.60 g, 23.7 mmol) in H_2O (20 mL) was heated to 80 ^oC under vigorous stirring. 35% (aq.) NH_3 solution (6 mL) was added to the orange solution which immediately turned black. After stirring for 5 min, the heat was removed and the solution was allowed to stir for a further 2 h at RT. The reaction mixture was filtered through celite and acidified to pH 4 using 1M HCl, then extracted with EtOAc (4 x 100 mL). The organic phases were dried over Na_2SO_4, filtered, and the solvent was evaporated to give **67** as an orange oil (325 mg, 76%). R_f = 0.75 (20% MeOH: DCM); R_t = 6.2 min (solvent system A); ^1H NMR ($CDCl_3$, 400 MHz) δ 3.77 (3H, s, OCH_3), 3.79 (3H, s, OCH_3), 6.06 (1H, s, Ar), 6.80 (1H, s, Ar), 6.61 (1H, d, J = 0.4, HC=O); ^{13}C NMR ($CDCl_3$, 100 MHz) δ 55.82 (OCH_3), 56.44 (OCH_3), 98.34 (Ar), 111.20 (Ar), 116.02 (Ar), 140.88 (Ar), 147.36 (Ar), 156.14 (Ar), 191.26 (C=O).

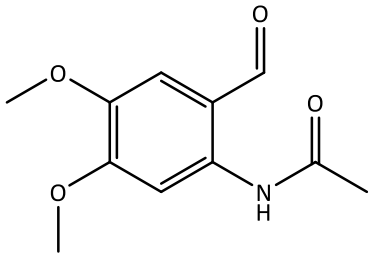

N-(2-Formyl-4,5-dimethoxyphenyl)acetamide (68)[198]

A solution of **67** (210 mg, 1.16 mmol) and Et_3N (195 µL, 1. 39 mmol) in anhydrous DCM (4 mL) was treated dropwise with acetyl chloride (100 µL, 1.39 mmol). The reaction was stirred under N_2 at RT for 30 min and then quenched with H_2O (20 mL), before extraction with sat. NH_4Cl (3

x 20 mL) and brine (3 x 20 mL). The organic phase was dried over Na_2SO_4, filtered and the solvent was evaporated to give **68** as a bright yellow solid (205 mg, 81%). R_f = 0.80 (3% MeOH: DCM); R_t = 6.8 min (solvent system A), mp = 174-178 °C (lit.[276] 178 -179 °C); ^{1}H NMR ($CDCl_3$, 400 MHz) δ 2.22 (3H, s, CH_3), 3.89 (3H, s, OCH_3), 3.97 (3H, s, OCH_3), 7.01 (1H, s, Ar), 8.45 (1H, s, Ar), 9.73 (1H, s, HC=O), 11.29 (1H, br s, NH); ^{13}C NMR ($CDCl_3$, 100 MHz) δ 25.32 (CH_3), 56.21 (OCH_3), 56.35 (OCH_3), 102.94 (Ar), 114.36 (Ar), 116.45 (Ar), 137.62 (Ar), 144.39 (Ar), 155.57 (Ar), 169.63 (C=O), 191.26 (C=O).

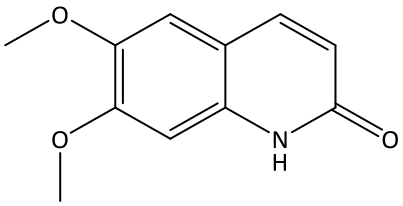

6,7-Dimethoxyquinolin-2(1H)-one (69)

Method A[198]:

A stirred mixture of **68** (122 mg, 0.56 mmol) and Cs_2CO_3 (920 mg, 2.8 mmol) in anhydrous DMF (5 mL) was heated to 60 °C under N_2 for 22 h. The solvent was evaporated and the remaining residue was dissolved in DCM (30 mL) and extracted with sat. NH_4Cl (3 x 30 mL), H_2O (3 x 30 mL) and brine (3 x 30 mL). The organic phase was dried over Na_2SO_4, filtered, and then the solvent was evaporated to give an orange residue which was purified by column chromatography eluting with 2-4% MeOH in DCM + 0.1% pyridine. This gave **69** as a pale yellow powder (11 mg, 10%).

Method B[194]:

A solution of **64** (55 mg, 0.25 mmol) and 4% HCl (2 mL) was heated to reflux and stirred for 2 h. The reaction was cooled in an ice bath and 1% (aq.) NH_3 solution (5 mL) was added, then extracted with DCM (3 x 10 mL). The organic phases were combined and extracted with brine (2 x 30 mL) and dried over Na_2SO_4, filtered and the solvent was evaporated to give **69** as a pale yellow solid (40 mg, 78%). R_f = 0.4 (5% MeOH: DCM); R_t = 5.7 min (solvent system A), mp

= 222-225 °C (lit[194] 229 °C); UV (EtOH) λ_{max} 214 (5575), 237 (4888), 344 (1890); ^{1}H NMR (DMSO-d_6, 400 MHz) δ 3.79 (3H, s, OCH_3), 3.82 (3H, s, OCH_3), 6.32 (1H, d, J = 7.6, Ar), 6.87 (1H, s, Ar), 7.19 (1H, s, Ar), 7.78 (1H, d, J = 7.6, Ar), 11.51 (1H, br s, NH); ^{13}C NMR (DMSO-d_6, 100 MHz) δ 55.52 (OCH_3), 55.73 (OCH_3), 97.67 (Ar), 108.86 (Ar), 112.26 (Ar), 118.72 (Ar), 134.52 (Ar), 139.64 (Ar), 144.69 (Ar), 151.81 (Ar), 161.78 (C=O); [Found (ESI+) 206.0831 $[M+H]^+$, $C_{11}H_{11}NO_3$ requires 206.0817].

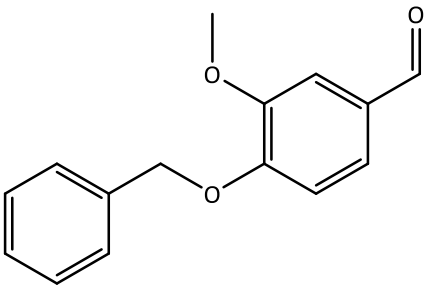

4-(Benzyloxy)-3-methoxybenzaldehyde (76)[209]

A mixture of vanillin (2.17 g, 14.27 mmol) and K_2CO_3 (2.37 g, 17.13 mmol) in MeOH (20 mL) was treated with benzyl bromide (2.03 mL, 17.13 mmol) and stirred at reflux for 4 h. After cooling, the solvent was evaporated and the residue was dissolved in $CHCl_3$ (40 mL). The organic phase was extracted with H_2O (3 x 40 mL) and brine (40 mL) and evaporated to give a yellow solid which was recrystallized from EtOH to give **76** as white needles (3.04 g, 93%). R_f = 0.39 (DCM); R_t = 8.7 min (solvent system A); mp = 59- 61°C (lit.[277] 58-60°C); ^{1}H NMR ($CDCl_3$, 400 MHz) δ 3.90 (3H, s, OCH_3), 5.20 (2H, s, CH_2), 6.94 (1H, d, J= 8.0, Ar), 7.25-7.40 (7H, m, Ar), 9.79 (1H, s, HC=O); ^{13}C NMR ($CDCl_3$, 100 MHz) δ 56.00 (OCH_3), 70.84 (CH_2), 109.43 (Ar), 112.43 (Ar), 126.43 (Ar), 127.12 (Ar), 128.12 (Ar), 128.64 (Ar), 130.30 (Ar), 135.98 (Ar), 150.07 (Ar), 153.57 (Ar), 190.75 (C=O).

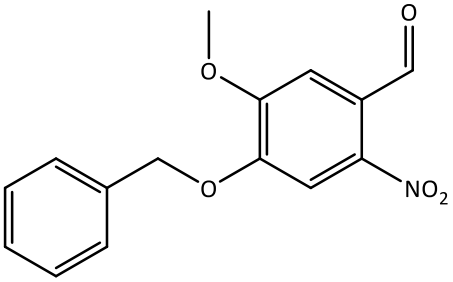

4-(Benzyloxy)-5-methoxy-2-nitrobenzaldehyde (77)[278]

65% (aq.) nitric acid (35 mL) was added slowly to **76** (2.80 g, 11.57 mmol) at 0°C and the resulting suspension was stirred for 1 h. The suspension was filtered and washed with H_2O and then recrystallized from EtOAc to give **77** as bright yellow crystals (1.99 g, 60%). R_f = 0.63 (DCM); R_t = 9.7 min (solvent system A); mp = 133°C (lit.[279] 132-133°C); ^{1}H NMR ($CDCl_3$, 400 MHz) δ 3.97 (3H, s, OCH_3), 5.22 (2H, s, CH_2), 7.29-7.42 (6H, m, Ar), 7.62 (1H, s, Ar), 10.39 (1H, s, HC=O); ^{13}C NMR ($CDCl_3$, 100 MHz) δ 56.64 (OCH_3), 71.52 (CH_2), 108.90 (Ar), 109.99 (Ar), 125.68 (Ar), 127.48 (Ar), 128.62 (Ar), 128.82 (Ar), 134.79 (Ar), 144.91 (Ar), 151.37 (Ar), 153.57 (Ar), 190.75 (C=O); [Found (ESI+) 310.0686. $[M+H]^+$, $C_{15}H_{13}NNaO_5$ requires 310.0691].

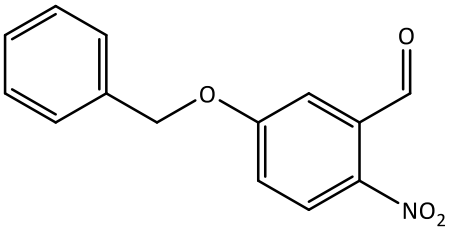

5-(Benzyloxy)-2-nitrobenzaldehyde (78)[209]

A mixture of 5-hydroxy-2-nitrobenzaldehyde (500 mg, 2.99 mmol) and K_2CO_3 (496 mg, 3.59 mmol) in MeOH (10 mL) was treated with benzyl bromide (430 µL, 3.62 mmol) and stirred at reflux for 4 h. After cooling, the solvent was evaporated and the residue was dissolved in $CHCl_3$ (30 mL). The organic phase was extracted with H_2O (3 x 30 mL) and brine (40 mL) and the solvent was evaporated to give a yellow solid which was recrystallized from EtOAc:hexane to give **78** as beige needles (580 mg, 80%). R_f = 0.84 (DCM); R_t = 9.8 min (solvent system A); mp = 73- 75°C (lit.[280] 70-72°C); ^{1}H NMR ($CDCl_3$, 400 MHz) δ 5.21 (2H, s, CH_2), 7.21 (1H, dd, J=

9.0, 3.0, Ar), 7.37-7.43 (6H, m, Ar), 8.15 (1H, d, J = 9.2, Ar), 10.47 (1H, s, HC=O); ^{13}C NMR ($CDCl_3$, 100 MHz) δ 71.02 (CH_2), 114.14 (Ar), 119.26 (Ar), 127.23 (Ar), 127.53 (Ar), 128.65 (Ar), 128.82 (Ar), 134.24 (Ar), 134.85 (Ar), 142.43 (Ar), 163.01 (Ar), 188.37 (C=O).

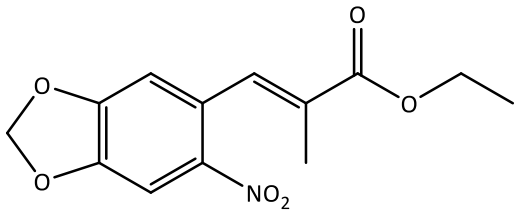

Ethyl (*E*)-2-methyl-3-(6-nitrobenzo[*d*][1,3]dioxol-5-yl)acrylate (79)[281]

A mixture of 2-nitropiperonal (1.50 g, 7.69 mmol) and ECETP (3.34 g, 9.22 mmol) in anhydrous toluene (60 mL) was stirred at 65°C under an argon atmosphere for 18 h. The solvent was evaporated and the resulting residue was purified by column chromatography (DCM) to give **79** as a bright yellow solid (2.13 g, 99%). R_f = 0.49 (DCM); R_t = 9.57 min (solvent system A); mp= 119-122°C (lit.[281] 115-117°C); ^{1}H NMR ($CDCl_3$, 400 MHz) δ 1.30 (3H, t, J = 8.0, $CH_2C\underline{H}_3$), 1.85 (3H, s, CH_3), 4.23 (2H, q, J = 8.0, $C\underline{H}_2CH_3$), 6.11 (2H, s, OCH_2O), 6.66 (1H, s, Ar), 7.60 (1H, s, Ar), 7.79 (1H, s, HC=C); ^{13}C NMR ($CDCl_3$, 100 MHz) δ 13.92 (CH_3), 14.19 (CH_3), 61.00 (CH_2), 103.13 (CH_2), 105.57 (Ar), 109.65 (Ar), 128.66 (C=C), 129.60 (Ar), 136.00 (C=C), 141.93 (Ar), 147.73 (Ar), 151.71 (Ar), 167.57 (C=O).

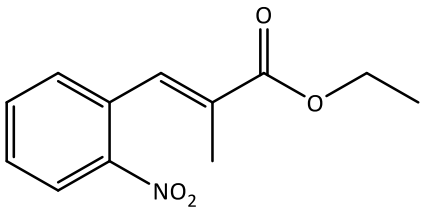

Ethyl (*E*)-2-methyl-3-(2-nitrophenyl)acrylate (80)[281]

A mixture of 2-nitrobenzaldehyde (1.00 g, 6.62 mmol) and ECETP (2.88 g, 7.94 mmol) in anhydrous toluene (40 mL) was stirred at 65°C under an argon atmosphere for 5 h. The solvent was evaporated and the resulting residue was purified by column chromatography (DCM) to give **80** as a yellow oil (1.55 g, 99%). R_f = 0.6 (DCM); R_t = 9.7 min (solvent system A); ^{1}H NMR

($CDCl_3$, 400 MHz) δ 1.29 (3H, t, J = 7.2, $CH_2C\underline{H}_3$), 1.83 (3H, s, CH_3), 4.22 (2H, q, J = 7.2, $C\underline{H}_2CH_3$), 7.30 (1H, dd, J = 7.6, 1.2, Ar), 7.44 (1H, td, J = 7.2, 1.6, Ar), 7.59 (1H, td, J = 7.6, 1.2, Ar), 7.83 (1H, s, HC=C), 8.06 (1H, dd, J = 8.4, 1.2, Ar); ^{13}C NMR ($CDCl_3$, 100 MHz) δ 13.85 (CH_3), 14.16 (CH_3), 61.00 (CH_2), 124.71 (Ar), 128.84 (C=C), 130.45 (Ar), 131.21 (Ar), 131.83 (Ar), 133.13 (Ar), 135.21 (C=C), 147.74 (Ar), 167.47 (C=O).

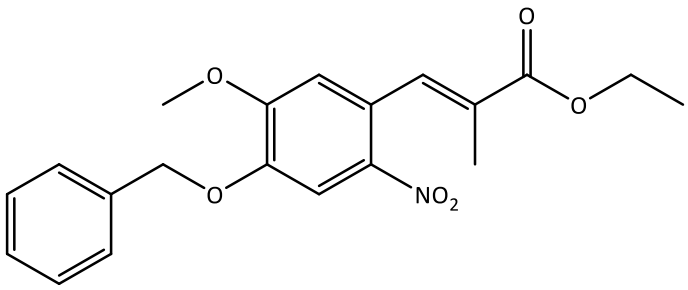

Ethyl (*E*)-3-(4-(benzyloxy)-5-methoxy-2-nitrophenyl)-2-methylacrylate (81)

A solution of **77** (1.65 g, 5.74 mmol) and ECETP (2.50 g, 6.89 mmol) in anhydrous toluene (50 mL) was stirred at 65°C under an argon atmosphere for 4 h. The solvent was evaporated and the resulting residue was purified by column chromatography (DCM) to give **81** as a bright yellow solid (2.09 g, 98%). R_f = 0.48 (DCM); R_t = 10.7 min (solvent system A); mp= 129-131°C; ^1H NMR ($CDCl_3$, 400 MHz) δ 1.35 (3H, t, J = 7.0, $CH_2C\underline{H}_3$), 1.92 (3H, d, J = 1.6, CH_3), 3.95 (3H, s, OCH_3), 4.29 (2H, q, J = 7.0, $C\underline{H}_2CH_3$), 5.22 (2H, s, CH_2), 6.73 (1H, s, Ar), 7.35-7.48 (5H, m, Ar), 7.80 (1H, s, Ar), 7.91 (1H, q, J = 0.7, HC=C); ^{13}C NMR ($CDCl_3$, 100 MHz) δ 14.03 (CH_3), 14.21 (CH_3), 56.64 (OCH_3), 60.97 (CH_2), 71.28 (CH_2), 109.79 (Ar), 112.56 (Ar), 126.80 (Ar), 127.53 (Ar), 128.39 (C=C), 128.71 (Ar), 129.34 (Ar), 135.46 (Ar), 136.39 (C=C), 140.08 (Ar), 147.54 (Ar), 153.47 (Ar), 167.70 (C=O); [Found (ESI+) 372.1461 $[M+H]^+$, $C_{20}H_{22}NO_6$ requires 372.1442].

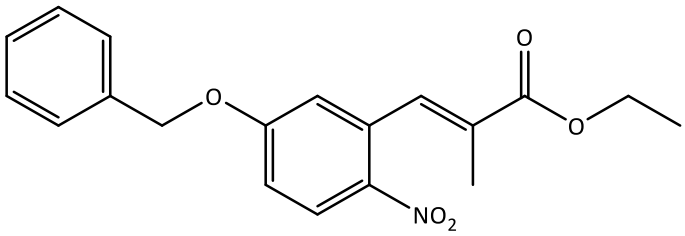

Ethyl (*E*)-3-(5-(benzyloxy)-2-nitrophenyl)-2-methylacrylate (82)

A solution of **78** (312 mg, 1.29 mmol) and ECETP (570 mg, 1.57 mmol) in anhydrous toluene (20 mL) was stirred at 65°C under an argon atmosphere for 3 h. The solvent was evaporated and the resulting residue was purified by column chromatography (DCM) to give **82** as a yellow oil (429 mg, 98%). R_f = 0.64 (DCM); R_t = 10.88 min (solvent system A); ^{1}H NMR ($CDCl_3$, 400 MHz) δ 1.35 (3H, t, J = 7.2, $CH_2C\underline{H}_3$), 1.81 (3H, d, J = 1.6, CH_3), 4.28 (2H, q, J = 7.2, $C\underline{H}_2CH_3$), 5.17 (2H, s, CH_2), 6.81 (1H, dd, J = 2.8, 0.8, Ar), 7.02 (1H, dd, J = 9.2, 2.8, Ar), 7.36-7.42 (5H, m, Ar), 7.91 (1H, q, J = 0.8, HC=C), 8.19 (1H, d, J = 9.2, Ar); ^{13}C NMR ($CDCl_3$, 100 MHz) δ 13.81 (CH_3), 14.21 (CH_3), 61.04 (CH_2), 70.65 (CH_2), 114.62 (Ar), 116.82 (Ar), 127.30 (Ar), 127.48 (Ar), 128.49 (Ar), 128.80 (Ar), 129.77 (C=C), 134.67 (Ar), 135.29 (Ar), 136.09 (C=C), 140.77 (Ar), 162.11 (Ar), 167.60 (C=O); [Found (ESI+) 342.1349 $[M+H]^+$, $C_{19}H_{20}NO_5$ requires 342.1336].

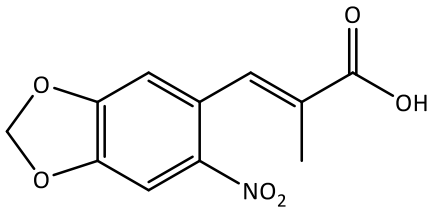

(*E*)-2-Methyl-3-(6-nitrobenzo[*d*][1,3]dioxol-5-yl)acrylic acid (83)

A solution of **79** (1.50 g, 5.37 mmol) in THF (30 mL) was treated with 1M NaOH (19 mL) and EtOH (8 mL) and the mixture was stirred at 40°C for 3 h. The organic solvents were evaporated and the remaining solution was diluted with H_2O (30 mL), the pH adjusted to 2 with 6M HCl, and the aqueous phase was extracted with EtOAc (3 x 100 mL). The combined organic layers were extracted with brine (100 mL) then dried over $MgSO_4$, filtered and the solvent was evaporated to give a pale peach powder (1.34 g, 99%). R_f = 0.63 (10% MeOH:DCM); R_t = 7.83 min (solvent system A); mp= 197-202°C; ^{1}H NMR (DMSO-d_6, 400

MHz) δ 1.82 (3H, s, CH_3), 6.29 (2H, s, CH_2), 7.07 (1H, s, Ar), 7.69 (1H, s, HC=C), 7.76 (1H, s, Ar), 12.64 (1H, s, CO_2H); ^{13}C NMR (DMSO-d_6, 100 MHz) δ 13.72 (CH_3), 103.67 (CH_2), 105.07 (Ar), 109.63 (Ar), 127.89 (C=C), 129.63 (Ar), 135.28 (C=C), 141.56 (Ar), 147.67 (Ar), 151.80 (Ar), 168.47 (C=O); [Found (ESI+) 274.0331 $[M+Na]^+$, $C_{11}H_9NNaO_6$ requires 274.0322].

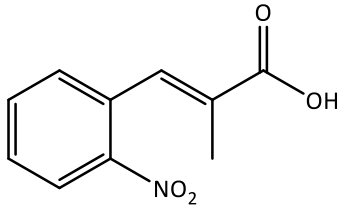

(*E*)-2-Methyl-3-(2-nitrophenyl)acrylic acid (84)

A solution of **80** (1.51 g, 6.42 mmol) in THF (32 mL) was treated with 1M NaOH (22 mL) and EtOH (8 mL) and the mixture was stirred at 40°C for 2 h. The organic solvents were evaporated and the remaining solution was diluted with H_2O (30 mL), the pH adjusted to 2 with 6M HCl and the aqueous phase was extracted with EtOAc (3 x 50 mL). The combined organic layers were extracted with brine (50 mL), then dried over $MgSO_4$, filtered and the solvent was evaporated to give **84** as a pale yellow solid (1.35 g, 99%). R_f = 0.51 (5% MeOH:DCM); R_t = 7.80 min (solvent system A); mp= 191-195°C (lit.[282] 196-196.5°C); ^1H NMR (DMSO-d_6, 400 MHz) δ 1.82 (3H, s, CH_3), 7.55 (1H, d, J = 7.6, Ar), 7.66 (1H, t, J = 7.6, Ar), 7.76 (1H, s, HC=C), 7.82 (1H, t, J = 7.6, Ar), 8.16 (1H, d, J = 8.0, Ar), 12.71 (1H, s, CO_2H); ^{13}C NMR (DMSO-d_6, 100 MHz) δ 13.72 (CH_3), 124.58 (Ar), 129.46 (C=C), 130.51 (Ar), 130.89 (Ar), 131.32 (Ar), 133.74 (Ar), 134.50 (C=C), 147.54 (Ar), 168.47 (C=O).

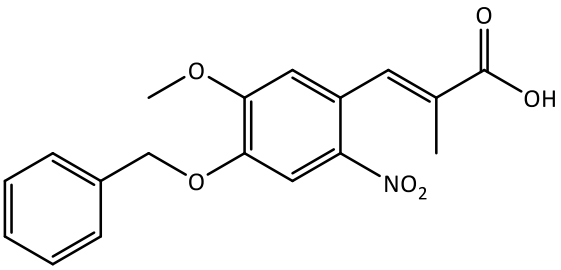

(*E*)-3-(4-(Benzyloxy)-5-methoxy-2-nitrophenyl)-2-methylacrylic acid (85)

A solution of **81** (940 mg, 2.53 mmol) in THF (20 mL) was treated with 1M NaOH (10 mL) and EtOH (5 mL) and the mixture was stirred at 40°C overnight. The organic solvents were evaporated and the remaining solution was diluted with H_2O (30 mL), the pH adjusted to 2 with 6M HCl and the aqueous phase was extracted with EtOAc (3 x 40 mL). The combined organic layers were extracted with brine (50 mL) and dried over $MgSO_4$, then filtered and the solvent evaporated to give a pale yellow solid (824 mg, 95%). R_f = 0.36 (5% MeOH:DCM); R_t = 9.41 min (solvent system A); mp= 167-170°C; ^{1}H NMR (DMSO-d_6, 400 MHz) δ 1.86 (3H, d, J = 1.6, CH_3), 3.93 (3H, s, OCH_3), 5.25 (2H, s, CH_2), 7.02 (1H, s, Ar), 7.35-7.50 (5H, m, Ar), 7.78 (1H, q, J = 0.8, HC=C), 7.86 (1H, s, Ar), 12.62 (1H, br s, CO_2H); ^{13}C NMR (DMSO-d_6, 100 MHz) δ 13.83 (CH_3), 56.53 (OCH_3), 70.39 (CH_2), 109.26 (Ar), 113.10 (Ar), 126.01 (Ar), 127.97 (Ar), 128.14 (C=C), 128.49 (Ar), 129.50 (Ar), 135.49 (Ar), 136.09 (C=C), 139.69 (Ar), 147.16 (Ar), 153.18 (Ar), 168.73 (C=O); [Found (ESI+) 366.1032 $[M+Na]^+$, $C_{18}H_{17}NNaO_6$ requires 366.0948].

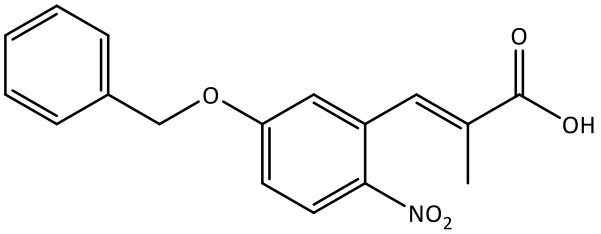

(*E*)-3-(5-(Benzyloxy)-2-nitrophenyl)-2-methylacrylic acid (86)

A solution of **82** (396 mg, 1.16 mmol) in THF (10 mL) was treated with 1M NaOH (5 mL) and EtOH (3 mL) and the mixture was stirred at 40°C for 3 h. The organic solvents were evaporated and the remaining solution was diluted with H_2O (20 mL), the pH adjusted to 2 with 6M HCl, and the aqueous phase was extracted with EtOAc (3 x 30 mL). The combined organic layers

were extracted with brine (40 mL) and dried over $MgSO_4$, then filtered and the solvent was evaporated to give a pale yellow solid (326 mg, 90%). R_f = 0.35 (5% MeOH:DCM); R_t = 9.46 min (solvent system A); mp = 175-180°C; ^{1}H NMR (DMSO-d_6, 400 MHz) δ 1.74 (3H, d, J = 1.6, CH_3), 5.30 (2H, s, CH_2), 7.04 (1H, dd, J = 2.8, 0.8, Ar), 7.24 (1H, dd, J = 9.2, 2.8, Ar), 7.36-7.49 (5H, m, Ar), 7.78 (1H, q, J = 0.8, HC=C), 8.21 (1H, d, J = 9.2, Ar), 12.72 (1H, br s, CO_2H); ^{13}C NMR (DMSO-d_6, 100 MHz) δ 13.63 (CH_3), 70.13 (CH_2), 115.31 (Ar), 116.71 (Ar), 127.44 (Ar), 127.79 (Ar), 128.14 (Ar), 128.54 (Ar), 129.82 (C=C), 134.04 (Ar), 135.43 (Ar), 135.94 (C=C), 140.30 (Ar), 161.99 (Ar), 168.60 (C=O); [Found (ESI+) 336.0864 $[M+Na]^+$, $C_{17}H_{15}NNaO_5$ requires 336.0842].

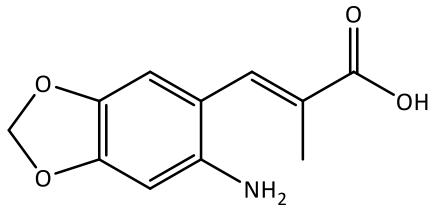

(*E*)-3-(6-Aminobenzo[*d*][1,3]dioxol-5-yl)-2-methylacrylic acid (87)

A suspension of **83** (590 mg, 2.35 mmol) and FeSO4.7H2O (6.67 g, 24.00 mmol) in H_2O (20 mL) was heated to 80°C under stirring. 35% (aq.) NH_3 solution (7 mL) was added. After stirring for 5 min, the heat was removed and the mixture was allowed to stir for a further 3 h at RT. Then the reaction mixture was filtered through celite and acidified to pH 3 using 1M HCl. The aqueous phase was extracted with EtOAc (3 x 100 mL) and brine (100 mL). The organic phases were dried over Na_2SO_4, filtered, and the solvent was evaporated to give **87** as a bright yellow solid (442 mg, 85%). R_f = 0.53 (10% MeOH: DCM); R_t = 5.08 min (solvent system A); mp = 197-200°C; ^{1}H NMR (DMSO-d_6, 400 MHz) δ 1.95 (3H, d, J = 1.2, CH_3), 4.95 (2H, br s, NH_2), 5.89 (2H, s, CH_2), 6.39 (1H, s, Ar), 6.69 (1H, s, Ar), 7.46 (1H, s, HC=C) 12.14 (1H, br s, CO_2H); ^{13}C NMR (DMSO-d_6, 100 MHz) δ 14.23 (CH3), 96.83 (CH_2), 100.35 (Ar), 108.25 (Ar), 111.38 (Ar), 125.50 (C=C), 134.69 (Ar), 138.23 (Ar), 143.46 (C=C), 148.31 (Ar), 169.44 (C=O). [Found (ESI-) 220.0628 $[M-H]^-$, $C_{11}H_{10}NO_4$ requires 220.0610].

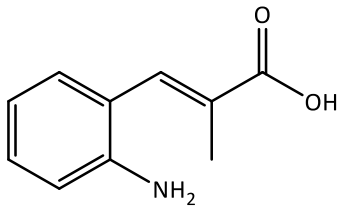

(*E*)-3-(2-Aminophenyl)-2-methylacrylic acid (88)

A suspension of **84** (1.34 g, 6.47 mmol) and FeSO4.7H2O (18.1 g, 65.0 mmol) in H_2O (60 mL) was heated to 80°C under stirring. 35% (aq.) NH_3 solution (20 mL) was added. After stirring for 5 min, the heat was removed and the mixture was allowed to stir for a further 2.5 h at RT. Then the reaction mixture was filtered through celite and acidified to pH 3 using 1M HCl then it was extracted with EtOAc (3 x 150 mL). The organic phases were dried over Na_2SO_4, filtered, and the solvent was evaporated to give **88** as a peach-coloured solid (1.07 g, 71%). R_f = 0.46 (10% $_i$PrOH:DCM); R_t = 5.20 min (solvent system A); mp = 143-145°C; ^{1}H NMR (DMSO-d_6, 400 MHz) δ 1.92 (3H, s, CH_3), 5.08 (2H, br s, NH_2), 6.58 (1H, t, J = 8.0, Ar), 6.71 (1H, d, J = 8.0, Ar), 7.04 (2H, m, Ar), 7.51 (1H, s, HC=C) 12.29 (1H, br s, CO_2H); ^{13}C NMR (DMSO-d_6, 100 MHz) δ 14.20 (CH3), 115.15 (Ar), 115.66 (Ar), 119.64 (Ar), 127.91 (C=C), 129.19 (Ar), 129.35 (Ar), 134.98 (C=C), 146.89 (Ar), 169.44 (C=O). [Found (ESI-) 176.0727 $[M-H]^-$, $C_{10}H_{10}NO_2$ requires 176.0712].

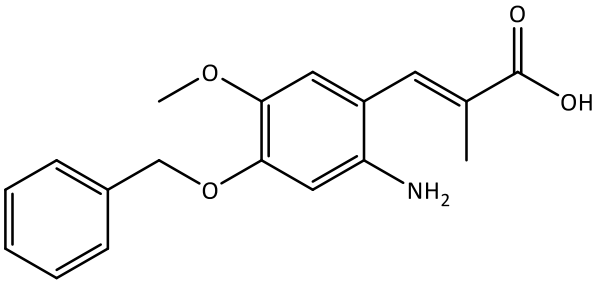

(*E*)-3-(2-Amino-4-(benzyloxy)-5-methoxyphenyl)-2-methylacrylic acid (89)

A suspension of **85** (1.18 g, 3.44 mmol) and $FeSO_4.7H_2O$ (9.56 g, 34.4 mmol) in H_2O (60 mL) was heated to 80°C under stirring. 35% (aq.) NH_3 solution (20 mL) was added. After stirring for 5 min, the heat was removed and the mixture was allowed to stir for 2.5 h at RT. Then the reaction mixture was filtered through celite and acidified to pH 3 using 1M HCl. The aqueous

phase was extracted with EtOAc (3 x 80 mL) and brine (100 mL). The organic phases were dried over Na2SO4, filtered, and the solvent was evaporated to give a residue which was purified by column chromatography eluting with 0-10% MeOH in DCM to give the product as a yellow solid (640 mg, 59%). R_f = 0.54 (10% MeOH: DCM); R_t = 6.79 min (solvent system A); mp = 127-131^oC; ^1H NMR (DMSO-d_6, 400 MHz) δ 1.98 (3H, d, J = 1.6, CH_3), 3.67 (3H, s, OCH_3), 4.85 (2H, br s, NH_2), 5.03 (2H, s, CH_2), 6.51 (1H, s, Ar), 6.74 (1H, s, Ar), 7.33-7.47 (5H, m, Ar), 7.50 (1H, s, HC=C), 12.14 (1H, br s, CO_2H); ^{13}C NMR (DMSO-d_6, 100 MHz) δ 14.31 (CH_3), 56.69 (OCH_3), 69.56 (CH_2), 101.64 (Ar), 111.55 (Ar), 114.79 (Ar), 125.38 (Ar), 127.71 (Ar), 127.80 (C=C), 128.37 (Ar), 134.62 (Ar), 136.99 (C=C), 140.11 (Ar), 142.52 (Ar), 149.74 (Ar), 169.69 (C=O); [Found (ESI-) 312.1243 $[M-H]^-$, $C_{18}H_{18}NO_4$ requires 312.1236].

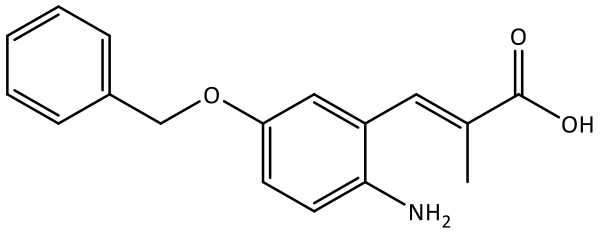

(*E*)-3-(2-Amino-5-(benzyloxy)phenyl)-2-methylacrylic acid (90)

A suspension of **86** (318 mg, 1.02 mmol) and $FeSO_4.7H_2O$ (2.84 g, 10.20 mmol) in H_2O (20 mL) was heated to 80^oC under stirring. 35% (aq.) NH_3 solution (7 mL) was added. After stirring for 5 min, the heat was removed and the mixture was allowed to stir for a further 20 h at RT. The reaction mixture was filtered through celite and acidified to pH 3 using 1M HCl. The aqueous phase was extracted with EtOAc (3 x 100 mL) and the combined organic phases were extracted with brine (100 mL), then dried over Na_2SO_4, filtered, and the solvent was evaporated to give **90** as a bright yellow solid (230 mg, 80%). R_f = 0.53 (10% MeOH:DCM); R_t = 6.73 min (solvent system A); mp= 118-123^oC; ^1H NMR (DMSO-d_6, 400 MHz) δ 1.86 (3H, d, J = 1.6, CH_3), 4.82 (2H, br s, NH_2), 5.00 (2H, s, CH_2), 6.67 (1H, d, J = 8.8, Ar), 6.70 (1H, d, J = 2.8, Ar), 6.81 (1H, dd, J = 8.8, 2.8, Ar), 7.29-7.43 (5H, m, Ar), 7.48 (1H, s, HC=C), 12.21 (1H, br s, CO_2H); ^{13}C NMR (DMSO-d_6, 100 MHz) δ 14.10 (CH_3), 69.80 (CH_2), 115.34 (Ar), 116.41 (Ar), 117.23 (Ar), 120.40 (Ar), 127.50 (Ar), 127.56 (Ar), 128.03 (C=C), 128.30 (Ar), 134.80 (Ar),

137.63 (Ar), 141.20 (C=C), 149.11 (Ar), 169.41 (C=O). [Found (ESI-) 282.1131 $[M-H]^-$, $C_{17}H_{16}NO_3$ requires 282.1136].

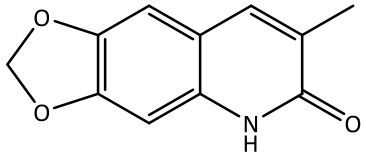

7-Methyl-[1,3]dioxolo[4,5-*g*]quinolin-6(5*H*)-one (91)

A solution of **87** (105 mg, 0.47 mmol) and 4% (aq.) HCl (6 mL) was heated to reflux and stirred overnight. After cooling, the solution was diluted with H_2O (10 mL) and extracted with DCM (4 x 20 mL) and brine (50 mL). The combined organic phases were evaporated to give **91** as a cream solid (38 mg, 57%). R_f = 0.63 (10% MeOH: DCM); R_t = 6.65 min (solvent system A); mp= 202-209°C; UV (EtOH) λ_{max} 212 (4433), 236 (2384), 343 (930); ^{1}H NMR (DMSO-d_6, 400 MHz) δ 2.04 (3H, d, J = 1.2, CH_3), 6.06 (2H, s, CH_2), 6.87 (1H, s, Ar), 7.09 (1H, s, Ar), 7.63 (1H, d, J = 1.2, Ar), 11.67 (1H, br s, NH); ^{13}C NMR (DMSO-d_6, 100 MHz) δ 16.32 (CH_3), 94.91 (CH_2), 99.48 (Ar), 101.43 (Ar), 104.58 (Ar), 113.56 (Ar), 134.43 (Ar), 136.26 (Ar), 142.90 (Ar), 148.85 (Ar), 164.31 (C=O); [Found (ESI+) 226.0467. $[M+H]^+$, $C_{11}H_9NNaO_3$ requires 226.0480].

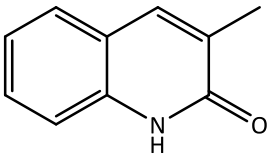

3-Methylquinolin-2(1*H*)-one (92)

***Method A:*[194]**

A solution of **88** (178 mg, 1.00 mmol) and 4% (aq.) HCl (8 mL) was heated to reflux and stirred overnight. No conversion of starting material was observed by TLC or HPLC analysis.

Method B:

A solution of **88** (89 mg, 0.50 mmol) and 70% (aq.) H_2SO_4 (4 mL) was heated to reflux overnight. The pH was adjusted 10 with 35% (aq.) NH_3 solution then the solution was extracted with DCM (3 x 15 mL) and brine (30 mL). The solvent was evaporated to give **92** as a white solid (20 mg, 25%). R_f = 0.55 (10% MeOH: DCM); R_t = 6.75 min (solvent system A); mp= 232-238°C (lit.[283] 226-228°C); UV (EtOH) λ_{max} 214 (2701), 269 (507), 323 (566); ^{1}H NMR ($CDCl_3$, 400 MHz) δ 2.25 (3H, s, CH_3), 7.14 (1H, t, J= 8.0, Ar), 7.30 (1H, d, J = 8.0, Ar), 7.40 (1H, t, J = 8.0, Ar), 7.45 (1H, d, J = 8.0, Ar), 7.60 (1H, s, Ar), 11.35 (1H, br s, NH); ^{13}C NMR ($CDCl_3$, 100 MHz) δ 16.74 (CH_3), 115.38 (Ar), 120.26 (Ar), 122.33 (Ar), 126.81 (Ar), 129.18 (Ar), 130.13 (Ar), 137.28 (Ar), 137.41 (Ar), 164.31 (C=O); [Found (ESI+) 160.0767 $[M+H]^+$, $C_{10}H_{10}NO$ requires 160.0762].

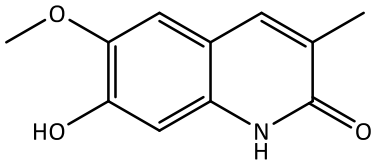

7-Hydroxy-6-methoxy-3-methylquinolin-2(1*H*)-one (93)

Method A:[194]

A solution of **89** (63 mg, 0.20 mmol) in 4% (aq.) HCl (4 mL) was heated to reflux and stirred for 2 h. After cooling, the solution was diluted with H_2O (10 mL) and the solvent was evaporated. The resulting oil was purified by column chromatography (5-10% MeOH:DCM) to give **93** as a brown oil (31 mg, 76%). R_f = 0.20 (10% MeOH: DCM); R_t = 4.3 min (solvent system A); UV (EtOH) λ_{max} 214 (12073), 235 (7559), 341 (4710); ^{1}H NMR (DMSO-d_6, 400 MHz) δ 1.98 (3H, d, J = 1.2, CH_3), 3.65 (3H, s, OCH_3), 6.29 (1H, s, Ar), 6.69 (1H, s, Ar), 7.50 (1H, d, J = 1.2, Ar), 9.18 (1H, br s, NH); ^{13}C NMR (DMSO-d_6, 100 MHz) δ 14.36 (CH_3), 56.61 (OCH_3), 103.62 (Ar), 110.83 (Ar), 114.60 (Ar), 124.34 (Ar), 134.81 (Ar), 139.40 (Ar), 142.15 (Ar), 148.73 (Ar), 169.84 (C=O); [Found (ESI+) 206.0803. $[M+H]^+$, $C_{11}H_{12}NO_3$ requires 206.0812].

***Method B:*[218]**

A solution of **89** (47 mg, 0.15 mmol) in TFA (500 µL) was stirred at RT under a N_2 atmosphere overnight. The solution was diluted with H_2O (5 mL) and the solvent was evaporated to give **93** as a brown oil (23 mg, 74%).

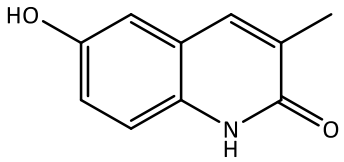

6-Hydroxy-3-methylquinolin-2(1*H*)-one (94)

A solution of **90** (60 mg, 0.21 mmol) in 4% (aq.) HCl (5 mL) was heated to reflux and stirred for 3 h. After cooling, the solution was diluted with H_2O (5 mL) and the solvent was evaporated to give **94** as a white solid (35 mg, 95%). R_f = 0.45 (20% MeOH:DCM); R_t = 3.78 min (solvent system A); mp = 239-245°C; UV (EtOH) λ_{max} 203 (9070); ^{1}H NMR (CD_3OD, 400 MHz) δ 2.02 (3H, d, J = 1.6, CH_3), 6.89- 6.92 (2H, m, Ar), 7.31 (1H, d, J = 8.0, Ar), 7.70 (1H, dd, J = 2.8, 1.6, Ar); ^{13}C NMR (CD_3OD, 100 MHz) δ 14.44 (CH_3), 117.34 (Ar), 118.23 (Ar), 121.23 (Ar), 125.83 (Ar), 133.05 (Ar), 133.36 (Ar), 135.38 (Ar), 159.30 (Ar), 170.59 (C=O); [Found (ESI+) 176.0704. $[M+H]^+$, $C_{10}H_{10}NO_2$ requires 176.0706].

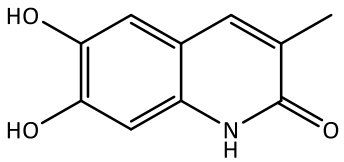

6,7-Dihydroxy-3-methylquinolin-2(1*H*)-one (95)

A solution of **60** (25 mg, 0.11 mmol) in anhydrous DCM (2 mL) was cooled to 0°C and treated with a solution of 1M BBr_3 in DCM (570 µL, 0.57 mmol) under an argon atmosphere. The reaction was allowed to warm to RT and stirred for 18 h. The mixture was treated with ice-water (10 mL) and then stirred for 30 min. A white precipitate formed which was filtered and dried to give **95** (18 mg, 82%). R_f = 0.18 (10% MeOH: DCM); R_t = 5.03 min (solvent system A);

mp = 245-247°C; UV (EtOH) λ_{max} 213.5 (32166), 233.5 (16306), 344.5 (10130); ^{1}H NMR (DMSO-d_6, 400 MHz) δ 2.01 (3H, d, J = 1.2, CH_3), 6.72 (1H, s, Ar), 6.86 (1H, s, Ar), 7.52 (1H, d, J = 1.2, Ar), 11.34 (1H, br s, NH); ^{13}C NMR (DMSO-d_6, 100 MHz) δ 16.36 (CH_3), 100.51 (Ar), 111.17 (Ar), 112.40 (Ar), 125.25 (Ar), 132.54 (Ar), 135.95 (Ar), 141.45 (Ar), 148.34 (Ar), 162.20 (C=O); [Found (ESI+) 214.0474. $[M+H]^+$, $C_{10}H_9NNaO_3$ requires 214.0475].

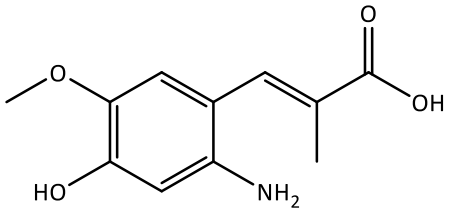

(*E*)-3-(2-Amino-4-hydroxy-5-methoxyphenyl)-2-methylacrylic acid (96)

***Method A:*[218]**

A solution of **89** (47 mg, 0.15 mmol) in TFA (500 µL) was stirred at RT under a N_2 atmosphere overnight. The solution was diluted with H_2O (5 mL) and the solvent was evaporated. ^{1}H NMR analysis showed that the resulting brown oil was pure **93** (23 mg, 74%), rather than the desired product.

Method B:

A mixture of **89** (52 mg, 0.17 mmol) and 10% Pd/C (5 mg) in EtOAc (10 mL) was stirred at RT for 12 h under a H_2 atmosphere. No conversion of the starting material was observable by TLC.

Method C:

A mixture of **89** (25 mg, 0.08 mmol) and 10% Pd/C (3 mg) in AcOH (5 mL) was stirred at RT for 3 h under a H_2 atmosphere. The reaction mixture was filtered through celite and the solvent was evaporated. ^{1}H NMR and mass spectrometry analysis of the crude material showed that the alkene unit had been saturated.

Method D:[220]

A solution of **89** (134 mg, 0.43 mmol) in anhydrous DCM (10 mL) under an argon atmosphere was treated with trimethylsilyl iodide (80 µL, 0.56 mmol) and heated to reflux for 2 h after which time there was no conversion of starting material observable on TLC.

Method E:[220]

A solution of **89** (127 mg, 0.40 mmol) in anhydrous MeCN (10 mL) under an argon atmosphere was treated with trimethylsilyl iodide (74 µL, 0.52 mmol) and heated to reflux for 5 h after which time there was no conversion of starting material observable on TLC.

Method F:[194]

A suspension of **98** (530 mg, 2.09 mmol) and $FeSO_4.7H_2O$ (5.80 g, 21.0 mmol) in H_2O (30 mL) was heated to 80°C under stirring. 35% (aq.) NH_3 solution (10 mL) was added. After stirring for 5 min, the heat was removed and the mixture was allowed to stir for a further 22 h at RT. The reaction mixture was filtered through celite and acidified to pH 3 using 1M HCl. The H_2O was evaporated and the residue was dissolved in hot MeOH, filtered and the solvent was evaporated. This gave a complex mixture of products on TLC analysis.

Method G:[193]

A suspension of **98** (456 mg, 1.8 mmol), iron powder (402 mg, 7.2 mmol) and NH_4Cl (144 mg, 2.7 mmol) in 80% (aq.) EtOH (15 mL) was stirred at 80 °C for 5 h. The hot reaction mixture was filtered through celite and the solvent was evaporated to give a brown solid which was a complex mixture of products on TLC and ^1H NMR.

Method H:[221]

Hydrazinium monoformate was generated by neutralising one equivalent of hydrazine monohydrate (1 mL, 2.06 mmol) with formic acid (778 µL, 2.06 mmol). The mixture was stirred

for 1 h at 0 °C. Hydrazinium monoformate (500 µL) was added to a suspension of **98** (142 mg, 0.56 mmol) and zinc dust (73 mg, 1.12 mmol) in MeOH (2 mL). The reaction mixture was stirred at 30 °C under an argon atmosphere for 2 h after which time there was no conversion of the starting material observable on TLC.

Method I:

A solution of **102** (75 mg, 0.30 mmol) in THF (4 mL) was treated with 1M NaOH (1.2 mL) and EtOH (1 mL) and stirred at 40 °C overnight. The organic solvents were evaporated and the remaining solution was diluted with H_2O (10 mL), the pH adjusted to 2 with 6M HCl, and the aqueous phase was extracted with EtOAc (3 x 10 mL). The combined organic layers were extracted with brine (10 mL) then dried over $MgSO_4$, filtered and the solvent was evaporated to give an orange residue. TLC and HPLC analysis showed a mixture of products including carbostyril **93**.

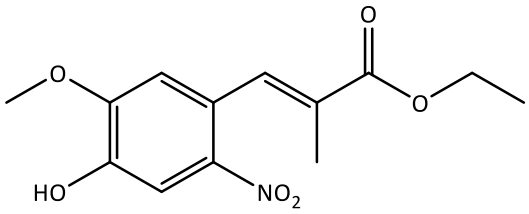

Ethyl (*E*)-3-(4-hydroxy-5-methoxy-2-nitrophenyl)-2-methylacrylate (97)

A solution of **81** (300 mg, 0.81 mmol) in TFA (3 mL) was stirred at 30°C under an argon atmosphere overnight. The solution was diluted with H_2O (20 mL) and extracted with DCM (3 x 20 mL). The combined organic phases were extracted with sat. $NaHCO_3$ (2 x 20 mL) and brine (20 mL), then were dried over $MgSO_4$, filtered and the solvent was evaporated to give an orange oil. Purification by column chromatography (DCM) gave **97** as an orange oil (213 mg, 93%). R_f = 0.32 (DCM); R_t = 8.7 min (solvent system A); ^{1}H NMR ($CDCl_3$, 400 MHz) δ 1.29 (3H, t, J = 7.2, CH_3), 1.85 (3H, d, J = 1.2, CH_3), 3.92 (3H, s, OCH_3), 4.23 (2H, q, J= 7.2, CH_2), 6.06 (1H, s, OH), 6.66 (1H, s, Ar), 7.71 (1H, s, Ar), 7.83 (1H, d, J = 0.4, C=CH); ^{13}C NMR ($CDCl_3$, 100 MHz) δ 13.96 (CH_3), 14.18 (CH_3), 56.48 (OCH_3), 61.03 (CH_2), 111.51 (Ar), 111.86 (Ar), 125.52 (Ar), 129.21 (Ar), 136.46 (C=C), 140.96 (Ar), 145.39 (C=C), 150.39 (Ar), 167.86 (C=O); [Found (ESI-) 280.0826 $[M+H]^-$, $C_{13}H_{14}NO_6$ requires 280.0827].

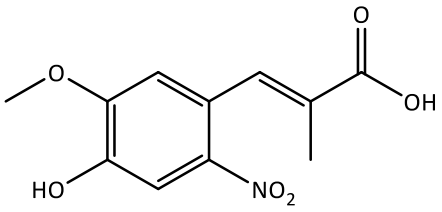

(E)-3-(4-Hydroxy-5-methoxy-2-nitrophenyl)-2-methylacrylic acid (98)

A solution of **97** (600 mg, 2.13 mmol) in THF (15 mL) was treated with 1M NaOH (9 mL) and EtOH (5 mL) and stirred at 40 ^{o}C overnight. The organic solvents were evaporated and the remaining solution was diluted with H_2O (30 mL), the pH was adjusted to 2 with 6M HCl and the aqueous phase was extracted with EtOAc (4 x 30 mL). The combined organic layers were extracted with brine (40 mL) and dried over $MgSO_4$, filtered and the solvent was evaporated to give an orange oil (530 mg, 98%). R_f = 0.40 (10% MeOH: DCM); R_t = 6.95 min (solvent system A); ^{1}H NMR (DMSO-d_6, 400 MHz) δ 1.86 (3H, s, CH_3), 3.91 (3H, s, OCH_3), 6.95 (1H, s, Ar), 7.61 (1H, s, Ar), 7.76 (1H, s, HC=C), 10.31 (1H, br s, OH), 12.57 (1H, br s, CO_2H); ^{13}C NMR (DMSO-d_6, 100 MHz) δ 13.82 (CH_3), 56.36 (OCH_3), 111.25 (Ar), 113.30 (Ar), 124.08 (Ar), 128.94 (C=C), 135.80 (C=C), 139.83 (Ar), 146.54 (Ar), 152.18 (Ar), 168.85 (C=O); [Found (ESI+) 276.0476 $[M+Na]^+$, $C_{11}H_{11}NNaO_6$ requires 276.0479].

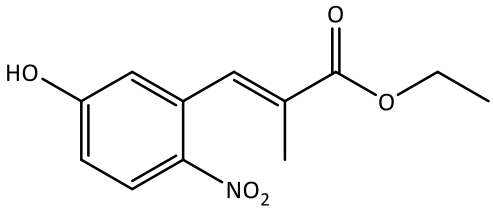

Ethyl (*E*)-3-(5-hydroxy-2-nitrophenyl)-2-methylacrylate (100)

A solution of **82** (400 mg, 1.17 mmol) was stirred in TFA (5 mL) at 40^{o}C under an argon atmosphere overnight. The mixture was diluted with H_2O (20 mL) and extracted with DCM (3 x 20 mL). The combined organic phases were extracted with sat. $NaHCO_3$ (2 x 20 mL) and brine (20 mL) then dried over $MgSO_4$, filtered and the solvent was evaporated to give a yellow oil. Purification by column chromatography (0-6% MeOH in DCM) gave **100** as a yellow oil (273 mg, 93%). R_f = 0.70 (10% MeOH:DCM) ; R_t = 8.70 min (solvent system A); ^{1}H NMR ($CDCl_3$, 400 MHz) δ 1.36 (3H, t, J = 7.2, CH2C$\underline{H_3}$), 1.90 (3H, d, J = 1.6, CH_3), 4.31 (2H, q, J= 7.2, C$\underline{H_2}$$CH_3$), 6.46

(1H, br s, OH), 6.74 (1H, d, J = 2.8, Ar), 6.91 (1H, dd, J = 8.8, 2.8, Ar), 7.91 (1H, s, C=CH), 8.16 (1H, d, J = 8.8, Ar); ^{13}C NMR ($CDCl_3$, 100 MHz) δ 13.96 (CH_3), 14.57 (CH_3), 62.20 (CH_2), 116.53 (Ar), 118.17 (Ar), 128.83 (Ar), 130.20 (C=C), 135.92 (Ar), 138.25 (C=C), 140.93 (Ar), 163.86 (Ar), 169.34 (C=O); [Found (ESI+) 274.0687 $[M+Na]^+$, $C_{12}H_{13}NNaO_5$ requires 274.0686].

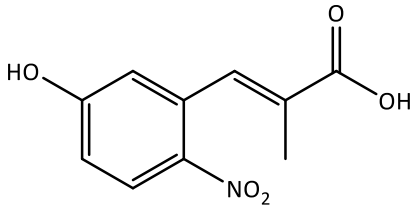

(*E*)-3-(5-Hydroxy-2-nitrophenyl)-2-methylacrylic acid (101)

A solution of **100** (333 mg, 1.33 mmol) in THF (8 mL) was treated with 1M NaOH (6 mL) and EtOH (2 mL) and stirred at 40 °C overnight. The organic solvents were evaporated and the remaining solution was diluted with H_2O (30 mL), the pH was adjusted to 2 with 6M HCl, and the aqueous phase was extracted with EtOAc (4 x 30 mL). The combined organic layers were extracted with brine (40 mL) and dried over $MgSO_4$, filtered and the solvent was evaporated to give **101** as an orange oil (292 mg, 98%). R_f = 0.25 (10% MeOH:DCM); R_t = 3.68 min (solvent system A); ^{1}H NMR (DMSO-d_6, 400 MHz) δ 1.81 (3H, d, J = 1.6, CH_3), 6.76 (1H, dd, J = 2.4, 0.8, Ar), 6.95 (1H, dd, J = 9.2, 2.4, Ar), 7.77 (1H, s, HC=C), 8.13 (1H, d, J= 9.2, Ar), 11.11 (1H, br s, OH), 12.60 (1H, br s, CO_2H); ^{13}C NMR (DMSO-d_6, 100 MHz) δ 13.97 (CH_3), 116.47 (Ar), 118.18 (Ar), 128.80 (C=C), 130.46 (Ar), 136.09 (Ar), 138.27 (C=C), 140.96 (Ar), 163.81 (Ar), 171.14 (C=O); [Found (ESI+) 246.0363 $[M+Na]^+$, $C_{10}H_9NNaO_5$ requires 246.0373].

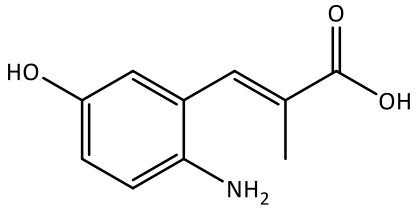

(*E*)-3-(2-Amino-5-hydroxyphenyl)-2-methylacrylic acid (99)[193]

A mixture of **101** (288 mg, 1.29 mmol), iron powder (288 mg, 5.16 mmol) and NH_4Cl (104 mg, 1.94 mmol) in 80% (aq.) EtOH (10 mL) was stirred at 80 °C for 5 h. The hot reaction mixture

was filtered through celite and the H_2O was evaporated to give a brown solid. TLC analysis gave a complex mixture of products.

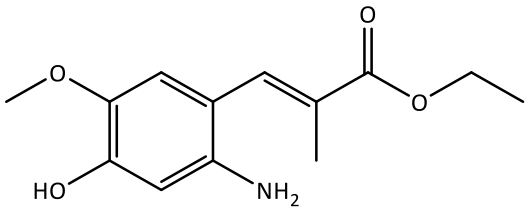

Ethyl (*E*)-3-(2-amino-4-hydroxy-5-methoxyphenyl)-2-methylacrylate (102)

A mixture of **97** (116 mg, 0.41 mmol), iron powder (87 mg, 1.56 mmol) and NH_4Cl (30 mg, 0.57 mmol) in 80% (aq.) EtOH (5 mL) was stirred at 80 °C for 2 h. The hot reaction mixture was filtered through celite and the solvent was evaporated to give a brown residue which was dissolved in EtOAc (10 mL) and washed with H_2O (3 x 10 mL) and brine (10 mL). The organic phase was dried over Na_2SO_4, filtered and the solvent was evaporated to give **102** as an orange oil (95 mg, 92%). %). R_f = 0.65 (10% MeOH: DCM); R_t = 8.50 min (solvent system A); ^{1}H NMR (CDCl3, 400 MHz) δ 1.29 (3H, t, J = 7.2, $CH_2C\underline{H}_3$), 1.98 (3H, d, J = 1.2, CH_3), 3.50 (2H, br s, NH_2), 3.76 (3H, s, OCH_3), 4.21 (2H, q, J = 7.2, $C\underline{H}_2CH_3$), 5.70 (1H, br s, OH), 6.30 (1H, s, Ar), 6.61 (1H, s, Ar), 7.52 (1H, s, HC=C); ^{13}C NMR (CDCl3, 100 MHz) δ 14.22 (CH_3), 14.27 (CH_3), 56.63 (OCH_3), 60.65 (CH_2), 102.72 (Ar), 112.49 (Ar), 112.67 (Ar), 127.99 (C=C), 134.69 (C=C), 139.38 (Ar), 139.90 (Ar), 147.18 (Ar), 168.52 (C=O); [Found (ESI+) 252.1230 $[M+H]^+$, $C_{13}H_{18}NO_4$ requires 252.1230].

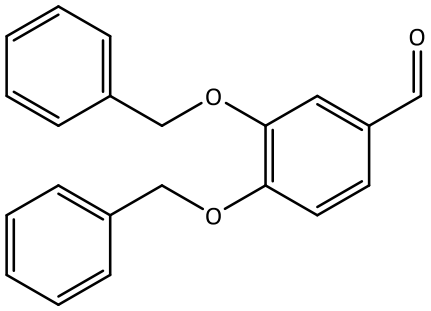

3,4-*bis*(Benzyloxy)benzaldehyde (103)[284]

A mixture of 3,4-dihydroxybenzaldehyde (1.52 g, 11.0 mmol) and K_2CO_3 (3.32 g, 24.0 mmol) in DMF (50 mL) was treated with benzyl chloride (2.76 mL, 24.0 mmol) and the mixture was stirred at 80 ^oC for 3 h. The solvent was evaporated and the residue was dissolved in $CHCl_3$ (30 mL) and extracted with H_2O (3 x 30 mL) and brine (50 mL). The organic phase was dried over $MgSO_4$, then filtered and the solvent was evaporated to give **103** as a brown oil (3.37 g, 96%). R_f = 0.55 (DCM); R_t = 10.50 min (solvent system A) ; ^1H NMR ($CDCl_3$, 400 MHz) δ 5.16 (2H, s, CH_2), 5.19 (2H, s, CH_2), 6.98 (1H, d, J= 8.0, Ar), 7.26- 7.47 (12H, m, Ar), 9.77 (1H, s, HC=O); ^{13}C NMR ($CDCl_3$, 100 MHz) δ 70.81 (CH_2), 70.97 (CH_2), 112.50 (Ar), 113.15 (Ar), 126.57 (Ar), 127.06 (Ar), 127.29 (Ar), 127.96 (Ar), 128.06 (Ar), 128.52 (Ar), 128.60 (Ar), 130.33 (Ar), 136.24 (Ar), 136.57 (Ar), 149.20 (Ar), 154.26 (Ar), 190.66 (C=O).

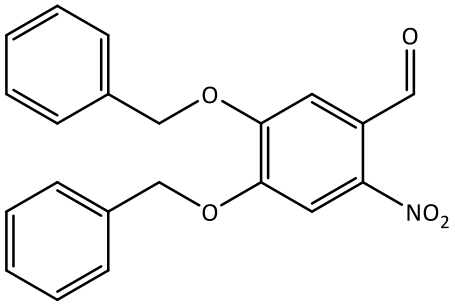

4,5-bis(benzyloxy)-2-nitrobenzaldehyde (104)

AH178 (3.30 g, 10.4 mmol) in $CHCl_3$ (20 mL) was treated slowly with 65% (aq.) nitric acid (30 mL) at 0^oC and allowed to stir for 4 h. The mixture was then treated with H_2O (50 mL) and the aqueous phase was extracted with EtOAc (3 x 60 mL). The combined organic phases were washed with brine (100 mL), dried over $MgSO_4$, filtered and the solvent evaporated. This gave

a yellow solid which was recrystallized from EtOAc to give **104** (3.35 g, 92%). R_f = 0.80 (DCM); R_t = 10.70 min (solvent system A); mp=140-142°C (lit.[285] 137.5-138.5°C); ^{1}H NMR ($CDCl_3$, 400 MHz) δ 5.24 (4H, s, CH_2), 7.29- 7.42 (10H, m, Ar), 7.44 (1H, s, Ar), 7.63 (1H, s, Ar), 10.35 (1H, s, HC=O); ^{13}C NMR ($CDCl_3$, 100 MHz) δ 71.25 (CH_2), 71.45 (CH_2), 109.46 (Ar), 111.92 (Ar), 125.58 (Ar), 127.23 (Ar), 127.26 (Ar), 128.40 (Ar), 128.48 (Ar), 128.69 (Ar), 128.75 (Ar), 135.05 (Ar), 135.21 (Ar), 143.70 (Ar), 151.83 (Ar), 152.82 (Ar), 187.50 (C=O).

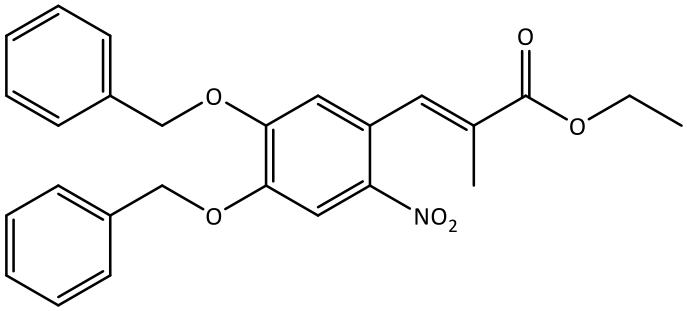

Ethyl (*E*)-3-(4,5-*bis*(benzyloxy)-2-nitrophenyl)-2-methylacrylate (105)

A solution of **104** (2.9 g, 7.98 mmol) and ECETP (4.34 g, 11.97 mmol) in anhydrous toluene (50 mL) was heated for 24 h at 65°C under N_2. The solvent was evaporated and the residue was purified by column chromatography (10-20% EtOAc in petroleum ether) to give **105** as a yellow oil (2.7 g, 76%). R_f = 0.60 (DCM); R_t= 11.55 min (solvent system A); ^{1}H NMR ($CDCl_3$, 400 MHz) δ 1.34 (3H, t, J = 7.0, $CH_2C\underline{H_3}$), 1.65 (3H, d, J = 1.6, CH_3), 4.27 (2H, q, J = 7.0, $C\underline{H_2}CH_3$), 5.25 (2H, s CH_2), 5.26 (2H, s, CH_2) 6.71 (1H, d, J = 0.8, Ar), 7.35- 7.50 (10H, m, Ar), 7.82 (1H, s, Ar), 7.85 (1H, q, J = 0.8, C=CH); ^{13}C NMR ($CDCl_3$, 100 MHz) δ 13.64 (CH_3), 14.19 (CH_3), 60.94 (CH_2), 71.11 (CH_2), 71.34 (CH_2), 110.44 (Ar), 115.28 (Ar), 126.56 (Ar), 126.78 (Ar), 127.39 (Ar), 128.26 (Ar), 128.30 (Ar), 128.67 (Ar), 128.77 (Ar), 129.34 (C=C), 135.58 (Ar), 135.68 (Ar), 136.10 (C=C), 140.35 (Ar), 148.07 (Ar), 152.37 (Ar), 167.72 (C=O); [Found (ESI+) 448.1768 $[M+H]^+$, $C_{26}H_{26}NO_6$ requires 448.1755].

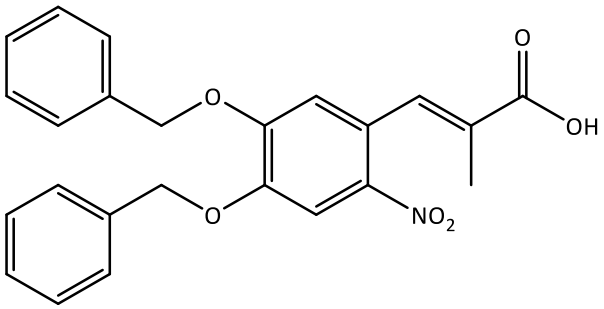

(E)-3-(4,5-*bis*(Benzyloxy)-2-nitrophenyl)-2-methylacrylic acid (106)

A solution of **105** (1.27 g, 2.84 mmol) in THF (40 mL) was treated with 1M NaOH (14 mL) and EtOH (10 mL) and stirred at 40^{o}C overnight. The organic solvents were evaporated and the remaining solution was diluted with H_2O (20 mL), the pH adjusted to 2 with 6M HCl, and the aqueous phase was extracted with $CHCl_3$ (3 x 30 mL). The combined organic layers were extracted with brine (50 mL) then dried over $MgSO_4$, filtered and the solvent was evaporated to give **106** as a yellow solid (1.10 mg, 92%). R_f = 0.21 (5% MeOH: DCM); R_t = 10.37 min (solvent system A); mp= 162-167^{o}C; ^{1}H NMR ($CDCl_3$, 400 MHz) δ 1.61 (3H, d, J = 1.2, CH_3), 5.21 (2H, s CH_2), 5.23 (2H, s, CH_2) 6.67 (1H, s, Ar), 7.27- 7.45 (10H, m, Ar), 7.78 (1H, s, Ar), 7.93 (1H, q, J = 0.8, C=CH); ^{13}C NMR ($CDCl_3$, 100 MHz) δ 13.31 (CH_3), 71.16 (CH_2), 71.35 (CH_2), 110.44 (Ar), 115.14 (Ar), 126.07 (Ar), 126.78 (Ar), 127.39 (Ar), 128.13 (C=C), 128.30 (Ar), 128.33 (Ar), 128.69 (Ar), 128.80 (Ar), 135.53 (Ar), 135.61 (Ar), 138.59 (C=C), 140.30 (Ar), 148.29 (Ar), 152.42 (Ar), 171.72 (C=O); [Found (ESI+) 442.1313 $[M+Na]^+$, $C_{24}H_{21}NNaO_6$ requires 442.1261].

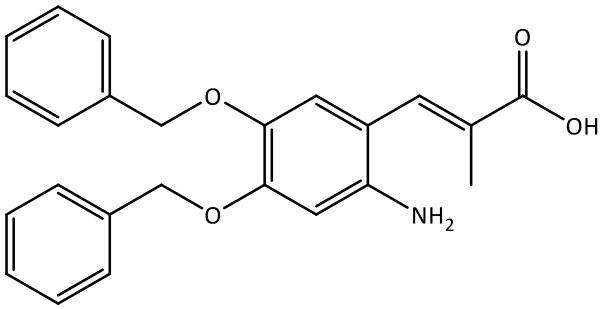

(*E*)-3-(2-Amino-4,5-bis(benzyloxy)phenyl)-2-methylacrylic acid (107)

A suspension of **106** (1.0 g, 2.38 mmol) and $FeSO_4.7H_2O$ (6.67 g, 24.00 mmol) in H_2O (60 mL) was heated to 80^oC under stirring. 35% (aq.) NH_3 solution (20 mL) was added. After stirring for 5 min, the heat was removed and the mixture was allowed to stir for a further 18 h at RT. The reaction mixture was filtered through celite and acidified to pH 3 using 1M HCl. The aqueous phase was extracted with EtOAc (3 x 100 mL) and the combined organic phases were washed with brine (150 mL), dried over Na_2SO4, filtered, and the solvent was evaporated to give **107** a yellow solid (149 mg, 16%). R_f = 0.37 (10% MeOH:DCM); R_t = 8.13 min (solvent system A); mp = 102-105^oC; ^1H NMR (CD_3OD, 400 MHz) δ 1.85 (3H, d, J = 1.2, CH_3), 5.01 (2H, s, CH_2), 5.12 (2H, s, CH_2), 6.56 (1H, s, Ar), 6.76 (1H, s, Ar), 7.27- 7.48 (10H, m, Ar), 7.57 (1H, s, C=CH); ^{13}C NMR (CD_3OD, 100 MHz) δ 14.46 (CH_3), 71.78 (CH_2), 74.27 (CH_2), 103.85 (Ar), 114.75 (Ar), 120.43 (Ar), 128.22 (C=C), 128.72 (Ar), 128.86 (Ar), 128.97 (Ar), 129.06 (Ar), 129.40 (Ar), 129.53 (Ar), 136.17 (C=C), 138.57 (Ar), 139.12 (Ar), 141.28 (Ar), 143.60 (Ar), 152.60 (Ar), 172.45 (C=O); [Found (ESI+) 390.1696 $[M+H]^+$, $C_{24}H_{24}NO_4$ requires 390.1700].

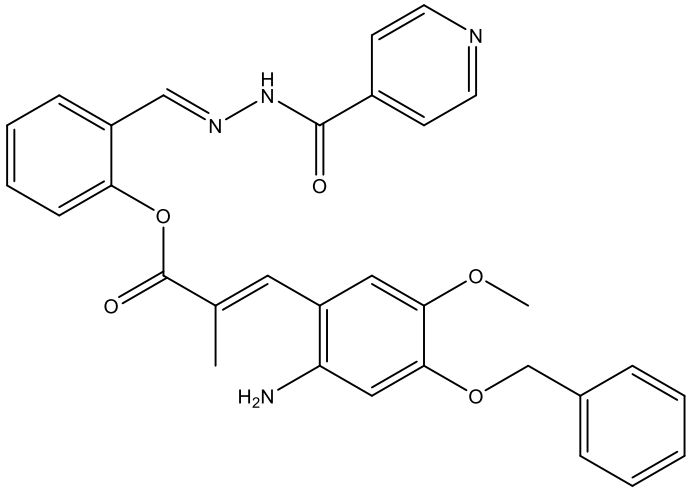

2-((*E*)-(2-Isonicotinoylhydrazineylidene)methyl)phenyl (*E*)-3-(2-amino-4-(benzyloxy)-5-methoxyphenyl)-2-methylacrylate (108)

A stirred solution of **89** (125 mg, 0.40 mmol) in anhydrous DMF (4 mL) under argon was cooled to 0 ^{o}C and treated with DMAP (49 mg, 0.40 mmol) and EDC.HCl (77 mg, 0.40 mmol). The mixture was allowed to stir for 10 min before **8** (53 mg, 0.22 mmol) was added. The mixture was allowed to warm to RT and stirred overnight. The solvent was evaporated and the remaining residue was dissolved in DCM (10 mL) and extracted with sat. NH_4Cl (3 x 10 mL), H_2O (3 x 10 mL) and brine (10 mL). The organic phase was dried over $MgSO_4$, filtered and the solvent was evaporated to give **108** as a yellow oil which was used without further purification (103 mg, 87%). R_f = 0.20 (20% acetone:DCM); R_t = 7.3 min (solvent system A); [Found (ESI+) 537.2114 $[M+H]^+$, $C_{31}H_{29}N_4O_5$ requires 537.2132].

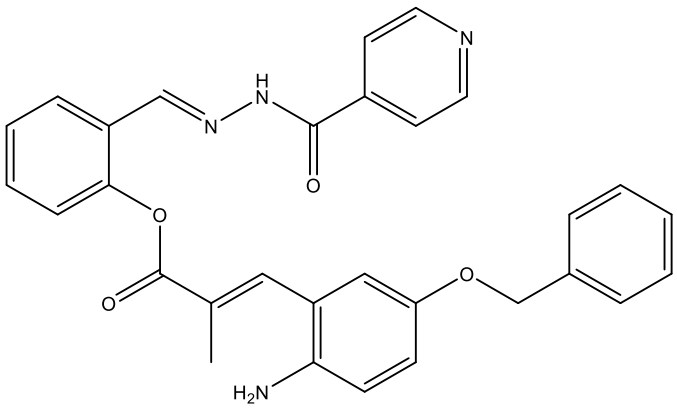

2-((*E*)-(2-Isonicotinoylhydrazineylidene)methyl)phenyl (*E*)-3-(2-amino-5-(benzyloxy)phenyl)-2-methylacrylate (109)

A stirred solution of **90** (154 mg, 0.54 mmol) in anhydrous DMF (4 mL) under argon was cooled to 0 ^{o}C and treated with DMAP (66 mg, 0.54 mmol) and EDC.HCl (104 mg, 0.54 mmol). The mixture was allowed to stir for 10 min before **8** (109 mg, 0.45 mmol) was added. The mixture was allowed to warm to RT and stirred overnight. The solvent was evaporated and the remaining residue was dissolved in DCM (10 mL) and extracted with sat. NH_4Cl (3 x 10 mL), H_2O (3 x 10 mL) and brine (10 mL). The organic phase was dried over $MgSO_4$, filtered and the solvent was evaporated to give **109 as** a yellow residue which was used without further purification (192 mg, 84%). R_f = 0.20 (20% acetone: DCM); R_t = 7.1 min (solvent system A); [Found (ESI+) 529.1855 $[M+Na]^+$, $C_{30}H_{26}N_4NaO_4$ requires 529.1846].

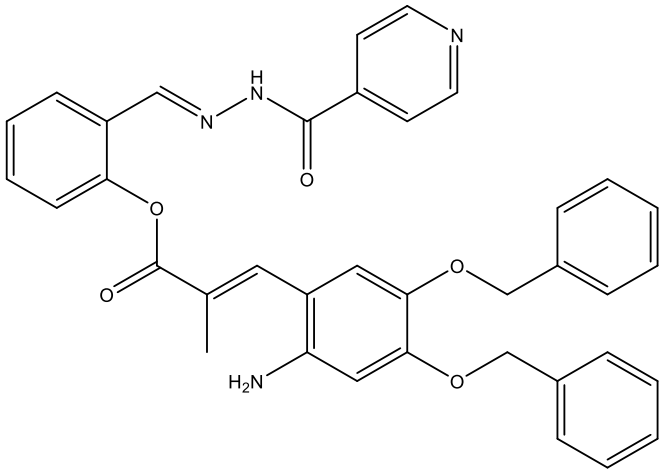

2-((*E*)-(2-Isonicotinoylhydrazineylidene)methyl)phenyl (*E*)-3-(2-amino-4,5-bis(benzyloxy)phenyl)-2-methylacrylate (110)

A stirred solution of **103** (143 mg, 0.37 mmol) in anhydrous DMF (4 mL) under argon was chilled to 0 ^{o}C and treated with DMAP (45 mg, 0.37 mmol) and EDC.HCl (71 mg, 0.37 mmol). The mixture was allowed to stir for 10 min before **8** (75 mg, 0.31 mmol) was added. The mixture was allowed to warm to RT and stirred for 24 h. The solvent was evaporated and the remaining residue was dissolved in DCM (10 mL) and extracted with sat. NH_4Cl (3 x 10 mL), water (3 x 10 mL) and brine (10 mL). The organic phase was dried over $MgSO_4$, filtered and the solvent was evaporated to give **110** as a yellow residue which was used without further purification (114 mg, 60%). R_f = 0.37 (30% acetone: DCM); R_t = 8.4 min (solvent system A); [Found (ESI+) 613.2452 $[M+H]^+$, $C_{37}H_{33}N_4O_5$ requires 613.2445].

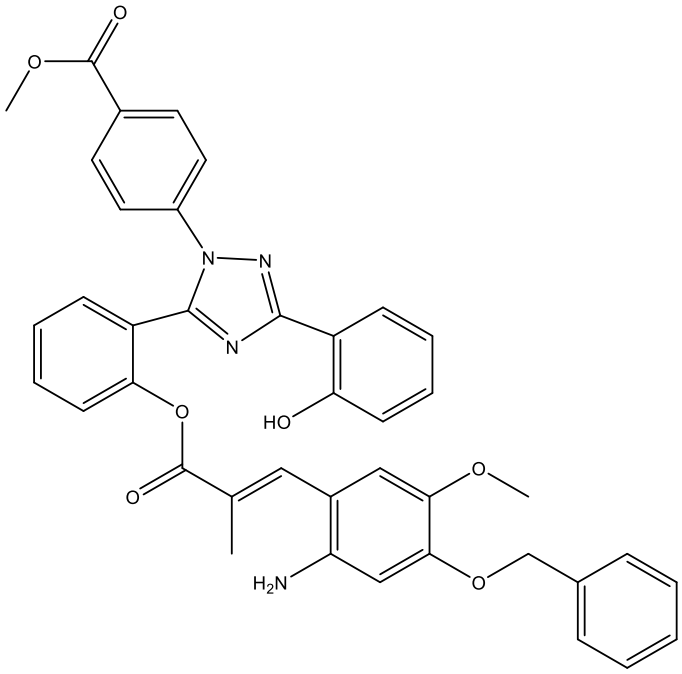

Methyl (*E*)-4-(5-(2-((3-(2-amino-4-(benzyloxy)-5-methoxyphenyl)-2-methylacryloyl)oxy)phenyl)-3-(2-hydroxyphenyl)-1H-1,2,4-triazol-1-yl)benzoate (111)

A stirred solution of **89** (116 mg, 0.37 mmol) in anhydrous DMF (4 mL) under argon was cooled to 0 ^{o}C and treated with DMAP (45 mg, 0.37 mmol) and EDC.HCl (71 mg, 0.37 mmol). The mixture was allowed to stir for 10 min before a solution of **33** (131 mg, 0.34 mmol) and DIPEA (59 μL, 0.34 mmol) in anhydrous DMF (4 mL) was added. The mixture was heated to 30 ^{o}C and stirred for 24 h. The solvent was evaporated and the remaining residue was dissolved in DCM (20 mL) and extracted with sat. NH_4Cl (3 x 20 mL), H_2O (3 x 20 mL) and brine (20 mL). The organic phase was dried over $MgSO_4$, filtered and the solvent was evaporated to give **111** as a yellow residue which was used without further purification (90 mg, 39%). R_f = 0.56 (4% acetone: DCM); R_t = 10.7 min (solvent system A); [Found (ESI+) 683.2497 $[M+H]^+$, $C_{40}H_{35}N_4O_7$ requires 683.2500].

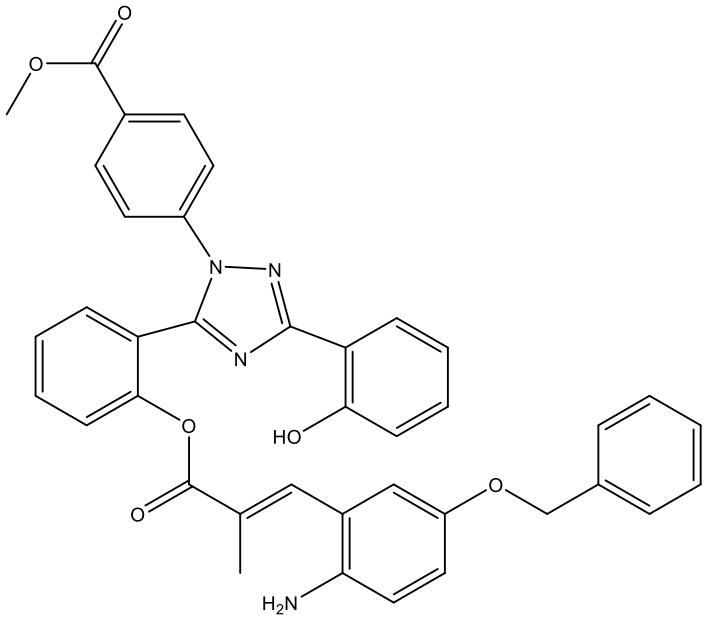

Methyl (*E*)-4-(5-(2-((3-(2-amino-5-(benzyloxy)phenyl)-2-methylacryloyl)oxy)phenyl)-3-(2-hydroxyphenyl)-1H-1,2,4-triazol-1-yl)benzoate (112)

A stirred solution of **90** (113 mg, 0.40 mmol) in anhydrous DMF (5 mL) under argon was cooled to 0 ^{o}C and treated with DMAP (49 mg, 0.40 mmol) and EDC.HCl (77 mg, 0.40 mmol). The mixture was allowed to stir for 10 min before a solution of **33** (139 mg, 0.36 mmol) and DIPEA (63 μL, 0.36 mmol) in anhydrous DMF (5 mL) was added. The mixture was heated to 30 ^{o}C and stirred for 24 h. The solvent was evaporated and the remaining residue was dissolved in DCM (20 mL) and extracted with sat. NH_4Cl (3 x 20 mL), H_2O (3 x 20 mL) and brine (20 mL). The organic phase was dried over $MgSO_4$, filtered and the solvent was evaporated to give **112** as a yellow residue which was used without further purification (76 mg, 32%). R_f = 0.60 (2% acetone: DCM); R_t = 10.1 min (solvent system A); [Found (ESI+) 653.2439 $[M+H]^+$, $C_{29}H_{33}N_4O_6$ requires 653.2395].

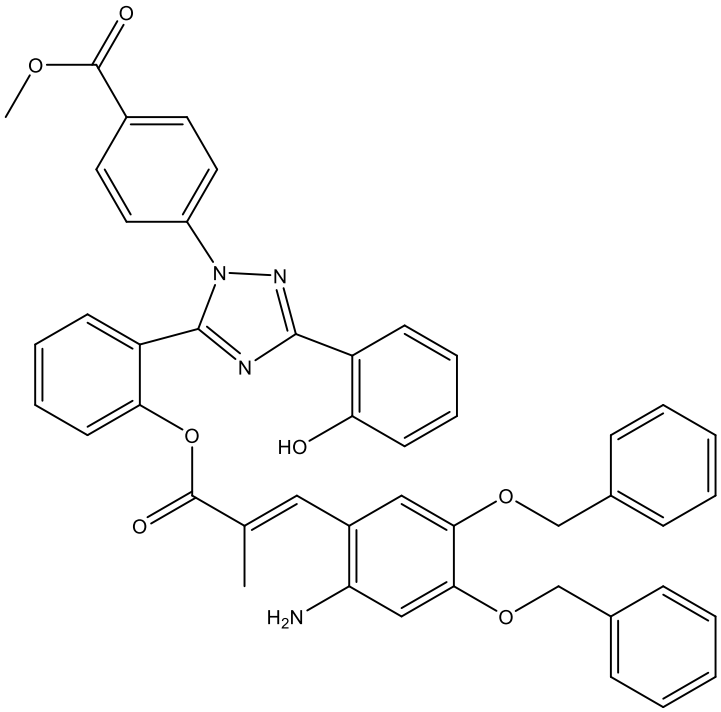

Methyl (*E*)-4-(5-(2-((3-(2-amino-4,5-bis(benzyloxy)phenyl)-2-methylacryloyl)oxy)phenyl)-3-(2-hydroxyphenyl)-1H-1,2,4-triazol-1-yl)benzoate (113)

A stirred solution of **103** (72 mg, 0.18 mmol) in anhydrous DMF (3 mL) under argon was cooled to 0 ^{o}C and treated with DMAP (22 mg, 0.18 mmol) and EDC.HCl (35 mg, 0.18 mmol). The mixture was allowed to stir for 10 min before a solution of **33** (66 mg, 0.17 mmol) and DIPEA (30 μL, 0.17 mmol) in anhydrous DMF (2 mL) was added. The reaction was heated to 30 ^{o}C and stirred for 24 h. The solvent was evaporated and the remaining residue was dissolved in DCM (20 mL) and extracted with sat. NH_4Cl (3 x 20 mL), H_2O (3 x 20 mL) and brine (20 mL). The organic phase was dried over $MgSO_4$, filtered and the solvent was evaporated to give **113** as a yellow residue which was used without further purification (24 mg, 19%). R_f = 0.50 (2% acetone: DCM); R_t = 11.56 min (solvent system A); [Found (ESI+) 759.2827 $[M+H]^+$, $C_{46}H_{39}N_4O_7$ requires 759.2813].

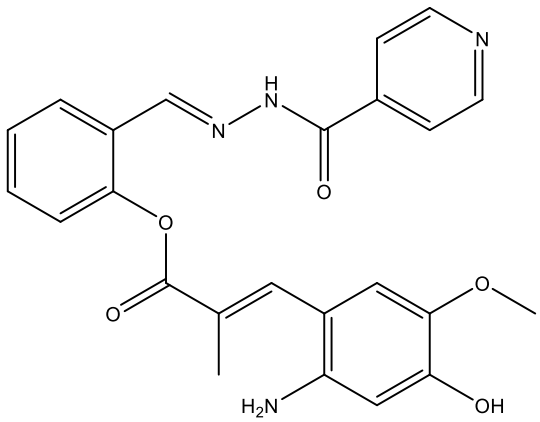

2-((*E*)-(2-Isonicotinoylhydrazineylidene)methyl)phenyl (*E*)-3-(2-amino-4-hydroxy-5-methoxyphenyl)-2-methylacrylate (114)

A solution of **108** (93 mg, 0.17 mmol) in TFA (2 mL) was stirred at 30°C under an argon atmosphere overnight. The TFA was evaporated and the residue was co-evaporated with MeCN (3 x 10 mL). The resulting oil was purified by column chromatography eluting with 5-10% MeOH in DCM to give **114** as a yellow oil (59 mg, 78%). R_f = 0.35 (10% MeOH: DCM); R_t = 5.7 min (solvent system A); UV (EtOH) 298 (14250); ^{1}H NMR (DMSO-d_6, 400 MHz) δ 2.21 (3H, d, J = 1.2, CH_3), 3.69 (3H, s, OCH_3), 5.07 (2H, br s, NH_2), 6.29 (1H, s, Ar), 6.82 (1H, s, Ar), 7.28 (1H, dd, J = 6.4, 0.8, Ar), 7.40 (1H, td, J = 6.0, 0.8, Ar), 7.55 (1H, td, J = 6.0, 1.2, Ar), 7.80 (2H, dd, J = 3.6, 1.2, Pyr), 7.89 (1H, q, J = 0.8, HC=C), 8.03 (1H, dd, J = 6.0, 1.2, Ar), 8.57 (1H, s, HC=N), 8.79 (2H, dd, J = 3.6, 1.2, Pyr), 9.30 (1H, s, OH), 12.13 (1H, s, NH); ^{13}C NMR (DMSO-d_6, 100 MHz) δ 14.63 (CH_3), 56.58 (OCH_3), 103.16 (Ar), 109.67 (Ar), 114.42 (Ar), 120.87 (Ar), 121.20 (Ar), 121.52 (Pyr), 123.52 Ar), 126.17 (Ar), 126.67 (C=C), 138.07 (Ar), 139.21 (Ar), 140.39 (Ar), 143.47 (C=C), 144.00 (C=N), 149.87 (Pyr), 150.12 (Ar), 150.29 (Ar), 150.60 (Pyr), 161.67 (C=O), 167.01 (C=O); [Found (ESI+) 469.1487 $[M+Na]^+$, $C_{24}H_{22}N_4NaO_5$ requires 469.1482].

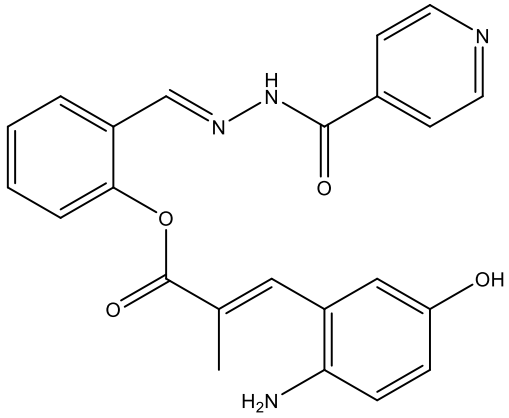

2-((*E*)-(2-Isonicotinoylhydrazineylidene)methyl)phenyl (*E*)-3-(2-amino-5-hydroxyphenyl)-2-methylacrylate (115)

A solution of **109** (236 mg, 0.47 mmol) in TFA (10 mL) was stirred at 30°C under an argon atmosphere overnight. The TFA was evaporated and the residue co-evaporated with MeCN (3 x 10 mL). The resulting oil was purified by column chromatography eluting with 5-15% MeOH in DCM to give **115** as a yellow oil (150 mg, 77%). R_f = 0.30 (10% MeOH: DCM); R_t = 5.4 min (solvent system A); UV (EtOH) 296 (5500); ^{1}H NMR (DMSO-d_6, 500 MHz) δ 2.15 (3H, d, J = 1.5, CH_3), 6.78 (1H, dd, J = 11.0, 3.0, Ar), 6.84 (1H, d, J = 3.5, Ar), 7.00 (1H, d, J = 11.0, Ar), 7.31 (1H, dd, J = 10.0, 1.5, Ar), 7.43 (1H, td, J = 9.5, 1.5, Ar), 7.53 (1H, td, J = 10.0, 2.0, Ar), 7.84 (2H, dd, J = 5.5, 2.0, Pyr), 7.91 (1H, d, J = 2.0, HC=C), 8.02 (1H, dd, J = 10.0, 2.0, Ar), 8.61 (1H, s, HC=N), 8.79 (2H, dd, J = 5.5, 2.0, Pyr), 9.46 (1H, br s, OH), 12.22 (1H, s, NH); ^{13}C NMR (DMSO-d_6, 125 MHz) δ 14.33 (CH_3), 115.89 (Ar), 117.32 (Ar), 118.53 (C=C), 121.55 (Pyr), 123.40 (Ar), 124.53 (Ar), 126.43 (Ar), 126.49 (Ar), 126.71 (Ar), 131.37 (Ar), 136.62 (Ar), 138.08 (Ar), 140.35 (C=C), 143.62 (Ar), 144.31 (C=N), 148.12 (Ar), 149.64 (Ar), 150.25 (Pyr), 161.63 (C=O), 166.25 (C=O); [Found (ESI+) 469.1487 $[M+Na]^+$, $C_{24}H_{22}N_4NaO_5$ requires 469.1482].

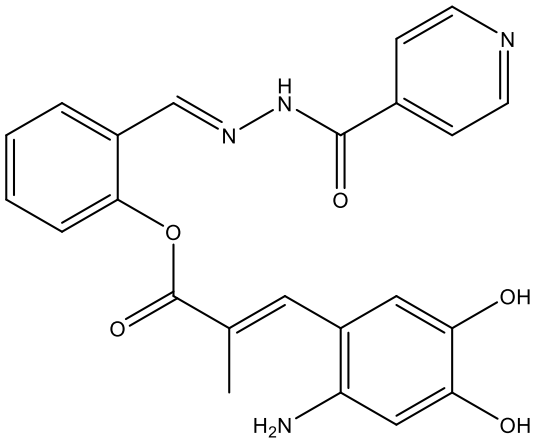

2-((*E*)-(2-Isonicotinoylhydrazineylidene)methyl)phenyl (*E*)-3-(2-amino-4,5-dihydroxyphenyl)-2-methylacrylate (116)

A solution of **110** (110 mg, 0.18 mmol) in TFA (10 mL) was stirred at 30°C under an argon atmosphere overnight. The TFA was evaporated and the residue was co-evaporated with MeCN (3 x 10 mL). The resulting oil was purified by column chromatography eluting with 30-70% acetone in DCM to give **116** as a yellow glass (29 mg, 37%). R_f = 0.25 (10% MeOH:DCM); R_t = 5.2 min (solvent system A); UV (EtOH) λ_{max} 298 (4800) ; ^{1}H NMR (DMSO-d_6, 500 MHz) δ 2.18 (3H, d, J= 0.8, CH_3), 6.76 (1H, s, Ar), 6.98 (1H, s, Ar), 7.28 (1H, dd, J= 7.6, 1.8, Ar), 7.42 (1H, t, J = 7.6, Ar), 7.57 (1H, td, J = 7.6, 1.8, Ar), 7.84 (2H, d, J = 4.4, Pyr), 7.91 (1H, d, J = 0.8, HC=C), 8.03 (1H, dd, J = 7.8, 1.6, Ar), 8.58 (1H, s, HC=N), 8.80 (2H, d, J = 4.6, Pyr), 12.19 (1H, s, NH); ^{13}C NMR (DMSO-d_6, 125 MHz) δ 14.40 (CH_3), 116.60 (Ar), 116.75 (Ar), 121.61 (Ar), 121.87 (Ar), 123.37 (Ar), 126.37 (Ar), 126.53 (C=C), 126.61 (Ar), 131.37 (Ar), 135.95 (Ar), 140.52 (Pyr), 143.63 (Pyr), 147.60 (Pyr), 149.60 (C=C), 149.75 (C=N), 149.99 (Ar), 150.08 (Ar), 158.15 (Ar), 161.59 (C=O), 166.50 (C=O); [Found (ESI+) 433.1533 $[M+H]^+$, $C_{23}H_{21}N_4O_5$ requires 433.1506].

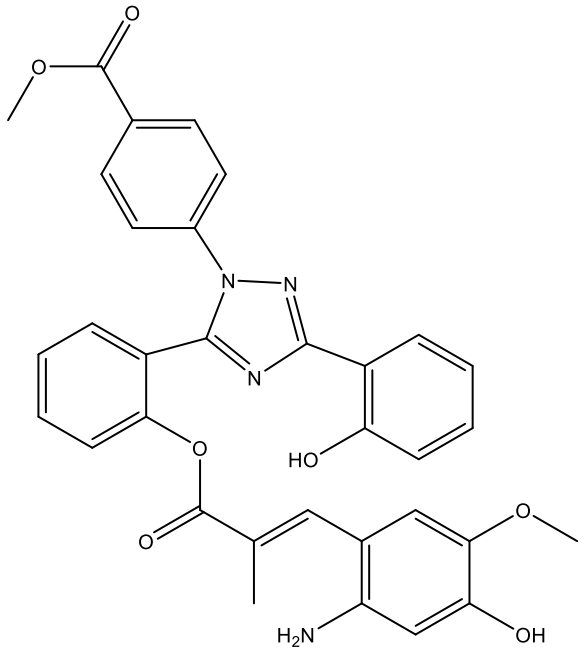

Methyl (*E*)-4-(5-(2-((3-(2-amino-4-hydroxy-5-methoxyphenyl)-2-methylacryloyl)oxy)phenyl)-3-(2-hydroxyphenyl)-1H-1,2,4-triazol-1-yl)benzoate (117)

A solution of **111** (90 mg, 0.13 mmol) in TFA (8 mL) was stirred at 30°C under an argon atmosphere overnight. The TFA was evaporated and the residue was co-evaporated with MeCN (3 x 10 mL). The resulting residue was purified by column chromatography eluting with 0-30% acetone in DCM to give **117** as a yellow oil (71 mg, 92%). R_f = 0.80 (5% MeOH: DCM); R_t = 8.8 min (solvent system A); UV (EtOH) λ_{max} 304 (1100), 378 (3630); ^{1}H NMR ($CDCl_3$, 500 MHz) δ 1.90 (3H, d, J = 1.0, CH_3), 3.69 (3H, s, OCH_3), 3.86 (3H, s, OCH_3), 5.07 (1H, s, OH), 6.24 (1H, s, Ar), 6.54 (1H, s, Ar), 6.87 (1H, td, J = 7.5, 1.0, Ar), 6.92 (1H, dd, J = 8.0, 1.0, Ar), 7.16-7.18 (2H, m, Ar), 7.24 (1H, td, J = 7.5, 2.0, Ar), 7.27 (1H, d, J = 8.5, Ar), 7.50 (1H, td, J = 6.0, 2.5, Ar), 7.54 (2H, d, J = 8.5, Ar), 7.60 (1H, d, J = 2.0, HC=C), 7.99 (2H, d, J = 8.5, Ar), 8.05 (1H, dd, J = 10.0, 2.5, Ar), 10.94 (1H, br s, OH). ^{13}C NMR ($CDCl_3$, 125 MHz) δ 14.48 (CH_3), 52.47 (OCH_3), 56.62 (OCH_3), 102.76 (Ar), 112.08 (Ar), 112.35 (Ar), 113.44 (Ar), 117.32 (Ar), 119.65 (Ar), 120.93 (Ar), 123.84 (Ar), 124.20 (Ar), 125.04 (C=C), 125.90 (Ar), 126.87 (Ar), 130.22 (Ar), 130.81 (Ar), 130.88 (Ar), 131.54 (Ar), 132.18 (Ar), 137.94 (C=C), 139.30 (Ar), 140.80 (Ar), 140.94 (Ar), 147.86 (Ar), 149.59 (Ar), 150.01 (Tri), 157.02 (Ar), 161.17 (Tri), 166.01 (C=O), 166.50 (C=O); [Found (ESI+) 593.2041 $[M+H]^+$, $C_{33}H_{29}N_4O_7$ requires 593.2031].

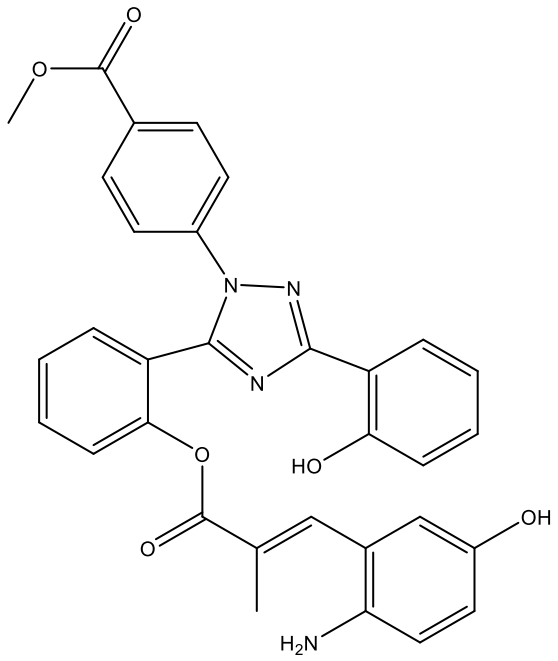

Methyl (*E*)-4-(5-(2-((3-(2-amino-5-hydroxyphenyl)-2-methylacryloyl)oxy)phenyl)-3-(2-hydroxyphenyl)-1H-1,2,4-triazol-1-yl)benzoate (118)

A solution of **112** (76 mg, 0.12 mmol) in TFA (5 mL) was stirred at 30°C under an argon atmosphere overnight. The TFA was evaporated and the residue was co-evaporated with MeCN (3 x 10 mL). The resulting oil was purified by column chromatography eluting with 0-30% acetone in DCM to give **118** as a yellow glass (39 mg, 57%). R_f = 0.80 (5% MeOH: DCM); R_t = 8.2 min (solvent system A); UV (EtOH) λ_{max} 290 (6500), 378 (1250); ^{1}H NMR (DMSO-d_6, 400 MHz) δ 1.86 (3H, d, J = 1.6, CH_3), 3.87 (3H, s, OCH_3), 4.59 (2H, br s, NH_2), 6.54 (1H, s, Ar), 6.59 (2H, d, J = 1.2, Ar), 6.99 (1H, td, J = 7.2, 1.2, Ar), 7.02 (1H, dd, J = 8.4, 1.6, Ar), 7.37 (1H, td, J = 7.6, 1.6, Ar), 7.40-7.47 (3H, m, Ar and HC=C), 7.58 (1H, dd, J = 7.6, 1.6, Ar), 7.63 (2H, d, J = 6.4, Ar), 7.70 (1H, td, J = 7.2, 1.6, Ar), 8.01-8.04 (3H, m, Ar), 8.62 (1H, s, OH), 10.70 (1H, s, OH); ^{13}C NMR (DMSO-d_6, 100 MHz) δ 14.09 (CH_3), 52.42 (OCH_3), 113.27 (Ar), 114.95 (Ar), 116.86 (Ar), 117.12 (Ar), 117.94 (Ar), 119.76 (Ar), 120.29 (Ar), 123.72 (Ar), 124.43 (Ar), 124.69 (C=C), 126.21 (Ar), 126.79 (Ar), 129.78 (Ar), 130.38 (Ar), 131.37 (Ar), 131.63 (Ar), 132.46 (Ar), 138.28 (C=C), 139.91 (Ar), 140.40 (Ar), 140.94 (Ar), 147.85 (Ar), 148.72 (Ar), 150.12 (Tri), 156.24 (Ar), 160.08 (Tri), 165.22 (C=O), 165.82 (C=O); [Found (ESI+) 563.1937 $[M+H]^+$, $C_{32}H_{27}N_4O_6$ requires 563.1925].

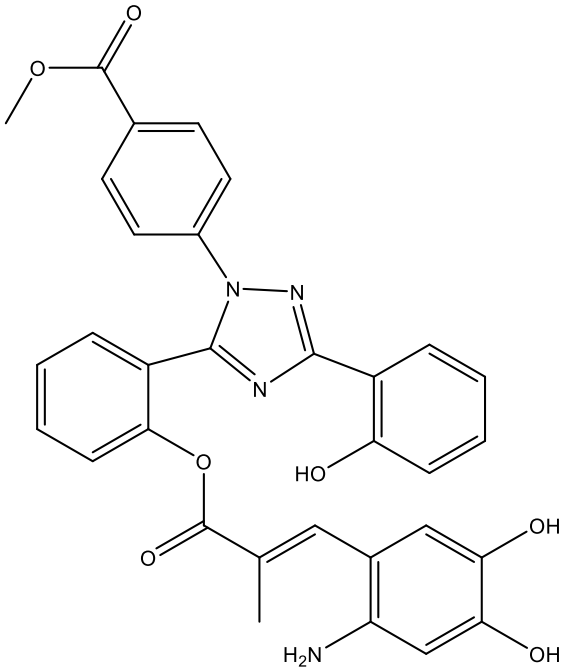

Methyl (*E*)-4-(5-(2-((3-(2-amino-4,5-dihydroxyphenyl)-2-methylacryloyl)oxy)phenyl)-3-(2-hydroxyphenyl)-1H-1,2,4-triazol-1-yl)benzoate (119)

A solution of **113** (24 mg, 0.032 mmol) in TFA (3 mL) was stirred at 30°C under an argon atmosphere overnight. The TFA was evaporated and the residue was co-evaporated with MeCN (3 x 10 mL). The resulting oil was purified by column chromatography eluting with 0-30% acetone in DCM to give **119** as a yellow glass (3 mg, 16%). R_f = 0.50 (20% acetone: DCM); R_t = 8.1 min (solvent system A); UV (EtOH) λ_{max} 300 (2675); ^{1}H NMR (DMSO-d_6, 500 MHz) δ 1.89 (3H, s, CH_3), 3.88 (3H, s, CO_2CH_3), 6.47 (1H, s, Ar), 6.72 (1H, s, Ar), 6.98 (1H, td, J = 8.2, 1.2, Ar), 7.02 (1H, dd, J = 8.4, 1.2, Ar), 7.37 (1H, td, J = 8.2, 1.6, Ar), 7.40- 7.43 (2H, m, Ar), 7.53 (1H, d, J = 1.2, C=CH), 7.58 (1H, dd, J = 8.0, 1.6), 7.62 (2H, d, J = 8.4, Ar), 8.07 (1H, td, J = 8.0, 1.2, Ar), 8.01- 8.05 (3H, m, Ar), 8.54 (1H, br s, OH), 9.50 (1H, br s, OH), 10.67 (1H, br s, OH); ^{13}C NMR (DMSO-d_6, 125 MHz) δ 14.18 (CH_3), 52.41 ($CO_2\underline{C}H_3$), 113.30 (Ar), 116.24 (Ar), 117.10 (Ar), 119.72 (Ar), 120.35 (Ar), 122.95 (Ar), 123.62 (Ar), 124.39 (Ar), 126.17 (Ar), 126.81 (C=C), 129.32 (Ar), 129.78 (Ar), 130.37 (Ar), 131.37 (Ar), 131.49 (Ar), 131.61 (Ar), 132.46 (Ar), 137.43 (Ar), 138.45 (Ar), 140.39 (C=C), 148.02 (Ar), 148.79 (Ar), 150.17 (Ar), 150.89 (Tri), 156.27 (Ar), 160.10 (Tri), 165.24 (C=O), 165.95 (C=O); [Found (ESI+) 679.1917 $[M+H]^+$, $C_{32}H_{27}N_4O_7$ requires 579.1874].

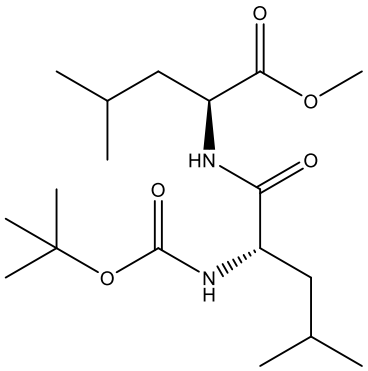

Methyl (*tert*-butoxycarbonyl)-*L*-leucyl-*L*-leucinate (122)[268]

A stirred solution of Boc-L-leucine (10 g, 43 mmol) in anhydrous DMF (60 mL) was cooled to 0 ^{o}C and treated with HOBt (8.8 g, 65 mmol) and EDC.HCl (12.5 g, 65 mmol) and the mixture was allowed to stir for 30 min. A solution of L-leucine methyl ester hydrochloride (7.8 g, 43 mmol) and DIPEA (22.6 mL, 130 mmol) in anhydrous DMF (40 mL) was added and the mixture was allowed to warm to RT and was stirred for 24 h. The solvent was evaporated and the residue was dissolved in DCM (150 mL) and washed with sat. NH_4Cl (3 x 150 mL), 10% $NaHCO_3$ (3 x 150 mL) and brine (100 mL). The organic phase was dried over $MgSO_4$, filtered and the solvent was evaporated to give **122** as a white solid (15.3 g, 74%). R_f = 0.50 (5% MeOH: DCM); mp = 128-134^{o}C (lit.[286] 135-136^{o}C); ^{1}H NMR ($CDCl_3$, 400 MHz) δ 0.86- 0.90 (12H, m, 2x $(CH_3)_2$), 1.39 (9H, s, $(CH_3)_3$), 1.41- 1.66 (6H, m, 2x $(CH_3)_2C\underline{H}C\underline{H_2}$), 3.67 (3H, s, OCH_3), 4.04 (1H, br s, CH), 4.56 (1H, td, J = 8.8, 4.4, CH), 4.81 (1H, br s, NH), 6.37 (1H, d, J = 8.8, NH); ^{13}C NMR ($CDCl_3$, 100 MHz) δ 21.75 (CH_3), 22.74 (CH_3), 24.62 (CH), 24.66 (CH), 28.19 (($CH_3)_3$), 40.77 (CH_2), 41.53 (CH_2), 50.56 (OCH_3), 52.12 (NHCH), 52.13 (NHCH), 77.10 ($\underline{C}(CH_3)_3$) 149.84 (C=O), 170.91 (C=O), 174.07 (C=O).

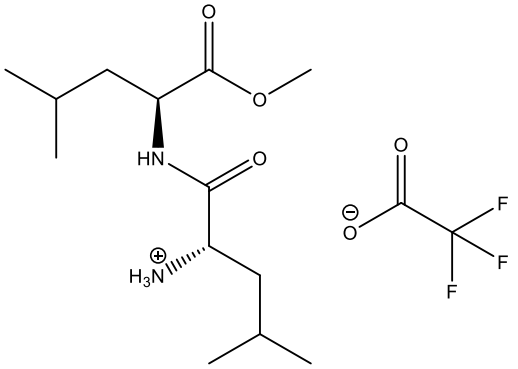

***L*-Leucyl-*L*-leucine methyl ester trifluoroacetate (123)**

A stirred solution of **122** (11.3 g, 31.7 mmol) in DCM (50 mL) was treated with TFA (50 mL) and the mixture was stirred at RT for 1.5 h. The solvent was evaporated and the product was dried to give **123** as a white solid (11.8 g, 99%). R_f = 0.63 (12% MeOH:DCM); mp = 115-120^oC; ^1H NMR (CD_3OD, 400 MHz) δ 0.96- 1.06 (12H, m, 2x $(CH_3)_2$), 1.65- 1.83 (6H, m, 2x $(CH_3)_2CHCH_2$), 3.74 (3H, s, OCH_3), 3.92 (1H, q, J= 8.0, CH), 4.53 (1H, t, J = 8.0, CH); ^{13}C NMR (CD_3OD, 100 MHz) δ 21.79 (CH_3), 22.10 (CH_3), 23.10 (CH_3), 23.23 (CH_3), 25.27 (CH), 25.92 (CH), 41.30 (CH_2), 41.80 (CH_2), 52.39 (CHNH), 52.75 (CHNH), 52.88 (OCH_3), 170.91 (C=O), 174.07 (C=O).

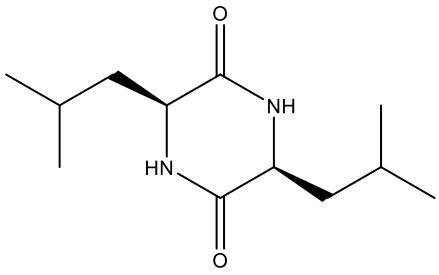

(3*S*,6*S*)-3,6-diisopentylpiperazine-2,5-dione (124)[268]

A solution of **122** (11.8 g, 31.7 mmol) in 0.1M acetic acid in butan-1-ol (200 mL) was treated with DIPEA (5.7 mL, 32.7 mmol) was added and the mixture was stirred at reflux under an argon atmosphere overnight. The mixture was cooled to RT and the solvent was evaporated. The resulting clear residue was dissolved in $CHCl_3$ (100 mL) and extracted with H_2O (4 x 100

mL) and brine (100 mL), then dried over $MgSO_4$, filtered and the solvent was evaporated to give **124** as a white solid (6.67 g, 93%). R_f = 0.40 (10% MeOH: DCM); mp = 275-278^oC (lit.[287] 270-272^oC); ^1H NMR ($CDCl_3$, 400 MHz) δ 0.90 (6H, d, J = 6.0z, 2x CH_3), 0.94 (6H, d, J = 6.0, 2x CH_3), 1.53- 1.61 (2H, m, 2x C<u>H</u>$(CH_3)_2$), 1.71- 1.83 (4H, m, 2x CH_2), 3.93 (2H, dt, J = 6.0, 2.8, 2x C<u>H</u>CH_2), 6.63 (2H, br s, 2x NH); ^{13}C NMR ($CDCl_3$, 100 MHz) δ 21.10 (CH_3), 23.16 (CH_3), 24.22 (CH), 43.39 (CH_2), 53.28 (CH), 168.81 (C=O); [Found (ESI+) 249.1574 $[M+Na]^+$, $C_{12}H_{22}N_2NaO_2$ requires 249.1573].

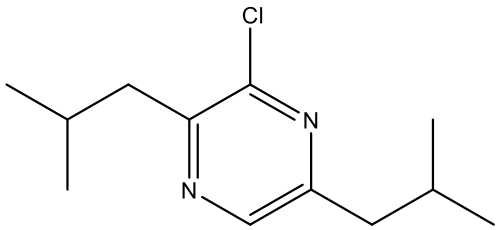

3-Chloro-2,5-diisobutylpyrazine (128)

Method A:[261]

A stirred suspension of **124** (625 mg, 2.76 mmol) in $POCl_3$ (5 mL) was heated overnight at 100 ^oC in a sealed pressure tube. The mixture was cooled to RT then poured onto ice water (50 mL) and allowed to stir for 30 min. The aqueous phase was extracted with DCM (3 x 50 mL) and the combined organic phases were washed with 1M NaOH (2 x 100 mL) and brine (100 mL), then dried over $MgSO_4$ and filtered. The solvent was evaporated to give an orange oil which was purified by column chromatography eluting with toluene to give **128** as a colourless oil (242 mg, 39%) along with **127** (120 mg, 17%). R_f = 0.30 (5% EtOAc: petroleum ether); R_t = 11.59 min (solvent system A); ^1H NMR ($CDCl_3$, 400 MHz) δ 0.79- 0.84 (12H, m, 4x CH_3), 1.97 (1H, nonet, J = 6.8, CH), 2.09 (1H, nonet, J = 6.8, CH), 2.48 (2H, d, J = 7.2, CH_2), 2.67 (2H, d, J = 7.2, CH_2), 8.11 (1H, s, Pyr); ^{13}C NMR ($CDCl_3$, 100 MHz) δ 22.12 (CH_3), 22.27 (CH_3), 27.77 (CH), 28.65 (CH), 43.01 (CH_2), 43.36 (CH_2), 141.62 (Pyr), 148.02 (Pyr), 152.25 (Pyr), 153.93 (Pyr); [Found (ESI-) 451.2383 $[(M)(M-H)]^-$, $C_{24}H_{37}N_4Cl_2$ requires 451.2390].

Method B:[260]

A suspension of **124** (132 mg, 0.58 mmol) in $POCl_3$ (1 mL) was stirred at RT overnight in a sealed pressure tube. The mixture was poured onto ice water (20 mL) and allowed to stir for 30 min. The aqueous phase was extracted with DCM (3 x 20 mL) and the combined organic phases were washed with 1M NaOH (2 x 50 mL) and brine (50 mL), then dried over $MgSO_4$ and filtered. The solvent was evaporated to give an orange oil which was purified by column chromatography eluting with toluene to give **128** as a colourless oil (39 mg, 30%).

Method C:[263]

A stirred suspension of **124** (1.01 g, 4.46 mmol) and pyridine (318 μL, 4.46 mmol) in $POCl_3$ (834 μL, 8.92 mmol) was heated for 2 h at 160°C in a sealed pressure tube. The mixture was cooled to RT then poured onto ice water (50 mL) and allowed to stir for 30 min. The aqueous phase was extracted with DCM (3 x 50 mL) and the combined organic phases were washed with 1M NaOH (2 x 100 mL) and brine (100 mL), then dried over $MgSO_4$ and filtered. The solvent was evaporated to give an orange oil which was purified by column chromatography eluting with toluene to give **128** as a colourless oil (575 mg, 56%) along with **127** (43 mg, 4%).

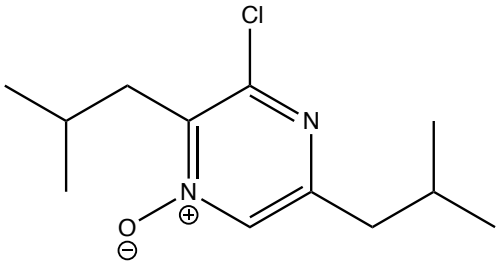

3-chloro-2,5-diisobutylpyrazine 1-oxide (129)

Method A:[261]

A solution of **128** (221 mg, 0.97 mmol) and 70% *m*-CPBA (717 mg, 2.91 mmol) in anhydrous DCM (10 mL) was stirred at 40 °C overnight. The organic phase was extracted with 5% $Na_2S_2O_5$ (3 x 20 mL) and brine (20 mL). Peroxide levels were tested using Merck peroxide test strips to

ensure that the concentration was <3 mg/L, then the organic phase was dried over $MgSO_4$, filtered and the solvent was evaporated to give a yellow oil which was a 4:1 mixture of **129** and **130** respectively (231 mg), determined by ^1H NMR integration.

Method B:

A solution of **128** (570 mg, 2.51 mmol) and 70% *m*-CPBA (1.85 g, 7.53 mmol) in anhydrous DCM (40 mL) was stirred at 40 °C for 3 h. The organic phase was extracted with 5% $Na_2S_2O_5$ (3 x 50 mL) and brine (50 mL). Peroxide levels were tested using Merck peroxide test strips to ensure that the concentration was <3 mg/L, then the organic phase was dried over $MgSO_4$, filtered and the solvent was evaporated to give **129** as a yellow oil (600 mg, 98%). R_f = 0.2 (5% EtOAc: petroleum ether); R_t = 10.37 min (solvent system A); ^1H NMR ($CDCl_3$, 400 MHz) δ 0.87-0.93 (12H, m, CH_3), 2.03 (1H, nonet, J = 6.8, CH), 2.19 (1H, nonet, J = 6.8, CH), 2.43 (2H, d, J = 7.2, CH_2), 2.85 (2H, d, J = 7.2, CH_2), 7.84 (1H, s, Pyr); ^{13}C NMR ($CDCl_3$, 100 MHz) δ 22.24 (CH_3), 22.63 (CH_3), 26.19 (CH), 28.41 (CH), 35.51 (CH_2), 43.93 (CH_2), 141.62 (Pyr), 151.22 (Pyr), 155.25 (Pyr), 155.93 (Pyr); ^{15}N NMR ($CDCl_3$, 40 MHz) δ 273.95 (N^+-O^-), 282.56 (C=N); [Found (ESI+) 243.1275 $[M+H]^+$, $C_{12}H_{20}N_2OCl$ requires 243.1259].

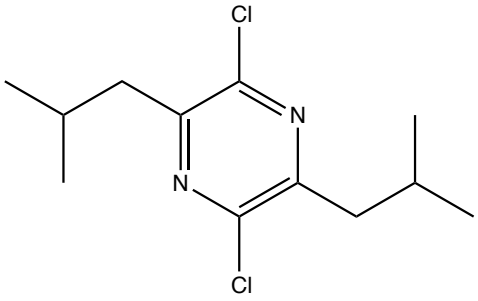

2,5-dichloro-3,6-diisobutylpyrazine (127)

Method A:[261]

A suspension of 4:1 **129** and **130** (200 mg, 0.82 mmol) in $POCl_3$ (2 mL) was stirred overnight at 100 °C in a sealed pressure tube. The mixture was cooled to RT then poured onto ice water (20 mL) and allowed to stir for 30 min. The aqueous phase was extracted with DCM (3 x 30 mL) and the combined organic phases were washed with 1M NaOH (2 x 80 mL) and brine (80

mL), then dried over $MgSO_4$ and filtered. The solvent was evaporated to give an orange oil which was purified by column chromatography eluting with toluene to give **127** as a colourless oil (125 mg, 59%).

Method B:

A suspension of **129** (600 mg, 2.47 mmol) in $POCl_3$ (6 mL) was stirred overnight at 100 ^oC in a sealed pressure tube. The mixture was cooled to RT then poured onto ice water (50 mL) and allowed to stir for 30 min. The aqueous phase was extracted with DCM (3 x 50 mL) and the combined organic phases were washed with 1M NaOH (2 x 100 mL) and brine (100 mL), then dried over $MgSO_4$ and filtered. The solvent was evaporated to give an orange oil which was purified by column chromatography eluting with toluene to give **127** as a colourless oil (540 mg, 84%). R_f = 0.75 (5% EtOAc: petroleum ether); R_t = 12.48 min (solvent system A); ^1H NMR ($CDCl_3$, 400 MHz) δ 0.92 (12H, d, J = 6.8, 2x CH_3), 2.16 (2H, nonet, J = 6.8, 2x CH), 2.72 (4H, d, J = 7.2, 2x CH_2); ^{13}C NMR ($CDCl_3$, 100 MHz) δ 22.27 (CH_3), 27.99 (CH), 42.60 (CH_2), 145.77 (Pyr), 152.45 (Pyr); ^{15}N NMR ($CDCl_3$, 40 MHz) δ 305.25 (C=N).

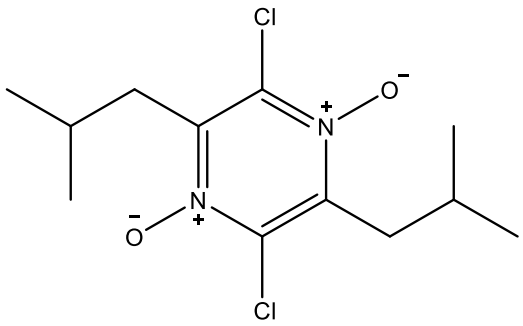

2,5-dichloro-3,6-diisobutylpyrazine 1,4-dioxide (131)

A solution of **127** (541 mg, 2.07 mmol) in TFA (5.4 mL) was treated with 50% H_2O_2 (1.10 mL, 19.3 mmol) added dropwise and then heated gently under stirring at 50 ^oC for 3 h. The mixture was cooled to RT and slowly poured onto ice cold sat. $Na_2S_2O_5$ (50 mL) and was neutralised with 1M NaOH (60 mL). Peroxide levels were tested using Merck peroxide test strips to ensure that the concentration was <3 mg/L, The aqueous phase was then extracted with DCM (3 x 50 mL) and washed with brine (100 mL), dried over $MgSO_4$, filtered and the solvent was

evaporated. Purification by column chromatography eluting with DCM gave **131** as a white solid (410 mg, 67%). R_f = 0.40 (DCM); R_f = 9.3 min (solvent system A); mp = 185- 190^oC; IR (KBr) 1466s (N^+-O^-); ^1H NMR ($CDCl_3$, 500 MHz) δ 0.95 (12H, d, J = 7.0, 4x CH_3), 2.27 (2H, nonet, J = 7.0, 2x CH), 2.96 (4H, d, J = 7.5, 2x CH_2);^{13}C NMR ($CDCl_3$, 125 MHz) δ 22.61 (CH_3), 26.23 (CH), 37.86 (CH_2), 139.70 (Pyr), 146.11 (Pyr); ^{15}N NMR ($CDCl_3$, 50 MHz) δ 248.05 (N^+-O^-); [Found (ESI+) 293.0825 $[M+H]^+$, $C_{12}H_{19}Cl_2N_2O_2$ requires 293.0818].

132 was also isolated (109 mg, 20%). R_f = 0.85 (DCM); R_f = 11.2 min (solvent system A); ^1H NMR ($CDCl_3$, 500 MHz) δ 0.92 (12H, m, 4x CH_3), 2.15 (1H, nonet, J = 7.0, CH), 2.23 (1H, nonet, J = 7.0, CH), 2.71 (2H, d, J = 7.0, CH_2), 2.89 (2H, d, J = 7.0, CH_2); ^{13}C NMR ($CDCl_3$, 125 MHz) δ 22.32 (CH_3), 22.69 (CH_3), 26.00 (CH), 27.95 (CH), 36.77 (CH_2), 43.60 (CH_2), 138.61 (Pyr), 144.83 (Pyr), 147.22 (Pyr), 154.01 (Pyr); ^{15}N NMR ($CDCl_3$, 50 MHz) δ 270.83 (N^+-O^-), 276.54 (C=N); [Found (ESI+) 277.0876 $[M+H]^+$, $C_{12}H_{19}Cl_2N_2O$ requires 277.0869].

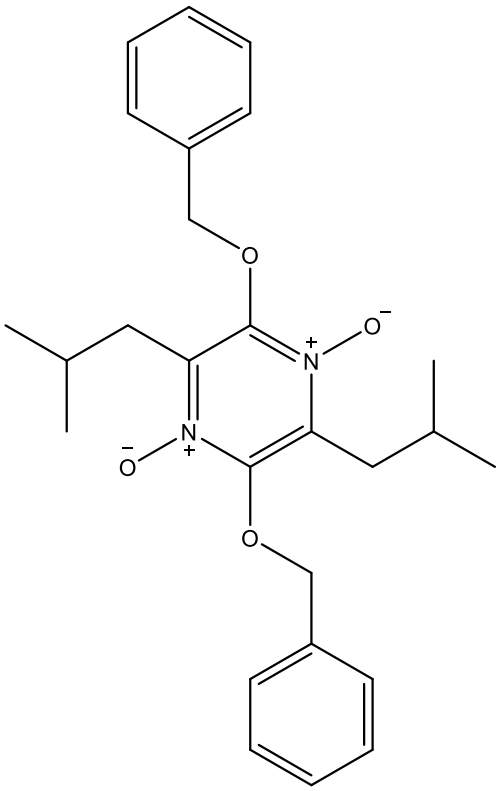

2,5-bis(benzyloxy)-3,6-diisobutylpyrazine 1,4-dioxide (133)

Method A:

A solution of **131** (112 mg, 0.38 mmol) in anhydrous THF (4 mL) was treated with KO^tBu (150 mg, 1.34 mmol) and benzyl alcohol (139 µL, 1.34 mmol) and stirred overnight at RT under an argon atmosphere. The mixture was quenched by addition of H_2O (20 mL) and extracted with DCM (3 x 20 mL). The combined organic phases were washed with brine (20 mL), then dried over $MgSO_4$, filtered and the solvent was evaporated to give an orange oil. Purification by column chromatography eluting with 0-2 % acetone in DCM gave **133** and **134** in a 6:1 ration respectively as a yellow oil (77 mg, 46%). R_f = 0.55 (DCM); R_t = 11.33 min (solvent system A); ^{1}H NMR (**133**) ($CDCl_3$, 400 MHz) δ 0.85 (12H, d, J = 6.8, 4x CH_3), 2.19 (2H, nonet, J = 6.8, 2x CH), 2.59 (4H, d, J = 7.6, 2x C$\underline{H_2}$CH), 5.44 (4H, s, CH_2), 7.28-7.35 (10H, m, Ar); ^{13}C NMR ($CDCl_3$, 100 MHz) δ 22.55 (CH_3), 25.91 (CH), 33.80 (CH_2), 74.06 (CH_2), 128.62 (Ar), 129.04 (Ar), 129.07 (Ar), 134.78 (Ar), 139.86 (Pyr), 150.66 (Pyr); [Found (ESI+) 459.2297 $[M+Na]^+$, $C_{26}H_{32}N_2NaO_4$ requires 459.2254].

Method B:[260]

A solution of **131** (28 mg, 0.096 mmol) in anhydrous THF (2 mL) was treated with NaO^tBu (28 mg, 0.29 mmol) and benzyl alcohol (30 µL, 0.29 mmol) and stirred overnight at RT under an argon atmosphere. The reaction was quenched by addition of H_2O (10 mL) and extracted with DCM (3 x 10 mL). The combined organic phases were washed with brine (20 mL), then dried over $MgSO_4$, filtered and the solvent was evaporated to give an orange oil. Purification by column chromatography eluting with 0-30 % EtOAc in petroleum ether gave **134** as a yellow oil (11 mg, 44%). R_f = 0.55 (DCM); R_t = 11.33 min (solvent system A); IR (KBr) 1644s (C=O), 1505s (N^+-O^-); ^{1}H NMR ($CDCl_3$, 400 MHz) δ 0.80 (6H, d, J = 6.8, 2x CH_3), 0.90 (6H, d, J = 6.8, 2x CH_3), 2.03 (1H, nonet, J = 6.8, CH), 2.25 (1H, nonet, J = 6.8, CH), 2.37 (2H, d, J = 7.6, C$\underline{H}_2$CH), 2.79 (2H, d, J = 7.6, C$\underline{H}_2$CH), 5.26 (2H, s, OCH_2), 5.29 (2H, s, OCH_2), 7.26-7.39 (10H, m, Ar).

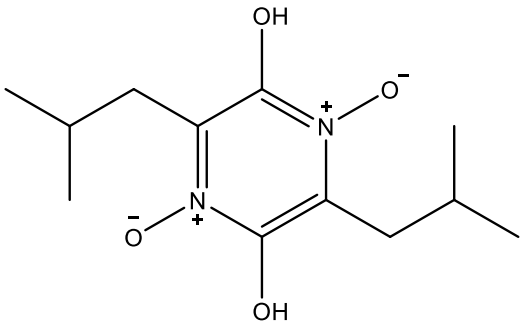

2,5-Dihydroxy-3,6-diisobutylpyrazine 1,4-dioxide, pulcherriminic acid (14)

A solution of **133** and **134** (62 mg, 0.14 mmol) in anisole (2 mL) was treated with TFA (2 mL) and the mixture was stirred for 2.5 h at RT under an argon atmosphere. The solvent was evaporated to give a yellow solid which was filtered off and washed with cold MeOH (3 x 10 mL) and then dried to give **14** as a pale yellow powder (27 mg, 75%). R_f = 0.30 (5% acetone: DCM); R_t = 7.7 min (solvent system A); mp = 160-165°C (lit.[248] 162-164°C); ^{1}H NMR (DMSO-d_6, 400 MHz) δ 0.90 (12H, d, J = 6.4, CH_3), 2.12 (2H, nonet, J = 6.8, CH), 2.68 (4H, d, J = 7.6, CH_2); ^{13}C NMR (DMSO-d_6, 100 MHz) δ 22.34 (CH_3), 26.17 (CH), 33.36 (CH_2), 129.56 (Pyr), 145.46 (Pyr); [Found (APCI+ direct probe) 257.1515 $[M+H]^+$, $C_{12}H_{21}N_2O_4$ requires 257.1496].

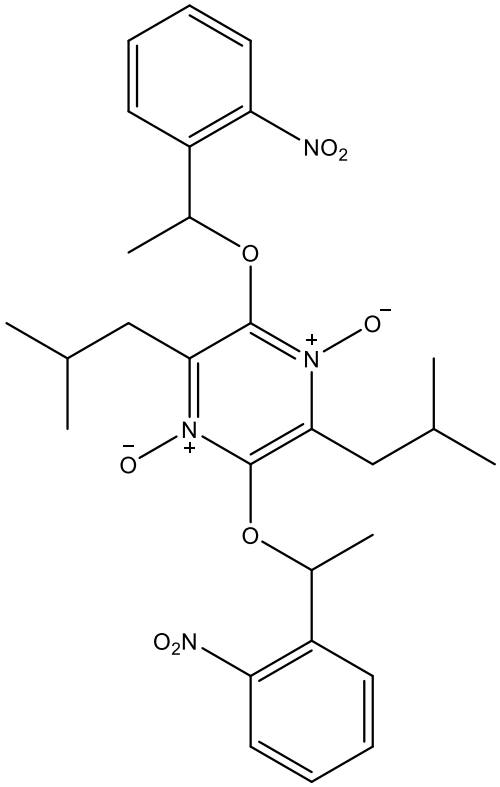

2,5-Diisobutyl-3,6-bis(1-(2-nitrophenyl)ethoxy)pyrazine 1,4-dioxide (135)

A solution of **131** (26 mg, 0.089 mmol) in anhydrous THF (2 mL) was treated with NaO^tBu (26 mg, 0.27 mmol) and 2-trimethylsilyl ethanol (36 µL, 0.27 mmol) and the mixture was stirred at RT overnight under an argon atmosphere. The reaction was quenched by addition of H_2O (10 mL) and extracted with DCM (3 x 10 mL). The combined organic phases were washed with brine (20 mL), then dried over $MgSO_4$, filtered and the solvent was evaporated. Purification by column chromatography eluting with 0-2% acetone in DCM gave a mixture of **135** and **136** (20 mg). **135**: [Found (ESI+) 555.2481 $[M+H]^+$, $C_{28}H_{35}N_4O_8$ requires 555.2449]; **136:** [Found (ESI+) 446.1485 $[M+Na]^+$, $C_{20}H_{26}ClN_3NaO_5$ requires 446.1459].

2. Biology

2.1. General

Chemical reagents and dyes were purchased from Sigma-Aldrich Chemical Co. (Poole, UK) and Invitrogen (Thermo Fischer Scientific). Cell culture media was obtained from Sigma-Aldrich Chemical Co. and foetal calf serum (FCS) was obtained from Gibco (Thermo Fischer Scientific). Nunclon Delta treated plasticware for adherent cells was purchased from Thermo Fisher Scientific. All buffers, solutions and phosphate buffered saline (PBS) were prepared from sterilised MilliQ water to minimize the presence of trace elements including transition metals. Stock solutions of 2.5% w/v trypsin, 200 mM glutamine, 10000 μg/mL penicillin/streptomycin and 50 mg/mL MTT were kept at -4 ^{o}C. Unless stated, all cell culture reagents were warmed to 37 ^{o}C prior to use.

2.2 Cell Culture

All cells were cultured and incubated in a 5% CO_2 cell culture incubator set at 37 ^{o}C. The cell model used was FEK4, a primary human dermal fibroblast cell line.[52] The medium used to culture the cells was 15% FCS EMEM with 0.22% w/v sodium bicarbonate, 2 mM L-glutamine, and 2.5 mg of penicillin/streptomycin premix. The FCS stock was heat-inactivated at 56 ^{o}C for 30 min before use. Stock cells were passaged by trypsinisation once or twice a week. Flasks were usually maintained in culture until they reached 80-90% confluency before being trypsinised as follows:

The medium was aspirated from the flask, and the cells were washed with PBS (10 mL) before being treated with 0.25% w/v trypsin (4-5 mL). Cells were incubated at 37 ^{o}C for 5 min until detached. Further medium (4-5 mL) was then added back to the flask to deactivate the trypsin. The cell suspension was transferred to a Falcon tube and centrifuged for 5 min at 1000 rpm (Jouan B3.11 centrifuge) followed by aspiration of the supernatant and resuspension of the remaining cell pellet in 15% FCS EMEM (4 mL). An aliquot (50 μL) of the cell suspension was mixed with 0.4% w/v trypan blue solution (50 μL) and counted under a

microscope using a Haemocytometer (Marienfeld, Germany). Cells were then diluted with 15% FCS EMEM at the required density for seeding. Passages up to 20 were used for experiments.

2.3 Chemical Treatment of Cells

Stock solutions at 20 mM and 100 mM in DMSO were prepared for all synthesised ICs, CICs and carbostyrils. These solutions were stored at -4 ^{o}C, wrapped in foil. For all experiments, including those with chemical treatment, cells were seeded at a density of 5 x 10^4 in media (2 mL/3.5 cm dish) and incubated for 48 h at 37 ^{o}C prior to treatment. 3 x 3.5 cm dishes per condition were typically used. The conditioned medium (CM, the medium in which the cells had grown for 48 h) was removed from the dish and the required amount of 20 mM stock solution was added to the CM to give a final concentration of 20 µM of compound. The CM was added back to the dishes and the cells were incubated at 37 ^{o}C for 18 h before irradiation to analyse the photoprotective effect of the compounds. For analysis of the cytotoxicity of compounds, CM containing 20-50 µM of compound was incubated with cells for 24-72 h.

2.4 Irradiation Procedures

UVA irradiation was carried out using a broad spectrum 4 kW lamp (Sellas, Germany) which emits in the range of 340- 400 nm, the spectral output of the UVA lamp is shown in Figure 73. The UVA doses were measured using an IL1700 radiometer (International light, Newbury, MA), with irradiation times varying from 15 s to 75 min depending on the experiment.

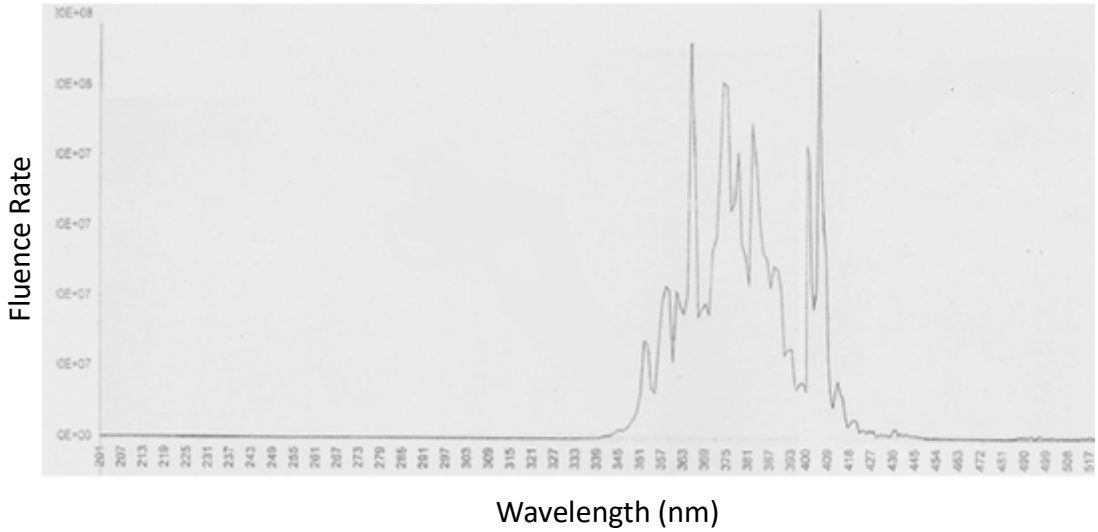

Figure 73. Output spectrum of the 4 kW UVA lamp (Sellas, Germany) in wavelength (nm).

2.4.1 Cellular Experiments

Irradiation of cells was carried out in an air-cooled room to keep the cells at 25 ^{o}C throughout the irradiation procedure. Before irradiation, the medium was aspirated from the cells which were then washed with PBS (1 mL/dish), aspirated and covered with PBS (1 mL/dish). Cells were irradiated in dishes covered by lids to prevent evaporation with UVA doses of 250-750 kJ/m^2. After irradiation, the PBS was aspirated and then either replaced by CM (1 mL/dish) followed by incubation of the cells at 37 ^{o}C for 24 h before carrying out an assay, or the assay was carried out immediately post-irradiation. Control cells were treated in the same manner, but were kept in the laminar flow cabinet in the dark.

2.4.2 Uncaging Experiments

Chemical irradiation of CICs to elucidate the uncaging profile was carried out on 1 mg/mL solutions in DMSO (500 μL) in a quartz cuvette at UVA doses of 5- 250 kJ/m^2 (see Figure 74). Aliquots (50 μL) were diluted 1 in 10 with MeOH at the required time points before injection on analytical HPLC. The following HPLC gradient programs were used for CIC uncaging analysis: **51, 44, 55, 117** and **118:** 5% to 95% over 10 min (solvent system A); **114-116** and

119: 5% to 95% over 10 min (solvent system B); **36:** 5% to 95% over 20 min (solvent system A); **52:** 5% to 95% over 20 min (solvent system B).

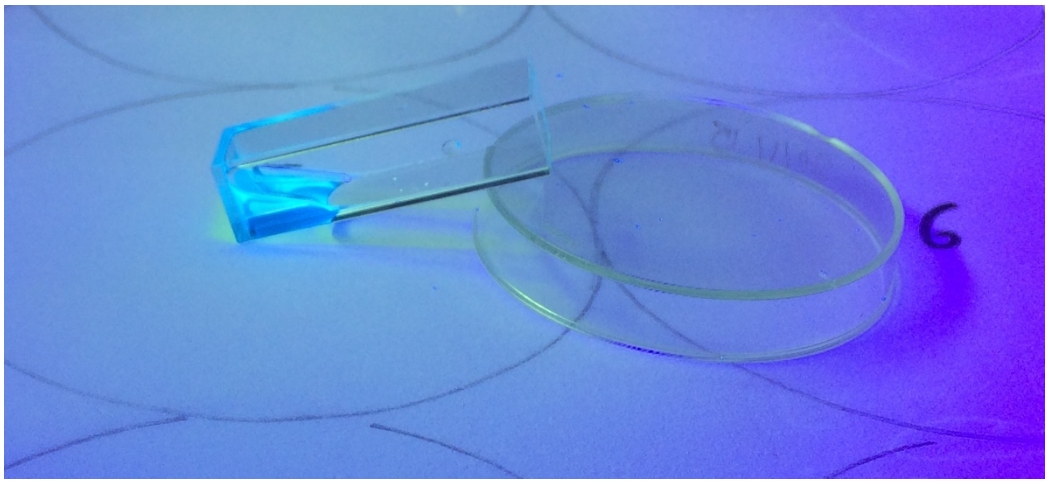

Figure 74. UVA uncaging of CICs (1 mg/mL in DMSO) carried out in a quartz cuvette under the Sellas UVA lamp.

2.4.3 Sunlight Radiometer Readings

The IL1700 radiometer was used outdoors to obtain readings for solar UVA on a British summer day (26th June 2017, University of Bath). The latitude of the test position was 51^{o} N, and the temperature in direct sunlight was 35 ^{o}C with readings being taken between 12.00 and 15.00 BST. The stability of a 1 mg/mL solution of avobenzone in DMSO was also tested under normal sunlight conditions during these experiments. The avobenzone solution was exposed to solar UVA doses of 100- 1000 kJ/m^2 and samples (50 μL) were diluted 1 in 10 with MeOH at the required time points before injection on analytical HPLC. In this way, any changes in the amount of the UVA-inactive keto tautomer of avobenzone in the solution could be observed.

2.5 Evaluation of the Efficiency of UV Filters/Sunscreen Formulations

Cells were seeded and treated in the same way as in the irradiation procedure described above, except that the dishes were covered with an extra dish containing a reservoir of a UV filter or sunscreen formulation in DMSO at varying concentrations relating to thickness of

sunscreen applications (Figure 75). After irradiation, the upper dish was removed, the PBS was aspirated and the cells were treated accordingly depending on the assay. The control samples were treated in the same manner, but were kept in the laminar flow cabinet in the dark.

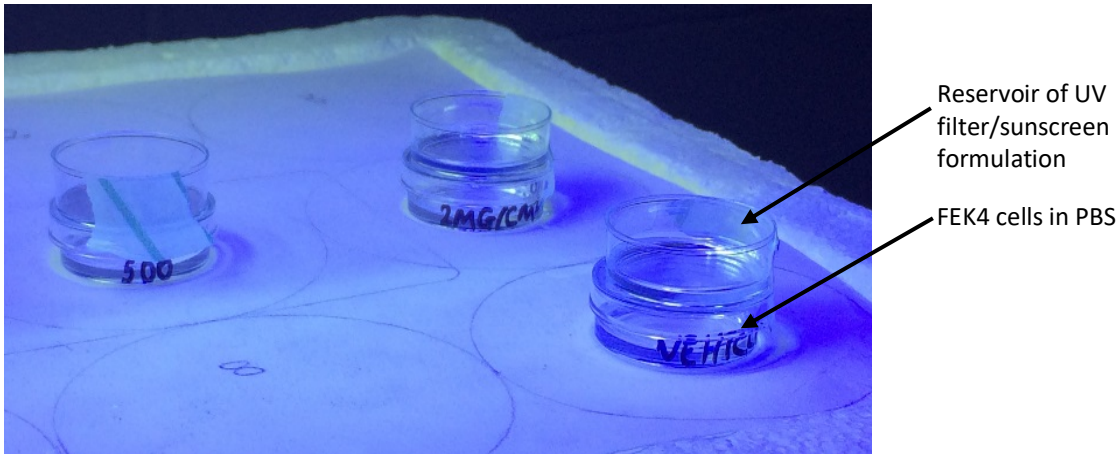

Figure 75. UV filter irradiation protocol. A 'reservoir' of filter or sunscreen formulation in DMSO is placed above the cells during irradiation. Using this technique it is possible to alter the concentration of sunscreen to mimic the thickness of sunscreen applied to the skin by a consumer.[71]

2.6 DPPH Assay

A stock solution of 1M DPPH in MeOH was stored at -4 °C and wrapped in foil. A working solution of 100 μM DPPH in MeOH was prepared from the stock solution immediately prior to use. All compounds to be tested were stored as 400 mM stock solutions in DMSO, and freshly diluted before the assay to 10- 400 μM in MeOH. Trolox was used as the positive control. An aliquot of each concentration of compound to be tested (50 μL) was added to 100 μM DPPH (150 μL) in triplicate in a 96-well plate (Figure 76). After mixing, the plate was incubated in the dark at room temperature for 30 min. The absorbance was read at 520 nm on a UV/Vis microplate reader (SPECTROstar, BMG Labtech, Ortenberg, Germany), with MeOH used as the blank (200 μL). The control was 100 μM DPPH (150 μL) and MeOH (50 μL). The percentage radical scavenging activity of each concentration of compound was calculated using the following expression =

$$\frac{(\text{control} - \text{sample})}{\text{control}} \times 100$$

The average percentage radical scavenging activity of n=3 was plotted against concentration and the IC_{50} value was determined from the line of best fit within the linear range of activity.

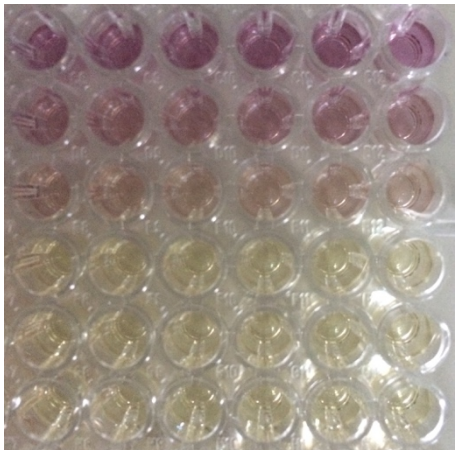

Figure 76. DPPH assay. The colour change is shown from violet (top line: control DPPH) to colourless at increasing concentrations of an active antioxidant compound.

2.7 MTT Assay

A solution of 0.5 mg/mL MTT in serum-free EMEM (SFM) was prepared as required from a stock solution of 50 mg/mL MTT in PBS and warmed at 37 ^{o}C prior to adding to cells. CM was aspirated from the dishes which were then washed with PBS before 0.5 mg/mL MTT/SFM (500 µL) was added to each dish. The cells were incubated at 37 ^{o}C for 3 h. The MTT solution was aspirated and DMSO (500 µL) was added to each dish to dissolve any formazan produced. Dishes were swirled for 3 min on a 3D rocking platform (Stuart Scientific, UK) and then triplicates (20 µL) from each dish were pipetted into a 96-well micro plate, diluted 1 in 5 with DMSO. The absorbance was read at 550 nm on a UV/Vis microplate reader (SPECTROstar, BMG Labtech, Ortenberg, Germany). DMSO (100 µL) was used as the blank. The mean values calculated from the raw data (optical density, OD) for the untreated unirradiated control were set as 100% enzymatic activity. The mean values of the triplicates for each treated and/or

irradiated sample were then expressed as a percentage of the unirradiated and untreated control.

2.8 CM-H_2DCFDA Assay

A vial of 50 μg CM-H_2DCFDA was thawed and dissolved in DMSO (17.3 μL) before use to make a 5 mM stock solution. This was diluted 1 in 1000 into PBS to give a working solution of 5 μM CM-H_2DCFDA, which was wrapped in foil. Immediately after irradiation at 250 kJ/m^2, the PBS was aspirated from the dishes and the cells were covered with 5 μM CM-H_2DCFDA (1 mL/dish), PBS (1 mL) was added to the unstained control. The cells were incubated at 37 ^oC for 20 min in the dark before the CM-H_2DCFDA solution was aspirated and the dishes were washed with PBS. 0.125% w/v Trypsin (1 mL) was added to each dish and the cells were incubated for 5 min. Once the cells were detached, the trypsin was neutralised with 15% FCS EMEM (1 mL) and the contents of the dishes for each condition were transferred to corresponding Falcon tubes. The Falcon tubes were centrifuged at 1000 rpm for 7 min, then the supernatant was aspirated and the cell pellet was resuspended in 0.1% BSA in PBS (200 μL). This volume was transferred to flow cytometry tubes which were kept on ice for a maximum of 15 min before analysis on the flow cytometer (FACS ARIA III, Becton Dickinson UK Ltd, Berkshire). 10,000 Events were recorded per condition and these were gated for intact cells, excluding cell debris. The median fluorescence of each condition was recorded and all medians were corrected for cell autofluorescence using the unstained control.

2.9 Annexin V/PI Assay

Stock solutions of incubation buffer (IB) ± Ca^{2+} were prepared in advance and stored at 2-8 ^oC. The composition of IB-Ca^{2+} was 140 mM NaCl and 10 mM HEPES-NaOH (pH 7.4) in MilliQ water. The composition of IB+Ca^{2+} was the same with the addition of 5 mM $CaCl_2$. After irradiation of cells in dishes at 500- 750 kJ/m^2, the PBS was aspirated and the cells were covered with CM (1 mL/dish) and incubated at 37 ^oC for 24 h. After this incubation, the CM in each dish was added to one Falcon tube per condition. The cells were then washed with PBS, which was also added to the respective Falcon tube. 0.125% w/v Trypsin (1 mL) was added to

each dish and incubated for 5 min and once the cells were detached the trypsin was neutralised with 15% FCS EMEM (1 mL) and the contents of the dishes were transferred to the corresponding Falcon tubes. The Falcon tubes were centrifuged at 1000 rpm for 7 min then the supernatant was aspirated and the cell pellet was resuspended in IB+Ca^{2+} (1 mL). A portion of each cell suspension was counted as previously described, and the volume of cell suspension correlating to 0.5 x 10^6 cells in each condition was transferred to flow cytometry tubes. These tubes were centrifuged at 1000 rpm for 5 min then supernatant from each tube was aspirated and each pellet was resuspended in annexin V premix (100 µL: 2 µL of annexin V and 98 µL of IB+Ca^{2+}). The cell suspensions were incubated for 20 min in the dark at RT, 10 µg/mL PI in IB-Ca^{2+} (100 µL) was then added to each tube to give a final concentration of 5 µg/mL PI. The cells were incubated for a further 5 min in the dark at RT before analysis on the flow cytometer (FACS ARIA III, Becton Dickinson UK Ltd, Berkshire). 10,000 events were recorded per condition and these were gated for intact cells, excluding cell debris. This selection of cells was then gated into quadrants Q1-4, where Q1= PI-positive cells only; Q2= dual stained annexin V/PI-positive cells; Q3= cells negative for both stains; Q4= annexin V-positive cells only.

2.10 Calcein (CA-AM) Assay

2.10.1 LIP Determination in a Cuvette

This method was adapted from the method laid out by Breuer *et al*.[288] A stock of fixing solution was prepared in advance and stored at 2-8 ^oC. The composition of fixing solution was 150 mM NaCl, 2 mM EDTA and 10 mM HEPES-NaOH (pH 7.4) in MilliQ water. All other solutions were made freshly before the assay. The composition of loading buffer (LB) was 20 mM HEPES-NaOH (pH 7.4) in SFM. Aliquots of CA-AM were as a 0.25 mM solution in DMSO and were stored at -4 ^oC. After irradiation at 250 kJ/m^2, the PBS was aspirated from the cells in dishes and 0.05 µM CA-AM in LB (1 mL/dish) was added. The dishes were incubated at 37 ^oC for 15 min in the dark. After the incubation the CA-AM solution was aspirated and each dish was washed with PBS. 0.125% w/v Trypsin (1 mL/dish) was added and incubated for 5 min. Once the cells were detached, the trypsin was neutralised with 3% w/v BSA in PBS (1 mL)

and the contents of the dishes for each condition were transferred to corresponding Falcon tubes. The Falcon tubes were centrifuged at 900 rpm for 7 min then the supernatant was aspirated and each cell pellet was resuspended in 0.3% w/v BSA in PBS (1 mL). This volume was transferred to 1.5 mL Eppendorf tubes. The Eppendorf tubes were centrifuged at 5000 rpm for 5 min then the supernatant was aspirated and each cell pellet was resuspended in 0.3% w/v BSA in fixing solution (1 mL). The cell suspension for each condition was transferred sequentially to a quartz cuvette for analysis on the spectrofluorimeter (F-4500, Hitachi High-Technologies). The fluorescence intensity (F_1) was read in real time and once the signal had stabilised (approximately 2 min), 40 mM SIH in DMSO (1 µL) was added to the cuvette. The cuvette was mixed and the fluorescence intensity (F_2) was read for at least 5 min. This was repeated for each cell suspension to give the ΔF as $(F_2 - F_1)/F_2$ which is equivalent to [CA-Fe]. After all the fluorescence readings were completed, a portion of cells from each condition was counted in order to normalize the ΔF per 10^6 cells. Experimental parameters used on the spectrofluorimeter were: time scan function, excitation slit: 5 nm, emission slit: 10 nm, PMT voltage: 950 V.

2.10.2 LIP Determination in a 96-well Plate Format

After irradiation of cells in dishes at 500 kJ/m^2 the PBS was aspirated from the dishes and 0.05 µM CA-AM in LB (1 mL/dish) was added. The dishes were incubated at 37 ^{o}C for 15 min in the dark. After the incubation, the CA-AM solution was aspirated and each dish was washed with PBS. 0.125% w/v Trypsin (1 mL/dish) was added and incubated for 5 min. Once the cells were detached, the trypsin was neutralised with 3% w/v BSA in PBS (1 mL) and the contents of the dishes for each condition were transferred to corresponding Falcon tubes. The Falcon tubes were centrifuged at 900 rpm for 7 min then the supernatant was aspirated and each cell pellet was resuspended in 0.3% w/v BSA in PBS (1 mL). This volume was transferred to 1.5 mL Eppendorf tubes. The Eppendorf tubes were centrifuged at 5000 rpm for 5 min then the supernatant was aspirated and each cell pellet was resuspended in 0.3% w/v BSA in fixing solution (500 µL). Duplicates of 200 µL of cell suspension per condition were pipetted into a black 96-well plate (Greiner CELLSTAR) for analysis on the CLARIOstar plate reader (BMG LABTECH). 0.3% w/v BSA in fixing solution (200 µL) was used as the blank. An initial fluorescence intensity reading was taken (F_1) before 5 mM SIH in DMSO (1.6 µL) was added

to each well. After mixing the wells with the pipette, the fluorescence was read again (F_2). As in the previous method, the ΔF for each condition was calculated as $(F_2 - F_1)/F_2$ which is equivalent to [CA-Fe]. A portion of the cell suspension of each condition (remaining in the Eppendorf tube) was counted to normalize ΔF per 10^6 cells. An aliquot (200 μL) of the supernatant from the final centrifugation (of the untreated and irradiated condition) was also added to the 96-well plate to analyse CA leakage out of the cells due to the loss of membrane integrity during irradiation. The average CA leakage was 10.6% (n=6). The focal height was adjusted automatically by the CLARIOstar to ensure a gain of 1800 in every experiment.

2.10.3 Ferrous Ammonium Sulphate (FAS) Titration of CA-AM Loaded Cells

A stock of fixing solution- EDTA was prepared in advance and stored at 2-8 ^oC. The composition of fixing solution-EDTA was 150 mM NaCl and 10 mM HEPES-NaOH (pH 7.4) in MilliQ water. After 72 h incubation at 37 ^oC, the CM was aspirated from the cells in dishes and 0.05 μM CA-AM in LB (1 mL/dish) was added. The dishes were incubated at 37 ^oC for 15 min in the dark. During the incubation 100 μM FAS solution (10 mL) was prepared in de-oxygenated MilliQ water. After the incubation the CA-AM solution was aspirated and each dish was washed with PBS. 0.125% w/v Trypsin (1 mL/dish) was added and incubated for 5 min. Once the cells were detached, the trypsin was neutralised with 3% w/v BSA in PBS (1 mL) and the contents of the dishes were transferred to a Falcon tube. The Falcon tube was centrifuged at 900 rpm for 7 min then the supernatant was aspirated and the cell pellet was resuspended in 0.3% w/v BSA in PBS (1 mL). This volume was transferred to a 1.5 mL Eppendorf tube. The Eppendorf tube was centrifuged at 5000 rpm for 5 min then the supernatant was aspirated and the pellet was resuspended in 0.3% w/v BSA in fixing solution (500 μL). Duplicates of 200 μL of the cell suspension were pipetted into a black 96-well plate (Greiner CELLSTAR) for analysis on the CLARIOstar plate reader (BMG LABTECH). 0.3% w/v BSA in fixing solution (200 μL) was used as the blank. 1 mM ionophore (A23187) in DMSO (1 μL) was added to each well for a final ionophore concentration of 5 μM per well. After mixing the wells with the pipette, an initial fluorescence reading was taken (F_1). 100 μM aqueous FAS (1 μL) was sequentially added to each well every 2 min to give increasing increments of 0.5 μM FAS per well. The fluorescence was read after each addition and mixing to give F_2- F_8. The

ΔF after each addition was calculated using ($F_2 - F_1$) and plotted against FAS concentration. A portion of the cell suspension (remaining in the Eppendorf tube) was counted to normalize *the* ΔF per 10^6 cells. The focal height was adjusted automatically by the CLARIOstar to ensure a gain of 1800 in every experiment.

2.11 Statistical Analysis of Data

All results were expressed as an average of a minimum of n=3 experiments ± 1 standard deviation. GraphPad Prism and Microsoft Excel were used to statistically analyse data. An ANOVA test was initially carried out to determine whether there was any statistically significant differences between the means in a group of data. Following a positive ANOVA test the Student's one-tailed *t*-test was used to compare two sets of data within the group, using paired or unpaired as appropriate for the data. A p-value of <0.05 was considered to reflect a significant difference between two groups of data.

2.12 Assay Timelines

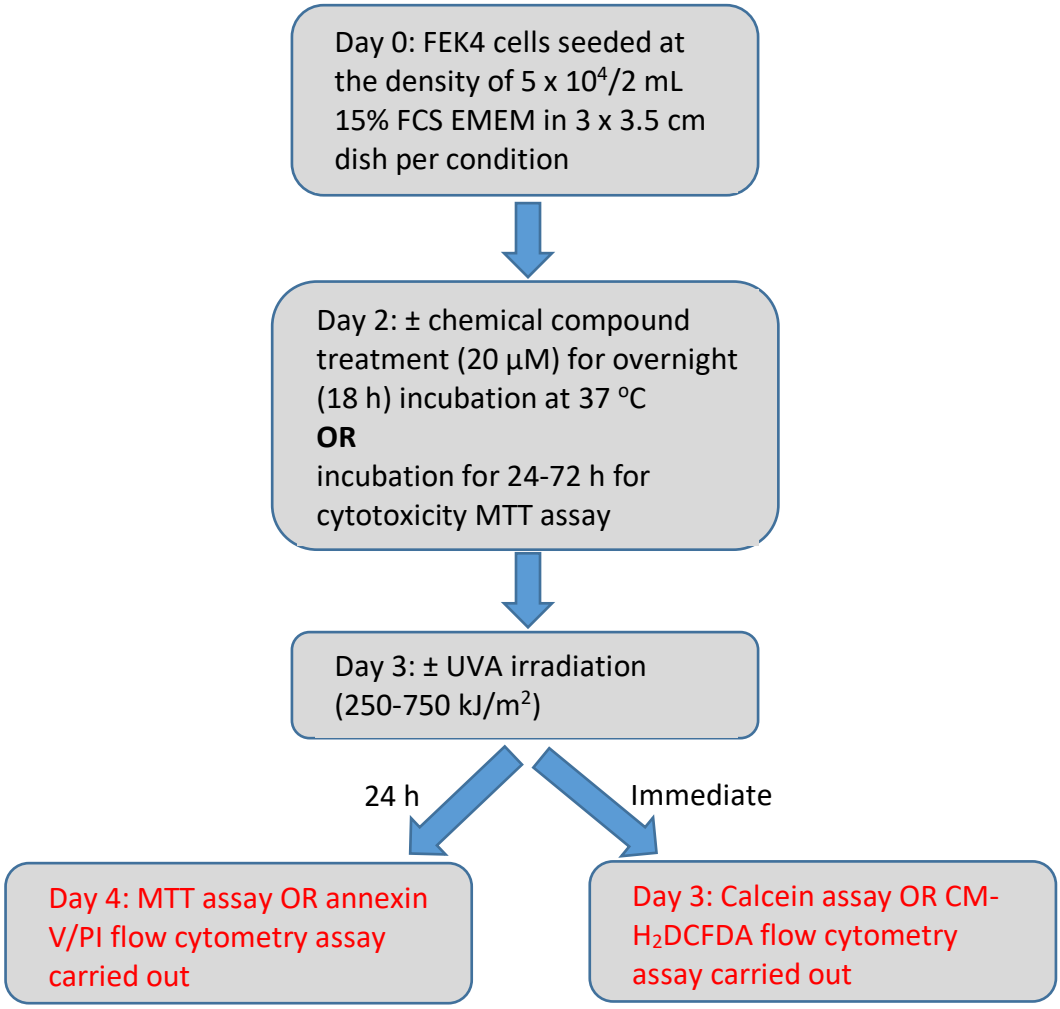

Appendix 1

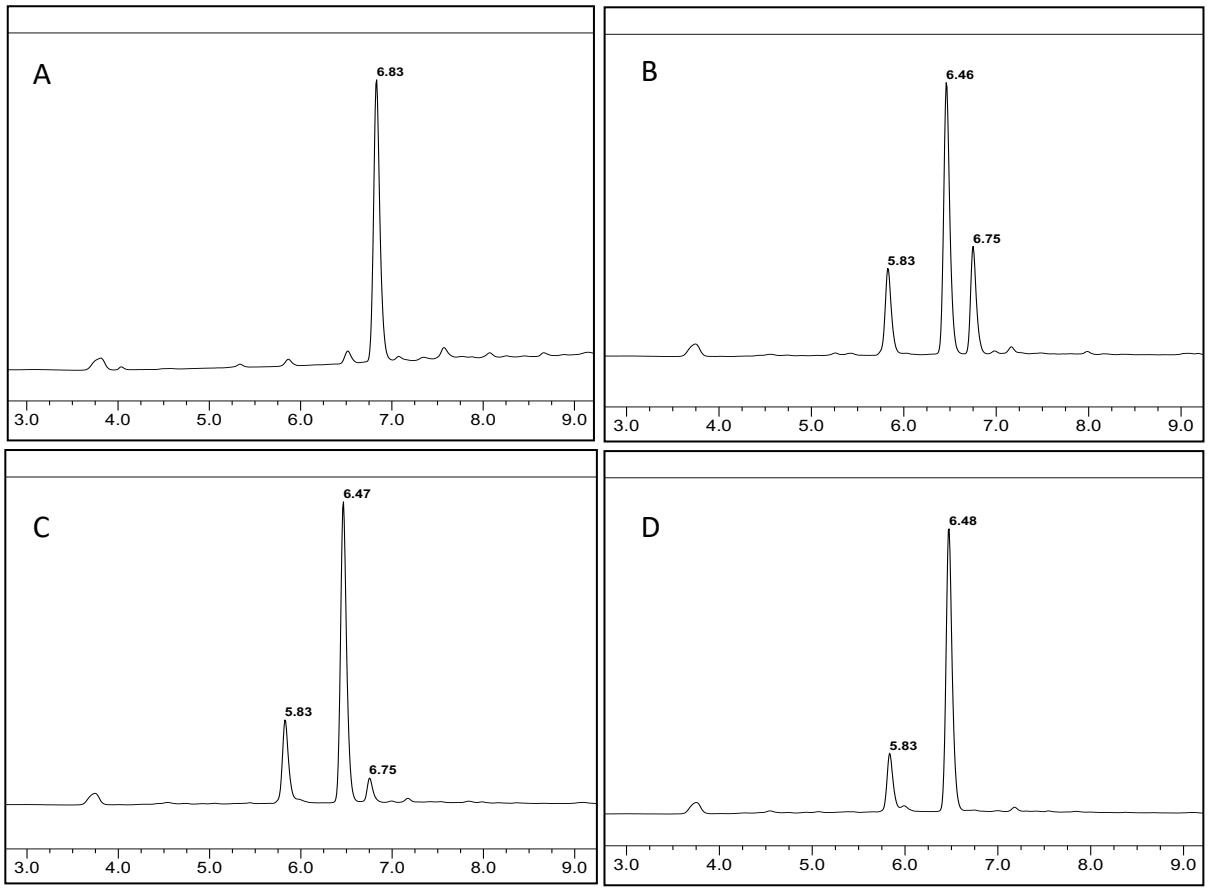

Figure 63. HPLC chromatograms of CIC **114**: **A.** Non-irradiated control of 'intact' **114**; **B.** 25 kJ/m^2 irradiation; **C.** 50 kJ/m^2 irradiation; **D.** 100 kJ/m^2 irradiation showing complete uncaging. Irradiated using a 4 kW UVA lamp (Sellas, Germany).

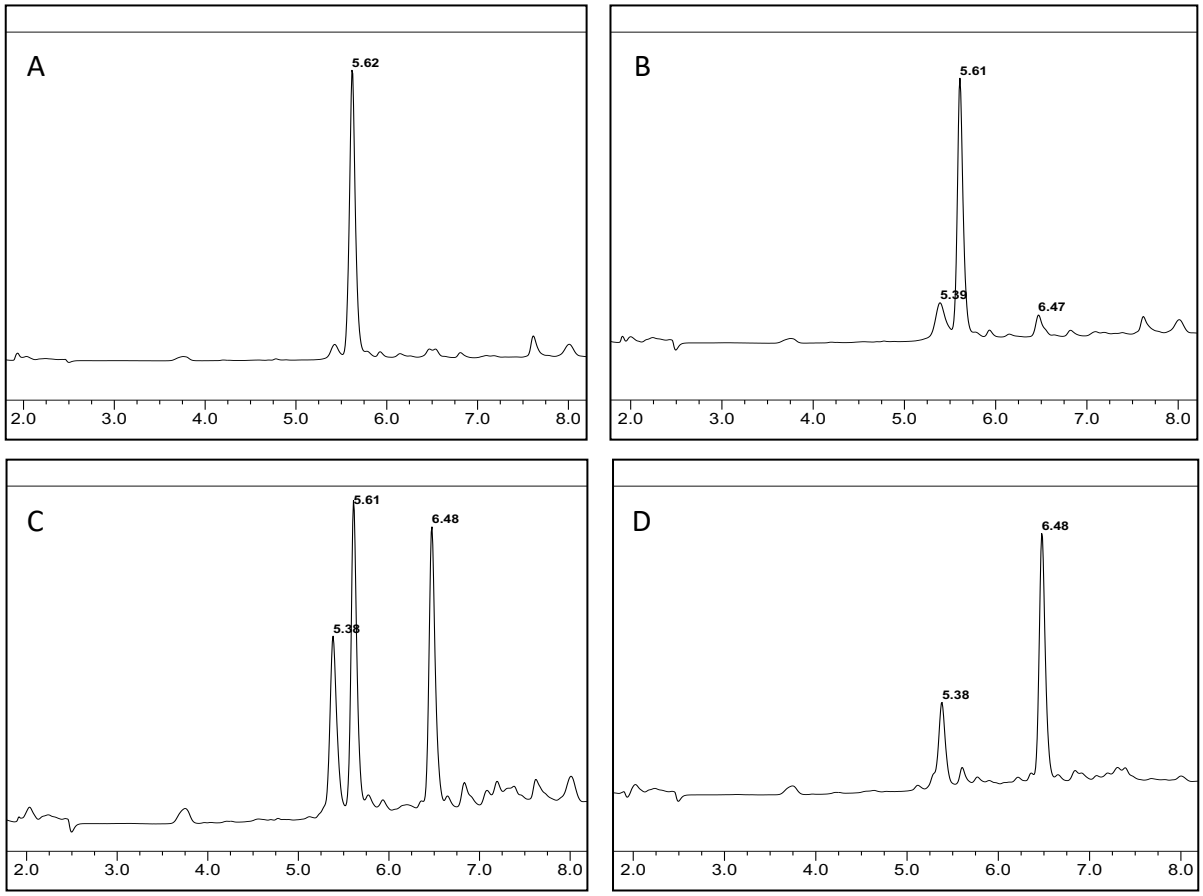

Figure 64. HPLC chromatograms of CIC **115**: **A.** Non-irradiated control of 'intact' **115**; **B.** 50 kJ/m^2 irradiation; **C.** 100 kJ/m^2 irradiation; **D.** 250 kJ/m^2 irradiation showing complete uncaging. Irradiated using a 4 kW UVA lamp (Sellas, Germany).

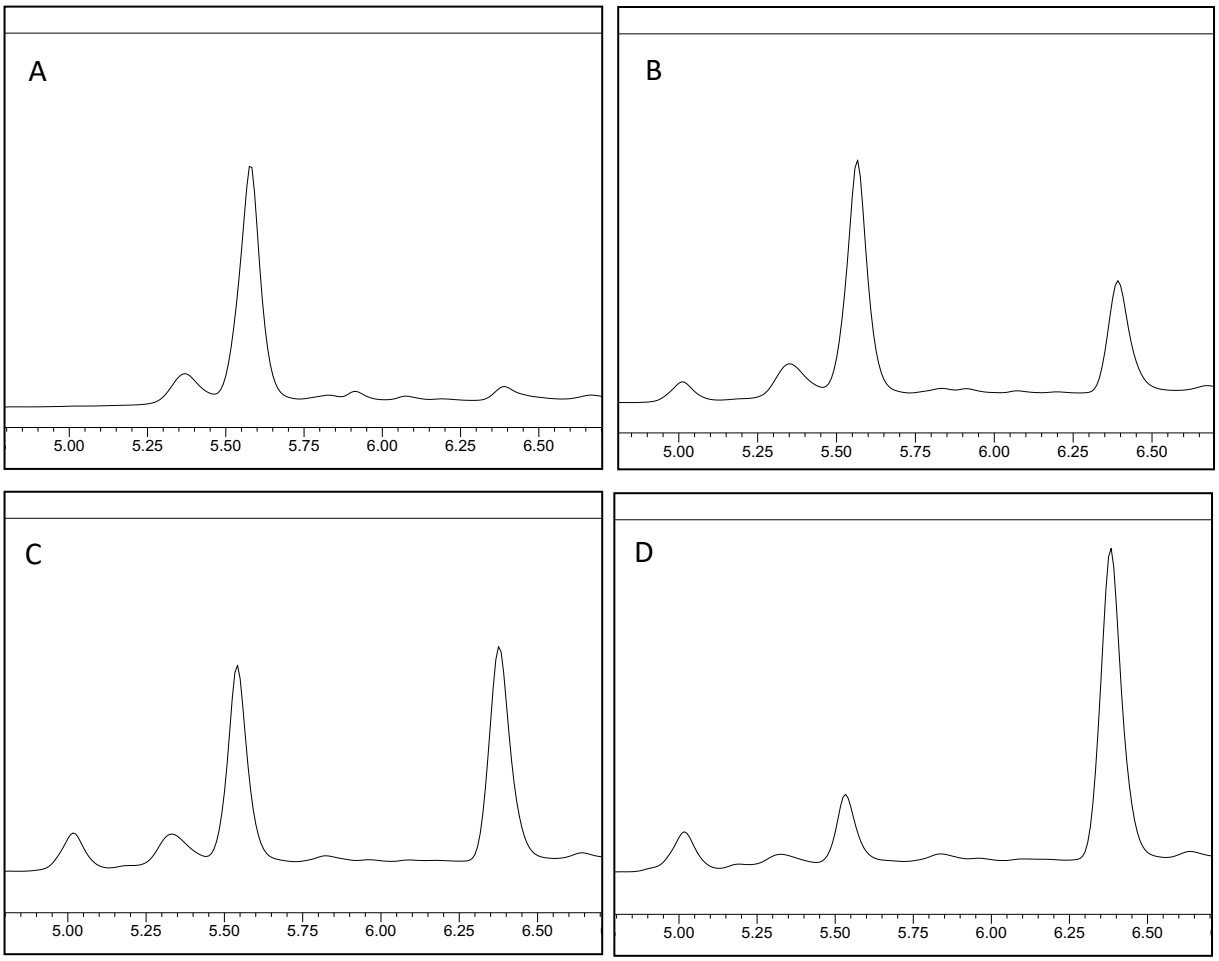

Figure 65. HPLC chromatograms of CIC **116**: **A.** Non-irradiated control of 'intact' **116**; **B.** 50 kJ/m^2 irradiation; **C.** 100 kJ/m^2 irradiation; **D.** 250 kJ/m^2 irradiation showing nearly complete uncaging. Irradiated using a 4 kW UVA lamp (Sellas, Germany).

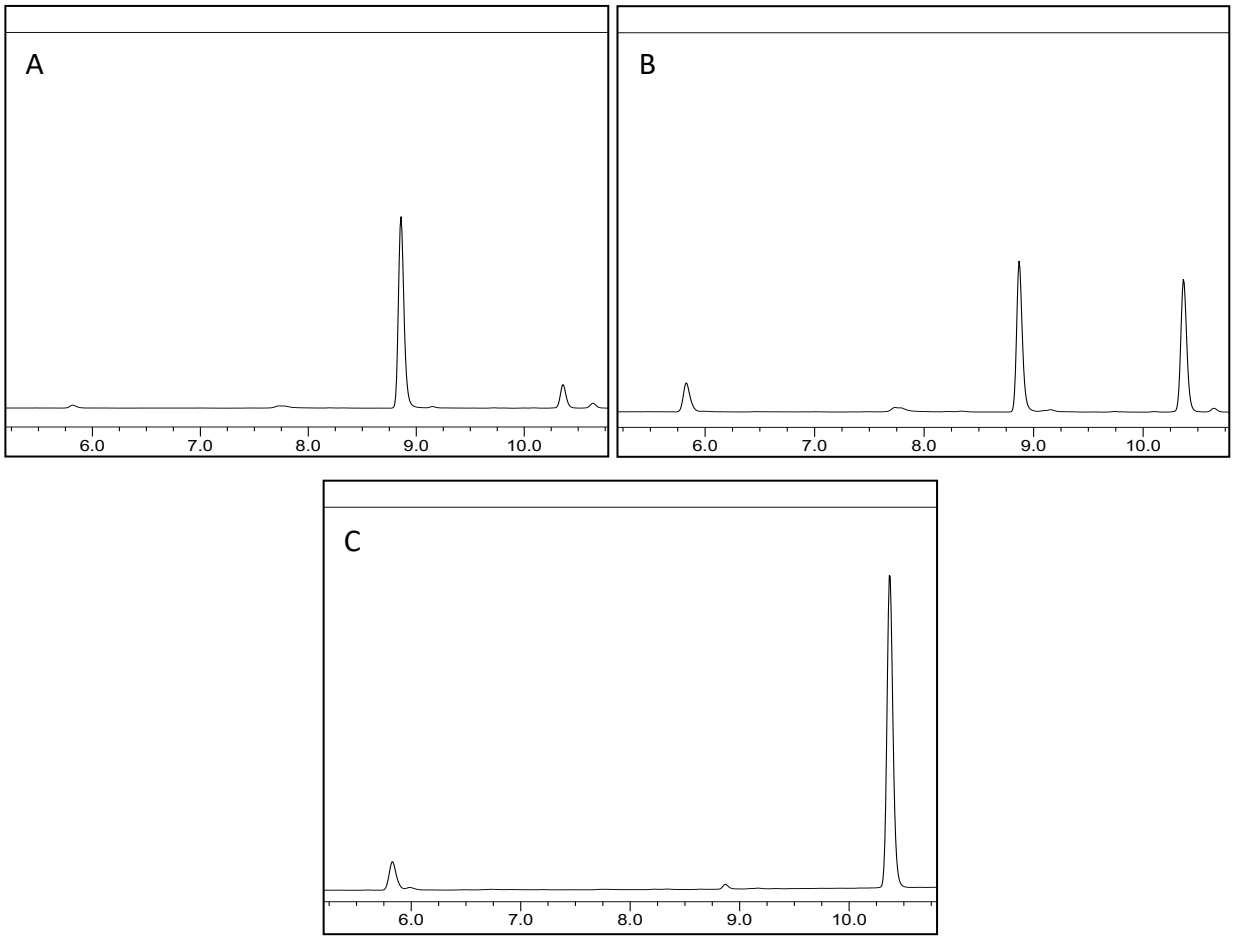

Figure 66. HPLC chromatograms of CIC **117**: **A.** Non-irradiated control of 'intact' **117**; **B.** 10 kJ/m^2 irradiation; **C.** 25 kJ/m^2 irradiation showing complete uncaging. Irradiated using a 4 kW UVA lamp (Sellas, Germany).

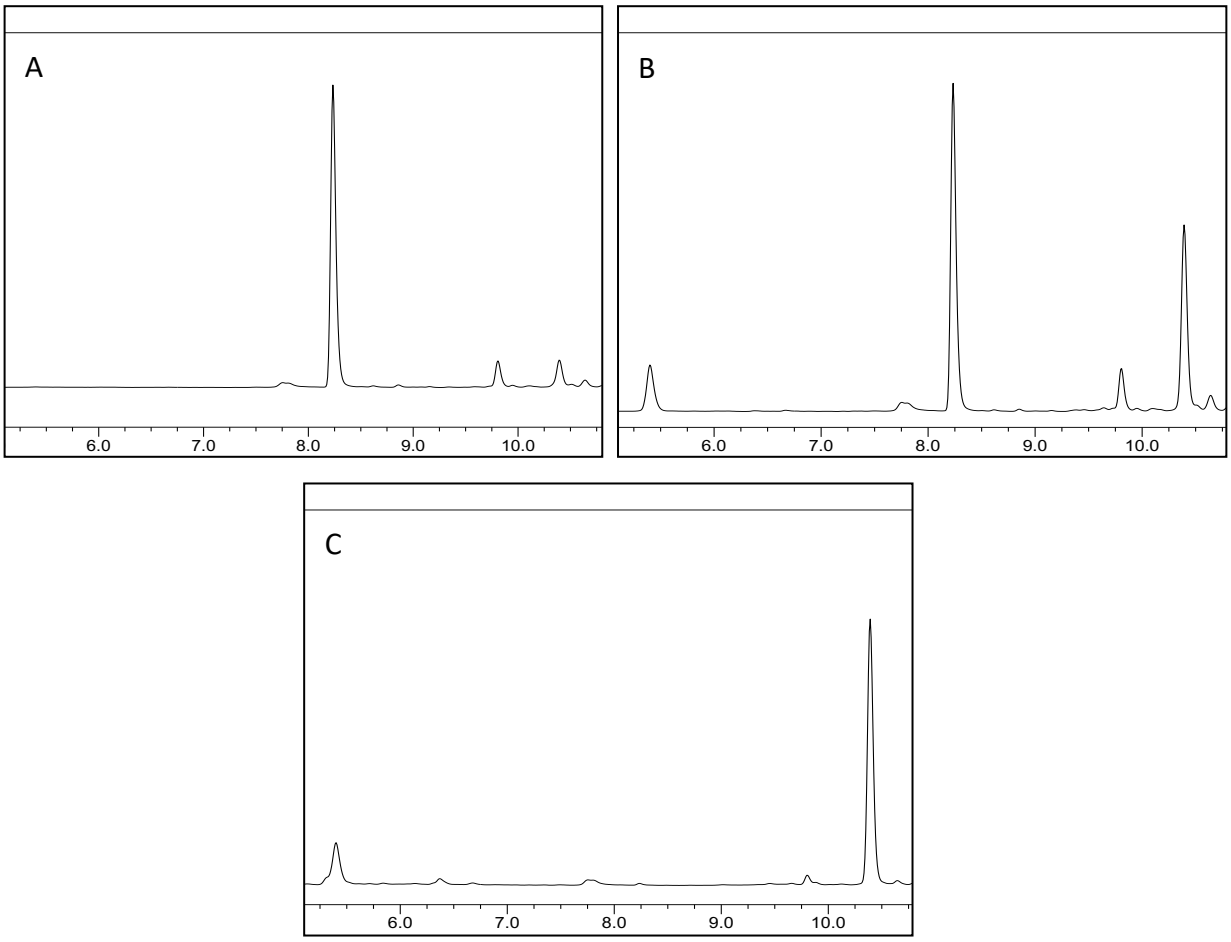

Figure 67. HPLC chromatograms of CIC **118**: **A.** Non-irradiated control of 'intact' **118**; **B.** 25 kJ/m^2 irradiation; **C.** 50 kJ/m^2 irradiation showing complete uncaging. Irradiated using a 4 kW UVA lamp (Sellas, Germany).

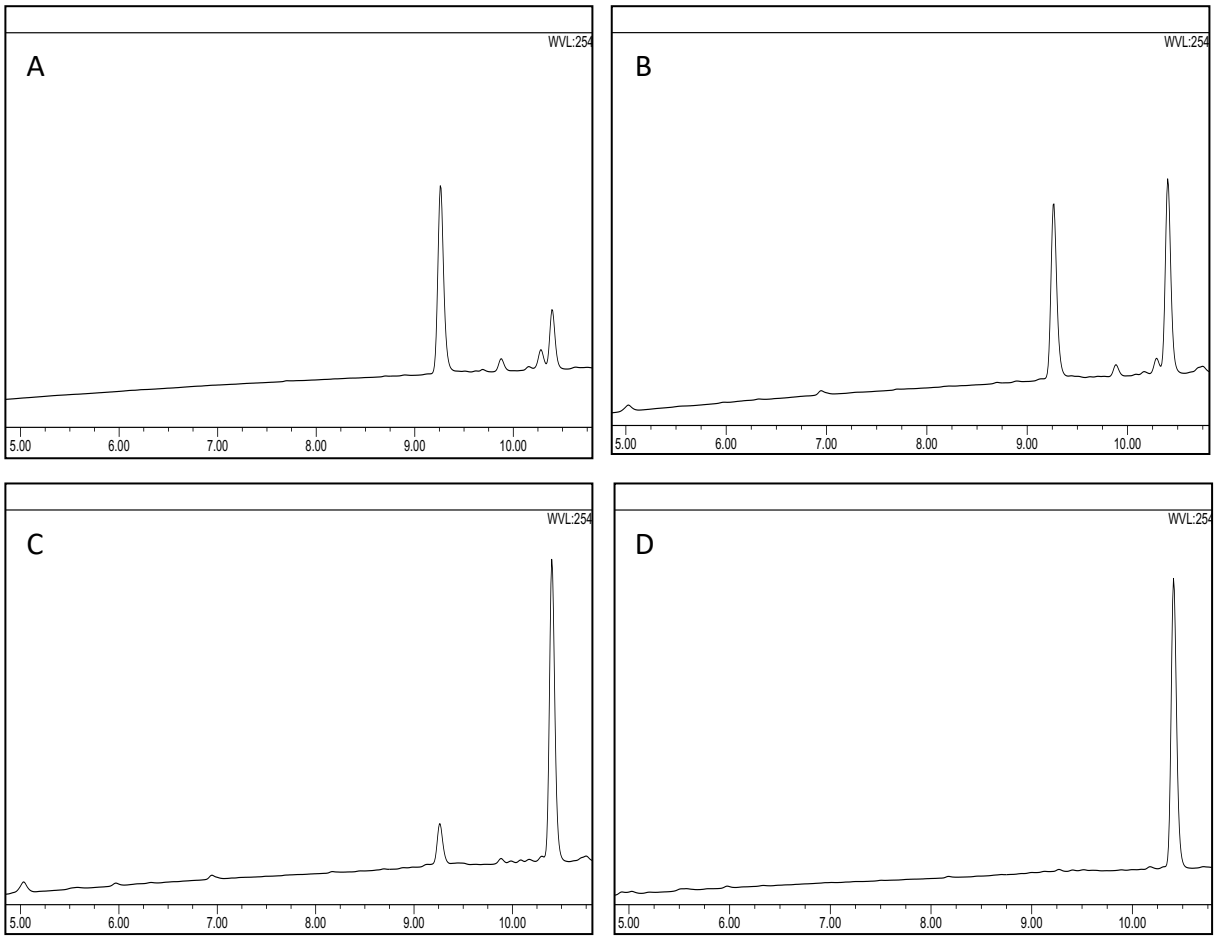

Figure 68. HPLC chromatograms of CIC **119**: **A.** Non-irradiated control of 'intact' **119**; **B.** 10 kJ/m^2 irradiation; **C.** 25 kJ/m^2 irradiation; **D.** 50 kJ/m^2 irradiation showing complete uncaging. Irradiated using a 4 kW UVA lamp (Sellas, Germany).

REFERENCES

(1) Ahmad, S.I. *Ultraviolet Light in Human Health, Diseases and Environment*; Springer International Publishing: New York, 2017.
(2) Diffey, B. L. *Phys. Med. Biol.* **1991**, *36*, 299.
(3) D'Orazio, J., Jarrett, S., Amaro-Ortiz, A. and Scott, T. *Int. J. Mol. Sci.* **2013**, *14*, 12222.
(4) Gamlen, H. E. *Br. Med. J.* **1903**, *1*, 1310.
(5) Nicholls, A. G. *Can. Med. Assoc. J.* **1928**, *18*, 321.
(6) Fioletov, V. E., Kerr, J. B. and Fergusson, A. *Can. J. Public Health* **2010**, *101*, 15.
(7) Sugibayashi, K. *Skin permeation and disposition of therapeutic and cosmeceutical compounds*; Springer: Japan, 2017.
(8) Eckert, R. L. and Rorke, E. A. *Environ. Health Perspect.* **1989**, *80*, 109.
(9) Antony, R. Y. *Phys. Med. Biol.* **1997**, *42*, 789.
(10) Eucerin basic skin knowledge. www.eucerin.co.uk/about-skin/basic-skin-knowledge/skin-structure-and-function (accessed Nov 2018).
(11) Wang, S. Q., Setlow, R., Berwick, M., Polsky, D., Marghoob, A. A., Kopf, A. W. and Bart, R. S. *J. Am. Acad. Dermatol.* **2001**, *44*, 837.
(12) Ash, C., Dubec, M., Donne, K. and Bashford, T. *Lasers. Med. Sci.* **2017**, *32*, 1909.
(13) Penta, D., Somashekar, B. S. and Meeran, S. M. *Photodermatol. Photoimmunol. Photomed.* **2018**, *34*, 42.
(14) Reichrath, J. *Sunlight, Vitamin D and Skin Cancer*; Springer: New York, 2014.
(15) Lomas, A., Leonardi-Bee, J. and Bath-Hextall, F. *Br. J. Dermatol.* **2012**, *166*, 1069.
(16) Nguyen, T. H. *Clin. Dermatol.* **2004**, *22*, 209.
(17) Strickland, L. R., Pal, H. C., Elmets, C. A. and Afaq, F. *Cancer Lett.* **2015**, *359*, 20.
(18 Office for National Statistics https://www.ons.gov.uk/peoplepopulationandcommunity/healthandsocialcare/healthandlifeexpectancies/bulletins/healthstatelifeexpectanciesuk/2015to2017 (accessed Dec 2018).
(19) Petersen, B., Thieden, E., Philipsen, P., Heydenreich, J., Young, A. and Wulf, H. *Photodermatol. Photoimmunol. Photomed.* **2013**, *29*, 221.
(20) Office for National Statistics https://www.ons.gov.uk/peoplepopulationandcommunity/birthsdeathsandmarriages/deaths/adhocs/004981deathsfrommalignantmelanomaoftheskinbysexandageengland1982to2011 (accessed Nov 2018)
(21) Brenner, M. and Hearing, V. J. *Photochem. Photobiol.* **2008**, *84*, 539.
(22) Ito, S. *Pigment Cell Res.* **2003**, *16*, 230.
(23) Watt, A. A. R., Bothma, J. P. and Meredith, P. *Soft Matter* **2009**, *5*, 3754.
(24) D'Mello, S. A. N., Finlay, G. J., Baguley, B. C. and Askarian-Amiri, M. E. *Int. J. Mol. Sci.* **2016**, *17*, 1144.
(25) Gilchrest, B. A., Eller, M. S., Geller, A. C. and Yaar, M. *N. Engl. J. Med.* **1999**, *340*, 1341.
(26) Soehnge, H., Ouhtit, A. N. and Ananthaswamy, O. *Front. Biosci.* **1997,** *2*, 538
(27) Kim, Y., Lee, J., Kim, J., Choi, C. W., Hwang, Y.-I., Kang, J. S. and Lee, W. J. *PloS one* **2017**, *12*, e0178567, https://doi.org/10.1371/journal.pone.0178567
(28) Lo, H.-L., Nakajima, S., Ma, L., Walter, B., Yasui, A., Ethell, D. W. and Owen, L. B. *BMC Cancer* **2005**, *5*, 135.

(29) Benjamin, C. L. and Ananthaswamy, H. N. *Toxicol. Appl. Pharmacol.* **2007**, *224*, 241.
(30) Ananthaswamy, H. N., Ullrich, S. E. and Kripke, M. L. *Exp. Dermatol.* **2002**, *11*, 40.
(31) Tyagi, N., Bhardwaj, A., Srivastava, S. K., Arora, S., Marimuthu, S., Deshmukh, S. K., Singh, A. P., Carter, J. E. and Singh, S. *Sci. Rep.* **2015**, *5*, 13894.
(32) Mullenders, L. H. F. *Photochem. Photobiol. Sci.* **2018**, *17*, 1842.
(33) Niedernhofer, L. J., Bohr, V. A., Sander, M. and Kraemer, K. H. *Mech. Ageing Dev.* **2011**, *132*, 340.
(34) Young, A. R., Claveau, J. and Rossi, A. B. *J. Am. Acad. Derm.* **2017**, *76*, S100.
(35) Sola, Y. and Lorente, J. *Photochem. Photobiol. B* **2015**, *143*, 5.
(36) Osterwalder, U. and Herzog, B. *Photochem. Photobiol. Sci.* **2010**, *9*, 470.
(37) Peak, J. G. and Peak, M. J. *Mutat. Res. Fundam. Mol. Mech. Mutagen.* **1991**, *246*, 187.
(38) Wenczl, E., Smit, N. P. M., Pavel, S., Schothorst, A. A., Van der Schans, G. P., Timmerman, A. J., Roza, L. and Kolb, R. M. *J. Invest. Dermatol.* **1998**, *111*, 678.
(39) Hill, H. Z. and Hill, G. J. *Pigment Cell Res.* **2000**, *13*, 140.
(40) Kvam, E. and Tyrrell, R. M. *Carcinogenesis* **1997**, *18*, 2379.
(41) Mouret, S., Forestier, A. and Douki, T. *Photochem. Photobiol. Sci.* **2012**, *11*, 155.
(42) Tewari, A., Grage, M. M. L., Harrison, G. I., Sarkany, R. and Young, A. R. Photochem. Photobiol. Sci. 2013, 12, 95.
(43) Mouret, S., Baudouin, C., Charveron, M., Favier, A., Cadet, J. and Douki, T. *Proc. Natl. Acad. Sci. U.S.A.* **2006**, *103*, 13765.
(44) Pattison, D. I., Rahmanto, A. S. and Davies, M. J. *Photochem. Photobiol. Sci.* **2012**, *11*, 38.
(45) Karran, P. and Brem, R. *DNA Repair* **2016**, *44*, 178.
(46) Aguilar, T. A. F., Navarro, B. C. H. and Perez, J. A. M. *The Transcription Factor Nrf2*; Morales-Gonzalez, J. A., Ed. *Endogenous Antioxidants: A Review of their Role in Oxidative Stress;* InTechOpen, 2016; https://www.intechopen.com/books/a-master-regulator-of-oxidative-stress-the-transcription-factor-nrf2/endogenous-antioxidants-a-review-of-their-role-in-oxidative-stress.
(47) Masella, R., Di Benedetto, R., Varì, R., Filesi, C. and Giovannini, C. *J. Nutr. Biochem.* **2005**, *16*, 577.
(48) Reelfs, O., Eggleston, I. M. and Pourzand, C. *Curr. Drug Metab.* **2010**, *11*, 242.
(49) Punnonen, K., Jansén, C. T., Puntala, A. and Ahotupa, M. *J. Invest. Dermatol.* **1991**, *96*, 255.
(50) Hoerter, J., Eisenstark, A. and Touati, D. *Mutat. Res. Fundam. Mol. Mech. Mutagen.* **1989**, *215*, 161.
(51) Aust, S. D., Morehouse, L. A. and Thomas, C. E. *J. Free Radic. Biol. Med.* **1985**, *1*, 3.
(52) Vile, G. F. and Tyrrell, R. M. *Free Radic. Biol. Med.* **1995**, *18*, 721.
(53) Harrison, P. M. and Arosio, P. *Biochim. Biophys. Acta Bioenerg.* **1996**, *1275*, 161.
(54) Breuer, W., Epsztejn, S. and Ioav Cabantchik, Z. *FEBS Lett.* **1996**, *382*, 304.
(55) Balla, G., Jacob, H. S., Balla, J., Rosenberg, M., Nath, K., Apple, F., Eaton, J. W. and Vercellotti, G. M. *J. Biol. Chem.* **1992**, *267*, 18148.
(56) Pourzand, C., Watkin, R. D., Brown, J. E. and Tyrrell, R. M. *Proc. Natl. Acad. Sci. U.S.A.* **1999**, *96*, 6751.
(57) Aroun, A., Zhong, J. L., Tyrrell, R. M. and Pourzand, C. *Photochem. Photobiol. Sci.* **2011**, *11*, 118.
(58) Witkowski, J. A. and Parish, L. C. *Clin. Dermatol.* **2001**, *19*, 367.

(59) Couteau, C., Couteau, O., Alami-El Boury, S. and Coiffard, L. J. M. *Int. J. Pharm.* **2011**, *415*, 181.
(60) Diffey, B. L. and Farr, P. M. *Br. J. Dermatol.* **1985**, *112*, 83.
(61) Young, A. R., Orchard, G. E., Harrison, G. I. and Klock, J. L. *J. Invest. Dermatol.* **2007**, *127*, 975.
(62) Osterwalder, U. and Herzog, B. *Br. J. Dermatol.* **2009**, *161*, 13.
(63) Wang, S. Q., Osterwalder, U. and Jung, K. *J. Am. Acad. Dermatol.* **2011**, *65*, 525.
(64) Herrling, T., Jung, K. and Fuchs, J. *Spectrochim. Acta A* **2006**, *63*, 840.
(65) Diffey, B. *Photodermatol. Photoimmunol. Photomed.* **2009**, *25*, 233.
(66) Rueegg, C. S., Stenehjem, J. S., Egger, M., Ghiasvand, R., Cho, E., Lund, E., Weiderpass, E., Green, A. C. and Veierød, M. B. *Int. J. Cancer* **2019**, *144*, 2651.
(67) Iannacone, M. R., Hughes, M. C. B. and Green, A. C. *Photodermatol. Photoimmunol. Photomed.* **2014**, *30*, 55.
(68) Ghiasvand, R., Weiderpass, E., Green, A. C., Lund, E. and Veierød, M. B. *J. Clin. Oncol.* **2016**, *34*, 3976.
(69) Bech-Thomsen, N. and Wulf, H. C. *Photodermatol. Photoimmunol. Photomed.* **1992**, *9*, 242.
(70) Reich, A., Harupa, M., Bury, M., Chrzaszcz, J. and Starczewska, A. *Photodermatol. Photoimmunol. Photomed.* **2009**, *25*, 242.
(71) Teramura, T., Mizuno, M., Asano, H., Naito, N., Arakane, K. and Miyachi, Y. *Clin. Exp. Dermatol.* **2012**, *37*, 904.
(72) Narbutt, J., Philipsen, P. A., Lesiak, A., Sandberg Liljendahl, T., Segerbäck, D., Heydenreich, J., Chlebna-Sokol, D., Olsen, P., Harrison, G. I., Pearson, A., Baczynska, K., Rogowski-Tylman, M., Wulf, H. C. and Young, A. R. *Br. J. Dermatol.* **2018**, *179*, 940.
(73) Springbett, P., Buglass, S. and Young, A. R. *Photochem. Photobiol. B* **2010**, *101*, 160.
(75) Shaath, N. *Photochem. Photobiol. Sci.* **2010**, *9*, 464.
(76) Osmond-McLeod, M. J., Oytam, Y., Rowe, A., Sobhanmanesh, F., Greenoak, G., Kirby, J., McInnes, E. F. and McCall, M. J. *Part. Fibre Toxicol.* **2016**, *13*, 44.
(77) Gonzalez, H. *Photochem. Photobiol. Sci.***2010**, *9*, 482.
(78) Mturi, G. J. and Martincigh, B. S. *J. Photochem. Photobiol. A* **2008**, *200*, 410.
(79) Cantrell, A. and McGarvey, D. J. *Photochem. Photobiol. B* **2001**, *64*, 117.
(80) Chatelain, E. and Gabard, B. *Photochem. Photobiol.* **2001**, *74*, 401.
(81) Fourtanier, A., Moyal, D. and Seité, S. *Photodermatol. Photoimmunol. Photomed.* **2008**, *24*, 164.
(82) Young, A. R., Sheehan, J. M., Chadwick, C. A. and Potten, C. S. *J. Invest. Dermatol.* **2000**, *115*, 37.
(83) Tarazona, I., Chisvert, A., León, Z. and Salvador, A. *J. Chromatogr. A* **2010**, *1217*, 4771.
(84) He, T., Tsui, M. M. P., Tan, C. J., Ma, C. Y., Yiu, S. K. F., Wang, L. H., Chen, T. H., Fan, T. Y., Lam, P. K. S. and Murphy, M. B. *Environ. Pollut.* **2019**, *245*, 462.
(85) Rehfeld, A., Egeberg, D. L., Almstrup, K., Petersen, J. H., Dissing, S. and Skakkebæk, N. E. *Endocr. Connect.* **2017**, *7*, 16.
(86) Lawrence, K. P., Gacesa, R., Long, P. F. and Young, A. R. *Br. J. Dermatol.* **2018**, *178*, 1353.
(87) Oren, A. and Gunde-Cimerman, N. *FEMS Microbiol. Lett.* **2007**, *269*, 1.
(88) Ellison, A. J. and Raines, R. T. *Org. Biomol. Chem.* **2018**, *16*, 7139.

(89) Matsui, M. S., Hsia, A., Miller, J. D., Hanneman, K., Scull, H., Cooper, K. D. and Baron, E. *J. Investig. Dermatol. Symp. Proc.* **2009**, *14*, 56.
(90) Ebrahimzadeh, M. A., Enayatifard, R., Khalili, M., Ghaffarloo, M., Saeedi, M. and Yazdani Charati, J. *Iran. J. Pharm. Res* **2014**, *13*, 1041.
(91) Hassan, I., Dorjay, K., Sami, A. and Anwar, P. *Our Dermatol. Online*, **2013**, *4*, 369
(92) Wu, C.-M., Cheng, Y.-L., Dai, Y.-H., Chen, M.-F. and Wang, C.-C. *Biomed. Rep.* **2014**, *2*, 419.
(93) Geissler, C. and Singh, M. *Nutrients* **2011**, *3*, 283.
(94) Ganz, T. *Physiol. Rev.* **2013**, *93*, 1721.
(95) Robson, K. J. H. and Drakesmith, H. *Digestion* **2005**, *72*, 22.
(96) Yu, Y., Kalinowski, D., Kovacevic, Z., Siafakas, A., Jansson, P., Stefani, C., Lovejoy, D., Sharpe, P. C., Bernhardt, P. and Richardson, D. *J. Med. Chem.* **2009**, *52*, 5271.
(97) Muckenthaler, M. U., Galy, B. and Hentze, M. W. *Annu. Rev. Nutr.* **2008**, *28*, 197.
(98) Steinhauser, S., Heinz, U., Bartholomä, M., Weyhermüller, T., Nick, H. and Hegetschweiler, K. *Eur. J. Inorg. Chem.* **2004**, *2004*, 4177.
(99) Ma, Y., Zhou, T., Kong, X. and Hider, R. C. *Curr. Med. Chem.* **2012**, *19*, 2816.
(100) Kielar, F., Wang, Q., Boyle, P. D. and Franz, K. J. *Inorganica Chim. Acta* **2012**, *393*, 294.
(101) Porter, J. B. *Iron Physiology and Pathophysiology in Humans*; McLaren, G. D., Anderson, G. J., Ed.; Humana Press: New York, 2012, 591.
(102) Osredkar, J. and Sustar, N. *J. Clinic. Toxicol.* **2011**, S3:001, doi: 10.4172/2161-0495.S3-001.
(103) Rae, T. D., Schmidt, P. J., Pufahl, R. A., Culotta, V. C. and O'Halloran, T. V. *Science* **1999**, *284*, 805.
(104) Harris, D. C. and Aisen, P. *Biochim. Biophys. Acta* **1973**, *329*, 156.
(105) Chen, Y.-L., Kong, X., Xie, Y. and Hider, R. C. *J. Inorg. Biochem.* **2018**, *180*, 194.
(106) Pepe, A., Meloni, A., Capra, M., Cianciulli, P., Prossomariti, L., Malaventura, C., Putti, M. C., Lippi, A., Romeo, M. A., Bisconte, M. G., Filosa, A., Caruso, V., Quarta, A., Pitrolo, L., Missere, M., Midiri, M., Rossi, G., Positano, V., Lombardi, M. and Maggio, A. *Haematologica* **2011**, *96*, 41.
(107) Richardson, D. R. *J. Lab. Clin. Med.* **2001**, *137*, 324.
(108) Cragg, L., Hebbel, R., Miller, W., Solovey, A., Selby, S. and Enright, H. *Blood* **1998**, *92*, 632
(109) Singh, S., Epemolu, R. O., Dobbin, P.S., Tilbrook, G. S., Ellis, B.L., Damani, L. A., Hider, R.C. *Drug. Metab. Dispos.* **1992**, *20*, 256.
(110) Porter, J. B., Abeysinghe, R. D., Hoyes, K. P., Barra, C., Huehns, E. R., Brooks, P. N., Blackwell, M. P., Araneta, M., Brittenham, G., Singh, S., Dobbin, P. and Hider, R. C. *Br. J. Haematol.* **1993**, *85*, 159
(111) Sergejew, T., Forgiarini, P., Schnebli, H.-P. *Br. J. Haematol.* **2000**, *110*, 985.
(112) Hershko, C., Konijn, A. M., Nick, H. P., Breuer, W., Cabantchik, Z. I. and Link, G. *Blood* **2001**, *97*, 1115.
(113) Galanello, R., Piga, A., Alberti, D., Rouan, M.-C., Bigler, H. and Séchaud, R. *J. Clin. Pharmacol.* **2003**, *43*, 565.
(114) Hancock, R. D. *Acc. Chem. Res.* **1990**, *23*, 253.
(115) Miliordos, E. and Xantheas, S. S. *J. Chem. Theory Comput.* **2015**, *11*, 1549.
(116) Poňka, P., Borová, J., Neuwirt, J., Fuchs, O. and Nečas, E. *Biochim. Biophys. Acta* **1979**, *586*, 278.

(117) Richardson, D. R., Wis Vitolo, L. M., Hefter, G. T., May, P. M., Clare, B. W., Webb, J. and Wilairat, P. *Inorganica Chim. Acta* **1990**, *170*, 165.
(118) Baker, E., Vitolo, M. L. and Webb, J. *Biochem. Pharmacol.* **1985**, *34*, 3011.
(119) Richardson, D. R., Tran, E. H. and Ponka, P. *Blood* **1995**, *86*, 4295.
(120) Konijn, A. M., Glickstein, H., Vaisman, B., Meyron-Holtz, E. G., Slotki, I. N. and Cabantchik, Z. I. *Blood* **1999**, *94*, 2128.
(121) Shvartsman, M., Fibach, E. and Cabantchik, Z. I. *Biochem. J.* **2010**, *429*, 185.
(122) Whitney, P., Bowe, S. P. *J. Drugs Dermatol.* **2014**, *13*, 1021.
(123) Philip, C. S., Des, R. R., Danuta, S. K. and Paul, V. B. *Curr. Top. Med. Chem.* **2011**, *11*, 591.
(124) Newman, D. J. and Cragg, G. M. *J. Nat. Prod.* **2016**, *79*, 629.
(125) Wilson, B. R., Bogdan, A. R., Miyazawa, M., Hashimoto, K. and Tsuji, Y. *Trends Mol. Med.* **2016**, *22*, 1077.
(126) Wang, D., Zhan, Y., Cai, D., Li, X., Wang, Q. and Chen, S. *Appl. Environ. Microbiol.* **2018**, *84*, e00262.
(127) Raymond, K. N., Dertz, E. A. and Kim, S. S. *Proc. Natl. Acad. Sci. U.S.A.* **2003**, *100*, 3584.
(128) Hatcher, H. C., Singh, R. N., Torti, F. M. and Torti, S. V. *Future Med. Chem.* **2009**, *1*, 1643.
(129) Perez, C. A., Wei, Y. and Guo, M. *J. Inorg. Biochem.* **2009**, *103*, 326.
(130) Zhang, Y., Li, H., Zhao, Y. and Gao, Z. *Eur. J. Pharmacol.* **2006**, *535*, 263.
(131) Reznichenko, L., Amit, T., Zheng, H., Avramovich-Tirosh, Y., Youdim, M. B. H. and Mandel, S. *J. Neurochem.* **2006**, *97*, 527.
(132) Sipiczki, M. *Appl. Environ. Microbiol.* **2006**, *72*, 6716.
(133) Cook, A. H. and Slater, C. A. *J. Chem. Soc.* **1956**, 4118.
(134) Richardson, D. R. and Milnes, K. *Blood* **1997**, *89*, 3025.
(135) Franz, K. J., Besse, D. M. and Seed, P. C., 2018 *Antimicrobial prochelators to target drug-resistant bacteria and the methods of making and using the same* US2018/01947788 A1.
(136) Liu, G., Men, P., Perry, G. and Smith, M. A. *Methods Mol. Biol.* **2010**, *610*, 123.
(137) Van der Schyf, C. J., Mandel, S., Geldenhuys, W. J., Amit, T., Avramovich, Y., Zheng, H., Fridkin, M., Gal, S., Weinreb, O., Orit, B., Sagi, Y. and Moussa, B.H. *Curr. Alzheimer Res.* **2007**, *4*, 522.
(138) Rogers, J. T. and Lahiri, D. K. *Curr. Drug Targets* **2004**, *5*, 535.
(139) Sanchez-Barcelo, E. J. and Mediavilla, M. D. *Recent Pat. Endocr. Metab. Immune Drug Discov.* **2014**, *8*, 1.
(140) Abrahamse, H. and Hamblin, M. R. *Biochem. J.* **2016**, *473*, 347.
(141) Tewari, K. M. and Eggleston, I. M. *Photochem. Photobiol. Sci.***2018**, *17*, 1553.
(142) De Rosa, F. S. and Bentley, M. V. L. B. *Pharm. Res.* **2000**, *17*, 1447.
(143) Taneja, S. S., Bennett, J., Coleman, J., Grubb, R., Andriole, G., Reiter, R. E., Marks, L., Azzouzi, A.-R. and Emberton, M. *J. Urol.* **2016**, *196*, 1096.
(144) Pereira, P. M. R., Korsak, B., Sarmento, B., Schneider, R. J., Fernandes, R. and Tomé, J. P. C. *Org. Biomol. Chem.* **2015**, *13*, 2518.
(145) Kharkwal, G. B., Sharma, S. K., Huang, Y.-Y., Dai, T. and Hamblin, M. R. *Lasers Surg. Med.* **2011**, *43*, 755.
(146) Patrizi, A., Raone, B. and Ravaioli, G. M. *Clin. Cosmet. Investig. Dermatol.* **2015**, *8*, 511.

(147) British Association of Dermatologists, *Phototherapy*, 2018, www.bad.org.uk/leaflets/phototherapy
(148) Tran, D., Kwok, Y. K. and Goh, C. L. *Photoderm. Photoimmunol. Photomed.* **2001**, *17*, 164.
(149) Archier, E., Devaux, S., Castela, E., Gallini, A., Aubin, F., Le Maître, M., Aractingi, S., Bachelez, H., Cribier, B., Joly, P., Jullien, D., Misery, L., Paul, C., Ortonne, J. P. and Richard, M. A. *J. Eur. Acad. Dermatol. Venereol* **2012**, *26*, 22.
(150) Glickstein, H., Ben El, R., Shvartsman, M. and Cabantchik, Z. I. *Blood* **2005**, *106*, 3242.
(151) Zhong, J. L., Yiakouvaki, A., Holley, P., Tyrrell, R. M. and Pourzand, C. *J. Invest. Dermatol.* **2004**, *123*, 771.
(152) Eguchi, Y., Shimizu, S. and Tsujimoto, Y. *Cancer Res.* **1997**, *57*, 1835.
(153) Seité, S., Popovic, E., Verdier, M. P., Roguet, R., Portes, P., Cohen, C., Fourtanier, A. and Galey, J. B. *Photodermatol. Photoimmunol. Photomed.* **2004**, *20*, 47.
(154) Bendova, P., Mackova, E., Haskova, P., Vavrova, A., Jirkovsky, E., Sterba, M., Popelova, O., Kalinowski, D. S., Kovarikova, P., Vavrova, K., Richardson, D. R. and Simunek, T. *Chem. Res. Toxicol.* **2010**, *23*, 1105.
(155) Hasinoff, B. B., Patel, D. and Wu, X. *Free Radic. Biol. Med.* **2003**, *35*, 1469.
(156) Yiakouvaki, A., Savović, J., Al-Qenaei, A., Dowden, J. and Pourzand, C. *J. Invest. Dermatol.* **2006**, *126*, 2287.
(157) Galey, J.-B., Dumats, J., Genard, S., Destree, O., Pichaud, P., Cctroux, P., Marrot, L., Beck, I., Fernandez, B., Barre, G., Seite, M., Hussler, G. and Hocquaux, M. *Biochem. Pharmacol.* **1996**, *51*, 103.
(158) Wei, Y. and Guo, M. *Angew. Chem. Int. Ed.* **2007**, *46*, 4722.
(159) Smoum, R., Rubinstein, A., Dembitsky, V. M. and Srebnik, M. *Chem. Rev.* **2012**, *112*, 4156.
(160) Jansová, H., Macháček, M., Wang, Q., Hašková, P., Jirkovská, A., Potůčková, E., Kielar, F., Franz, K. J. and Šimůnek, T. *Free Radic. Biol. Med.* **2014**, *74*, 210.
(161) Pygmalion, M.-J., Ruiz, L., Popovic, E., Gizard, J., Portes, P., Marat, X., Lucet-Levannier, K., Muller, B. and Galey, J.-B. *Free Radic. Biol. Med.* **2010**, *49*, 1629.
(162) Klán, P., Šolomek, T., Bochet, C. G., Blanc, A., Givens, R., Rubina, M., Popik, V., Kostikov, A. and Wirz, J. *Chem. Rev.* **2013**, *113*, 119.
(163) Bochet, C. G. *J. Chem. Soc., Perkin 1* **2002**, 125.
(164) Lawrence, D. S. *Curr. Opin. Chem. Biol.* **2005**, *9*, 570.
(165) Porter, N. A., Thuring, J. W. and Li, H. *J. Am. Chem. Soc.* **1999**, *121*, 7716.
(166) Gagey, N., Neveu, P., Benbrahim, C., Goetz, B., Aujard, I., Baudin, J.-B. and Jullien, L. *J. Am. Chem. Soc.* **2007**, *129*, 9986.
(167) Walker, J. W., Reid, G. P., McCray, J. A. and Trentham, D. R. *J. Am. Chem. Soc.* **1988**, *110*, 7170.
(168) Lusic, H., Young, D. D., Lively, M. O. and Deiters, A. *Org. Lett.* **2007**, *9*, 1903.
(169) *CRC Handbook of Organic Photochemistry and Photobiology*; Horspool, W. and Lenci, F., Ed.; CRC Press: United States, 2003.
(170) Turner, A. D., Porter, N. A., Rozakis, G. and Pizzo, G. *J. Am. Chem. Soc.* **1988**, *110*, 244.
(171) Gagey, N., Neveu, P. and Jullien, L. *Angew. Chem. Int. Ed.* **2007**, *46*, 2467.
(172) Li, H., Yang, J. and Porter, N. A. *J. Photochem. Photobiol. A Chem.* **2005**, *169*, 289.
(173) Shiono, H. 2000 *Caged amino acids* US-6329546-B1.

(174) Pelle, E., Jian, J., Declercq, L., Dong, K., Yang, Q., Pourzand, C., Maes, D., Pernodet, N., Yarosh, D. B. and Huang, X. *Photodermatol. Photoimmunol. Photomed.* **2011**, *27*, 231.
(175) Franks, A. T., Wang, Q. and Franz, K. J. *Bioorg. Med. Chem. Lett.* **2015**, *25*, 4843.
(176) Edward, J. T.; Gauthier, M.; Chubb, F. L.; Ponka, P. *J. Chem. Eng. Data* **1988**, *33*, 538.
(177) Reelfs, O., Tyrrell, R. M. and Pourzand, C. *J. Invest. Dermatol.* **2004**, *122*, 1440.
(178) Mosmann, T. *J. Immunol. Methods* **1983**, *65*, 55.
(179) Thuong, P. T., Hung, T. M., Ngoc, T. M., Ha, D. T., Min, B. S., Kwack, S. J., Kang, T. S., Choi, J. S. and Bae, K. *Phytother. Res.* **2010**, *24*, 101.
(180) Witaicenis, A., Seito, L. N., Da Silveira Chagas, A., De Almeida Jr, L. D., Luchini, A. C., Rodrigues-Orsi, P., Cestari, S. H. and Di Stasi, L. C. *Phytomedicine* **2014**, *21*, 240.
(181) Tsakos, M., Schaffert, E. S., Clement, L. L., Villadsen, N. L. and Poulsen, T. B. *Nat. Prod. Rep.* **2015**, *32*, 605.
(182) Neises, B. and Steglich, W. *Angew. Chem. Int. Ed.* **1978**, *17*, 522.
(183) Greene, T. W. and Wuts, P. G. M. *Greene's protective groups in organic synthesis*; 4th ed.; John Wiley & Sons, 2007.
(184) Crouch, R. D. *Tetrahedron* **2013**.
(185) Patschinski, P., Zhang, C. and Zipse, H. *J. Org. Chem.* **2014**, *79*, 8348.
(186) Corey, E. J. and Venkateswarlu, A. *J. Am. Chem. Soc.* **1972**, *94*, 6190.
(187) Okamoto, K., Hamada, N., Okamura, T., Ueyama, N. and Yamamoto, H. *Org. Biomol. Chem.* **2009**, *7*, 3782.
(188) Wissner, A. and Grudzinskas, C. V. *J. Org. Chem.* **1978**, *43*, 3972.
(189) Frederick, J. E., Snell, H. E. and Haywood, E. K. *Photochem. Photobiol.* **1989**, *50*, 443.
(190) Harrison, G. I. and Young, A. R. *Methods* **2002**, *28*, 14.
(191) Tyrrell, R. M. Mol. Aspects Med. 1994, 15, 1.
(192) Young, B., PhD thesis, University of Bath, 2013.
(193) Wang, H. 2013 *Compound of camptothecin and preparation and use thereof* EP2862571A4.
(194) Kefford, J. F. *J. Chem. Soc.* **1940**, 1208.
(195) Meth-Cohn, O., Narine, B. and Tarnowski, B. *J. Chem. Soc. Perkin 1* **1981**, 1531.
(196) Yamashita, H., Sakurai, Y., Miyamoto, M., Nakamura, Y., Kuroda, H. and Minowa, T. 2012 *Piperazine-substituted benzothiophene derivatives as antipsychotic agents* US9260420B2.
(197) Whitcombe, N. J., Hii, K. K. and Gibson, S. E. *Tetrahedron* **2001**, *57*, 7449.
(198) Park, K. K. and Jung, J. Y. *Heterocycles* **2005**, *65*, 2095.
(199) Tashima, T. *Bioorg. Med. Chem. Lett.* **2015**, *25*, 3415.
(200) Kinga, K., Anna, E. P. and Elzbieta, B. *Lett. Drug Des. Discov.* **2016**, *13*, 465.
(201) Lawrence, K. P., Douki, T., Sarkany, R. P. E., Acker, S., Herzog, B. and Young, A. R. *Sci. Rep.* **2018**, *8*, 12722.
(202) Sankaran, M., Kumarasamy, C., Chokkalingam, U. and Mohan, P. S. *Bioorg. Med. Chem. Lett.* **2010**, *20*, 7147.
(203) Chung, H. S. and Woo, W. S. *J. Nat. Prod.* **2001**, *64*, 1579.
(204) Lee, C. Y., Nanah, C. N., Held, R. A., Clark, A. R., Huynh, U. G. T., Maraskine, M. C., Uzarski, R. L., McCracken, J. and Sharma, A. *Biochimie* **2015**, *111*, 125.
(205) Mondal, M. A., Mandal, D. and Mitra, K. *J. Chem. Sci.* **2017**, *129*, 39.
(206) Tiberghien, A. C., Levy, J.-N., Masterson, L. A., Patel, N. V., Adams, L. R., Corbett, S., Williams, D. G., Hartley, J. A. and Howard, P. W. *ACS Med. Chem. Lett.* **2016**, *7*, 983.

(207) Janett, E., Bernardinelli, Y., Müller, D. and Bochet, C. G. *Bioconjugate Chem.* **2015**, *26*, 2408.
(208) Rakshit, S., Lakshminarasimhan, T., Guturi, S., Kanagavel, K., Kanusu, U. R., Niyogi, A. G., Sidar, S., Luzung, M. R., Schmidt, M. A., Zheng, B., Eastgate, M. D. and Vaidyanathan, R. *Org. Process Res. Dev.* **2018**, *22*, 391.
(209) Shen, L. and Sun, D. *Tetrahedron Lett.* **2011**, *52*, 4570.
(210) Chen, N., Jain, N., Xu, J., Reuman, M., Li, X., Russell, R. K. and Sui, Z. *Tetrahedron Lett* **2006**, *47*, 5909.
(211) Roussaki, M., Kontogiorgis, C. A., Hadjipavlou-Litina, D., Hamilakis, S. and Detsi, A. *Bioorg. Med. Chem. Lett.* **2010**, *20*, 3889.
(212) Fabian, W. M. F., Niederreiter, K. S., Uray, G. and Stadlbauer, W. *J. Mol. Struct.* **1999**, *477*, 209.
(213) Aksoy, L., Kolay, E., Ağılönü, Y., Aslan, Z. and Kargıoğlu, M. *Saudi J. Biol. Sci.* **2013**, *20*, 235.
(214) Kulišić, T., Verica, D.-U. and Milos, M. *Food Technol. Biotechnol.* **2006**, *44*, 485.
(215) Kedare, S. B. an Singh, R. P. *J. Food Sci. Technol.* **2011**, *48*, 412.
(216) Bendary, E., Francis, R. R., Ali, H. M. G., Sarwat, M. I. and El Hady, S. *Ann. Agric. Sci.* **2013**, *58*, 173.
(217) Eruslanov, E. and Kusmartsev, S. *Advanced Protocols in Oxidative Stress II*, Armstrong, D. Ed., Humana Press: Totowa, 2010, p 57.
(218) Lai, Y.-S., Kao, C.-L., Chen, Y.-P., Fang, C.-C., Hu, C.-C. and Chu, C.-C. *New J. Chem.* **2016**, *40*, 2601.
(219) Tungler, A., Tarnai, T., Hegedûs, L., Fodor, K. and Máthé, T. *Platin. Met. Rev.* **1998**, *42*, 108.
(220) Jung, M. E. and Lyster, M. A. *J. Org. Chem.* **1977**, *42*, 3761.
(221) Gowda, S., Kempe Gowda, B. K. and Channe Gowda, D. *Syn. Comm.* **2003**, *33*, 281.
(222) Liu, W., Wang, X., Lai, W., Yan, T., Wu, Y., Wan, M., Yi, J. and Matsui, M. S. *Photodermatol. Photoimmunol. Photomed.* **2012**, *28*, 120.
(223) Narbutt, J., Philipsen, P. A., Harrison, G. I., Morgan, K. A., Lawrence, K. P., Baczynska, K. A., Grys, K., Rogowski-Tylman, M., Olejniczak-Staruch, I., Tewari, A., Bell, M., O'Connor, C., Wulf, H. C., Lesiak, A. and Young, A. R. *Br. J. Dermatol.* **2019**, *180*, 604.
(224) Stokes, R. and Diffey, B. *Photodermatol. Photoimmunol. Photomed.* **1997**, *13*, 186.
(225) Rhodes, L. E. and Diffey, B. L. *J. Cosmet. Sci.* **1996**, *47*, 109
(226) Autier, P., Boniol, M., Severi, G. and Doré, J. F. *Br. J. Dermatol.* **2001**, *144*, 288.
(227) Neale, R., Williams, G. and Green, A. *Arch. Dermatol.* **2002**, *138*, 1319.
(228) Rai, R., Shanmuga, S. C. and Srinivas, C. *Indian J. Dermatol.* **2012**, *57*, 335.
(229) Fourtanier, A., Moyal, D. and Seite, S. *Photodermatol. Photoimmunol. Photomed.* **2008**, *24*, 164.
(230) Chen, L. L. and Wang, S. Q. *Nanoscience in Dermatology*, Hamblin, M. R., Avci, P., Prow, T. W., Ed., Academic Press: Boston, 2016, p 229.
(231) Schalka, S., Dos Reis, V. M. S. and Cucé, L. C. *Photodermatol. Photoimmunol. Photomed.* **2009**, *25*, 175.
(232) Faurschou, A. and Wulf, H. C. *Br. J. Dermatol.* **2007**, *156*, 716.
(233) Kim, S. M., Oh, B. H., Lee, Y. W., Choe, Y. B. and Ahn, K. J. *J. Am. Acad. Dermatol.* **2010**, *62*, 218.
(234) Sohn, M., Korn, V. and Imanidis, G. *Skin Pharmacol. Physiol.* **2015**, *28*, 31.
(235) Gasparro, F. P. *Environ. Health Perspect.* **2000**, *108*, 71.

(236) Breuer, W., Epsztejn, S., Millgram, P. and Cabantchik, I. Z. *Am. J. Physiol. Cell Physiol.* **1995**, *268*, 1354.
(237) Cabantchik, Z. I., Glickstein, H., Milgram, P. and Breuer, W. *Anal. Biochem.* **1996**, *233*, 221.
(238) Epsztejn, S., Kakhlon, O., Glickstein, H., Breuer, W. and Cabantchik, Z. I. *Anal. Biochem.* **1997**, *248*, 31.
(239) Vermes, I., Haanen, C. and Reutelingsperger, C. *Clin. Chem.* **1995**, *41*, S91.
(240) Pustisek, N. and Situm, M. *Coll. Antropol.* **2011**, *35(2)*, 339.
(241) Eggermont, A. M. M., Liénard, D., Guggisberg, D., Lejeune, F. J., Doré, J.-F., Autier, P., Panizzon, R., Négrier, S. *J. Natl. Cancer Inst.* **1999**, *91*, 1304.
(242) Beijerinck, M. W. *Arch. Neerland. Physiol.* **1918**, *2*, 609.
(243) Roberts, C. *Am. J. Bot.* **1946**, *33*, 237.
(244) Kupfer, D., Uffen, R. and Canale-Parola, E. *Arch. Microbiol.* **1967**, *56*, 9.
(245) Kluyver, A. J., Van Der Walt, J. P. and Van Triet, A. J. *Proc. Natl. Acad. Sci. U.S.A.* **1953**, *39*, 583.
(246) Dutcher, J. D. *J. Biol. Chem.* **1947**, *171*, 321.
(247) Fan, J., Santomauro, F., Budarin, V. L., Whiffin, F., Abeln, F., Chantasuban, T., Gore-Lloyd, D., Henk, D., Scott, R. J., Clark, J. and Chuck, C. J. *J. Clean. Prod.* **2018**, *198*, 776.
(248) MacDonald, J. C. *Can. J. Chem.* **1963**, *41*, 165.
(249) Borthwick, A. D. *Chem. Rev.* **2012**, *112*, 3641.
(250) Zhao, S., Smith, K. S., Deveau, A. M., Dieckhaus, C. M., Johnson, M. A., Macdonald, T. L. and Cook, J. M. *J. Med. Chem.* **2002**, *45*, 1559.
(251) Gomez-Monterrey, I., Campiglia, P., Carotenuto, A., Stiuso, P., Bertamino, A., Sala, M., Aquino, C., Grieco, P., Morello, S., Pinto, A., Ianelli, P. and Novellino, E. *J. Med. Chem.* **2008**, *51*, 2924.
(252) Manchineella, S., Voshavar, C. and Govindaraju, T. *Eur. J. Org. Chem.* **2017**, *17*, 4363.
(253) Ohta, A. *Chem. Pharm. Bull*. **1964**, *12*, 125.
(254) Ohta, A., Yamamoto, F., Arimura, Y. and Watanabe, T. *J. Heterocycl. Chem.* **1982**, *19*, 781.
(255) Cook, B., Hill, R. R. and Jeffs, G. E. *J. Chem. Soc. Perkin 1* **1992**, *10,* 1199.
(256) Valeur, E. and Bradley, M. *Chem. Soc. Rev.* **2009**, *38*, 606.
(257) Suzuki, K., Sasaki, Y., Endo, N. and Mihara, Y. *Chem. Pharm. Bull.* **1981**, *29*, 233.
(258) Fischer, E. *Chem. Ber.* **1906**, *39*, 2893.
(259) Nitecki, D. E., Halpern, B. and Westley, J. W. *J. Org. Chem.* **1968**, *33*, 864.
(260) Göktürk, A. K., Porter, A. A. E. and Sammes, P. G. *J. Chem. Soc. Perkin 1* **1982**, 953.
(261) Usui, I., Lin, D., Masuda, T. and Baran, P. S. *Org. Lett.* **2013**, *15*, 2080.
(262) Ohta, A., Akita, Y. and Hara, M. *Chem. Pharm. Bull.* **1979**, *27*, 2027.
(263) Wang, H., Wen, K., Wang, L., Xiang, Y., Xu, X., Shen, Y. and Sun, Z. *Molecules* **2012**, *17*, 4533.
(264) Matts, P. J., Alard, V., Brown, M. W., Ferrero, L., Gers-Barlag, H., Issachar, N., Moyal, D. and Wolber, R. *Int. J. Cosmet. Sci.* **2010**, *32*, 35.
(265) Ferrero, L., Pissavini, M. and Doucet, O. *Photochem. Photobiol. Sci.* **2010**, *9*, 540.
(266) Sohn, M., Malburet, C., Baptiste, L. and Prigl, Y. *Skin Pharmacol. Physiol.* **2017**, *30*, 159.
(267) Cordery, S. F., Pensado, A., Chiu, W. S., Shehab, M. Z., Bunge, A. L., Delgado-Charro, M. B. and Guy, R. H. *Int. J. Pharm.* **2017**, *529*, 55.

(268) Furukawa, T., Akutagawa, T., Funatani, H., Uchida, T., Hotta, Y., Niwa, M. and Takaya, Y. *Bioorg. Med. Chem.* **2012**, *20*, 2002.
(269) Sah, P. *J. Pharm. Sci.* **1954**, *43*, 513.
(270) Jarussophon, S., Pongwan, P. and Srikun, O. *Org. Prep. Proced. Int.* **2015**, *47*, 483.
(271) Rao, V. J., Mukkanti, K., Vekariya, N. A., Gupta, P. B. and Islam, A. *Syn. Comm.* **2012**, *42*, 3200.
(272) Frater, G. and Anderson, D. 2010 *Aryl-acrylic esters useful as precursors for organoleptic compounds* EP0936211B1.
(273) Chaisan, N., Kaewsri, W., Thongsornkleeb, C., Tummatorn, J. and Ruchirawat, S. *Tetrahedron Lett.* **2018**, *59*, 675.
(274) Saikia, U. P., Hussain, F. L., Suri, M. and Pahari, P. *Tetrahedron Lett* **2016**, *57*, 1158.
(275) Somasekhara, P. *J. Indian I. Sci.* **1955**, *37*, 120.
(276) Lempert-Sreter, M., Lempert, K. and Moller, J. *J. Chem. Soc. Perkin 1* **1983**, 2011.
(277) Zhang, H.-Q., Gong, F.-H., Ye, J.-Q., Zhang, C., Yue, X.-H., Li, C.-G., Xu, Y.-G. and Sun, L.-P. *Eur. J. Med. Chem.* **2017**, *125*, 245.
(278) Tsai, S.-C. and Klinman, J. P. *Bioorg. Chem.* **2003**, *31*, 172.
(279) Kobayashi, S., Okimoto, K. and Imakura, Y. *Chem. Pharm. Bull.* **1982**, *30*, 1567.
(280) Skiles, J. W. and Cava, M. P. *J. Org. Chem.* **1979**, *44*, 409.
(281) Yadav, M. *Synthesis* **1984**, *10*, 862.
(282) Gensler W. J. and Berman, E. *J. Am. Chem. Soc.* **1958**, *80*, 4949.
(283) Hou, J., Ee, A., Feng, W., Xu, J.-H., Zhao, Y. and Wu, J. *J. Am. Chem. Soc.* **2018**, *140*, 5257.
(284) Nemecek, G., Cudai, J. and Podlech, J. *Eur. J. Org. Chem.* **2012**, *20*, 3863.
(285) Avery, M. A., Verlander, M. S. and Goodman, M. *J. Org. Chem.* **1980**, *45*, 2750.
(286) Miyake, M., Kirisawa, M. and Tokutake, N. *Chem. Lett.* **1985**, *14*, 123.
(287) Gnanaprakasam, B., Balaraman, E., Ben-David, Y. and Milstein, D. *Angew. Chem. Int. Ed.* **2011**, *50*, 12240.
(288) Breuer, W., Epsztejn, S. and Cabantchik, Z. I. *J. Biol. Chem.* **1995**, *270*, 24209.